

2

AFWAL-TR-81-2101

ADA111939

VOLUME I

LIFE AND UTILIZATION CRITERIA IDENTIFICATION IN DESIGN (LUCID)



Pratt & Whitney Aircraft Group
Government Products Division
United Technologies Corporation
West Palm Beach Fla. 33402

October 1981

Final Report - August 1978 - May 1981

Approved for Public Release: Distribution Unlimited

DTIC FILE COPY

Aero Propulsion Laboratory
Air Force Wright Aeronautical Laboratories
Air Force Systems Command
Wright-Patterson Air Force Base, Ohio 45433

DTIC
ELECTE
MAR 11 1982
E

NOTICE

When Government drawings, specifications, or other data are used for any purpose other than in connection with a definitely related Government procurement operation, the United States Government thereby incurs no responsibility nor any obligation whatsoever; and the fact that the government may have formulated, furnished, or in any way supplied the said drawings, specifications, or other data, is not to be regarded by implication or otherwise as in any manner licensing the holder or any other person or corporation, or conveying any rights or permission to manufacture, use, or sell any patented invention that may in any way be related thereto.

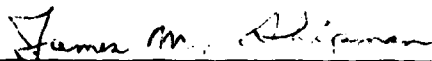
This report has been reviewed by the Office of Public Affairs (ASD/PA) and is releasable to the National Technical Information Service (NTIS). At NTIS, it will be available to the general public, including foreign nations.

This technical report has been reviewed and is approved for publication.



For the Commander





JAMES M. SHIPMAN, Major, USAF
Deputy Director
Turbine Engine Division

"If your address has changed, if you wish to be removed from our mailing list, or if the addressee is no longer employed by your organization please notify AFWAL/POTA, W-PAFB, OH 45433 to help us maintain a current mailing list."

Copies of this report should not be returned unless return is required by security considerations, contractual obligations, or notice on a specific document.

UNCLASSIFIED

SECURITY CLASSIFICATION OF THIS PAGE (When Data Entered)

REPORT DOCUMENTATION PAGE		READ INSTRUCTIONS BEFORE COMPLETING FORM
1. Report Number AFWAL-TR-81-2101, Volume I	2. Govt Accession No. AD -A111939	3. Recipient's Catalog Number
4. Title (and Subtitle) LIFE AND UTILIZATION CRITERIA IDENTIFICATION IN DESIGN (LUCID) Volume I	5. Type of Report & Period Covered Final Report Aug 78 - May 81	
	6. Performing Org. Report Number FR-14961	
7. Author(s) J. G. Osmer C. C. Dietrick	8. Contract or Grant Number(s) F33615-78-C-2032	
9. Performing Organization Name and Address United Technologies Corporation Pratt & Whitney Aircraft Group Government Products Division P.O. Box 2691, West Palm Beach, FL 33402	10. Program Element, Project, Task Area & Work Unit Numbers 30661128	
11. Controlling Office Name and Address Aero Propulsion Laboratory (AFWAL/POTA) Air Force Wright Aeronautical Laboratories (AFSC) Wright Patterson AFB, Ohio 45433	12. Report Date October 1981	
	13. Number of Pages 164	
14. Monitoring Agency Name & Address (if different from Controlling Office)	15. Security Class. (of this report) Unclassified	
	15a. Declassification/Downgrading Schedule	
16. Distribution Statement (of this Report) Approved for Public Release; Distribution Unlimited.		
17. Distribution Statement (of the abstract entered in Block 20, if different from Report)		
18. Supplementary Notes		
19. Key Words (Continue on reverse side if necessary and identify by block number) Turbine Engines, Engine Usage, Life Prediction, Conceptual Design, Engine Duty Cycle, Computer Aided Design, Engine Performance		
<p>20. Abstract (Continue on reverse side if necessary and identify by block number)</p> <p>In early gas turbine engine conceptual design, a complex interactive aircraft engine design effort is conducted. The primary objective of the Life and Utilization Criteria Identification in Design (LUCID) Program was to develop and demonstrate techniques which will aid in identifying, during conceptual design, balanced and consistent performance and life capability goals with which to proceed to engineering development.</p>		

DD FORM 1 JAN 73 1473

EDITION OF 1 NOV 65 IS OBSOLETE

UNCLASSIFIED

SECURITY CLASSIFICATION OF THIS PAGE (When Data Entered)

UNCLASSIFIED

SECURITY CLASSIFICATION OF THIS PAGE (When Data Entered)

29. Abstract (Continued)

In Volume I, a methodology for quantifying relative life/performance trades during the conceptual design phase of gas turbine engine development is presented. As part of this methodology, a computer-aided design system employing regression techniques has been developed and demonstrated. Major elements of this system are performing satisfactorily. However, certain component subroutines are exhibiting unacceptable error levels. Further effort is required in this innovative application of standard regression techniques.

In Volume II, procedures to predict engine usage are presented. Peacetime missions were defined for an advanced tactical strike aircraft and were employed by the usage models to generate a composite engine duty cycle. The engine duty cycle was analyzed and compared to engine usage projections for other advanced tactical aircraft. The analysis demonstrated significant variations in engine usage due to weapon delivery tactics associated with advanced air-to-surface missiles, as well as variations in peacetime mission frequencies and aircraft performance.

Accession For	
NTIS GRA&I	<input checked="" type="checkbox"/>
DTIC TAB	<input type="checkbox"/>
Unannounced	<input type="checkbox"/>
Justification	
By _____	
Distribution/	
Availability Codes	
Dist	Avail and/or Special
A	

0110
COPY
INSURE

DD FORM 1 JAN 73 1473

EDITION OF 1 NOV 65 IS OBSOLETE

UNCLASSIFIED

SECURITY CLASSIFICATION OF THIS PAGE (When Data Entered)

SUMMARY

In early gas turbine conceptual design, a complex interactive aircraft/ engine design effort is conducted. In this effort, the major objective is the determination of engine cycle variables (pressure ratio, turbine temperature, bypass ratio) and engine size. In the Life and Utilization Criteria Identification in Design 'LUCID' program (Contract F33615-78-C-2032), an effective computer-aided design procedure was developed, with the objective of producing an enhanced gas turbine conceptual design. This enhancement is the integration of component designs with the attributes of long design life goals, minor penalty to system size, and no change to system capability.

In the development of the design procedure, supportive mechanical design systems were developed, modified, and adapted to LUCID requirements. Matrices were developed (both aerodynamic and mechanical) for analysis of critical rotating components. These component models interact with a gas turbine performance model, engine steady-state and cyclic utilization, life goals, turbine airfoil cooling system analyses, and blade/disk material properties. Output of the computer-aided design system is engine performance and weight consistent with the engine cycle, life, and usage specified. Five to six stages of compressor and turbine components are addressed, and a comprehensive component weight program translates these stage weights to module and total engine weights.

The design system has been demonstrated. Selected fan, compressor, high pressure turbine, and low pressure turbine blade, attachment, and disk designs were generated for an advanced turbofan engine. The utilization specified was a composite steady-state and cyclic mission usage at multiple conditions in the flight envelope. Life-related and other design criteria were addressed for the gamut of stresses and design-limiting modes of the various components.

CONTENTS

Section	Page
SUMMARY	iii
1 INTRODUCTION.	1
2 LIFE, PERFORMANCE, AND WEIGHT TECHNIQUE (LPWT).	3
2.1 LIFE PREDICTION TECHNIQUES	4
2.1.1 Blade/Disk Attachment Synthesis.	8
2.1.2 Live Disk Synthesis.	19
2.1.3 Disk Radial Thermal Gradient Program	29
2.1.4 Turbine Airfoil Life Prediction.	34
2.1.5 Material Properties.	47
2.2 FLOWPATH COMPUTER ROUTINE.	51
2.2.1 Fan Flowath Subroutine	53
2.2.2 Compressor Flowpath Subroutine	57
2.2.3 High Pressure Turbine Flowpath Subroutine.	60
2.2.4 Low Pressure Turbine Flowpath Subroutine	65
2.3 WEIGHT PREDICTION ROUTINE.	71
2.3.1 Engine Weight Summary.	71
2.3.2 Fan Module Weight.	71
2.3.3 Compressor Module Weight	81
2.3.4 Diffuser/Combustor Weight.	81
2.3.5 High and Low Pressure Turbine Weight	85
2.3.6 Turbine Exhaust Case	85
2.3.7 Augmentor and Nozzle Weights	85
2.4 MECHANICAL MATRICES.	90
2.4.1 Compressor Blade/Disk Attachments.	90
2.4.2 High Pressure Turbine Blade/Disk Attachment.	95
2.4.3 Matrix Design Generation	101
2.4.4 Fan Disk	108
2.4.5 Compressor Disks	111
2.4.6 High Pressure Turbine Disk	115
2.4.7 Low Pressure Turbine Disks	116
2.5 MATRIX BASE DATA REGRESSION.	124
2.5.1 Compressor Attachment Regression	126
2.5.2 High Pressure Turbine (HPT) Attachment Regression.	128
2.5.3 Low Pressure Turbine (LPT) Attachment Regression	130
2.5.4 Aerodynamic Matrices' Regression	131
2.5.5 Fan Disk Matrix Regression	137
2.5.6 Compressor Disk Matrices Regression.	138
2.5.7 High-Pressure Turbine (HPT) Low-Pressure Turbine (LPT) Disk Matrix Regression.	140
2.6 LIFE, PERFORMANCE, WEIGHT TECHNIQUE (LPWT) CAD SYSTEM.	142
2.6.1 Engine Performance Simulation and Associated Driver Deck Routines.	144
2.6.2 LIFE/STRESS DECK	148
2.6.3 Life, Performance, Weight Technique Validation	151
3 RESULTS AND CONCLUSIONS	159

ILLUSTRATIONS

Figure	Page
2-1. LPWT Block Diagram.	3
2-2. Life Prediction Routine, Simplified Schematic	5
2-3. Blade/Disk Attachment Nomenclature and Optimization Parameters.	9
2-4. Blade/Disk Attachment Design Criteria Summary	10
2-5. Comparison of Boundary Integral Equation and Finite Element Values for K_T vs R/D	11
2-6. Blade/Disk Attachment Basic Flow Chart.	12
2-7. Single Tooth Attachment Synthesis Solution.	13
2-8. Blade/Disk Attachment Stresses.	15
2-9. Metal and Composite Fan Blade Attachment Failure Modes.	16
2-10. Composite Fan Blade Attachment	18
2-11. Initial Geometry From Synthesis of a Compressor Disk	22
2-12. First Iteration Geometry From Synthesis of a Compressor Disk.	23
2-13. Second Iteration Geometry From Synthesis of a Compressor Disk.	24
2-14. Third Iteration Geometry From Synthesis of a Compressor Disk.	25
2-15. Fourth Iteration Geometry From Synthesis of a Compressor Disk.	26
2-16. Final Iteration Geometry From Synthesis of a Compressor Disk.	27
2-17. Verification of the Disk Synthesis Program	28
2-18. Six Node Heat Transfer Model	30
2-19. Compressor Disk Radial Thermal Gradient, 3rd Disk (Non-Bleed Stage) 6 Second Acceleration	31
2-20. Compressor Disk Radial Thermal Gradient, 5th Disk (Bleed Stage) 6 Second Acceleration.	32
2-21. Compressor Disk Radial Thermal Gradient, 5th Disk (Bleed Stage) 6 Second Acceleration.	33
2-22. Typical Turbine Disk Thermal Gradients	35
2-23. Comparison of Turbine Disk Radial Thermal Gradient Models For Acceleration Transient	36
2-24. Comparison of Turbine Disk Radial Thermal Gradient Models For Deceleration Transient	37
2-25. Turbine Airfoil Cooling Effectiveness.	39
2-26. Centrifugal Stress (P/A) Blade Design Experience	40
2-27. Gas and Metal Temperature Trends (Left) and Critical Stress Section for Cooled Turbine Blades.	40
2-28. Uncooled Blade Temperature and Stress Characteristics.	41
2-29. Oxidation/Erosion Life Limits for Coated Turbine Blade and Vane Materials.	42
2-30. Relative Strain Range for First Vane and First Blade	44
2-31. First Vane Low Cycle Fatigue Life Relative to a Type III Cycle	45
2-32. First Blade Low Cycle Fatigue Life Relative to a Type III Cycle.	46

ILLUSTRATIONS (Cont.)

Figure	Page
2-33. Transient Strain Range Prediction	48
2-34. Vane Strain and Temperature for 22% to 43% Intermediate Thrust Transient.	49
2-35. Vane Strain and Temperature for Idle to 43% Intermediate Thrust Transient.	49
2-36. Acceleration and Deceleration Data For Transient Low Cycle Fatigue Life Analysis	50
2-37. Disk and Blade Material Properties Definition Format	52
2-38. LUCID Fan Parametric Screening Results	54
2-39. Fan Flowpath At Average Aspect Ratio of 2.3 and 1600 ft/sec Tip Speed.	55
2-40. Fan Pressure Ratio As A Function of Tip Speed and Number of Stages.	55
2-41. Fan Pressure Ratio As A Function of Aspect Ratio Tip Speed	56
2-42. Estimated Fan Efficiency	56
2-43. Typical Compressor Flowpaths Illustrating the Effect of Aspect Ratio With Seven Compressor Stages	58
2-44. Effect of Compressor Aspect Ratio on Pressure Ratio and Efficiency.	59
2-45. Estimated Pressure Ratio and Efficiency Trend With Number of Stages.	61
2-46. Estimated Pressure Ratio and Efficiency Variation With Compressor Tip Speed	62
2-47. Estimated Effect of Hub/Tip Ratio on Pressure Ratio and Efficiency.	63
2-48. Typical HPT Aerodynamic Matrix Results	66
2-49. Typical Low Pressure Turbine Meanline Designs.	67
2-50. Effect of Chord, Low Pressure Turbine.	68
2-51. Effect of Inlet Temperature, Low Pressure Turbine.	69
2-52. Effect of Mean Velocity Ratio, Low Pressure Turbine.	70
2-53. Fan Module Components and Materials Summary.	72
2-54. Boron Aluminum Solid Composite Fan Blade Construction.	73
2-55. Boron Aluminum Solid Composite Airfoil Construction.	74
2-56. Fan Module Weight Subroutine	75
2-57. Fan Stator Weight as a Function of Size.	76
2-58. Relative Fan Stator Weight as a Function of Tip Speed.	76
2-59. Relative Fan Stator Weight as a Function of Number of Stages and Average Aspect Ratio	77
2-60. Fan Weight Correlation, Normalized Rotor Weight.	78
2-61. Fan Weight Correlation, First and Second Stage Wheel Weights	78
2-62. Fan Weight Correlation, Disk Weight and Geometry Variation With Cyclic Life Capability	79
2-63. Fan Weight Correlation, Bias Curves.	80

ILLUSTRATIONS (Cont.)

Figure	Page
2-64. Schematic Representation of Compressor Weight Correlator. (Normalized Weight Is Total Rotor Weight Divided by First and Next-to-Last-Stage Wheel Weights).	82
2-65. Compressor Module Weight Summary	83
2-66. Materials and Geometric Input for Diffuser/Combustor Weight Prediction	84
2-67. High Pressure Turbine Summary.	86
2-68. Turbine Exhaust Case Components.	87
2-69. Augmentor Components	88
2-70. Balance Beam Nozzle Component and Material Summary	89
2-71. Summary of Fan, Compressor, and Turbine Attachment and Disk Matrices	91
2-72. Blade Design Data Initiates Sequential Attachment and Disk Solutions (Turbine Example).	92
2-73. Compressor Blade/Disk Circumferential Attachment	94
2-74. Typical Results of Front Compressor Blade/Disk Attachment Matrix Designs	96
2-75. Typical Results of Front Compressor Blade/Disk Matrix Design.	97
2-76. Sensitivity of Cooling Hole Area to Cooling Flow	98
2-77. Sensitivity of Coolant Mach Number to Cooling Flow	99
2-78. Effect of LCF Life on the Turbine Attachment	102
2-79. Effect of Stress Rupture Life on Turbine Attachment.	103
2-80. Effect of Number of Blades on Turbine Attachment	104
2-81. Effect of Total Airfoil Pull on Turbine Attachment	105
2-82. Life Ratio Effect on HPT Attachment.	106
2-83. Size Range of Turbine Attachments.	107
2-84. Low Pressure Turbine Attachment Response to Total Blade Pull Variation.	109
2-85. Low Pressure Turbine Attachment Response to LCF and Stress Rupture Capability	110
2-86. Typical Matrix Fan Disk with Four Slope-Limited Rings.	111
2-87. Effect of Cycles on Disk Weight and Geometry, First Compressor Disk	113
2-88. Effect of Rim Pull and Rim Width on Disk Weight and Geometry, First Compressor Disk	114
2-89. Effect of Cycles on High Pressure Turbine Disk Weight and Geometry	117
2-90. Effect of Disk Radial Temperature Gradient on High Pressure Turbine Disk Weight and Geometry	118
2-91. Effect of Rim Width on High Pressure Turbine Disk Weight and Geometry	119
2-92. Effect of Rim Pull on High Pressure Turbine Disk Weight and Geometry	120
2-93. Low Pressure Turbine Disk Weight and Geometry as a Function of Cyclic Life Capability.	122

ILLUSTRATIONS (Cont.)

Figure	Page
2-94. Effect of Rim Pull on Low Pressure Turbine Disk Geometry and Weight	123
2-95. IPT Blade/Disk Attachment Rim Width Trend Comparison of Data and Regression Equations.	132
2-96. LPT Blade/Disk Attachment Blade Second Neck Nominal Tensile Stress Regression Error Comparison.	133
2-97. Cooled Efficiency and Blade Pull Trends.	136
2-98. Schematic of SOAPP, LPWT Engine Performance Simulation, and Associated Driver Deck Routines	145
2-99. Pictorial Representation of SOAPP System	147
2-100. Flowchart of LUCID Life Prediction Procedure.	163

TABLES

Table	Page
2-1. Simplified/Detailed Meanline Analysis Comparison.	64
2-2. Referee Turbine Cooling Air	64
2-3. Front Compressor Attachment Independent Variable Levels	93
2-4. Rear Compressor Attachment Independent Variables Levels	93
2-5. High Pressure Turbine Blade/Disk Attachment Independent Variable Levels	100
2-6. High Pressure Turbine Variable Level Ranges	107
2-7. Low Pressure Turbine Attachment	108
2-8. Fan Disk Independent Variable Levels.	111
2-9. First Stage Compressor Disk Matrix.	112
2-10. Next-to-Last Stage Compressor Disk Independent Variables and Ranges.	115
2-11. High Pressure Turbine Disk Matrix Independent Variables and Ranges.	116
2-12. Low Pressure Turbine Disk Independent Variables and Ranges.	124
2-13. First Stage Compressor Blade/Disk Attachment Regression Results	127
2-14. Rear Compressor Blade/Disk Attachment Regression Results	128
2-15. High Pressure Turbine Blade/Disk Attachment Regression Results	129
2-16. Regression Results for Low Pressure Turbine Blade/Disk Attachment Matrix.	130
2-17. Compressor Aerodynamic Matrix Regression Analysis Results	134
2-18. Regression Results for High Pressure Turbine Aerodynamic Matrix.	134
2-19. Regression Results for Single-Stage Low Pressure Turbine Aerodynamic Matrix.	135

TABLES (Cont.)

Table	Page
2-20. Two-Stage Low Pressure Turbine Aerodynamic Matrix Regression Results.	137
2-21. Fan Disk Matrix Regression Results	138
2-22. Front Compressor Disk Regression Accuracy Summary (Second Order Polynomial)	139
2-23. Rear Compressor Disk Regression Accuracy Summary (Second Order Polynomial)	139
2-24. High Pressure Turbine Disk Regression Accuracy Summary (Second Order Polynomial)	141
2-25. Low Pressure Turbine Disk Regression Accuracy Summary (Second Order Polynomial)	142
2-26. Life, Performance, Weight Technique (LPWT) Size of Major Elements/Subroutines.	143
2-27. LPWT Driver and Life/Stress Deck Major Subroutines.	144
2-28. Comparison of LPWT-Generated Fan Aerodynamic Variables with Existing Conceptual Design	152
2-29. Comparison of LPWT-Generated Compressor Aerodynamic Variables with an Existing Conceptual Design.	153
2-30. Comparison of LPWT-Generated High Pressure Turbine Aerodynamic Variables with an Existing Conceptual Design.	153
2-31. Comparison of LPWT-Generated Low Pressure Turbine Aerodynamic Variables with an Existing Conceptual Design.	154
2-32. Fan Disk Validation.	156
2-33. Fan Turbine Disk Validation.	157

SECTION 1
INTRODUCTION

The military aircraft gas turbine conceptual design phase initially focuses on selection of the cycle parameters (turbine temperature, pressure ratio, bypass ratio) and engine size. The trend in conceptual design is toward more complex analyses, with emphasis on lessons learned during the maturation of previous system deployments. The propulsion systems of tactical aircraft deployed in the last decade were designed and developed to duty cycles far different from those of actual service operations. There is consensus in the propulsion community that this inaccurate perception of engine utilization has penalized the durability characteristics of today's propulsion systems.

Selection criteria for future gas turbine developments shall rank durability goals higher on the priority list. Future engine designs will reflect a larger degree of life/performance trades. High engine life goals can be accommodated with little increase in system size and constant capability, because of the logarithmic response of life to stress.

The overall objective of the LUCID program is the development and demonstration of effective procedures for more comprehensive early conceptual design, addressing engine life and utilization variables in more detail. McDonnell Aircraft Company (McAir), the subcontractor to Pratt and Whitney Aircraft Group Government Products Division, has developed a procedure for estimating engine utilization for advanced Air Force tactical aircraft. Pratt and Whitney Aircraft has developed a gas turbine conceptual design technique in the form of a computer-aided design system. The system is operational, and major elements of the computer program are performing satisfactorily. However, certain mechanical component subroutines are exhibiting

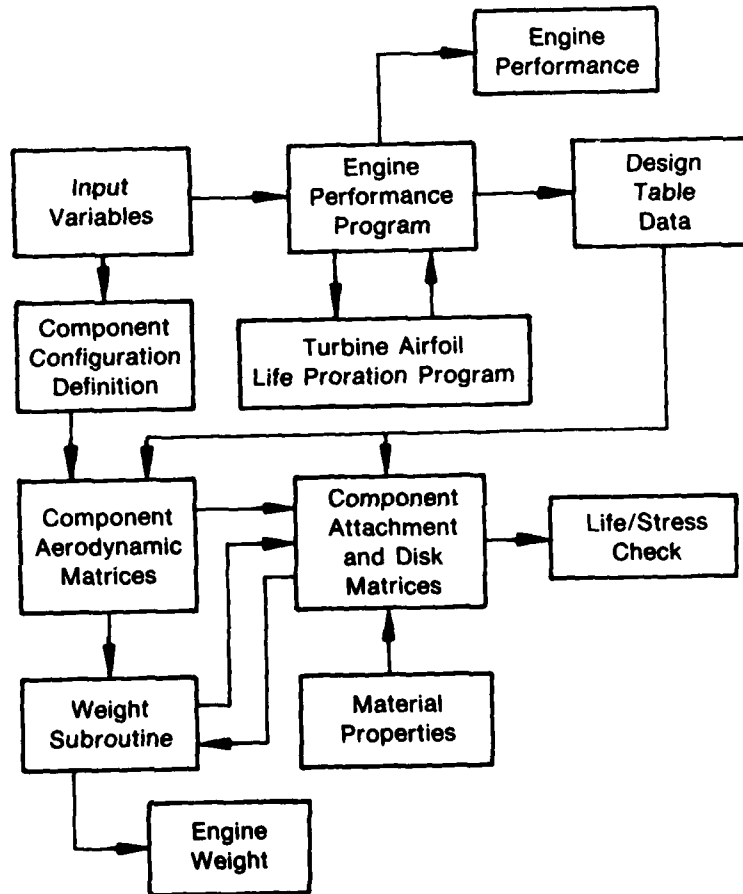
unacceptable error levels. These problems are principally in the areas of regression of attachment and disk matrices. Further effort is required in this innovative application of standard regression techniques.

This report summarizes both the approach used to generate the computer-aided design system and the development and execution of supportive effort. Successful completion of the program required the performance and coordination of virtually all technical disciplines in the advanced design area.

SECTION 2

LIFE, PERFORMANCE, AND WEIGHT TECHNIQUE (LPWT)

Figure 2-1 is a block diagram showing a schematic representation of the major subroutines which comprise the LPWT program developed under the LUCID contract. This computer-aided design (CAD) system has been developed to analyze the impact of engine life requirements and usage on engine cycle and component configuration selections during early conceptual design. A major program goal is the programming and checkout of the LPWT. The LPWT in its present form provides a framework within which one may add or delete selected engine design variables (fan, compressor, and turbine rotor components are analyzed; other aircraft gas turbine components are not currently addressed).



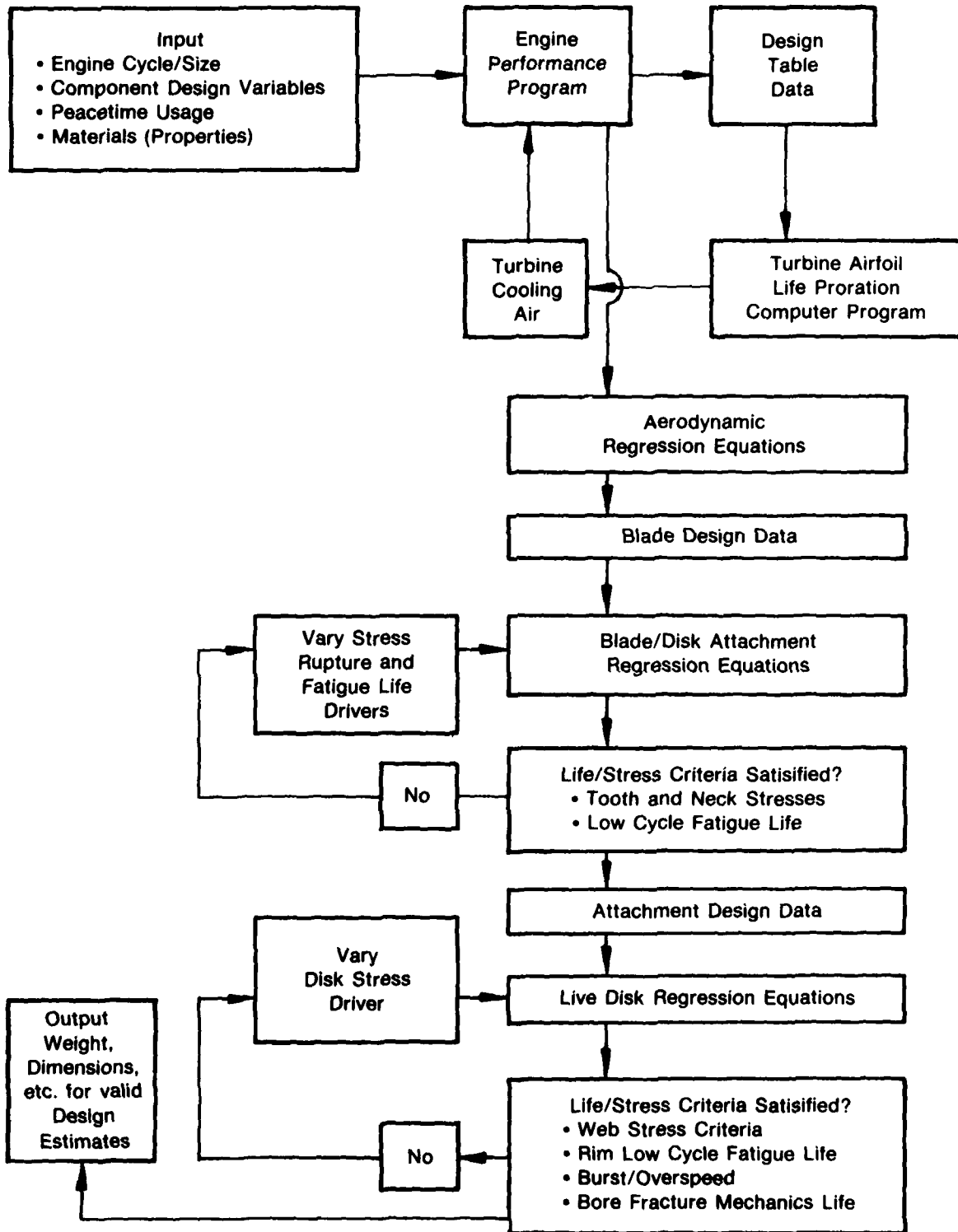
FD 223741

Figure 2-1. LPWT Block Diagram.

2.1 LIFE PREDICTION TECHNIQUES

The sequence of analyses used in estimating airfoil, blade/disk attachment, and disk lives is shown in simplified schematic form in Figure 2-2. Peacetime mission composite usage and required life are critical elements in the analyses. Gas turbine cycle requirements and turbine design variables interact with the turbine aerodynamic matrix regression equations, defining the number of blades, airfoil pull, flowpath root radius, and blade root chord. With these parameters, a matrix of blade/disk attachments is accessed (the matrix is in the form of regression equations). Two independent variables, which alter blade and disk lug tooth and neck stresses, are varied until empirical attachment stress criteria and low cycle fatigue lives are met or exceeded. For the fan, compressor, and turbine components, selected design variables are presently available (for example, tip speed, average aspect ratio and number of stages may be varied in the compressor design, but compressor exit Mach number and flowpath shape are fixed at representative levels).

With the LPWT, the designer has the capability to study the effects of component design variables, engine life, and engine usage concurrent with solving the usual conceptual design problem of optimizing the gas turbine cycle and size variables. The LPWT studies may be accomplished at a fraction of the cost of similar studies performed with existing design systems. Given engine cycle, size, life, and usage, a matrix of engine designs is defined encompassing ranges of the component design variables. The LPWT develops engine performance (at the critical design mission and usage flight conditions) and engine weight. With aircraft takeoff gross weight as the figure of merit, an optimum engine component configuration definition is selected from the LPWT-developed matrix.



FD 223742

2-2. Life Prediction Routine, Simplified Schematic.

The LPWT is comprised of the following three major elements.

o Driver Deck

This computer routine initiates the component design process, given the engine cycle, size, and component design variable levels. This routine assures the compatibility of the fan/fan-drive turbine and compressor/compressor-drive turbine, as well as continuity of gas path and secondary flow systems. In addition, the Driver Deck includes the Turbine Life Proration subroutine which estimates cooling air for turbine airfoils. With convergence of the Driver Deck, the flowpath variables required for analysis of blade/disk attachments and disks are estimated, as well as rotor speeds and engine temperatures at engine usage conditions.

o Life/Stress Deck

This portion of the LPWT determines the blade/disk attachment and disk configurations required to meet the engine life specified. Multiple design criteria are checked in determining the attachment and disk designs: (1) empirically-derived stress criteria, (2) burst/overspeed stress criteria, and (3) both steady-state and cyclic life criteria.

o Weight Routine

This routine builds up total engine weight, utilizing design information developed by both the Driver and Life/Stress Decks. Weight for the fan and compressor components utilize weight correlations to develop total rotor weights given the weights of the three bladed disks analyzed by the Life/Stress Deck. Case, stator, seal/spacer, etc. weights are added to these rotor weights in estimating module weights. Weights of other engine modules (combustor, augmentor, nozzle, control) are estimated using design variables generated by the Driver Deck.

The bladed disks selected for analysis in the LPWT Life/Stress Deck are:

- o First fan stage
- o First compressor stage
- o Next-to-last compressor stage
- o Single stage high pressure turbine
- o Single stage low pressure turbine, or first stage of two-stage low pressure turbine.

The fan, compressor, and turbine stages were selected because they are major weight drivers of the rotor systems and would be indicative of the respective modules. Only turbine airfoils are analyzed by the LPWT; fan and compressor airfoils were not selected because experience shows that their useful lives are limited by high cycle fatigue or foreign object damage. The turbine airfoils were selected for analysis because of the impact that their cooling air requirements have on engine performance, weight, and turbine cooled efficiency (cooling flows for all turbine airfoils will be estimated).

It is felt that the selected components provide the most effective life, weight, and performance visibility.

Primary independent variables of the LPWT are the cycle variables (overall pressure ratio, maximum combustor exit temperature, and throttle ratio), engine size, composite utilization, life required, and component configuration definitions. The engine performance program, configuration definitions, and the aerodynamic matrices interact, and blade data is generated for the 5 or 6 stages to be analyzed.

Blade design variables (number of blades, flowpath inside radius, airfoil pull, rotor speed, and airfoil root axial chord) are output from the component aerodynamic matrices and the weight subroutine. This blade design data provides for initiation of the blade/disk attachment designs via the attachment matrices. Attachment matrix output stresses are changed through the variation of one compressor attachment independent variable or two turbine attachment independent

variables. These stress driver independent variables are varied until the attachments meet (or exceed) all life and stress margin ratio checks.

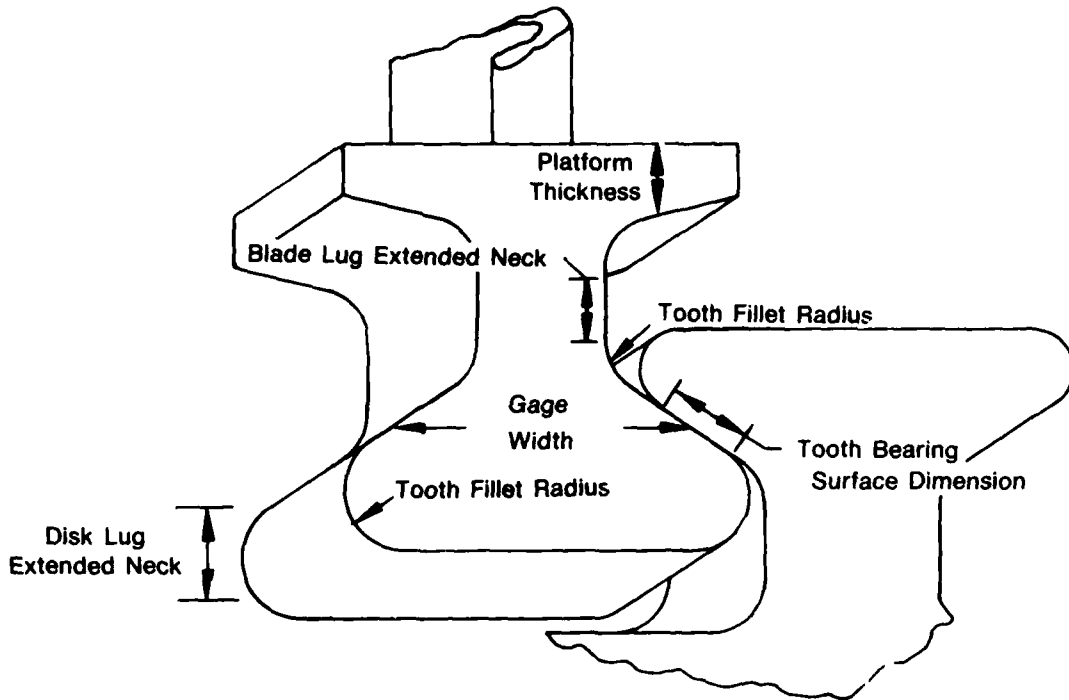
With the attachment design completed, the disk design variables (rim pull, live rim radius, and rim width) are available and the analysis may proceed with sizing the live disk. Similar to the turbine aerodynamic and the attachment matrices, the disk design variables are in the form of regression equations of a matrix of disk designs. A single independent variable is used in the disk regression equations to alter stresses until life and other disk design criteria are met or exceeded.

The foregoing discussion of the LPWT approach to life prediction of blade/disk attachments and disks demonstrates the reliance placed on design systems for attachments and disks. Since each component matrix is comprised of fifty-five to ninety designs, and there is potential for many of the design solutions to be iterative, the LUCID program needed attachment and disk design systems for generation of the multitude of component designs.

Sections 2.1.1 and 2.1.2 summarize the Blade/Disk Attachment Synthesis and Live-Disk Synthesis computer programs which were modified and adapted for use in the LUCID program.

2.1.1 Blade/Disk Attachment Synthesis

The axial broach Blade/Disk Attachment Synthesis computer program is an existing design system which optimizes blade and disk lug geometry for minimum dead rim weight, while meeting or exceeding empirical neck and tooth stress criteria and tooth fillet low cycle fatigue life. Figure 2-3 summarizes attachment nomenclature. In the figure, a dovetail attachment is shown (it is noted that in multi-tooth turbine attachments, a critical design parameter is the angle at which the teeth are set).



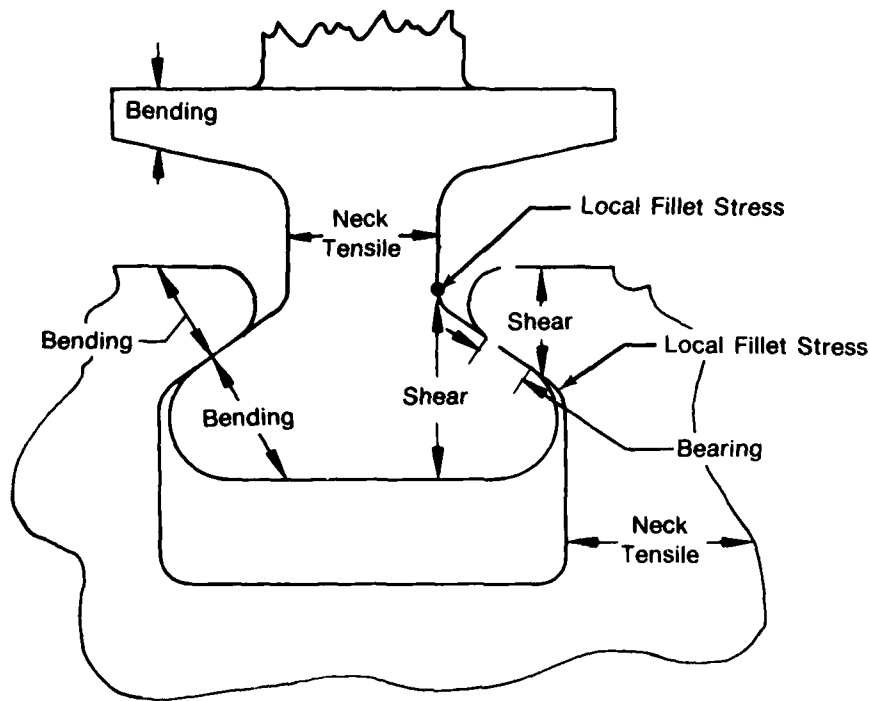
FD 167807

Figure 2-3. Blade/Disk Attachment Nomenclature and Optimization Parameters.

In Figure 2-4, the various design criteria are summarized. Tooth bearing, bending, and shear stresses are checked against allowable stresses at both operating speed and overspeed, as well as nominal neck tensile stress checks. Platform thickness is set by bending stress criteria. Fillet local maximum elastic stresses are estimated and low cycle fatigue life is compared with required life.

The Blade/Disk Attachment Synthesis program includes various stress concentration factors required for stress analyses. The stress concentration factor of primary importance in attachment design addresses the estimation of local maximum stress in the tooth fillet. This stress concentration factor (K_T) is a function of fillet radius (R), lug gage width (D), tooth bearing surface length (C), and tooth load distribution for multi-tooth attachments. The K_T values incorporated in the synthesis program were estimated with boundary integral equations. These equations produce stress values (and K_T 's) which are higher than actual stresses for coarse element size and approach actual stress values as element size is reduced. A

comparison of K_T estimated with boundary integral equations was made with K_T produced with finite element analysis (see Figure 2-5). The higher K_T value from the boundary integral equations will result in a bladed disk weight increase of approximately 1 percent. This is considered acceptable.



FD 167806

Figure 2-4. Blade/Disk Attachment Design Criteria Summary.

Figure 2-6 presents a schematic of the calculation procedure used by the Blade/Disk Attachment Synthesis program.

The calculations (see Figure 2-7) are repeated in a series of steps. In the first step, a "coarse grid" matrix of blade/disk attachment independent variable levels is constructed (the primary independent variables are fillet radius and rim width). After eliminating designs which are not feasible, values of gauge width and bearing surface length are determined for each design in the matrix which reduces calculated stresses to or below the stresses dictated by material properties. The optimum configuration selection is the last operation, with selection of the configuration with the minimum rim

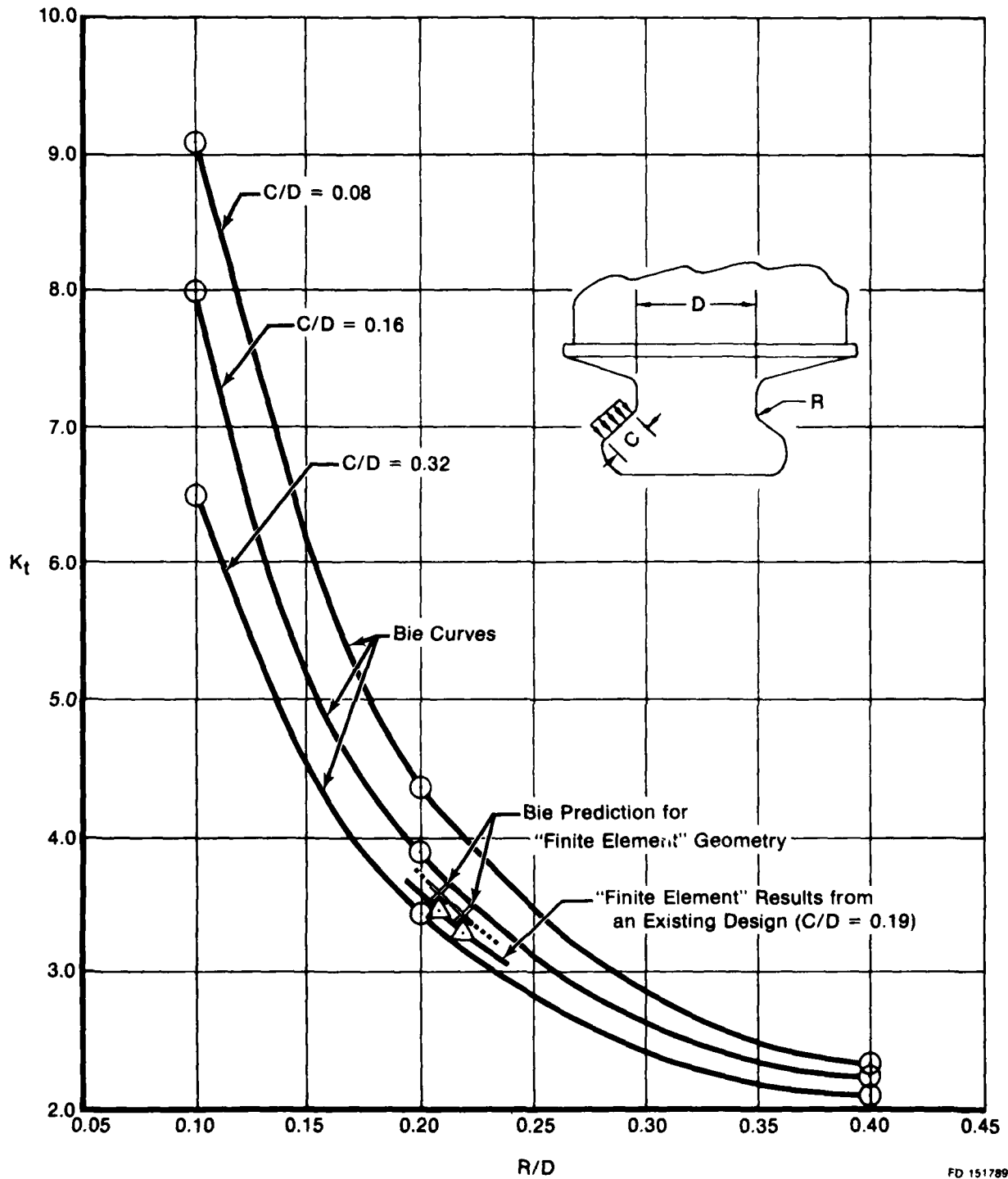
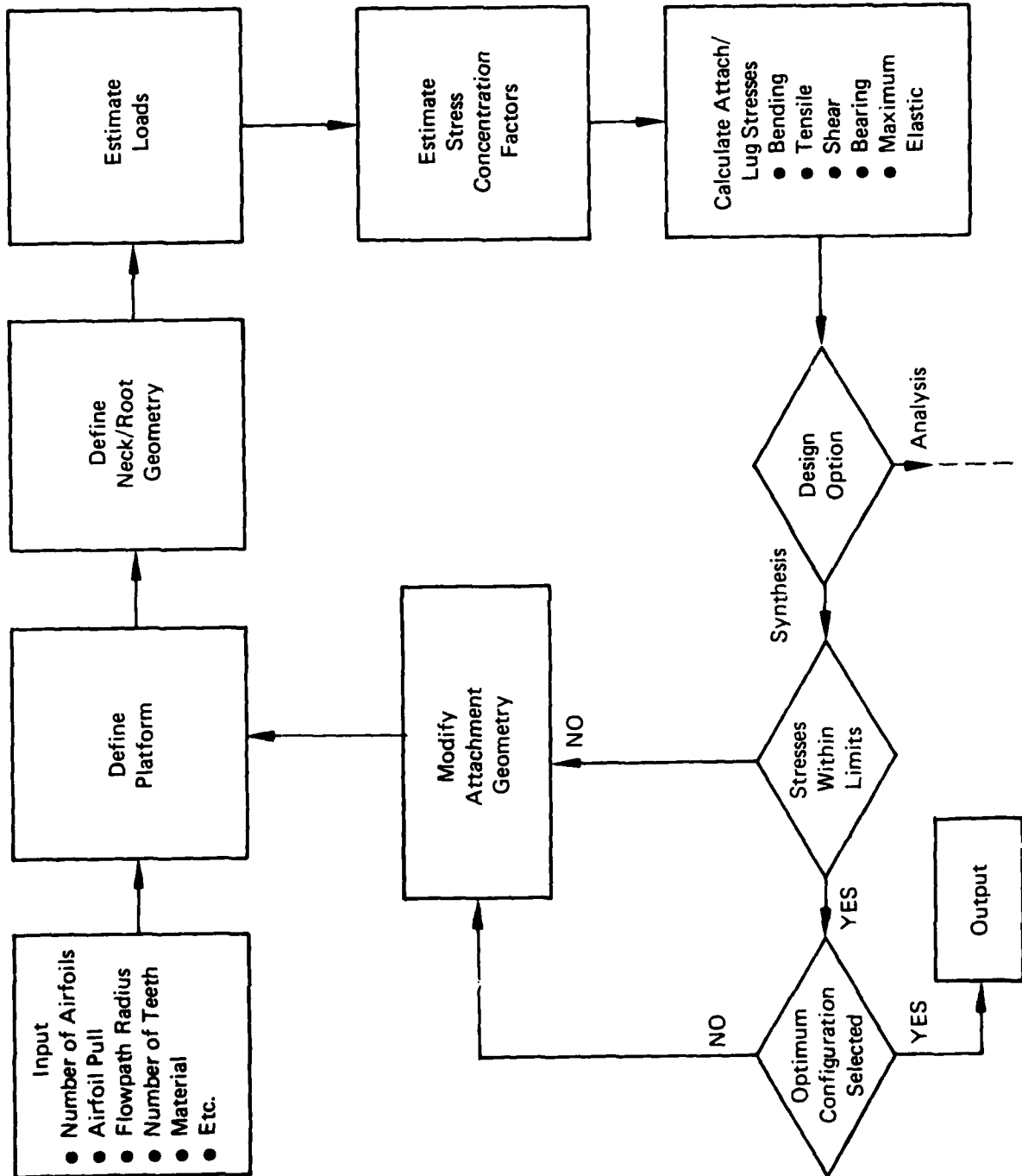


Figure 2-5. Comparison of Boundary Integral Equation and Finite Element Values for K_T vs R/D .



FD 167808

Figure 2-6. Blade/Disk Attachment Basic Flow Chart.

Step 1

		Gauge Width (GB)		
		0.4 in.	0.5 in.	0.6 in.
Fillet Radius (RCB)	0.12 in.	Rim Pull = 1.18×10^6 lb WRI = 0.973 in. LCE = 0.098 in.	1.094×10^6 lb 0.782 in. 0.123 in.	1.18×10^6 lb 0.924 in. 0.114 in.
	0.15 in.	1.34×10^6 lb 1.070 in. 0.096 in.	1.18×10^6 lb 0.804 in. 0.126 in.	1.42×10^6 lb 1.149 in. 0.105 in.
	0.18 in.	1.53×10^6 lb 1.189 in. 0.093 in.	1.38×10^6 lb 0.963 in. 0.116 in.	No Solution - Rim Width Exceeded Limit

Step 1 Attachment Definition

Step 2

		Gauge Width (GB)		
		0.45 in.	0.50 in.	0.55 in.
Fillet Radius (RCB)	0.12 in.	1.11×10^6 lb 0.829 in. 0.115 in.	1.09×10^6 lb 0.781 in. 0.123 in.	1.10×10^6 lb 0.795 in. 0.124 in.
	0.127 in.	1.14×10^6 lb 0.836 in. 0.115 in.	1.088×10^6 lb 0.735 in. 0.131 in.	1.13×10^6 lb 0.812 in. 0.123 in.
	0.135 in.	1.17×10^6 lb 0.853 in. 0.115 in.	1.11×10^6 lb 0.750 in. 0.130 in.	1.18×10^6 lb 0.853 in. 0.120 in.

Step 2 Attachment Definition

Note: Stresses Are Within Specified Limits for All Seventeen Designs Shown

FD 167809

Figure 2-7. Single Tooth Attachment Synthesis Solution.

pull (or disk dead load). The subsequent steps are merely repeats of the first step, with the exception that the fineness of the grid of independent variable levels is increased in each step. The program terminates when the minimum rim pull in step (N) is within the tolerance of the minimum rim pull in step (N-1).

Figure 2-8 illustrates the step 1 and step 2 stresses for the sample single tooth blade/disk attachment (note that the rim pull in step 2 is within 1/2 percent of the step 1 rim pull). The stresses which are limiting are denoted by boxes, and the stresses shown are for the minimum rim pull designs of steps 1 and 2.

The boron aluminum composite fan configuration created a unique problem in the blade/disk attachment area, since an established design system does not exist for this component configuration. The design limitations and failure modes for overspeed, low cycle fatigue, and creep are not as well understood as they are for existing metal blade designs. The composite fan blade failure modes are also different from metal blades, i.e., fiber breakage, interlaminar shear, and creep untwist. These differences are shown in Figure 2-9.

As a result, two approaches were considered for generating size and weight estimates of the composite boron aluminum blade attachment. Both of these approaches use the F100-PW-100 composite blade design developed under Contract F33615-76-C-5318 as a baseline for determining other attachment designs.

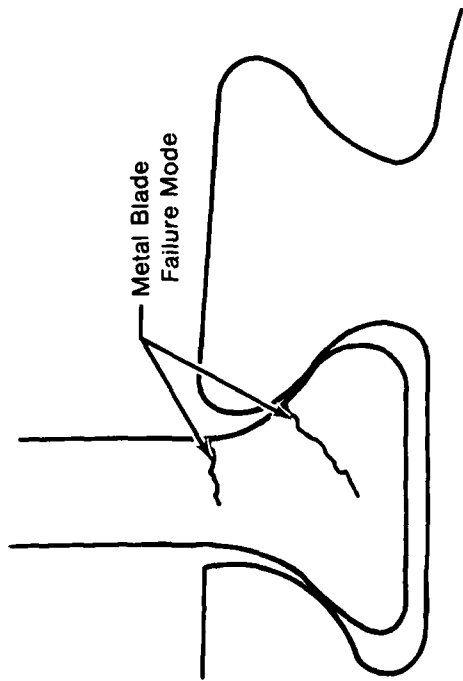
In approach 1, the attachment is synthesized using the metal blade synthesis program. Empiricized material properties that duplicate the F100 attachment dimensions and weight would be developed. The shape of the material properties used in the various designs would be based on calculations and engineering judgement. Since this approach implies more knowledge than is available about composite blade attachment design, approach 2 was selected.

	Step 1	Step 2
Disk Neck Tensile Stress, ksi	58.2	58.3
Blade Neck Tensile Stress, ksi	60.4	59.7
Tooth Bearing Stress, ksi	124.4	124.4
Tooth Bending Stress, ksi	1.95	2.24
Tooth Shear Stress, ksi	36.7	36.7
Blade Fillet Maximum Local Stress, ksi	133.6	133.8
Disk Fillet Maximum Local Stress, ksi	206.3	204.0

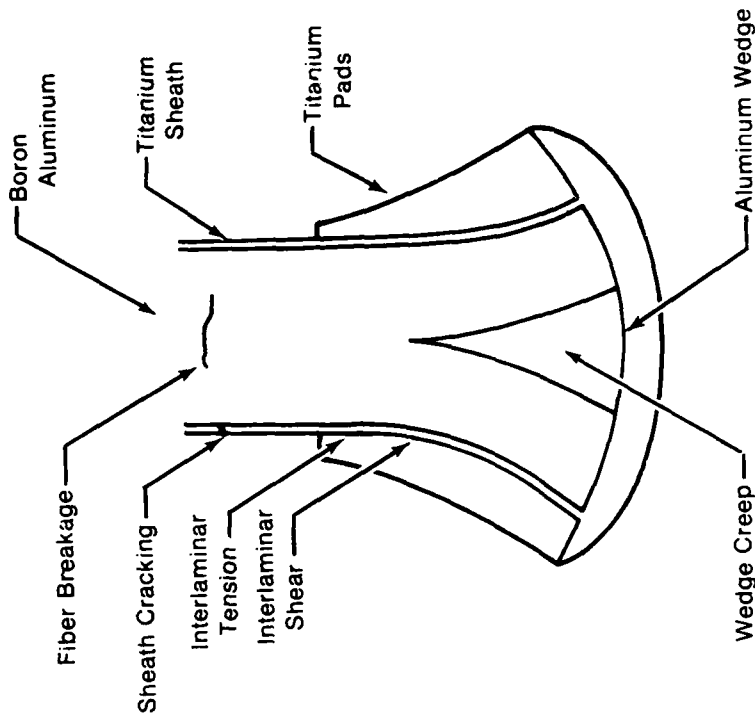
Note: Box Denotes Stresses at Specified Limits (± 1 Percent of Allowable), All Other Stresses Shown Are Below Limits

FD 167810

Figure 2-8. Blade/Disk Attachment Stresses.



Metal Blade



Composite Blade

FD 176051

Figure 2-9. Metal and Composite Fan Blade Attachment Failure Modes.

Approach 2 provides no life prediction capability. The approach is comprised of the following operations:

- o The airfoil is sized by aerodynamic considerations
- o The airfoil weight is estimated, and the weight is used in establishing the attachment weight and pull, by ratioing from the F100 blade design
- o The disk rim, web, and bore are then sized for minimum weight based on life and burst requirements.

The two approaches are shown in Figure 2-10.

The equations for total rim pull per blade, live rim diameter, and dead rim weight per blade are shown below:

PR = total rim pull/blade, pounds

LRD = live rim diameter, inches

WDR = Weight of blade/disk attachment per blade, pounds
(includes platform, but not airfoil)

RPM = Spool speed, revolutions/minute

N = number of airfoils

P_{af} = airfoil pull/blade, pounds

BC = axial blade chord, inches

GPD = flowpath inside diameter, inches

FPOD = flowpath outside diameter, inches

$$PR = 2.635 \times 10^{-10} \frac{(P_{af})(GPD)^2(RPM)^2}{N} + 1.775 \times 10^{-6} \frac{(BC)(GPD)^2(RPM)^2}{N} + P_{af}$$

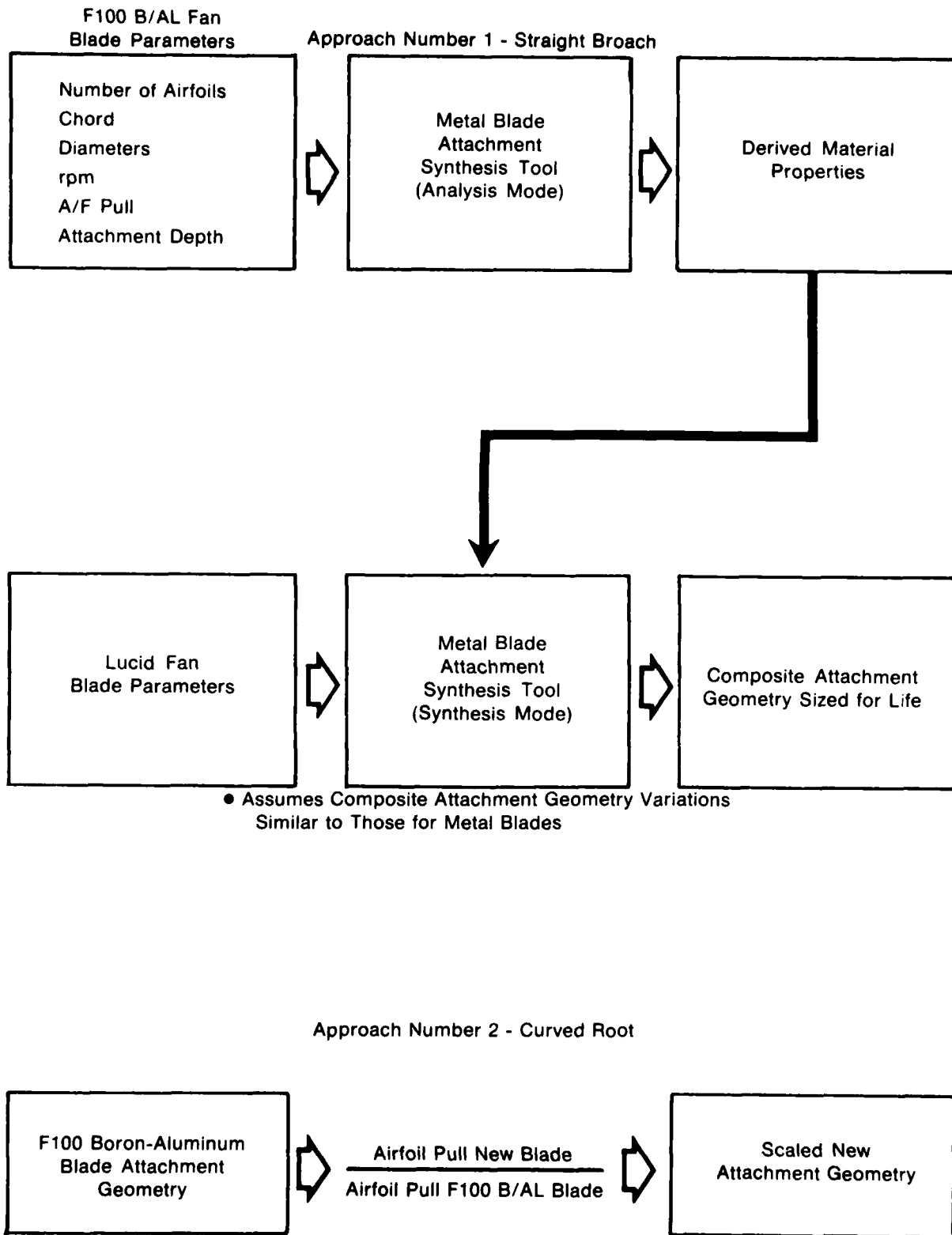


Figure 2-10. Composite Fan Blade Attachment.

FD 176052

$$\text{LRD} = \text{GPD} - 1.738 \times 10^{-4} \frac{P_{af}}{BC}$$

$$\text{WDR} = \frac{(70471)(PR - P_{af})}{(\text{LRD} + 0.444)(\text{GPD} - \text{LRD})(\text{RPM})^2}$$

2.1.2 Live Disk Synthesis

An existing computer program is used for synthesis of symmetric disks to provide preliminary disk profiles. It uses prescribed average tangential stress and radial stress patterns. The radial stress varies from zero at the bore to a value that will preclude failure through bolt holes to a value that will fair into a rim geometry generated by the Blade/Disk Attachment Synthesis Program. A maximum allowable radial stress is also prescribed.

The program generates the disk shape in two steps. The first step generates the tangential stresses by numerical integration of the solution of the compatibility equation using the prescribed stresses as shown by equation (1).

$$\frac{\sigma_t}{E} = \frac{1}{X^{(1+\mu)}} \left\{ \int_{X_1}^X \left[\frac{\sigma_r}{XE} (1+\mu) + \frac{d}{dX} \left(\mu \frac{\sigma_r}{E} \right) - \frac{d}{dX} (\alpha \Delta T) \right] X^{(1+\mu)} dX \right\} + \frac{\sigma_{ti}}{E_i} \left(\frac{X_i}{X} \right)^{(1+\mu)} \quad (1)$$

The disk profile is then determined by numerical integration of the solution of the equilibrium equation as shown by equation (2)

$$\log_e \left(\frac{y}{y_1} \right) = \int_{X_i}^X \left[\frac{\sigma_t - \sigma_r}{X} - \frac{d\sigma_r}{dX} - \rho \omega^2 X \right] \frac{dX}{\sigma_r} \quad (2)$$

where:

σ_t	= tangential stress	ω	= angular velocity
σ_r	= radial stress	E	= modulus of elasticity
μ	= Poisson's ratio	X	= radius
α	= coefficient of expansion	y	= axial thickness
T	= temperature change	i	= initial value subscript
ρ	= mass density		

The program can analyze for stresses at locations where geometry is specified and synthesize geometry where it is not given.

Input required includes:

- o Disk live rim load
- o Live rim geometry (width and height)
- o Rotor speed
- o Bore radius
- o Allowable average tangential stress for burst calculation
- o Maximum allowable radial stress in web disk metal thermal gradient.

The present program synthesizes bore and web widths by selecting values for the widths and iterating solutions of the equations until a minimum disk weight is achieved without exceeding input stress limits and geometry constraints.

The program has been modified as follows:

- o To calculate bore radius as a percentage of flowpath ID (based on experience and/or rotor dynamics requirements)
- o To vary live rim width
- o To set minimum rim width necessary for blade vibration control (based on experience for given solidity and aspect ratio)
- o To omit average tangential stress and web radial stress from the input.

These changes are necessary for the program to be used with the limited input data available during preliminary engine design. The output from the modified program includes:

- o Disk average tangential stress
- o Disk weight
- o Bore, bolt circle, web and rim radial, and tangential stresses.

An example of the Live-Disk Synthesis program iterative steps executed in arriving at a disk synthesis solution are shown in figures 2-11 through 2-16. The bore, bolt circle and rim diameter and rim width were held constant. Bore, bolt circle and web width were optimized for maximum speed conditions.

Synthesis was started with a bore width assumed to be 1.000 in. Figure 2-11 shows the synthesized values for bolt hole and web widths. The web width of 0.060 in. is a minimum machining limit which indicates low web stress.

The program then reduced bore width and increased bolt circle width as shown in figure 2-12. Web stresses were still low, as indicated by the machining limited width.

The program further reduced bore width while maintaining bolt circle width of 0.241 in., indicating that bolt circle stress was adequately high, as shown in figure 2-13.

In figure 2-14, bore and web widths were increased. This indicates that stresses were excessive in these locations for the dimensions in figure 2-13.

Bore width was again reduced, as shown in figure 2-15, indicating bore stress was low in figure 2-14. The bolt circle and web widths were unchanged, indicating adequately high stresses in those areas.

The final geometry is shown in figure 2-16. The bore width was increased, indicating high bore stress in figure 2-15. The program stops when tangential, radial and effective stresses in selected locations are within the selected tolerance of the maximum allowable values.

Figure 2-17 summarizes results of the Live Disk Synthesis program. Disk geometry comparisons show excellent agreement, with the exception of bore width; the synthesized disk weight is 7.65 lb, which is 17% lower than the actual F100 tenth stage disk. The synthesized disk was sized for criteria of: burst/overspeed with radial temperature gradient, bore tangential stress, and bolt circle and web radial stresses. However, the disk was not sized to bore low cycle fatigue life, since low cycle fatigue and fracture mechanics material property data were not available to the synthesis program. Were this data available, the bore would be thicker, thus a heavier disk would result.

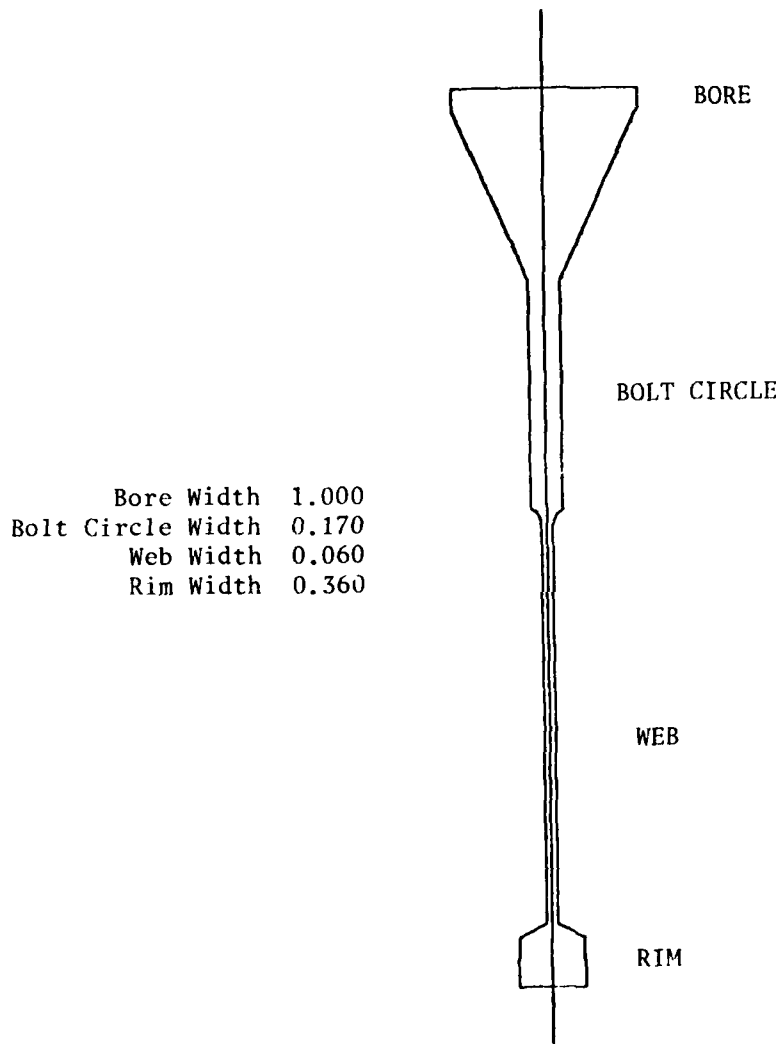


Figure 2-11. Initial Geometry From Synthesis of a Compressor Disk.

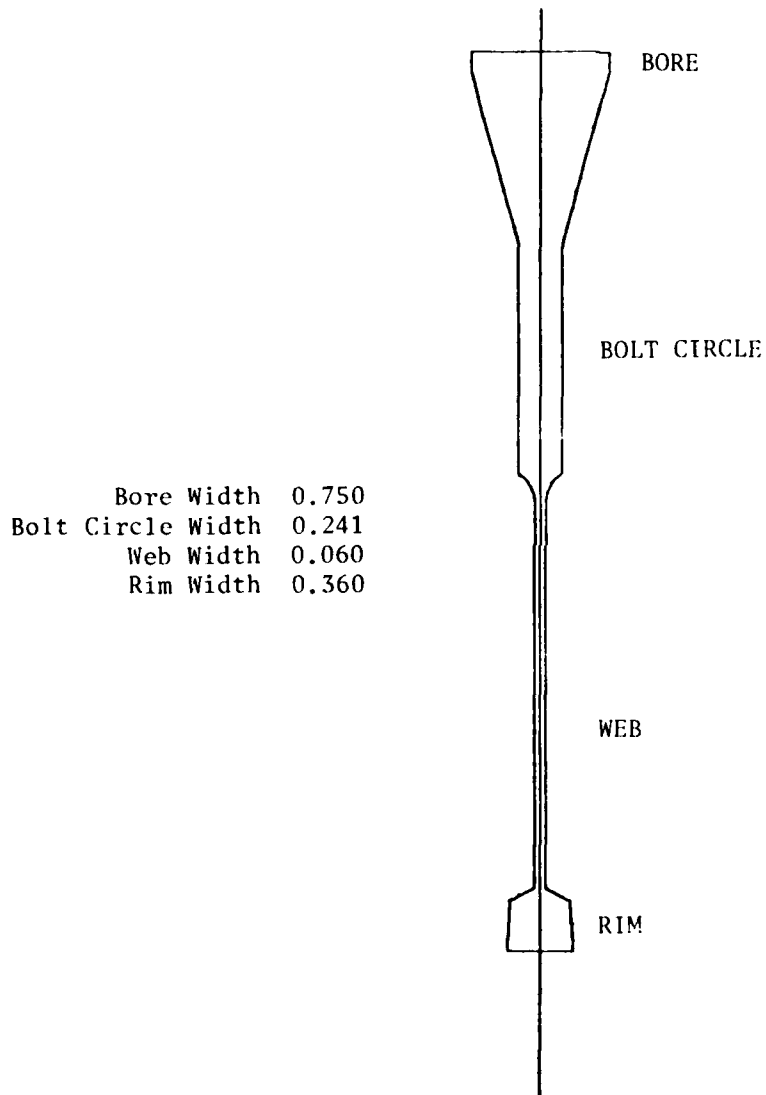


Figure 2-12. First Iteration Geometry From Synthesis of a Compressor Disk.

Bore Width 0.500
Bolt Circle Width 0.241
Web Width 0.060
Rim Width 0.360

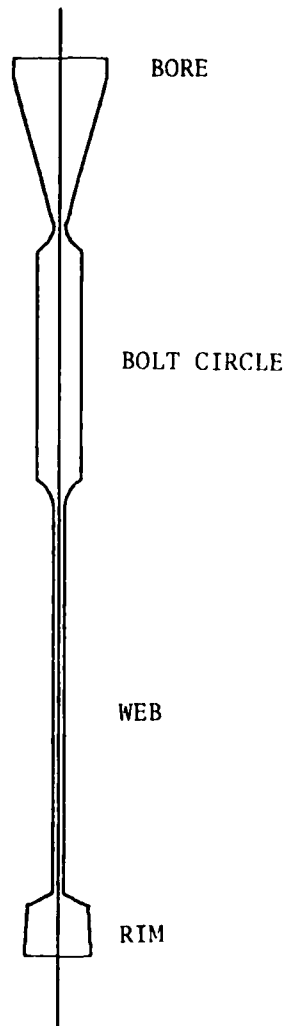


Figure 2-13. Second Iteration Geometry From Synthesis of a Compressor Disk.

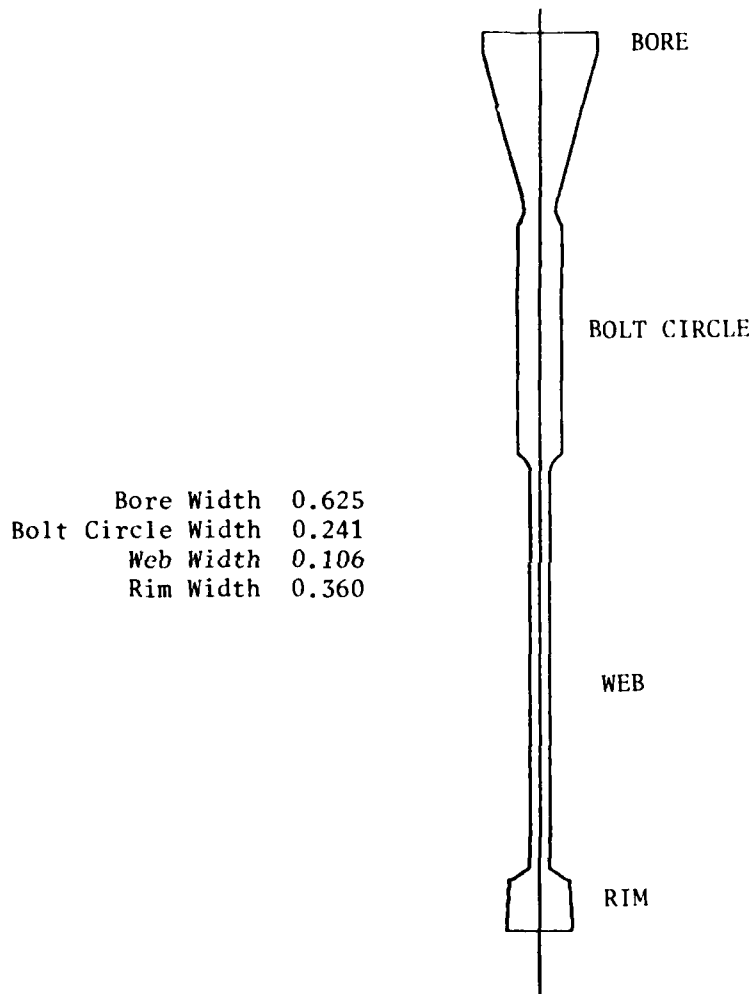


Figure 2-14. Third Iteration Geometry From Synthesis of a Compressor Disk.

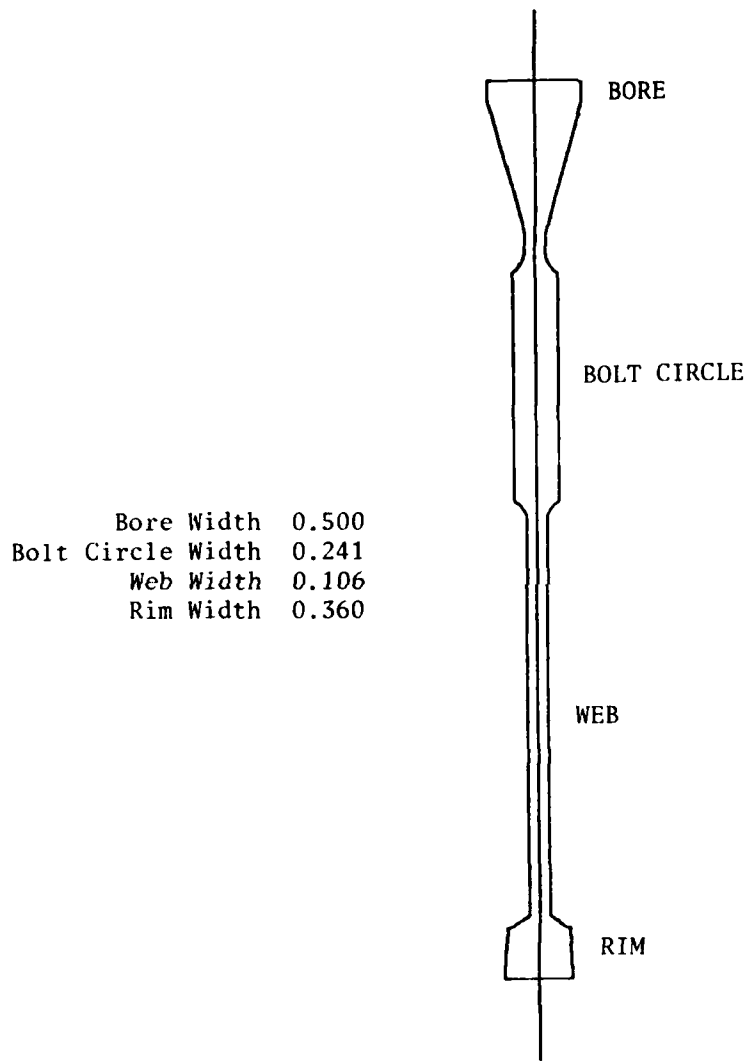


Figure 2-15. Fourth Iteration Geometry From Synthesis of a Compressor Disk.

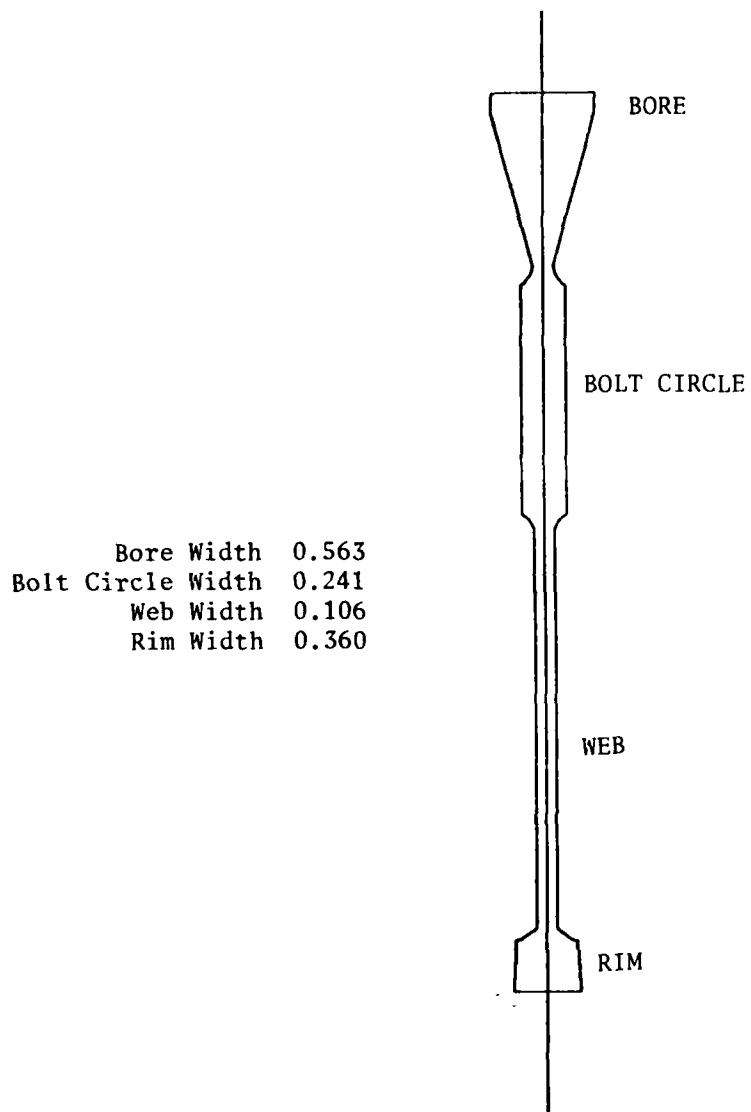
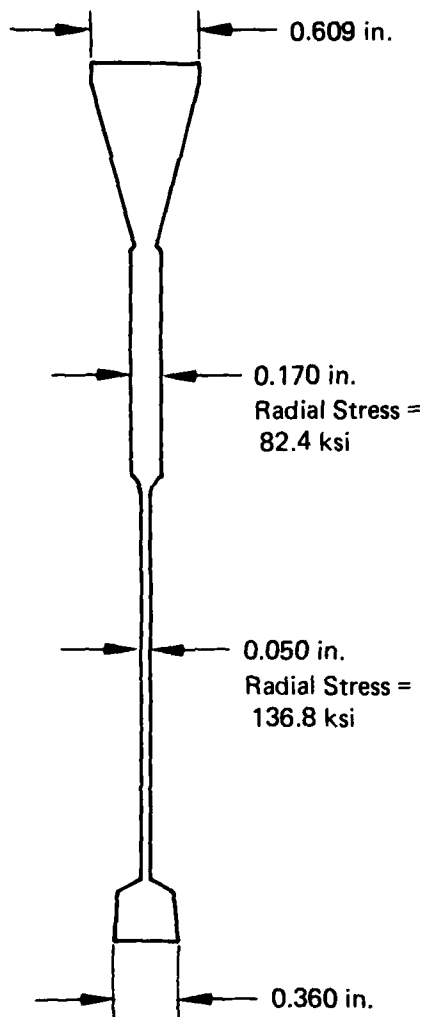
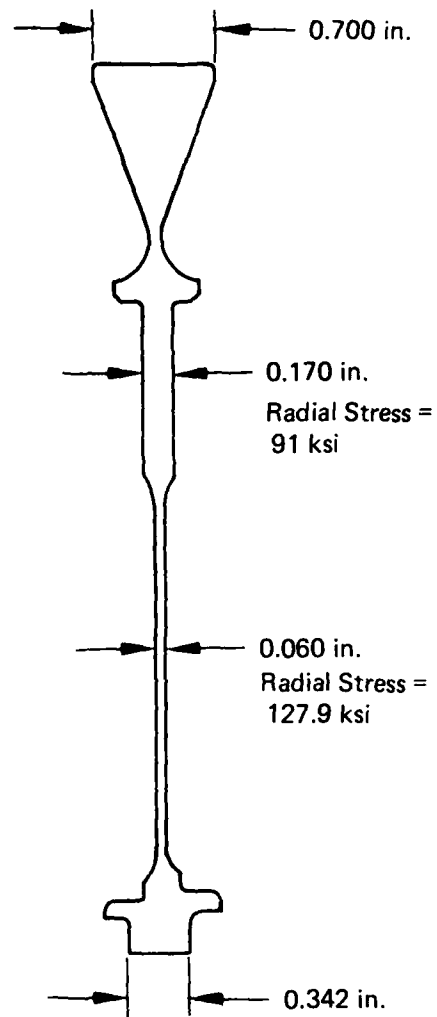


Figure 2-16. Final Iteration Geometry From Synthesis of a Compressor Disk.



Synthesized Disk

Rim Pull 163,900 lb
Disk Weight 7.650 lb
Average Tangential Stress 84.7 ksi



F100 Tenth Stage
Compressor Disk

Rim Pull 163,900 lb
Disk Weight 9.179 lb
Average Tangential Stress 81.7 ksi

FD 167811

Figure 2-17. Verification of the Disk Synthesis Program.

2.1.3 Disk Radial Thermal Gradient Program

A program was developed to predict the radial temperature gradients that occur in rear stage compressor disks and turbine disks during transient engine operation. A lumped mass thermal analysis was programmed accounting for mission requirements, engine operating conditions, and disk geometry. Empirical relations were developed as a function of general mechanical arrangement to account for conductive and convective heat transfer. These empirical relationships were established based on previous engine experience (including TF30-P-100 and F100-PW-100) and preliminary designs of advanced engines. The combination of empirical relations and lumped mass analysis in the program provide a time history of the radial temperature distribution of the disk from the time the transient is initiated until disk temperatures are stabilized. From this temperature-time history, the maximum temperature gradient is determined and used in the LPWT, modifying disk matrix output stresses.

2.1.3.1 Compressor For temperature level prediction, a six node model is used to describe heat transfer on a bleed stage compressor disk. There is one node each for the rim, web and bore and three fluid nodes, as shown in figure 2-18. Film coefficients and boundary temperatures are determined by main gas path pressures and temperatures which will be obtained from the engine performance computer simulation, the flowpath generation program, and mission input. Using the method of finite differences, a transient thermal analysis is performed. Five simultaneous equations are solved via matrix algebra techniques (the first fluid node pressure and temperature are constant at the bore air source condition).

Compressor disk radial thermal gradient program checkout is summarized in figures 2-19 through 2-21.

Figures 2-19 and 2-20 illustrate acceleration results of the 3-node routine, compared to a detailed 23-node model for representative compressor disks. The third disk rim-to-bore maximum gradient comparison of the models is not as good as the fifth stage.

Three-node model adjustments which give better maximum gradient values were explored, but results indicated these adjustments also result in more temperature prediction error at start and end conditions. Figure 2-21 presents deceleration disk temperature prediction comparison of the two models, and shows excellent agreement.

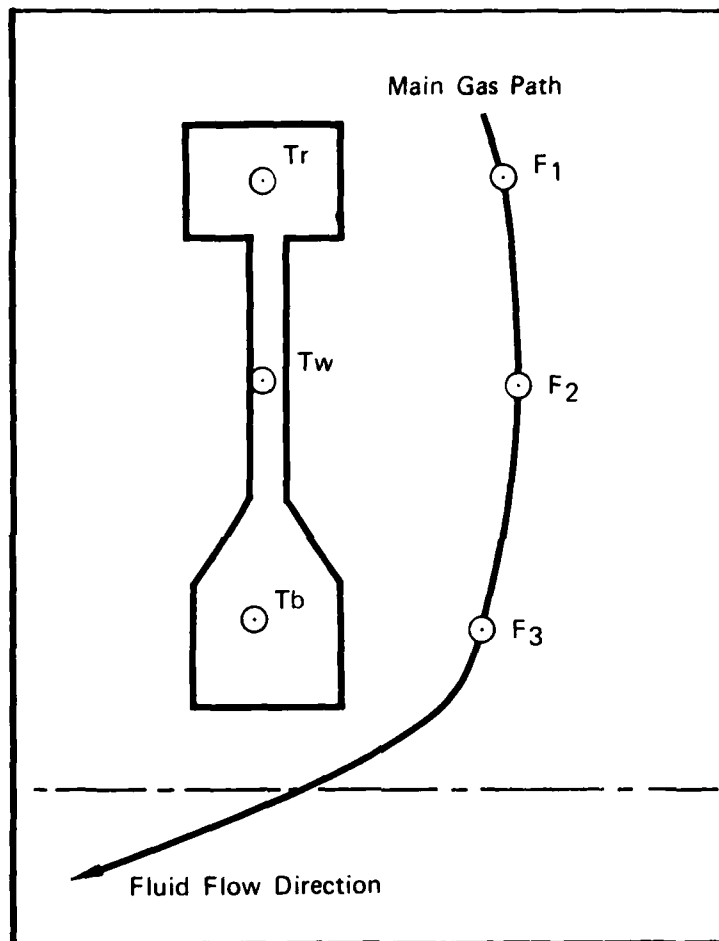
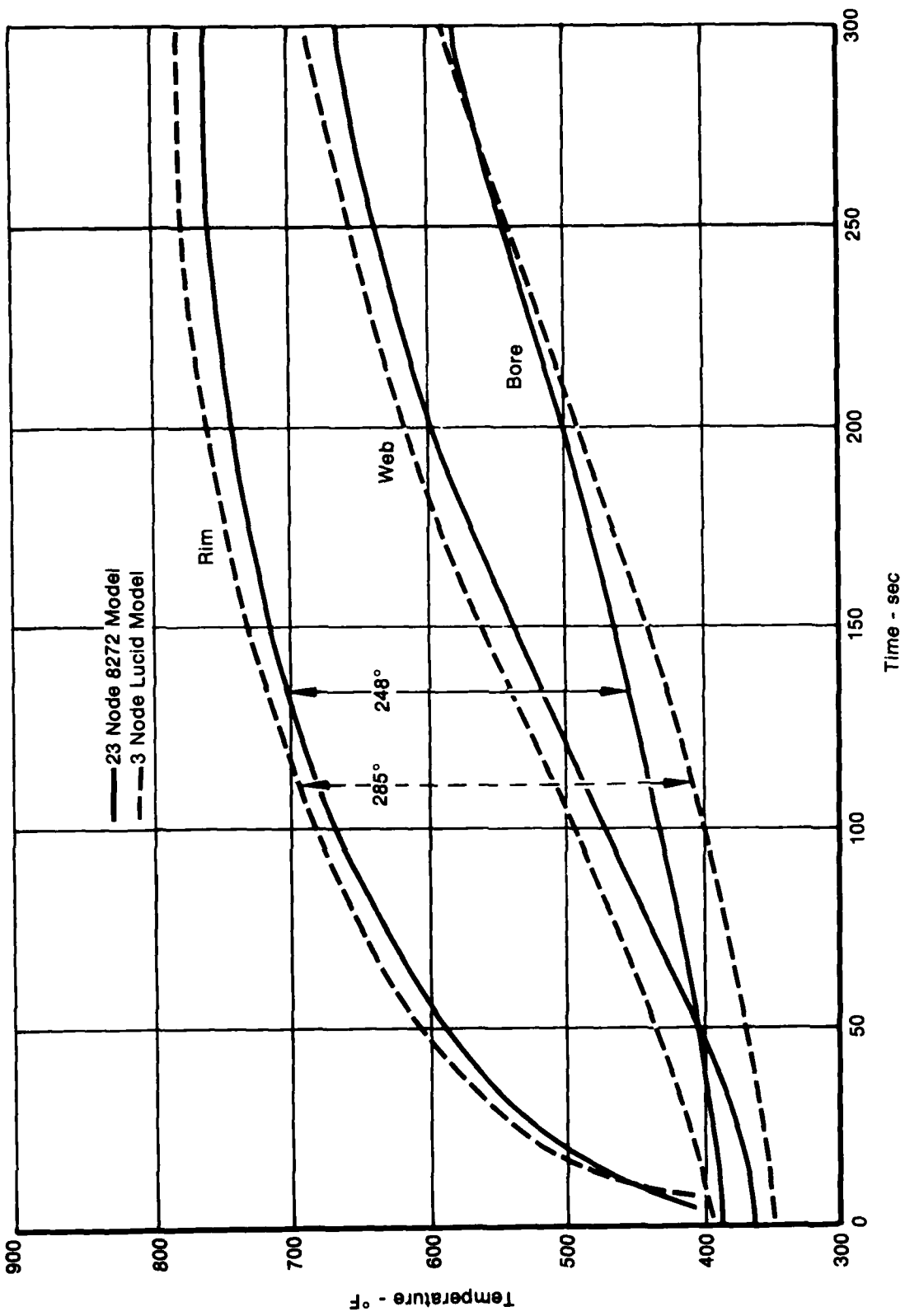
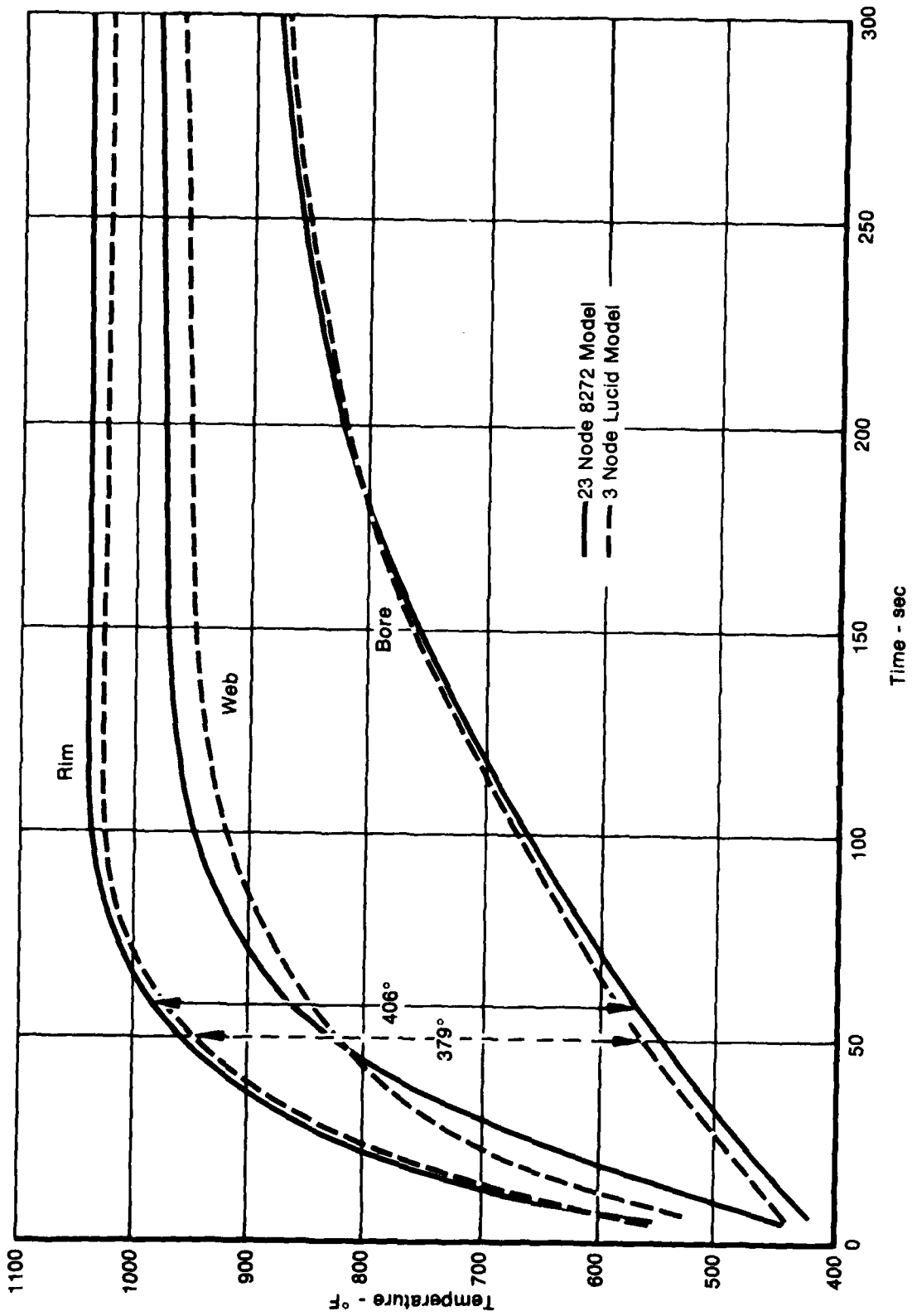


Figure 2-18. Six Node Heat Transfer Model.



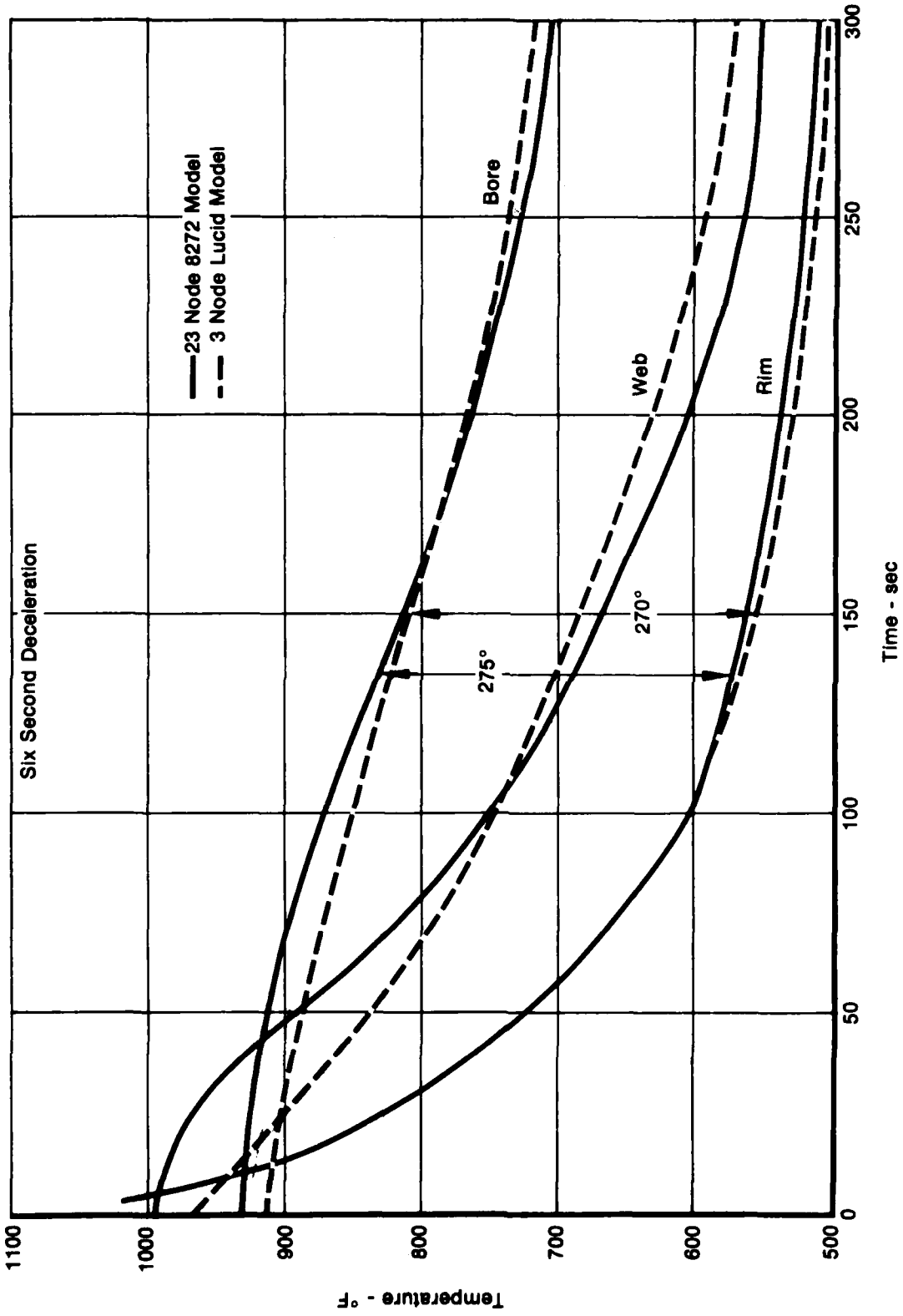
FD 170084

Figure 2-19. Compressor Disk Radial Thermal Gradient, 3rd Disk (Non-Bleed Stage) 6 Second Acceleration.



FD 176085

Figure 2-20. Compressor Disk Radial Thermal Gradient, 5th Disk (Bleed Stage) 6 Second Acceleration.



FD 170006

Figure 2-21. Compressor Disk Radial Thermal Gradient, 5th Disk (Bleed Stage) 6 Second Deceleration.

2.1.3.2 Turbine The estimation of the turbine disk radial thermal gradient is accomplished with an analysis similar to that of the compressor disk analysis, i.e., a rim-web-bore temperature prediction program to predict temperature levels and a curve fit program which matches the radial thermal gradient to the rim, web, and bore average temperatures. While compressor disk gradients are of uncomplicated shape, several factors complicate the turbine disk gradient shape: turbine on-board injection (TOBI) of blade cooling air, the rotating disk adjacent to static structure pumps air radially outward along the disk, and the windage work is converted to friction heating of the disk, and platform and blade attachment cooling and heating effects in the rim and the blade root areas. Typical acceleration and deceleration turbine disk radial thermal gradients are shown in figure 2-22. The effect of TOBI in heating and cooling the disk rim during the acceleration and deceleration transients is evident.

Figures 2-23 and 2-24 present comparisons of acceleration and deceleration temperature gradients of the LUCID program-generated 7-node model and the existing 230-node model detailed thermal analysis. The figures show excellent agreement of the two models in terms of both gradient shape and level as a function of time. As the Disk Radial Thermal Gradient Program was developed, it became apparent that adequate modelling of the rim temperature transient required inclusion of the heat transfer path from the blade root to the disk rim via the disk lug. It is noted that, while temperature levels of the two models are shown to be as much as twenty degrees apart, it is the shape (ΔT bore-to-web and ΔT bore-to-rim) that is important. The simplified model duplicates results of the detailed model very well.

2.1.4 Turbine Airfoil Life Prediction

2.1.4.1 Preliminary Design System A preliminary design system exists with the capability of determining turbine airfoil cooling airflows. The cooling airflows are calculated for steady-state (oxidation/erosion and stress-rupture) mission life requirements. The system has been linked with an engine-performance computer deck with

excellent results, substantially reducing the iterations between the performance and airfoil-durability disciplines. Modification of the system entails the addition of low cycle fatigue (LCF) life prediction analysis to the existing oxidation/erosion and stress-rupture failure modes.

2.1.4.2 Failure Modes Turbine airfoil failure modes can be classified as steady-state or cyclic.

Airfoil life-limiting failure modes at steady-state operation are oxidation/erosion or stress-rupture. Accumulation of creep damage causes a stress-rupture failure. All cooled and uncooled blades are evaluated for stress-rupture failure. An oxidation/erosion failure is caused by depleting the airfoil coating and base metal. All cooled and uncooled airfoils are also evaluated for oxidation/erosion failure. Experience indicates that the principal failure mode for turbine vanes is either oxidation/erosion or cyclic failure.

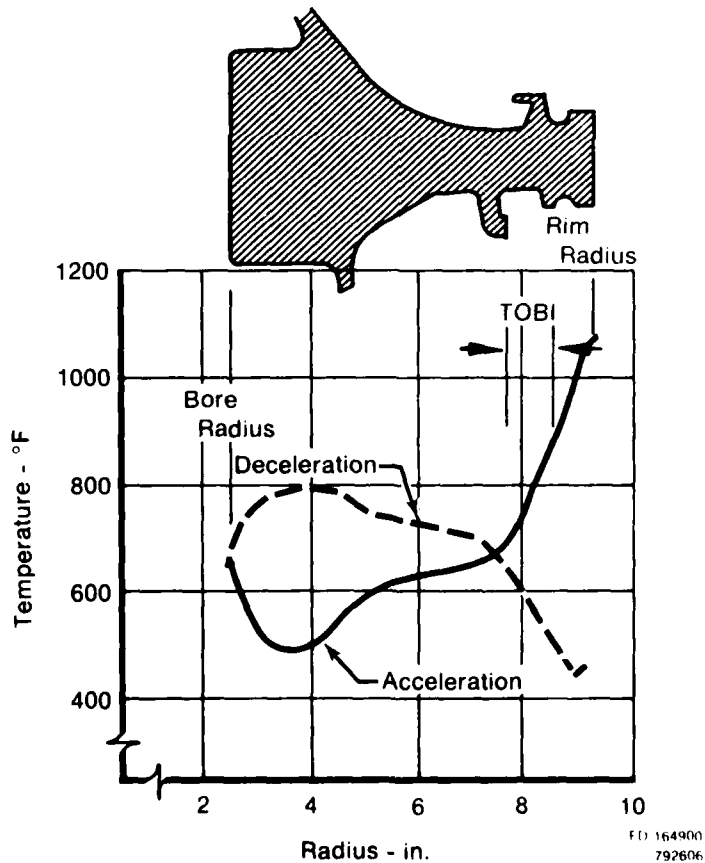
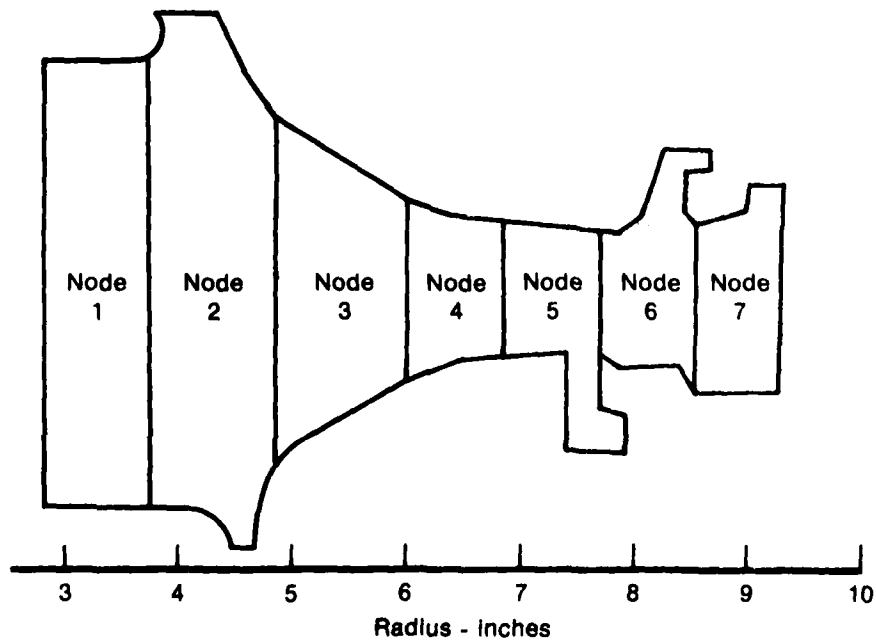
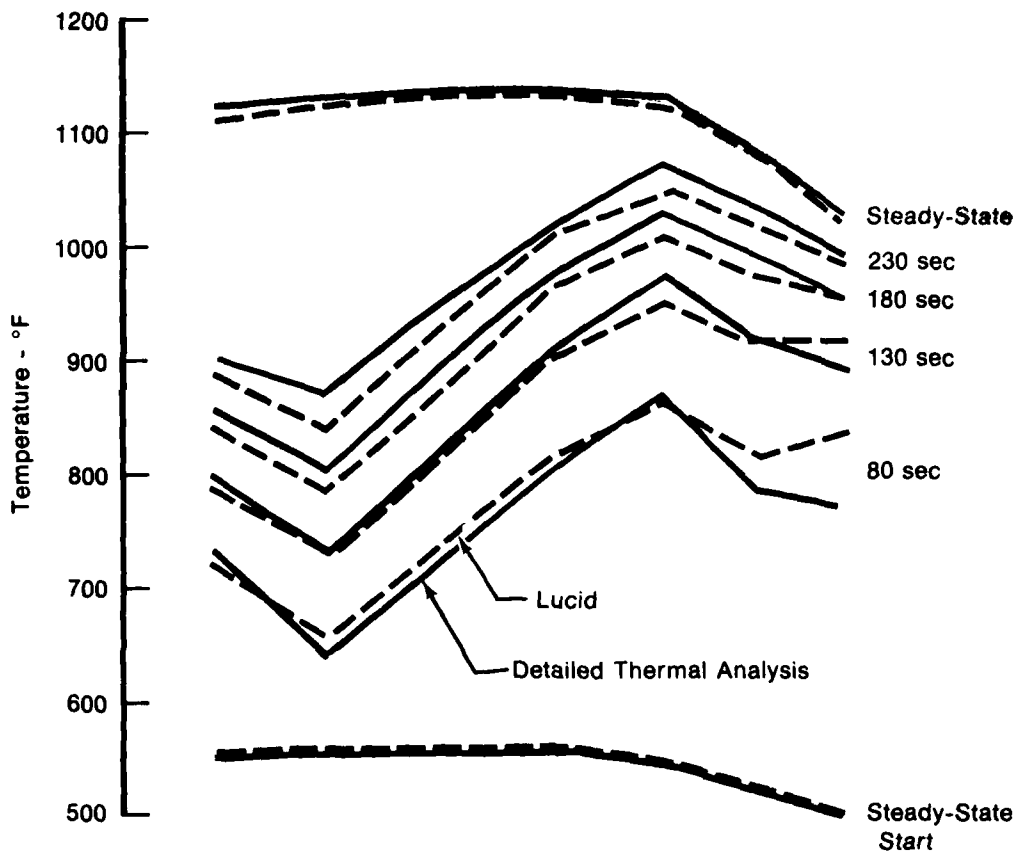
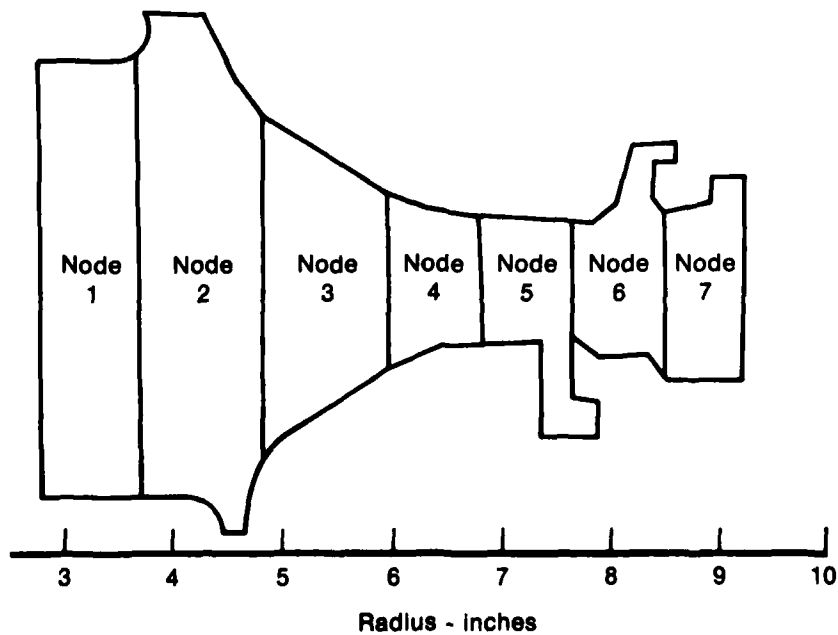
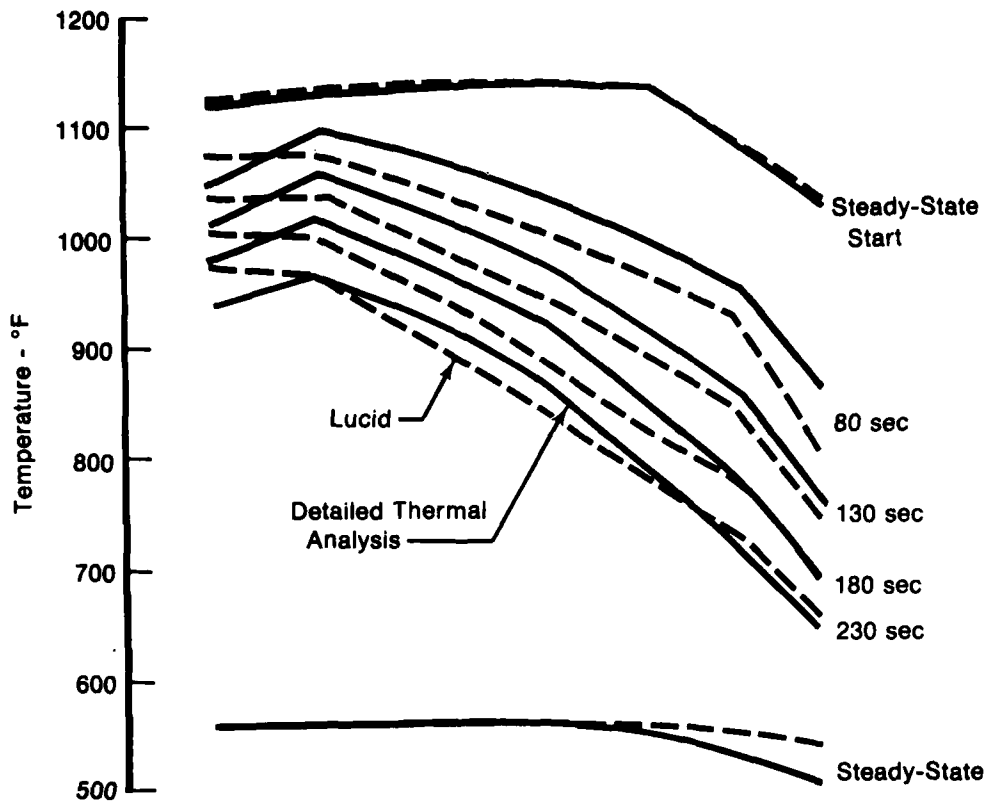


Figure 2-22. Typical Turbine Disk Thermal Gradients.



FD 184169

Figure 2-23. Comparison of Turbine Disk Radial Thermal Gradient Models For Acceleration Transient.



FD 184170

Figure 2-24. Comparison of Turbine Disk Radial Thermal Gradient Models For Deceleration Transient.

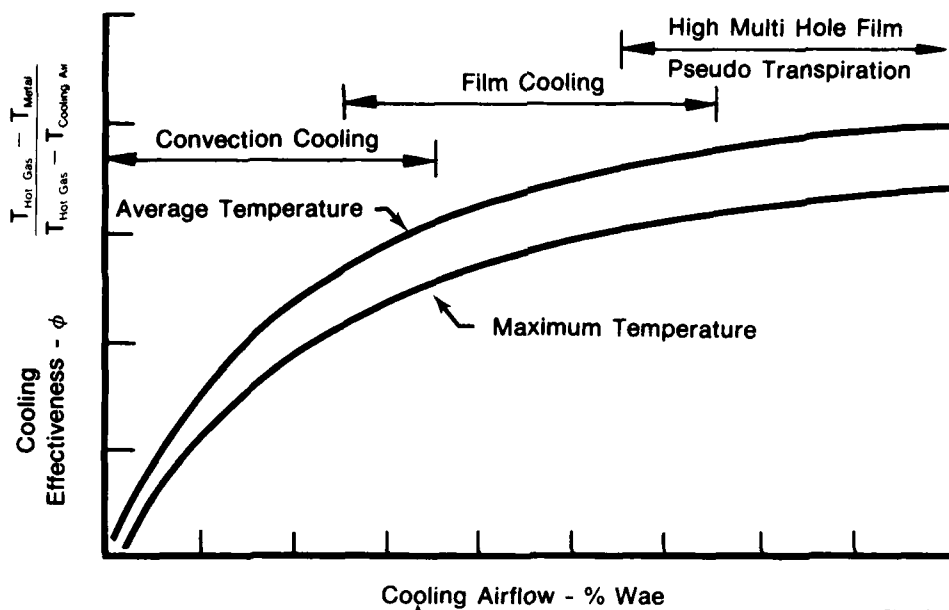
The cyclic failure mechanism is LCF and high cycle fatigue (HCF). HCF failure is caused by a combination of steady and vibratory stresses. This failure mode is not evaluated in preliminary design, since in the detailed design process, each airfoil is designed to ensure that HCF is not a life-limiting failure mode.

LCF failure is the result of rapid engine accelerations and decelerations that produce centrifugal and thermal distortions of the airfoil metal which induce large cyclic strains. Accumulation of creep strain also reduces the airfoil material cyclic strain capability, causing a creep-fatigue interaction failure mechanism. In preliminary design, only cooled airfoils are evaluated for LCF. Commercial and military engine experience indicates that fatigue of uncooled low-pressure turbine airfoils is not the life-limiting failure mode. LCF lives of cooled turbine blades are evaluated on the basis of creep-fatigue interaction. Cyclic lives of cooled turbine vanes are evaluated on the basis of fatigue only (no creep caused by centrifugal loads).

2.1.4.3 Airfoil Metal Temperatures Airfoil metal temperature estimates are required for the evaluation of oxidation/erosion, stress-rupture, and LCF lives.

Predictions of engine performance at all operating flight conditions, with initially estimated cooling flows, provide cooling-air temperatures, combustor exit temperatures, high- and low-pressure turbine exit temperatures, as well as the high- and low-rotor speeds. Average vane and blade inlet temperatures at each stage are calculated on the basis of the temperature drop through the turbine. The average vane inlet gas temperature is modified to obtain hot-spot gas temperature using the burner pattern factor and attenuation based upon experience. Average blade inlet temperatures are modified to include the burner temperature profile also attenuated by experience.

Airfoil metal temperature calculations are based on a design experience curve, such as that shown in figure 2-25, which has cooling effectiveness plotted against cooling airflow. With an initial estimate of cooling airflow and definition of gas and coolant temperatures, maximum and average section metal temperatures are calculated.



FD 140192

Figure 2-25. Turbine Airfoil Cooling Effectiveness.

2.1.4.4 Critical Blade Section Stress Blade stress predictions for preliminary stress-rupture and LCF considerations are based on design experience. As shown in figure 2-26, the blade stress at critical sections has been correlated to the flowpath annulus area and rotational speed. For a given value of annulus area times the rotational speed squared, there can be pull stress variations of +20%. These variations are a function of the metal area taper from tip to root for each design. A nominal taper is used for preliminary design evaluation.

The critical section for creep and fatigue of cooled blades is located near midspan. Burner dilution and cooling air reduce the endwall temperatures and cause the worst combination of temperature and stress to occur at midspan. Airfoil average metal temperatures transformed into allowable blade stresses for constant stress-rupture life indicate the least pull stress margin near midspan (i.e., the critical section), as shown in figure 2-27.

The critical section for uncooled low-pressure turbine blades is near 25% span. Gas temperature profiles in the low-pressure turbine are reduced due to attenuation. The relationship of the allowable to the actual stress levels for uncooled low-pressure turbine blades is shown in figure 2-28.

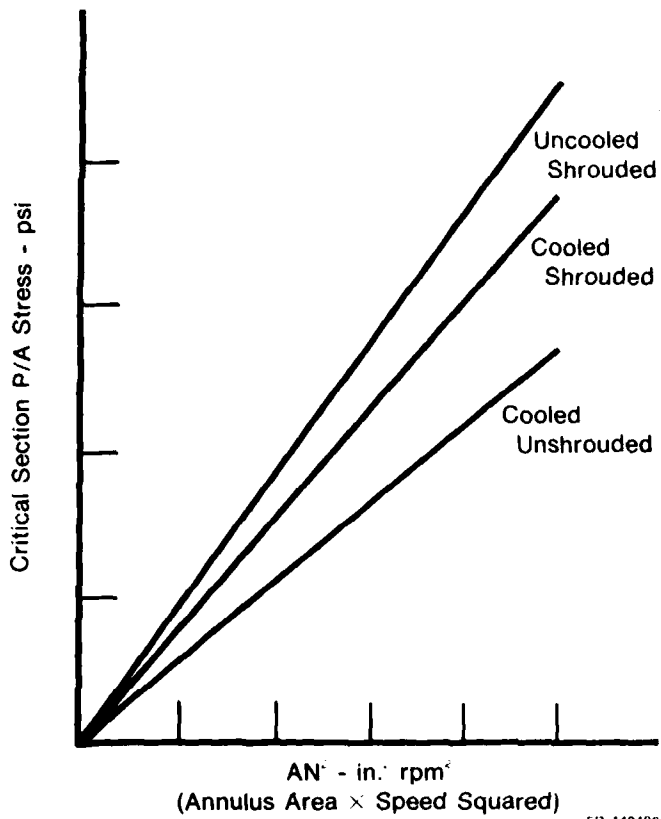


Figure 2-26. Centrifugal Stress (P/A) Blade Design Experience.

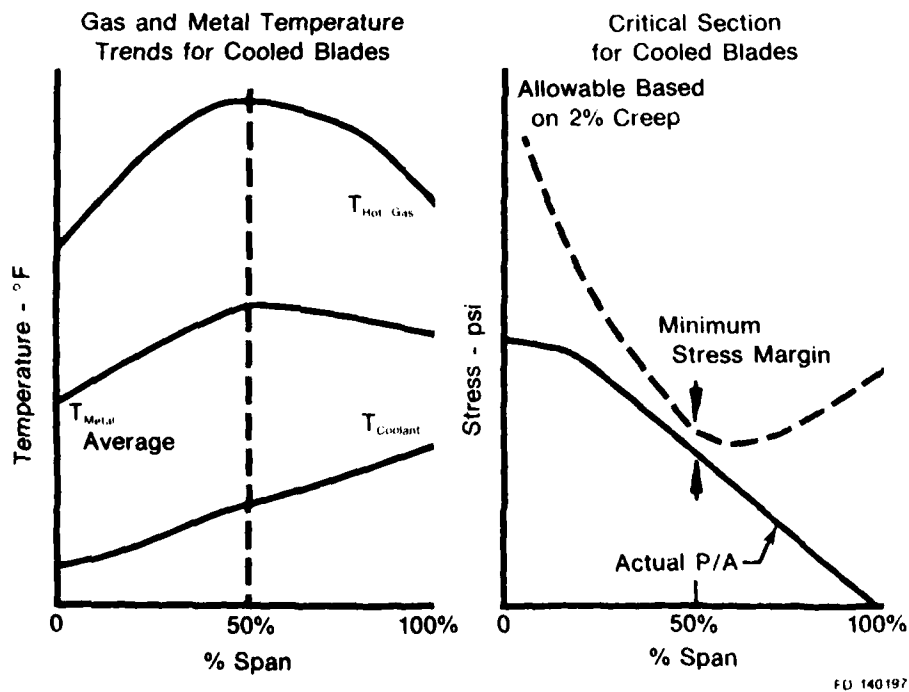
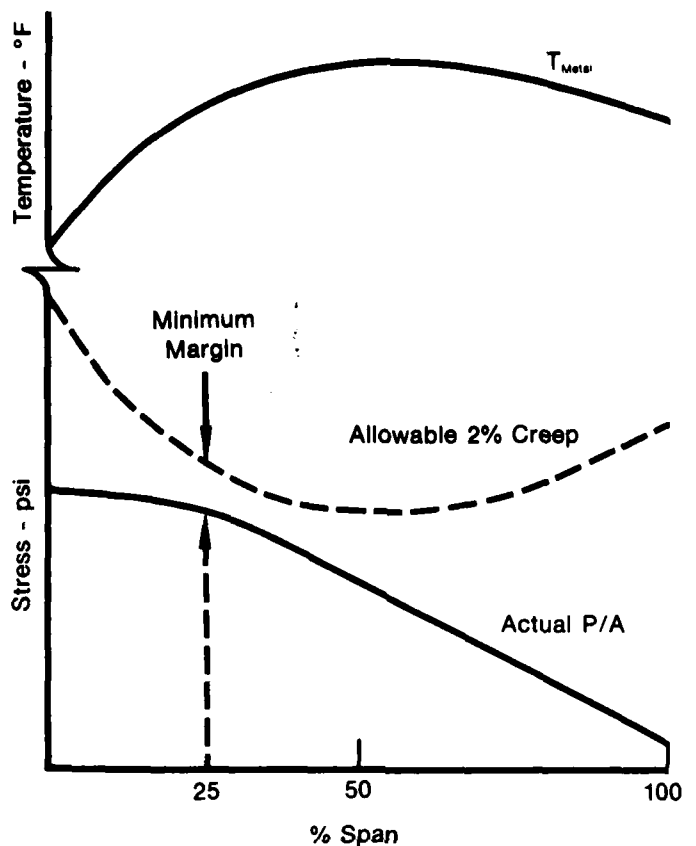


Figure 2-27. Gas and Metal Temperature Trends (Left) and Critical Stress Section for Cooled Turbine Blades.



FD 140198

Figure 2-28. Uncooled Blade Temperature and Stress Characteristics.

2.1.4.5 Airfoil Life Prediction Oxidation/erosion life for vanes and blades is calculated on the basis of the maximum metal temperature for each damaging flight condition. The resistance of various airfoil coatings to oxidation/erosion has been correlated to metal temperature, as shown in figure 2-29. This data was acquired in burner rig tests and has been calibrated to actual engine experience. The mission life is estimated, based on summation of the damage accumulated at each flight condition.

Preliminary design blade stress-rupture life is based on the critical-section pull stress and average metal temperature. Life is estimated using the Larson-Miller relationship for 2% creep. Critical-section stress, average metal temperature, and 2% creep properties in preliminary design have been used successfully as a method of estimating local stress-rupture life (the actual design criterion) in a detailed analysis. Actual local stress-rupture life

calculations require detailed knowledge of total thermal-mechanical stress distribution and degradation of the material for thin walls and coatings which are impossible to assess in preliminary design. Equivalent mission life is based on the sum of the life fraction damage at each flight condition.

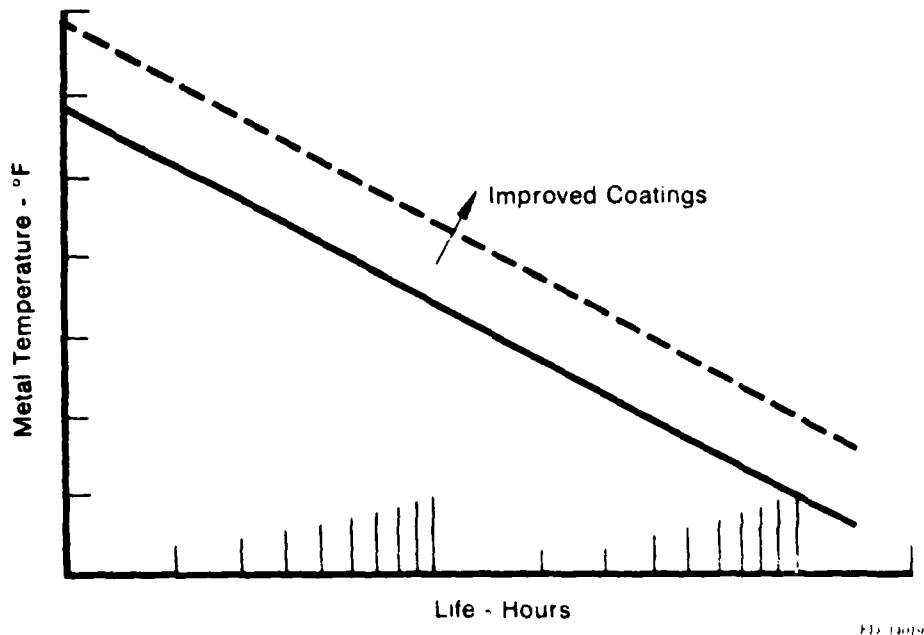


Figure 2-29. Oxidation/Erosion Life Limits for Coated Turbine Blade and Vane Materials.

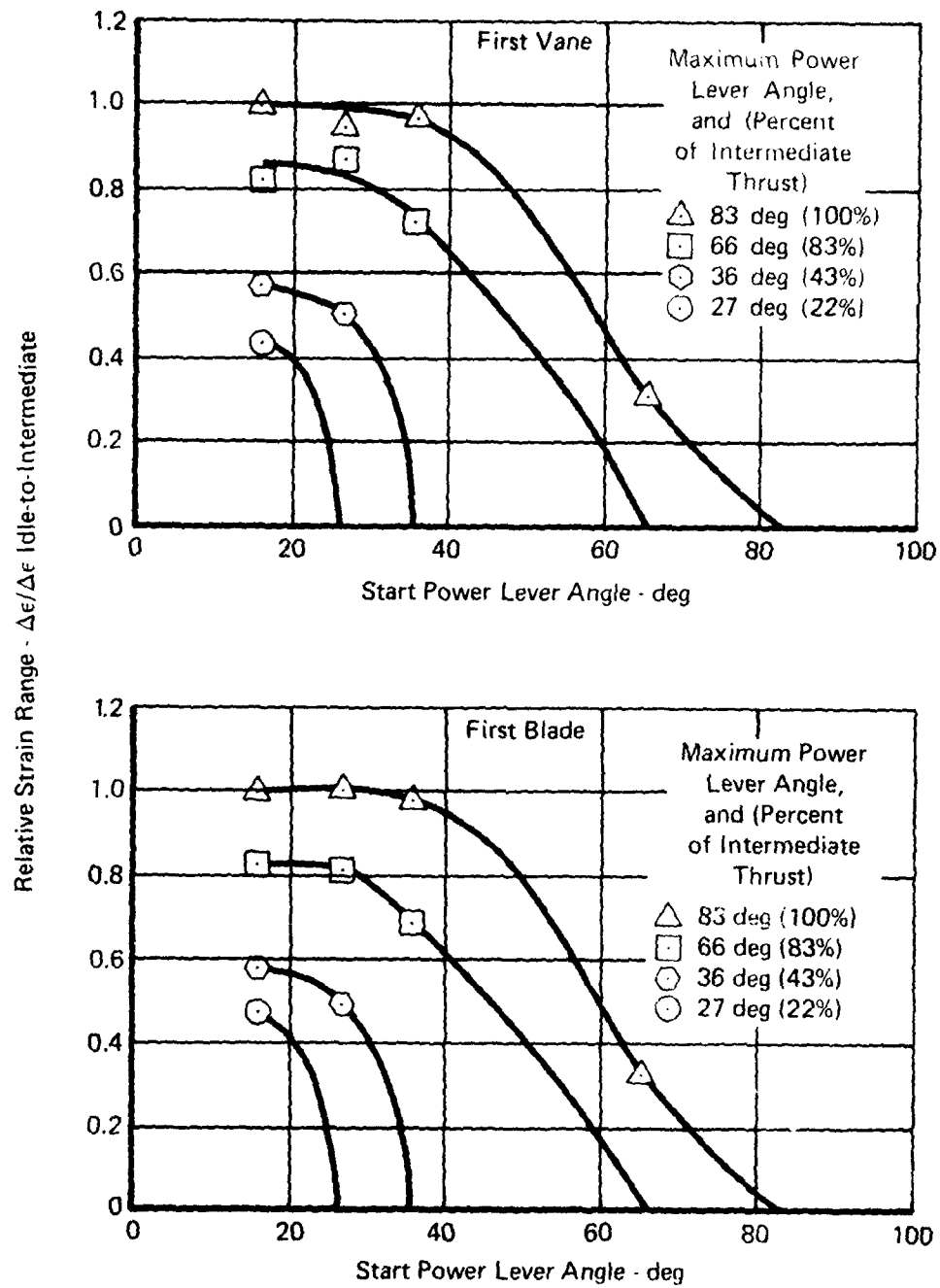
LCF life for vanes is based on the cyclic strain range calculated from the correlation and on thermal-mechanical fatigue data from coated specimens. Blade LCF life predictions are based on a ductility exhaustion theory for creep-fatigue interaction. The theory assumes that a decrement in available ductility resulting from a period of cycling could be represented as an increment of creep extension. The predicted damage interaction is nonlinear.

The ductility exhaustion model requires definition of the transient strain range, the average blade-section creep rate, time spent at intermediate power for each cycle, and the thermal-mechanical fatigue properties. Cyclic lives will be calculated for Type I and Type III cycles. Equivalent mission cyclic life is based on a life fraction ratio of Type I and Type III creep-fatigue damage.

Airfoil fatigue life improvements are possible with increased cooling flow. A reduction in average metal temperatures will improve blade fatigue life by reducing the impact of creep-fatigue interaction and allow use of stronger fatigue properties. A 10% improvement of fatigue life is possible with a 30°F reduction in metal temperature. Increased cooling for vanes will also reduce the cyclic strain range and provide stronger fatigue properties.

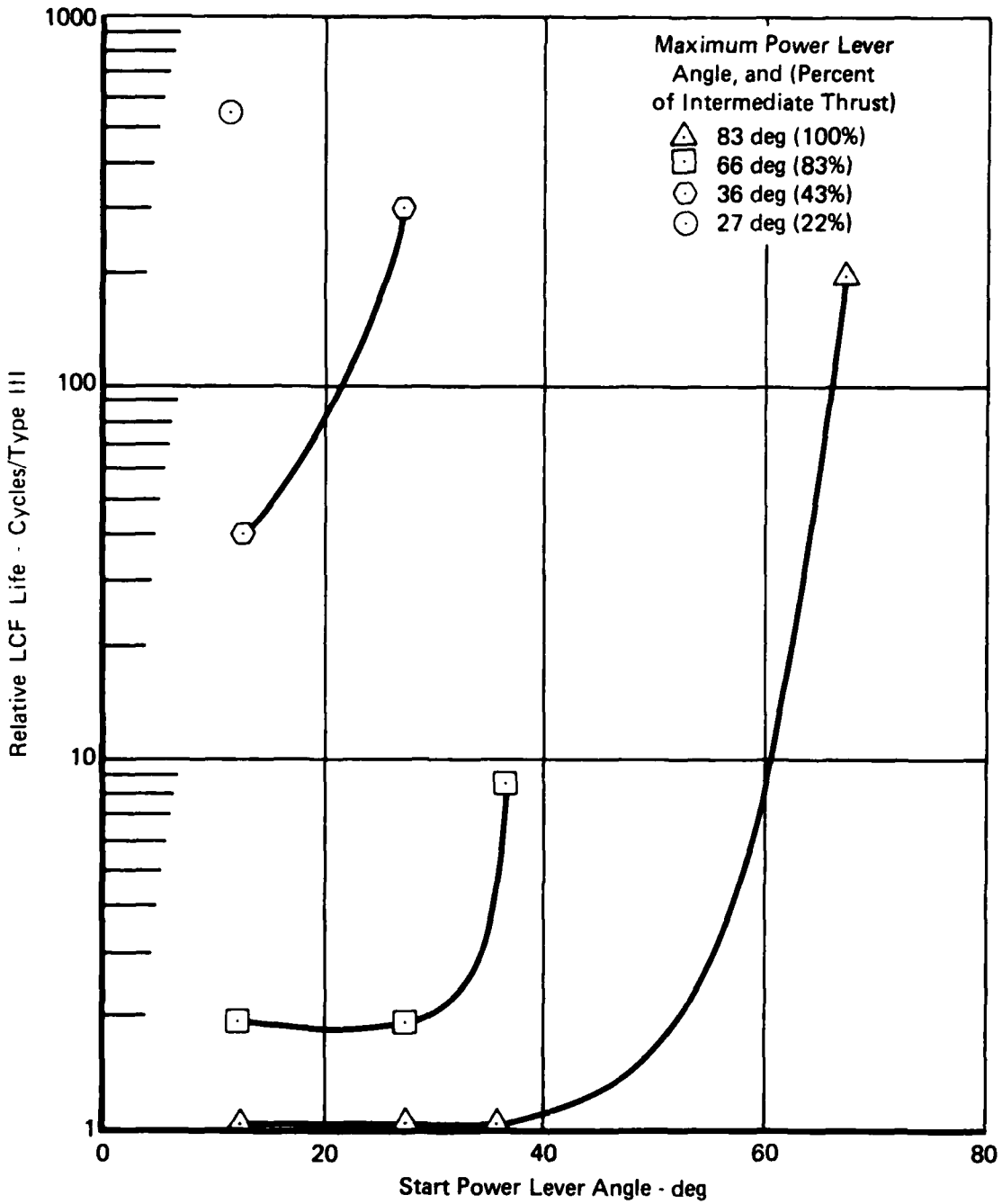
2.1.4.6 Partial Cycle Strain Range Correlation Extension The vane and blade strain range correlation for Type I and Type III cycles was extended to cover so-called partial cycles (partial cycles being cycles which are less than idle-to-intermediate power setting and back to idle power setting).

Transient heat transfer and stress analyses were conducted utilizing the F100-PW-100 high pressure turbine first vane and first blade. Ten partial cycle transients were analyzed, comparing strain range and cyclic life to that of a Type III cycle (idle-to-intermediate-to-idle). The relative strain range is shown in figure 2-30. Strain range for cycles from power lever angles slightly above idle to intermediate have maximum strain ranges equivalent to the Type III cycle. It is also noted that vane and blade strain ranges are essentially identical. Relative low cycle fatigue lives are shown for the vane and blade in figures 2-31 and 2-32, respectively. Cycles from idle to 83% of intermediate thrust have 20% less strain range and twice the low cycle fatigue life relative to the Type III cycle. As the magnitude of the transient decreases, damage decreases dramatically. For example, 560 transients from idle to 22% of intermediate thrust are the low cycle fatigue damage equivalent of one Type III cycle for the vane; for the blade approximately 13,000 of these cycles are the equivalent of the Type III cycle.



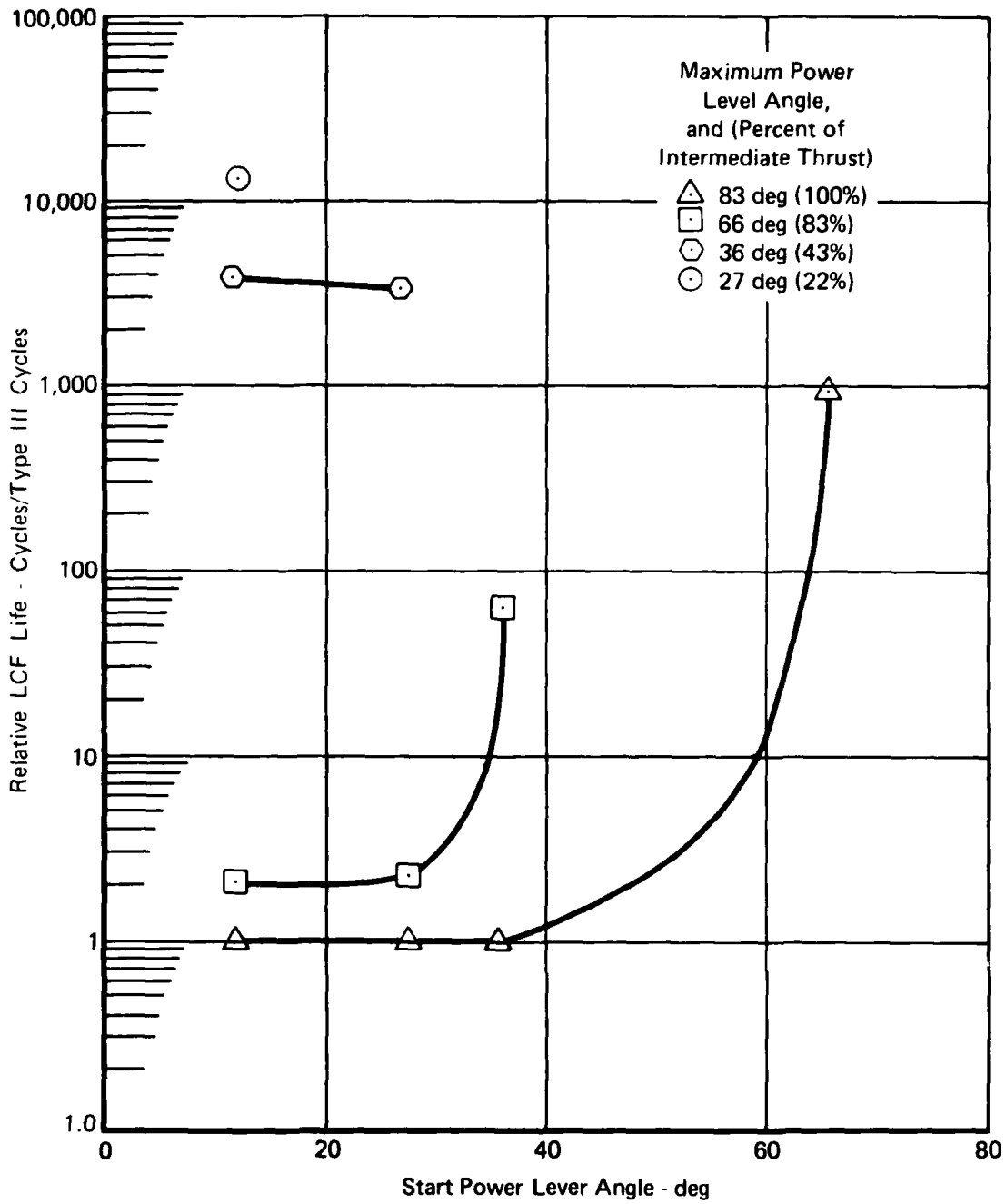
FD 183401

Figure 2-30. Relative Strain Range for First Vane and First Blade.



FD 184402

Figure 2-31. First Vane Low Cycle Fatigue Life Relative to a Type III Cycle.



FD 184403

Figure 2-32. First Blade Low Cycle Fatigue Life Relative to a Type III Cycle.

The Turbine Cooled Airfoil System (CAS) was used to perform this analysis. Figure 2-33 illustrates the CAS analysis approach. The two-dimensional airfoil cross-section is specified, and the internal section coring is defined, consistent with the cooling scheme requirements. The heat transfer and stress model consists of a finite element breakup of the airfoil, and internal/external flow and heat transfer analyses. The heat transfer and stress analysis determine both steady-state and transient metal temperatures, stresses, and strains for each airfoil element. The transient strain range is defined as the difference between the maximum and minimum strain during the transient for the life-limiting element in the cross-section. Figures 2-34 and 2-35 illustrate typical results of the analyses. Figure 2-36 illustrates typical F100-PW-100 transient data used for the low cycle fatigue life vane and blade analysis.

2.1.5 Material Properties

Pratt & Whitney Aircraft has an extensive computerized Material Data Library. This library includes stress versus creep and stress rupture lives and strain range - mean stress versus low cycle fatigue life as functions of temperature. The LUCID computer-aided design system makes extensive use of this system. The LPWT is capable of analysis of attachments and disks via the use of simple stress-ratioing techniques.

Blade materials selected for analysis are shown below:

- a. PWA 1202, 8-1-1 Titanium
- b. PWA 1005, Waspaloy
- c. PWA 1422, Directionally Solidified MAR M200

First stage fan blades will be boron aluminum composite with 8-1-1 Titanium being used in the later stages. When temperatures become too hot for titanium, WASPALOY will be used. Turbine blades will be sized for 1422. Advanced turbine blade alloys such as PWA 1480 single crystal will be synthesized through the use of the material properties ratio options.

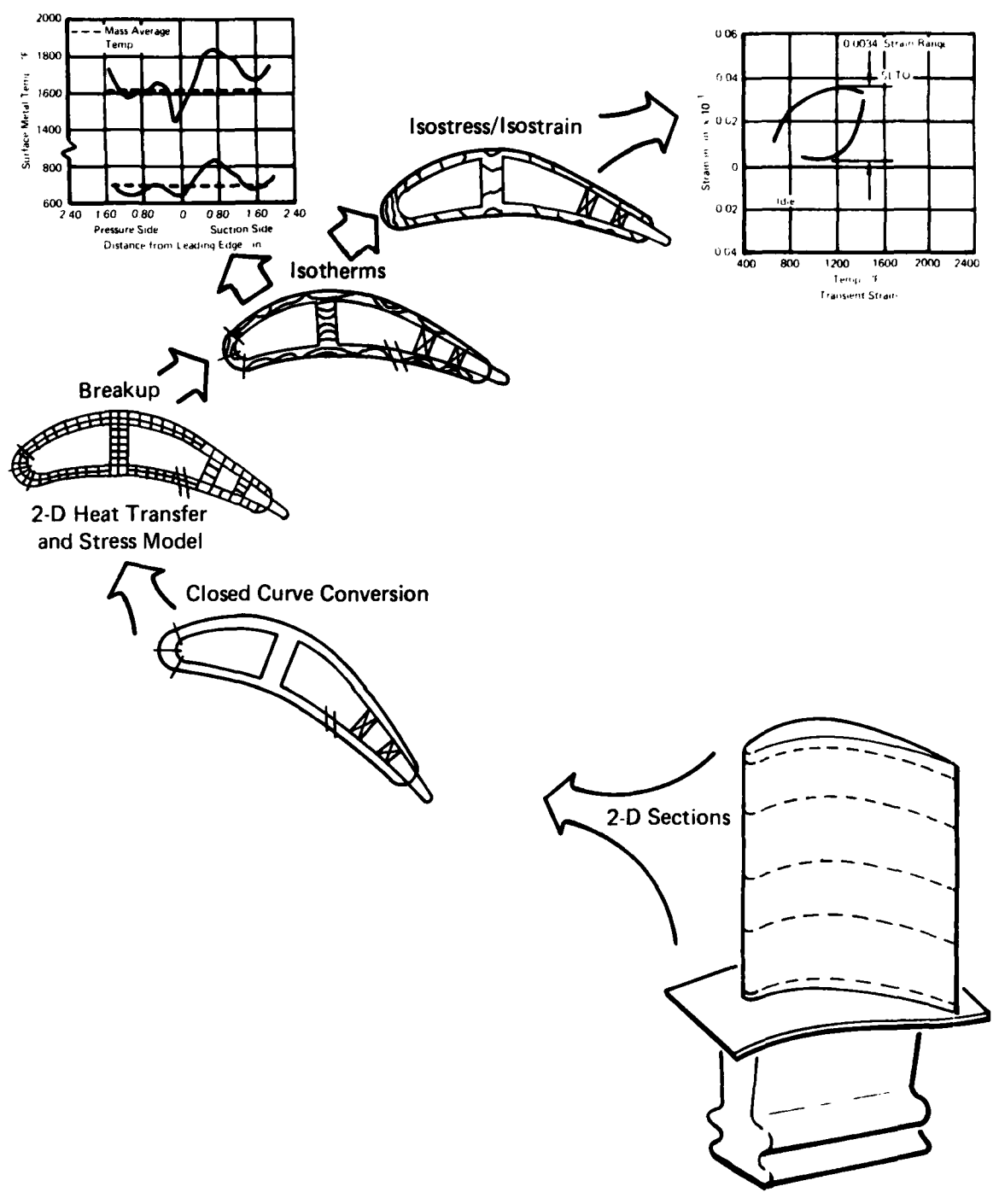


Figure 2-33. Transient Strain Range Prediction.

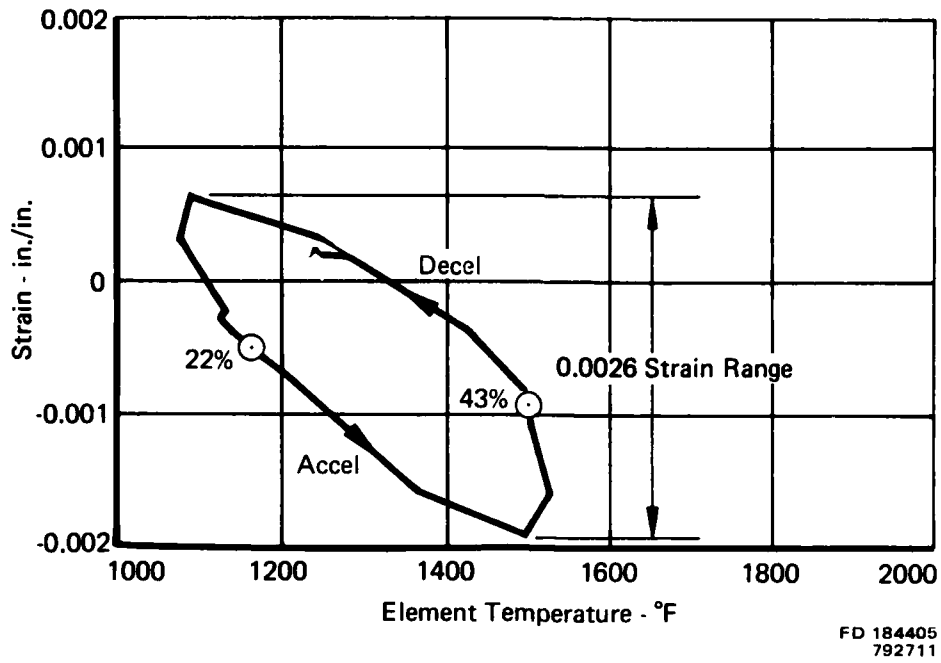


Figure 2-34. Vane Strain and Temperature for 22% to 43% Intermediate Thrust Transient.

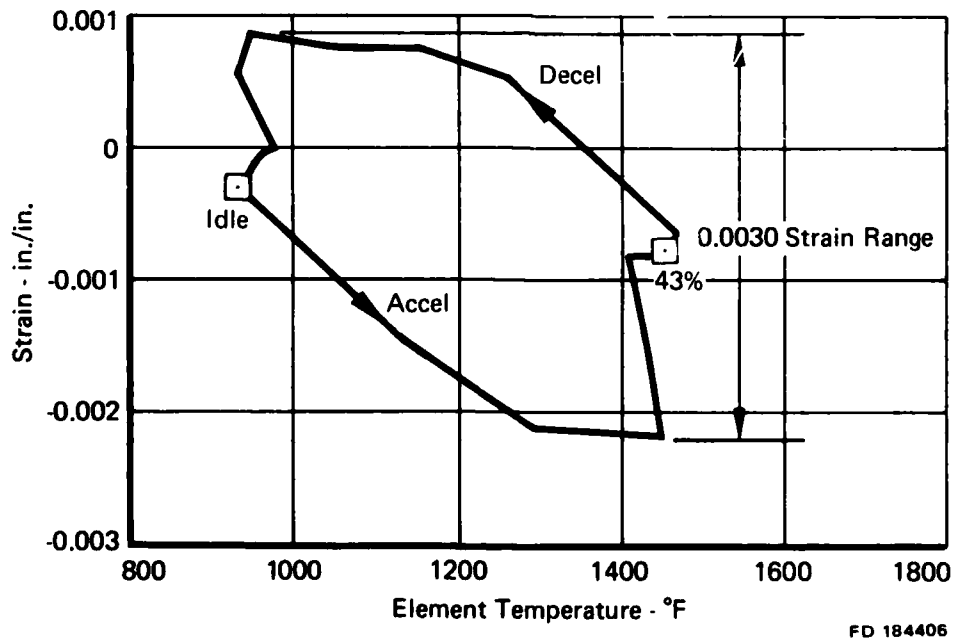
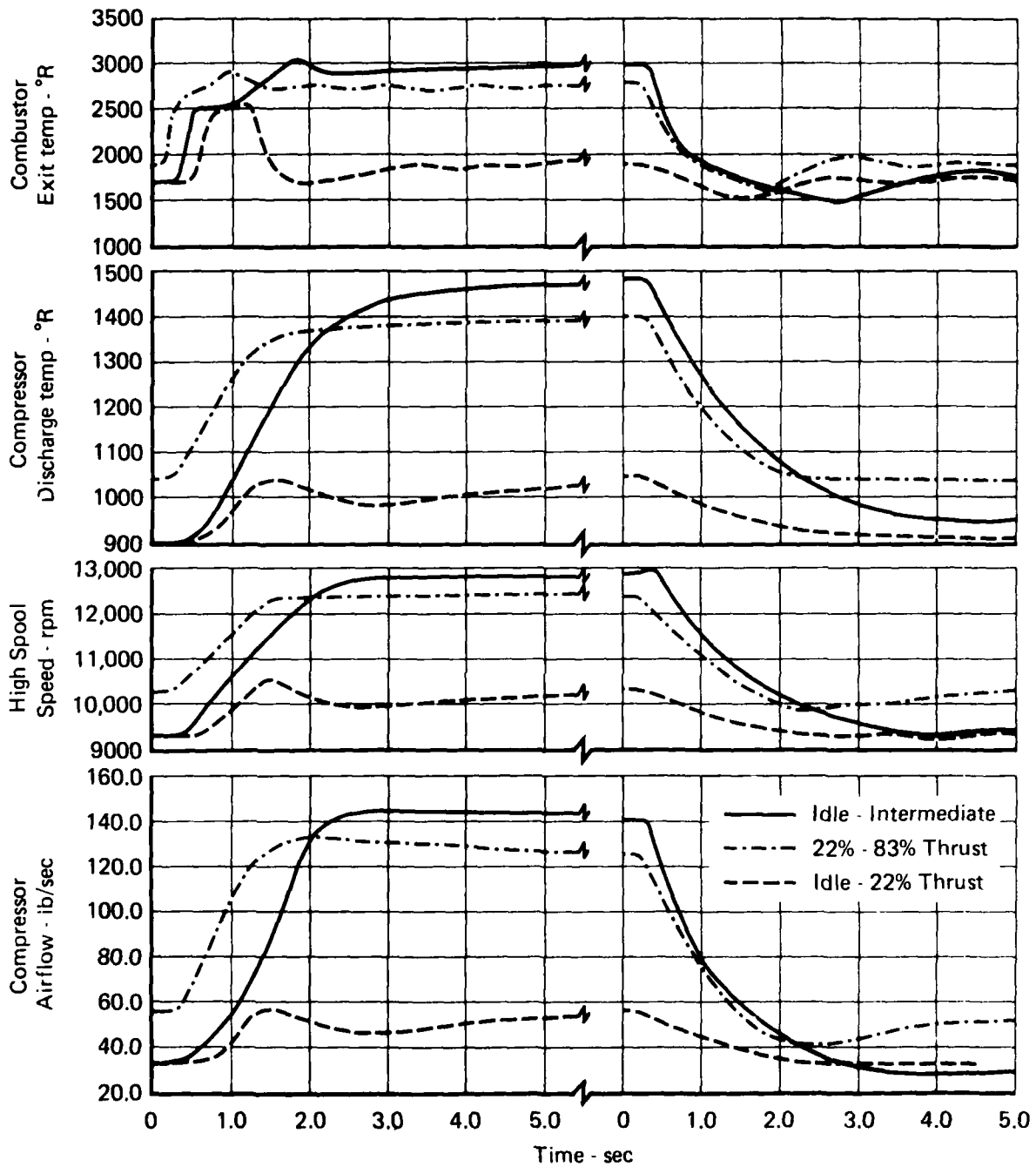


Figure 2-35. Vane Strain and Temperature for Idle to 43% Intermediate Thrust Transient.



FD 184407

Figure 2-36. Acceleration and Deceleration Data For Transient Low Cycle Fatigue Life Analysis.

Disk materials selected are shown below:

- a. AMS 4928, 6-4 Titanium
- b. PWA 1216, 6-2-4-6 Titanium
- c. PWA 1073, IN-100
- d. PWA 1010, IN-718

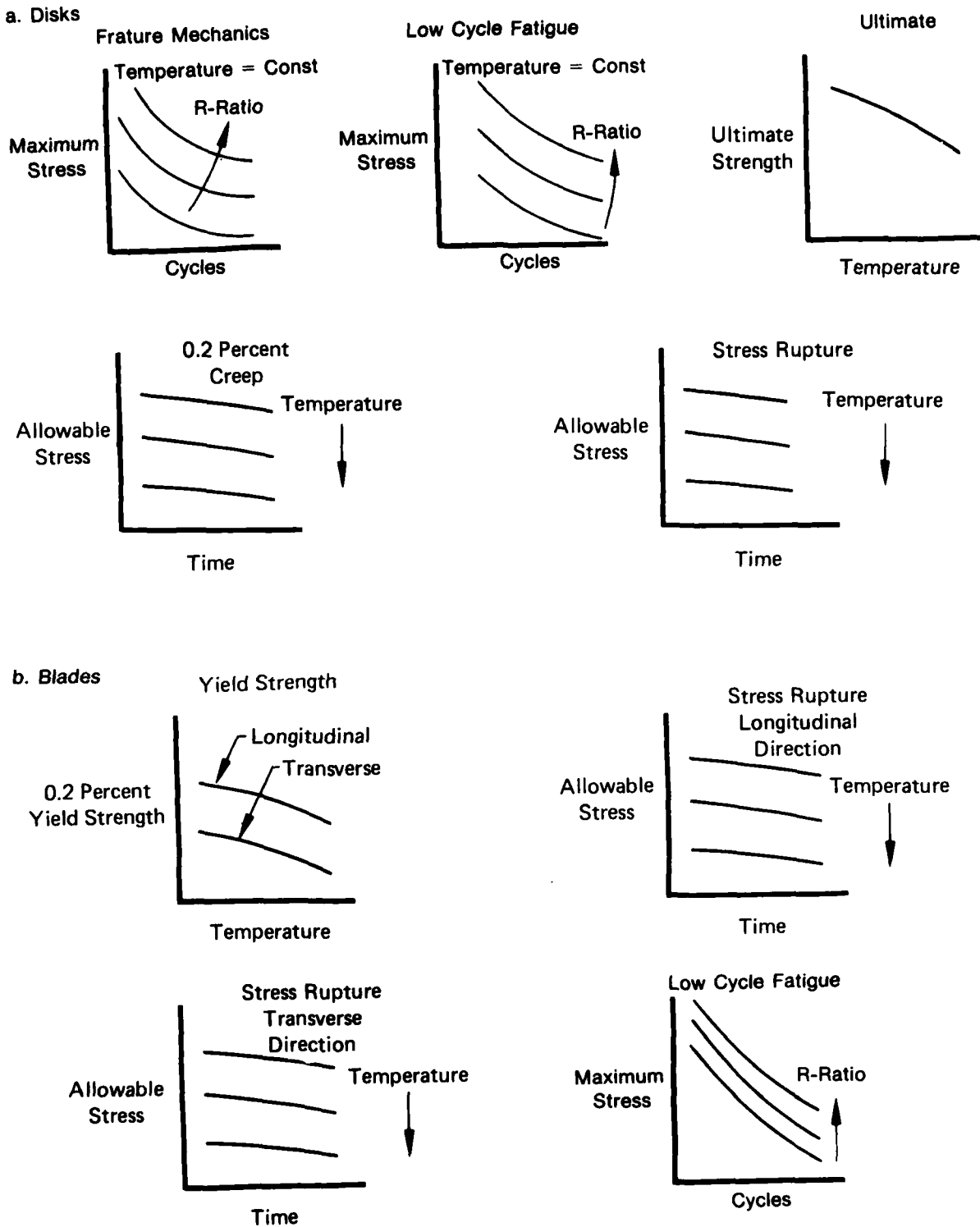
6-4 Titanium is currently the most satisfactory low temperature disk alloy. 6-2-4-6 Titanium is also included because of its exceptional creep and strength properties. It is hoped that its fracture mechanics properties can be improved in the future.

IN-100 is for use in high temperature disk applications. INCO-718 may be necessary for a future IN-100 substitute if cobalt availability becomes questionable.

Figure 2-37 summarizes the material properties required by the LUCID LPWT. The primary effort in generating the material data was generation of the low cycle fatigue properties for all seven materials and fracture mechanics properties for the four disk materials.

2.2 FLOWPATH COMPUTER ROUTINE

The LPWT Flowpath Computer Routine consists of four subroutines which provide component design parameters for the fan, compressor, high pressure turbine, and low pressure turbine. These flowpath data are parameters such as efficiencies, speeds, airfoil pulls, airfoil aspect ratios, critical dimensions, number of stages, and number of airfoils. The fan flowpath data subroutine consists of tables of output data which are accessed with the three independent variable levels. The compressor and turbine flowpath subroutines are in regression equation form, and are accessed with the levels of the four (or more) independent variables.



FD 167812

Figure 2-37. Disk and Blade Material Properties Definition Format.

2.2.1 Fan Flowpath Subroutine

The fan flowpath subroutine is required to cover a range of fan pressure ratios from 2.0:1 to 4.5:1. Since number of stages, tip speed, and average aspect ratio are the independent variables, and pressure ratio is one of the dependent variables, the range is actually much greater than required. The three independent variables and their ranges are:

<u>Fan Aerodynamic Variable</u>	<u>Range</u>
Corrected Tip Speed, ft/sec	1400 to 1800
Number of Stages	1 to 3
Average Aspect Ratio	1.6:1 to 2.9:1

Fan configuration independent variables which were fixed for generation of the matrix are shown below:

<u>Independent Variable</u>	<u>Level</u>
Inlet Specific Flow, lb/sec/ft ²	42.
Inlet Hub/Tip Ratio	0.40
Exit Mach Number	0.46
Flowpath Shape	Constant Mean Diameter
Gap/Chord Ratio	0.6
Corrected Flowrate, lb/sec	200.

With three levels of the three independent variables, the full 27-design matrix was generated with a simplified meanline design system. The results of this screening exercise are shown in figure 2-38.

To obtain the chord distribution, airfoil count by row, and axial projection for each fan in the matrix, the 3-stage 2.3 average aspect ratio 1600 foot-per-second design was generated using the conventional performance prediction meanline program (see figure 2-39).

Figures 2-40, 2-41, and 2-42 illustrate typical results. Figure 2-40 illustrates that at a constant fan pressure ratio of 3.2:1, the tip speed of a two-stage 1800 foot-per-second compressor may be

reduced to just over 1400 feet-per-second with the addition of a third stage. Figure 2-41 shows that at the low aspect ratio limit of 1.6 the two-stage fan may be reduced in tip speed to approximately 1700 feet per second. Figure 2-42 shows the efficiency estimates for the fan aerodynamic matrix; these estimates are for shroudless designs, reflecting the use of composite boron aluminum blades.

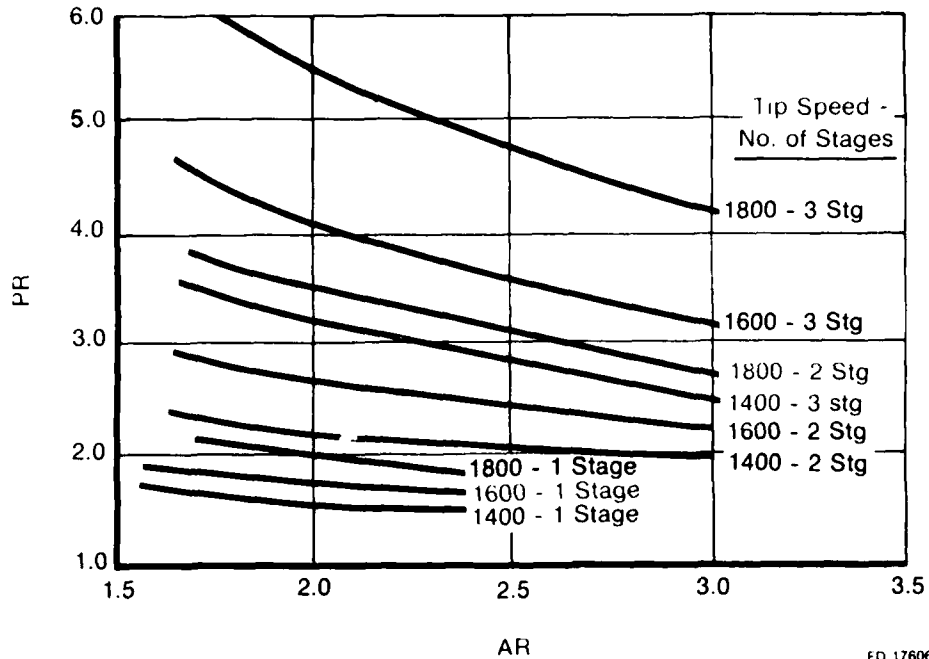
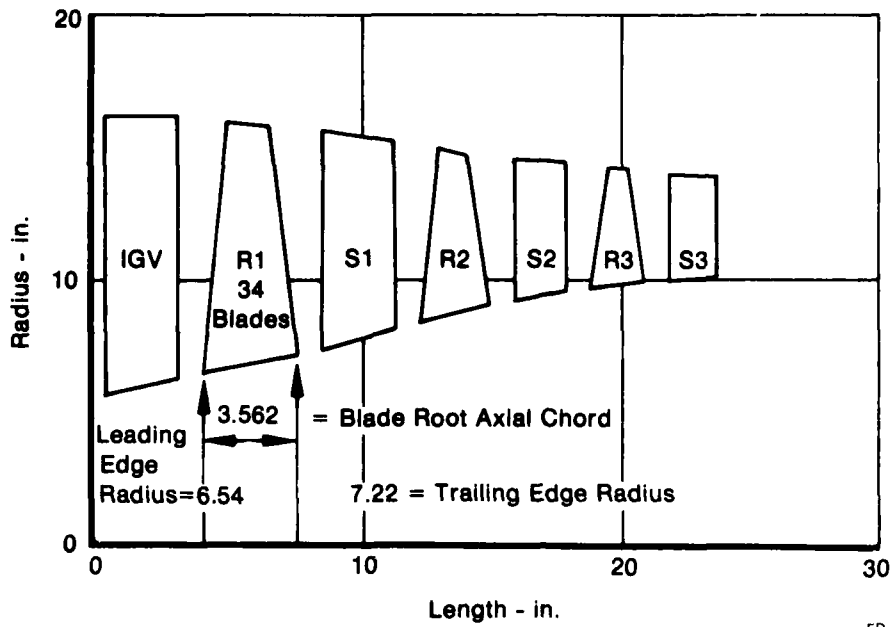
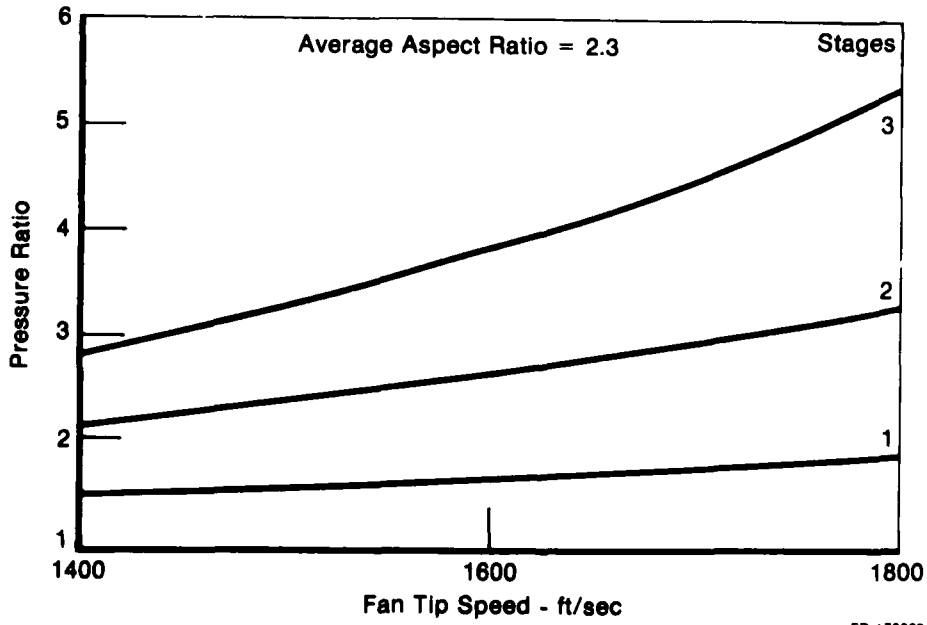


Figure 2-38. LUCID Fan Parametric Screening Results.



FD 176068

Figure 2-39. Fan Flowpath At Average Aspect Ratio of 2.3 and 1600 ft/sec Tip Speed.



FD 176069

Figure 2-40. Fan Pressure Ratio As A Function of Tip Speed and Number of Stages.

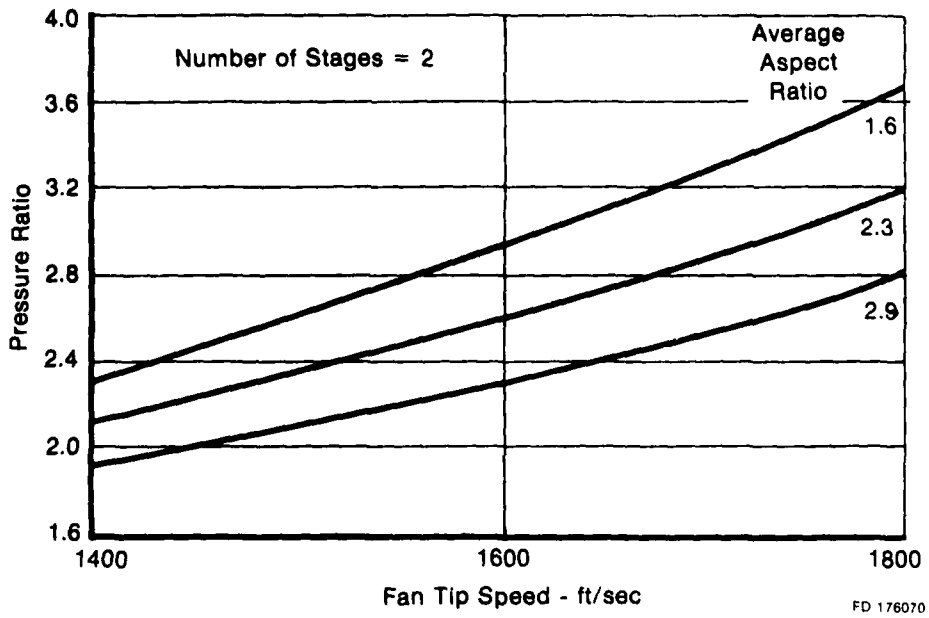


Figure 2-41. Fan Pressure Ratio As A Function of Aspect Ratio Tip Speed.

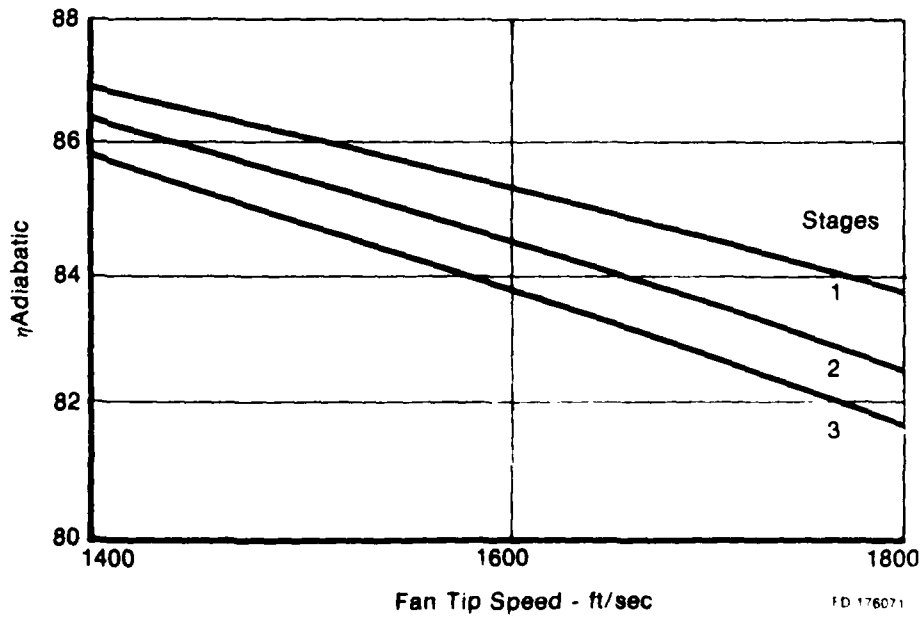


Figure 2-42. Estimated Fan Efficiency.

2.2.2 Compressor Flowpath Subroutine

The compressor aerodynamic matrix consists of twenty-five meanline designs comprising full replication of the four-variable central composite design.

The four independent variables and their ranges are shown below:

<u>Compressor Aerodynamic Matrix Independent Variable</u>	<u>Range</u>
Corrected tip speed, ft/sec	1150-1450
Average aspect ratio	1.0-2.0
Number of stages	4-10
Inlet hub/tip ratio	0.6-0.74
<u>Fixed Design Parameter</u>	<u>Level</u>
Stall Margin, percent	15
Inlet flow per annulus area, lb/sec-ft ²	37.5
Flowpath shape	Constant Mean Diameter
Exit Mach Number	0.45
Exit Swirl Angle	Axial
Airflow Size (corrected), lb/sec	40
Gap/Chord Ratio	0.70

The compressor meanline designs are generated by a one-dimensional meanline compressor preliminary design system. This design technique utilizes a "conical diffuser" analogy in conjunction with airfoil cascade test data correlations. The design system estimates performance and flow path based on Reynolds number, clearances, surface roughness, airfoil aspect ratio and thickness, and solidity.

Figure 2-43 illustrates three typical compressor meanlines, showing the effect of average aspect ratio (with seven stages) on pressure ratio, length, efficiency, etc. The higher pressure ratio per stage and pressure ratio per airfoil attributes of low aspect ratio are evident (these compressors are also shown in figure 2-44, illustrating a 1.2 change in polytropic efficiency with a 1.0 to 2.0

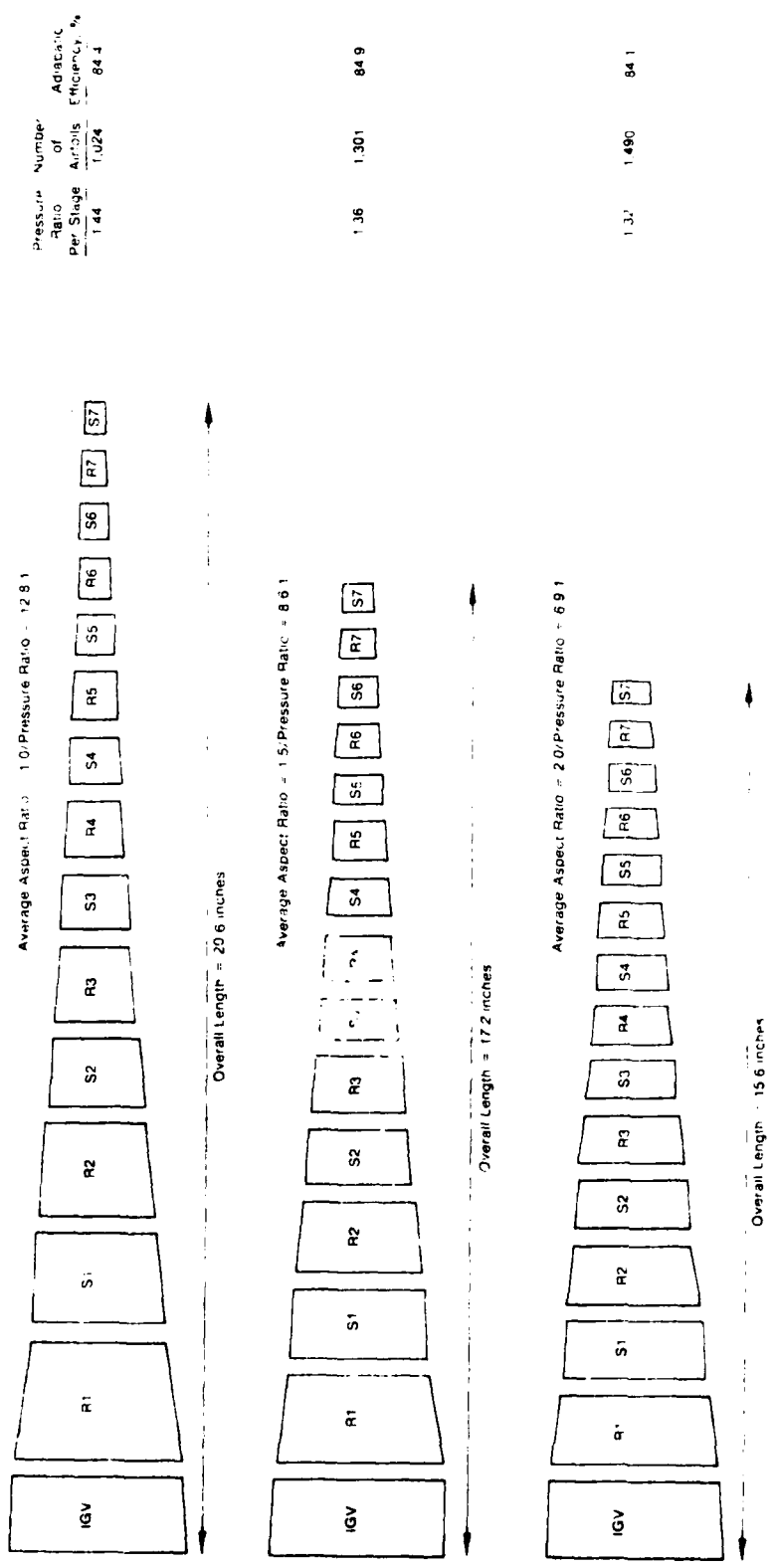
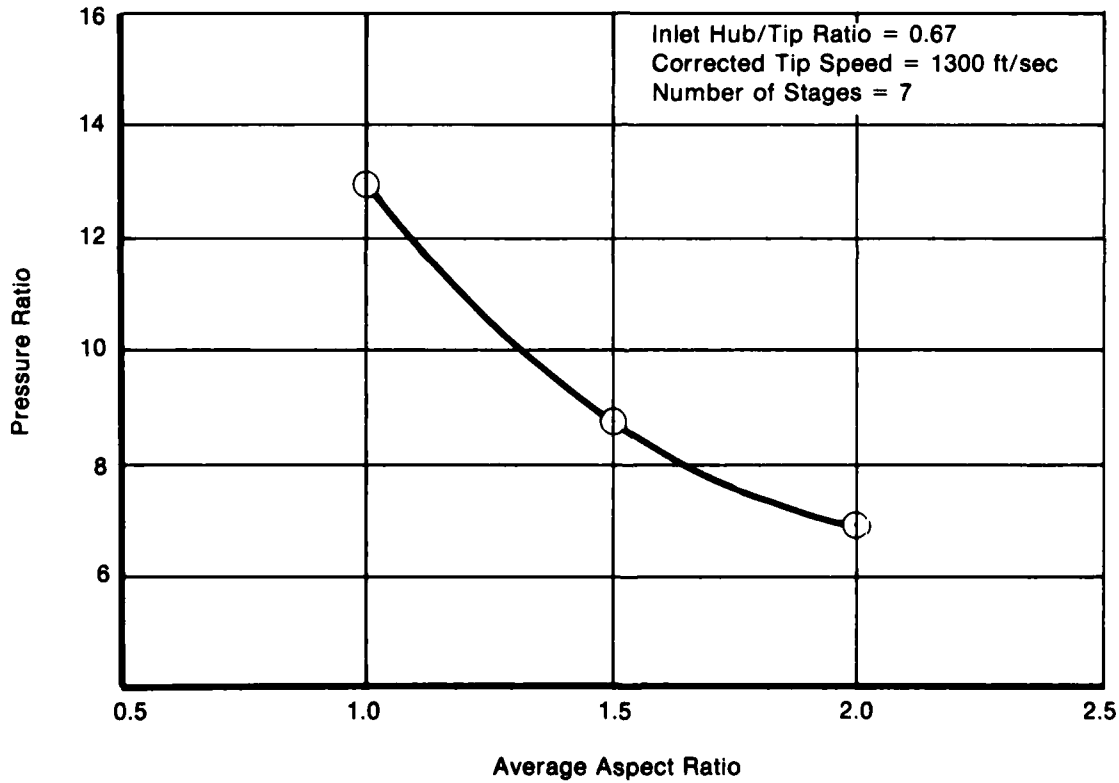
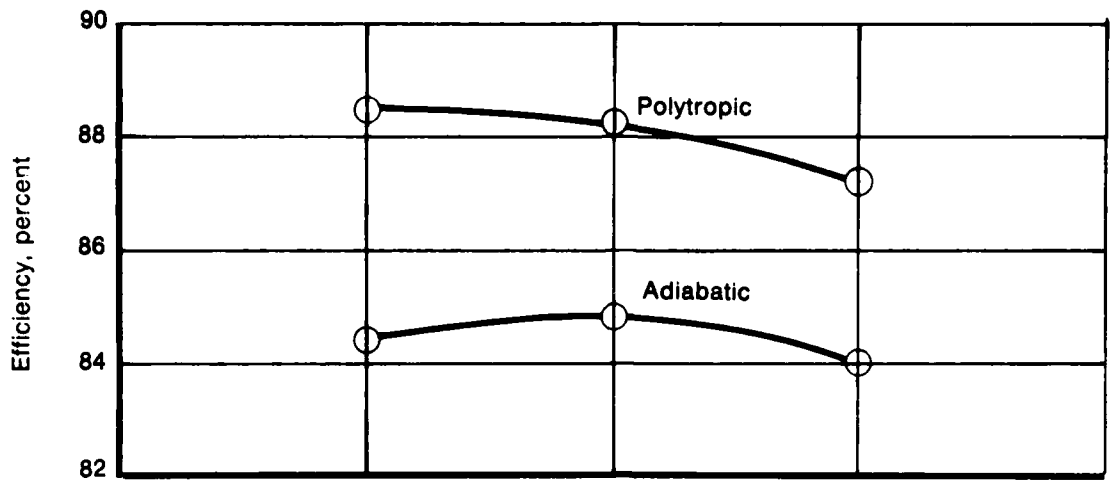


Figure 2-43. Typical Compressor Flowpaths Illustrating the Effect of Aspect Ratio With Seven Compressor Stages.



FD 184412

Figure 2-44. Effect of Compressor Aspect Ratio on Pressure Ratio and Efficiency.

change in average aspect ratio). Figures 2-45 through 2-47 show the trends in pressure ratio and efficiency with variations in the remaining three independent variables.

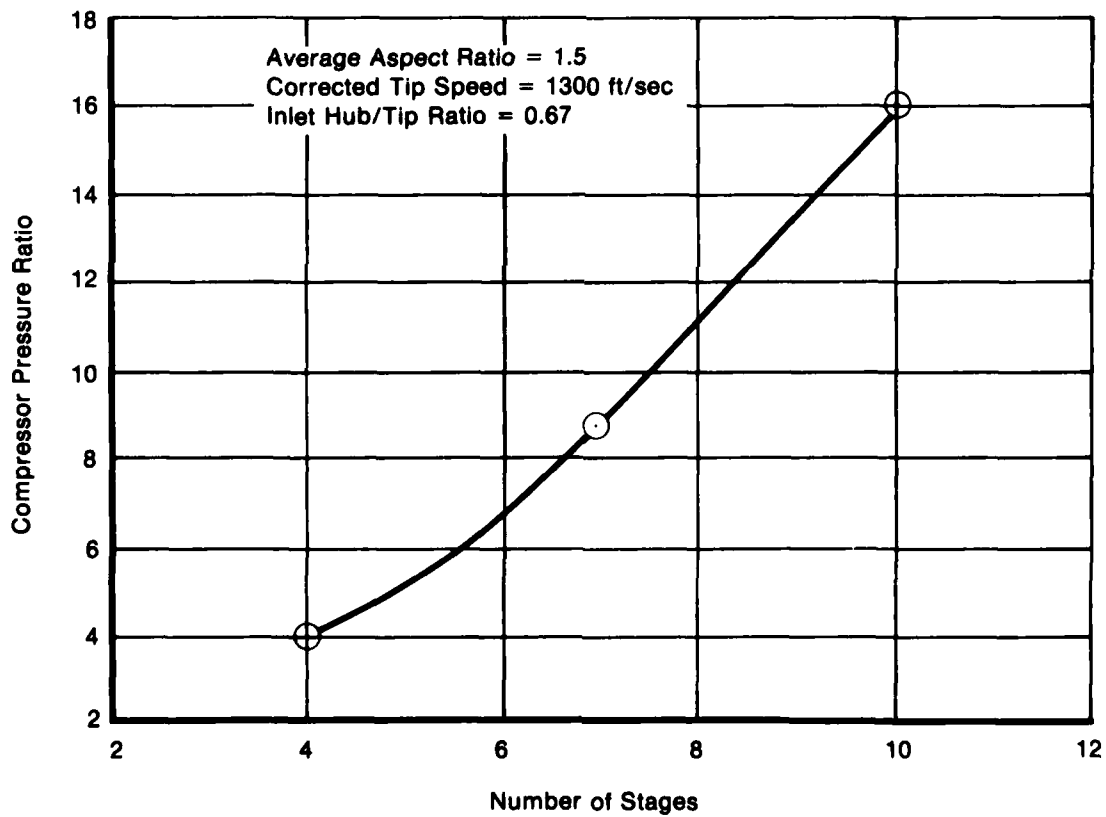
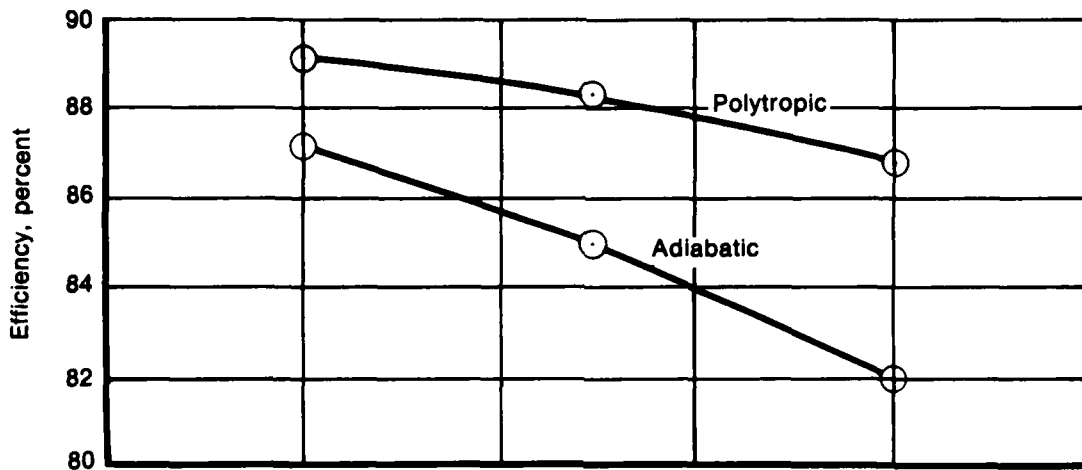
Polytropic (or "small stage") efficiency estimates range from 86.9 to 89.1% considering only the 9 meanlines comprising the main effects matrix design. This polytropic efficiency range increases (2.2% to 9.3%) for the entire matrix. Accuracy of the efficiency estimates is approximately ± 1.0 percent.

2.2.3 High Pressure Turbine Flowpath Subroutine

The high pressure turbine flowpath subroutine consists of six independent variables:

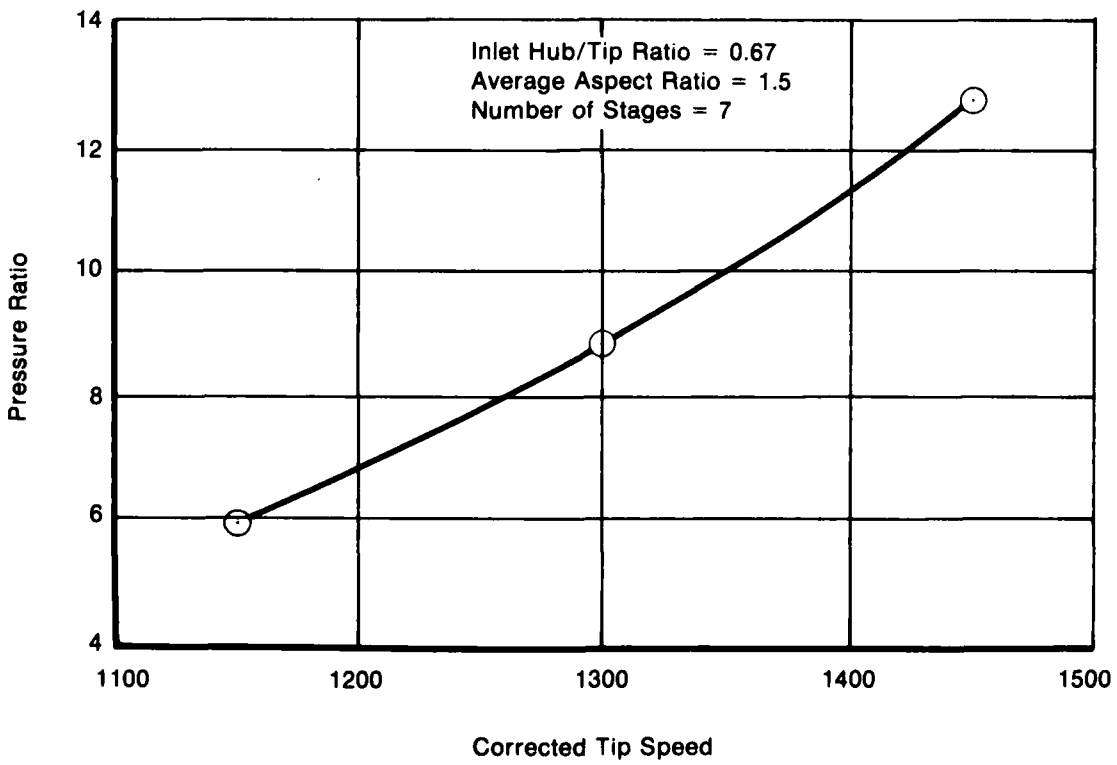
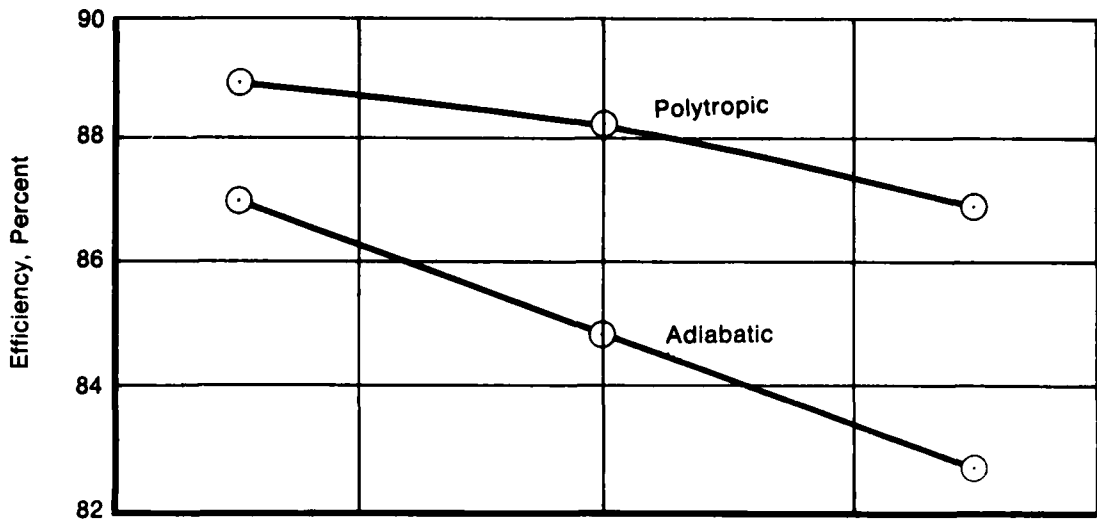
<u>Variable</u>	<u>Range</u>
1. Specific work, Δh , Btu/lbm	120-210
2. Combustor exit temperature, T_{T4} , °F	2,400-3,200
3. Product of exit annulus area and rotational speed squared, AN^2 , $\text{in}^2 \text{rpm}^2 \times 10^{-8}$	350-600
4. Mean velocity ratio, Vr_{mean} , dimensionless	.45-.65
5. Exit axial Mach number, Mx_{exit} , dimensionless	.3-.6
6. Blade axial chord, b_x , inches	1-2

The high-pressure turbine matrix output data is cooled efficiency (for a "referee" level of turbine airfoil/platform cooling air and disk cooling/seal leakage air), number of vanes and blades for the single stage high-pressure turbine, and flowpath dimensions. This data was generated with the Turbine Meanline Design Program. The "referee" nomenclature refers to our approach, setting a level of turbine cooling/leakage air as a function of combustor exit temperature for generation of the turbine meanline designs. Outputs of the matrix will be corrected to the level of cooling/leakage air for the specific case to be exercised by the LPWT.



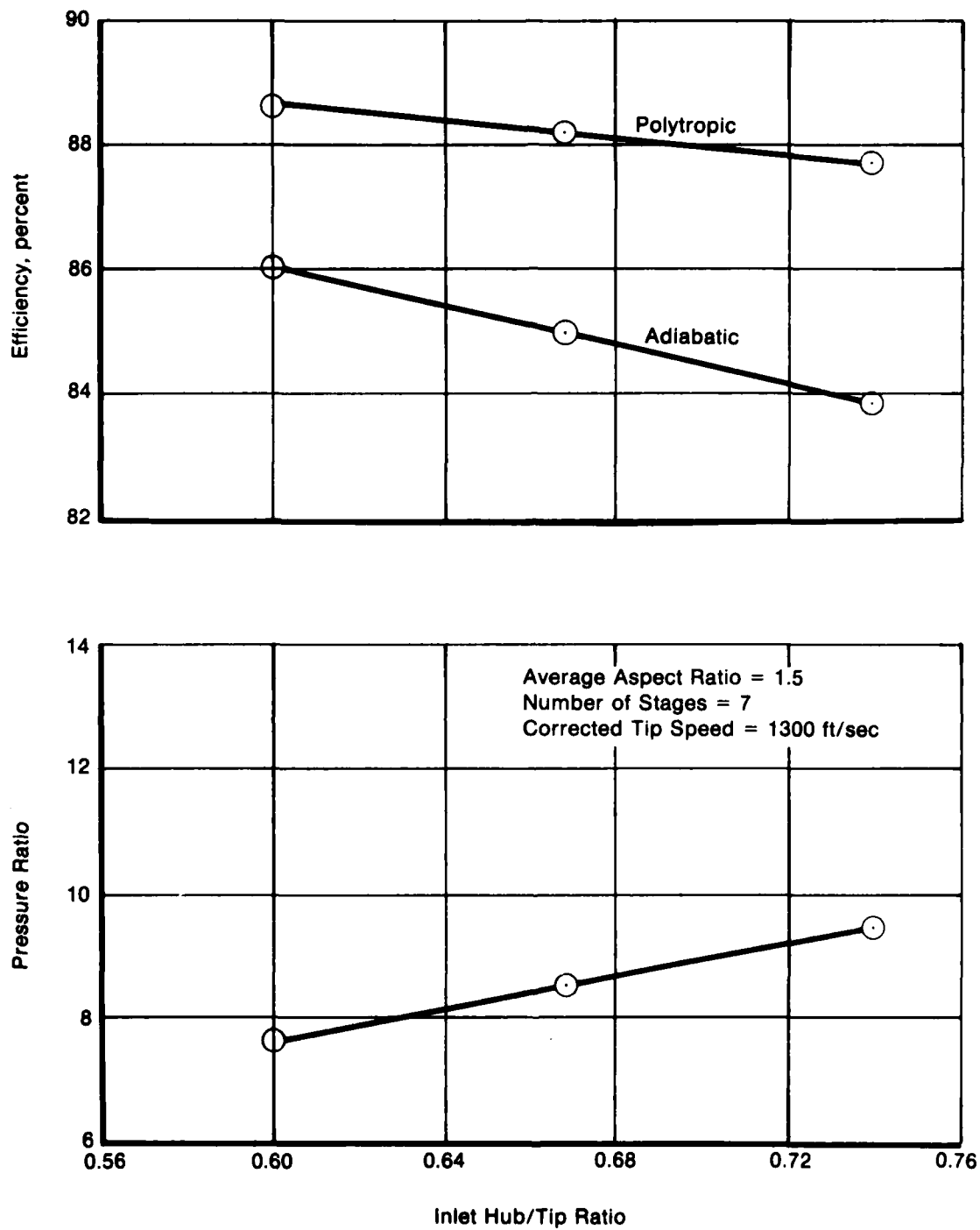
FD 184413

Figure 2-45. Estimated Pressure Ratio and Efficiency Trend With Number of Stages.



FD 184414

Figure 2-46. Estimated Pressure Ratio and Efficiency Variation With Compressor Tip Speed.



FD 184415

Figure 2-47. Estimated Effect of Hub/Tip Ratio on Pressure Ratio and Efficiency.

Dependent variables of interest for the single-stage high pressure turbine matrix are cooled efficiency, vane and blade airfoil count, rotor speed, exit annulus area, blade root axial chord and radius, and blade pull per airfoil. All dependent variables are output by the meanline design program with the exception of airfoil pull. A simplified turbine aerodynamic program was generated and linked to a computer program which generates airfoil pull. A comparison of blade pulls generated by velocity triangles of the detailed meanline design system and the simplified system is shown in Table 2-1. The average total pull error is 4.3%, and the maximum error is 9.7%.

TABLE 2-1. SIMPLIFIED/DETAILED MEANLINE ANALYSIS COMPARISON

	Case 1 Simplified/ Detailed	Case 2 Simplified/ Detailed	Case 3 Simplified/ Detailed	Case 4 Simplified/ Detailed
Tip inlet angle, deg.	37.9/40.7	35.9/37.2	55.7/59.7	42.4/42.8
Tip exit angle, deg.	27.2/26.8	21.2/22.8	35.2/38.8	26.5/26.7
Mean radius, in.	9.32/9.33	10.16/10.25	5.63/5.74	11.84/11.74
Number of blades	56/51	45/41	48/42	52/52
Total pull, thou- sands of pounds	414.5/393.8	549.1/500.5	337.6/343.6	532.3/528.9
Total pull error, %	+5.3	+9.7	-1.7	+0.6

Referee turbine cooling airs were estimated at three combustor exit temperature levels and are shown in Table 2-2.

TABLE 2-2. REFEREE TURBINE COOLING AIR

Maximum Combustor Exit Temperature, °F	2400	2800	3200
Vane Cooling Air, % of Core Airflow	3.9	5.9	10.4
Blade Cooling Air, % of Core Airflow	2.5	2.9	4.8

Fifty-one high pressure turbine meanlines were generated. A half-replicate six variable central composite design requires forty-five designs, and six check cases make up the balance of designs.

Typical results of turbine meanline design matrix generation are shown in figure 2-48. The efficiency and airfoil count estimates a function of velocity ratio and specific work are shown on 6 of the 51 meanline designs.

2.2.4 Low Pressure Turbine Flowpath Subroutine

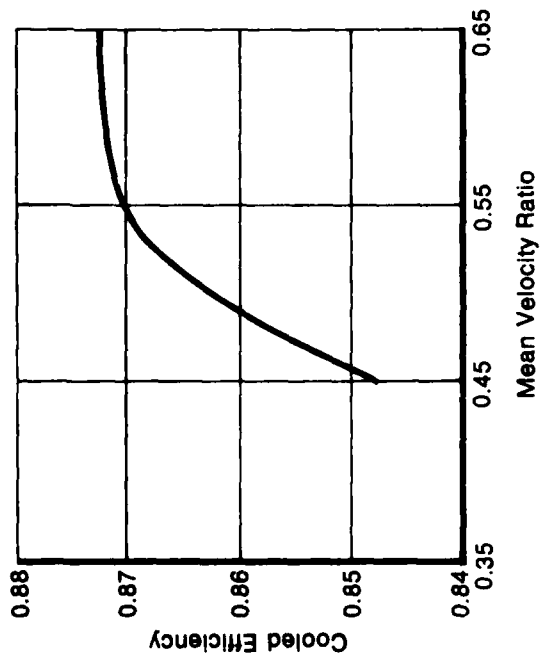
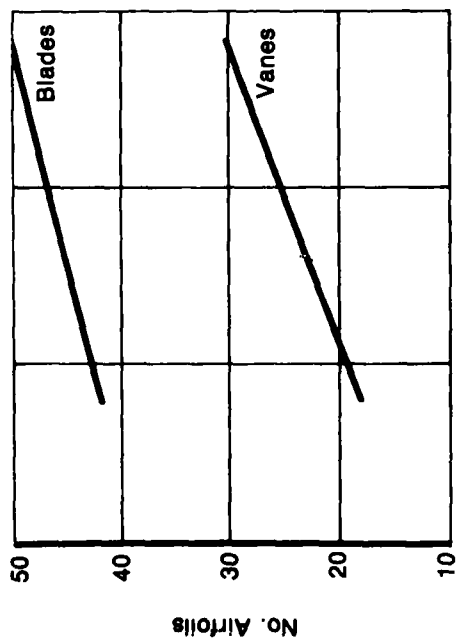
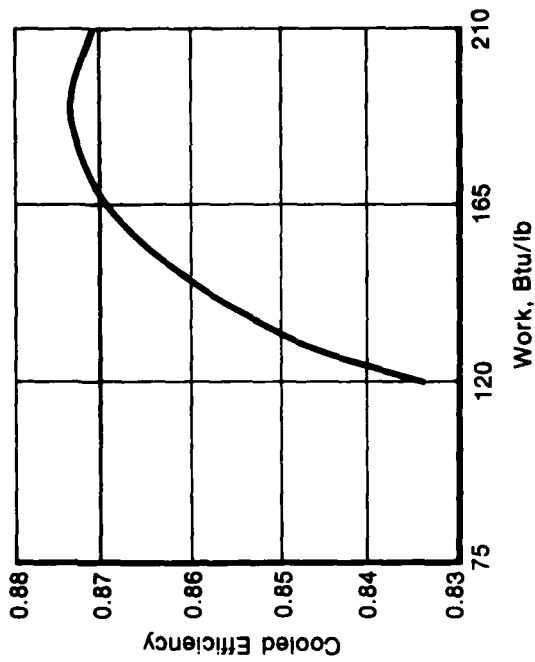
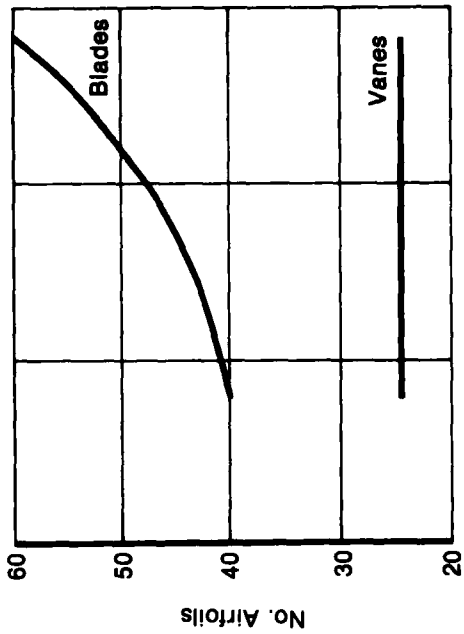
The low pressure turbine aerodynamic matrix is basically similar to the high pressure turbine; i.e., the same six independent variables, half replicate central composite design, forty-five base designs and six check cases. However, the magnitude of effort was doubled because the requirement to cover the medium bypass ratio range (greater than 2.0:1) dictated two turbine aerodynamic matrices covering both single- and two-stage designs.

Figure 2-49 illustrates single- and two-stage flowpaths at the centroid values of the six independent variables. The mean radius of the two-stage turbine is essentially $2^{-0.5}$ lower than that of the single-stage design (both turbines at same specific work and mean velocity ratio). The lower vane and blade count per row reflects both the lower level of turning and lower mean radius of the two-stage design at the same level of Zweifel load coefficient. The turbines have the same design speed and exit area (i.e., the same level of the product of exit annulus area and speed-squared).

Figures 2-50 through 2-52 show the effects of chord, fan turbine inlet temperature, and velocity ratio on blade count and cooled efficiency.

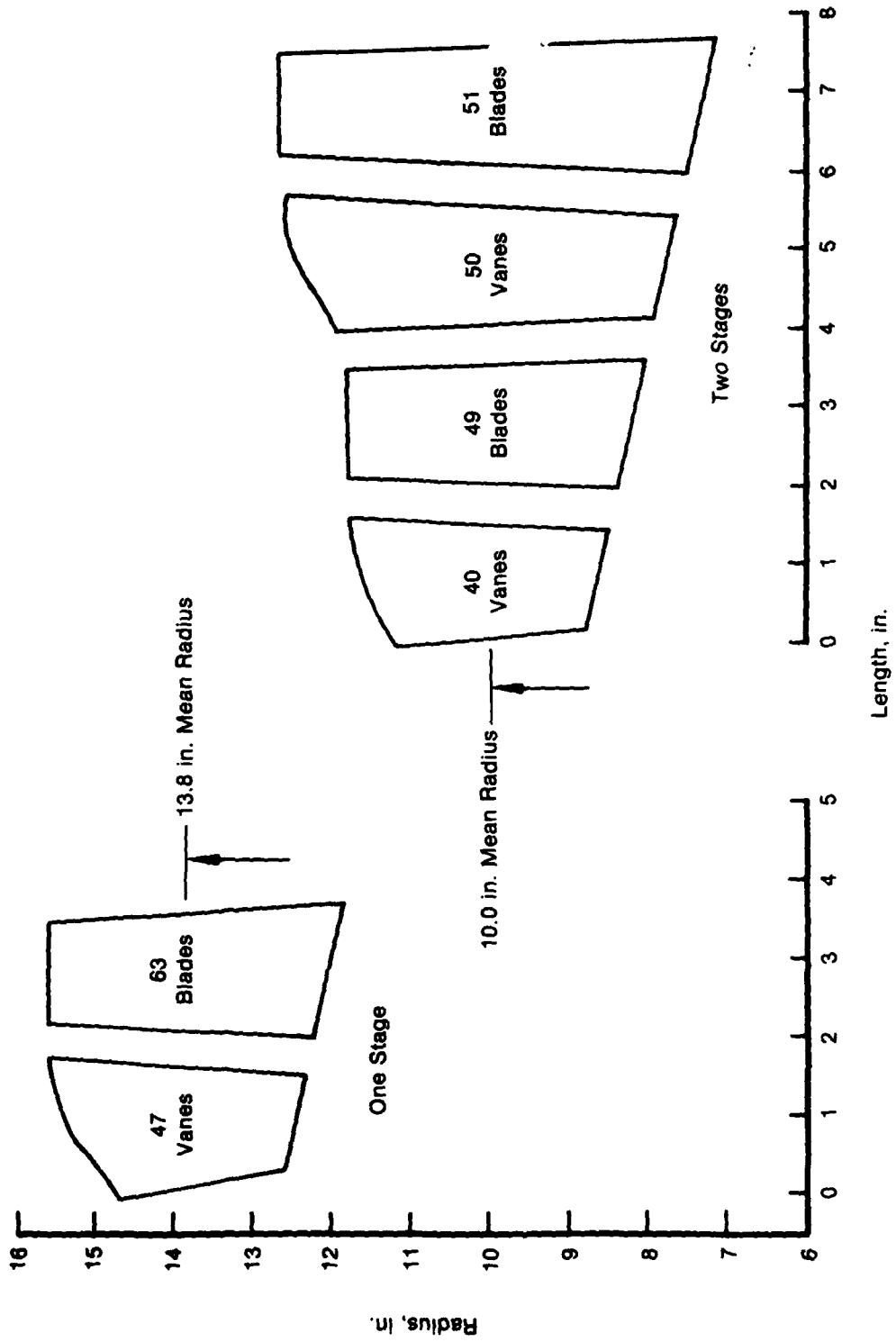
The following table shows the six independent variables and their ranges.

<u>Variable</u>	<u>Range</u>
Mean velocity ratio, dimensionless	0.45-0.65
Exit axial Mach number, dimensionless	0.3-0.6
Fan turbine inlet temperature, °F	1640-2440
Mean axial chord, inches	1.0-2.0
Product of exit annulus area and speed-squared, in ² x rpm ² x 10 ⁻⁸	300-500
Specific work, Btu/lb	70-160



FD 176073

Figure 2-48. Typical HPT Aerodynamic Matrix Results.



FD 164171

Figure 2-49. Typical Low Pressure Turbine Meanline Designs.

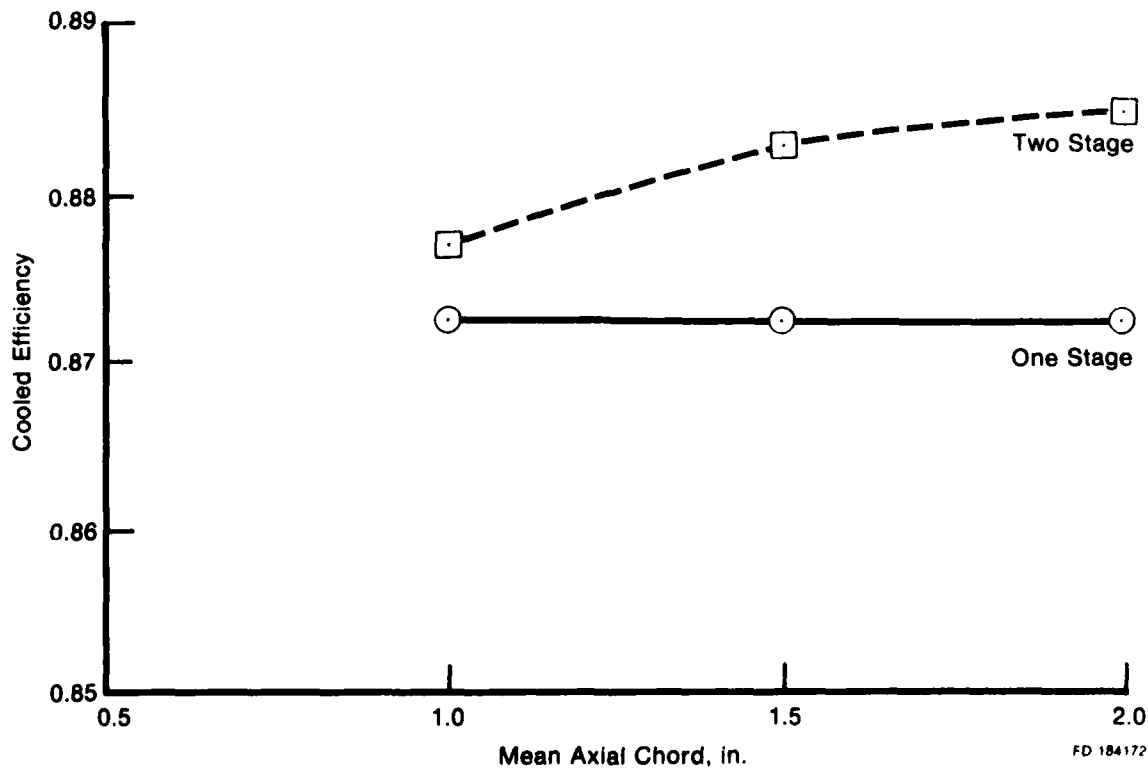
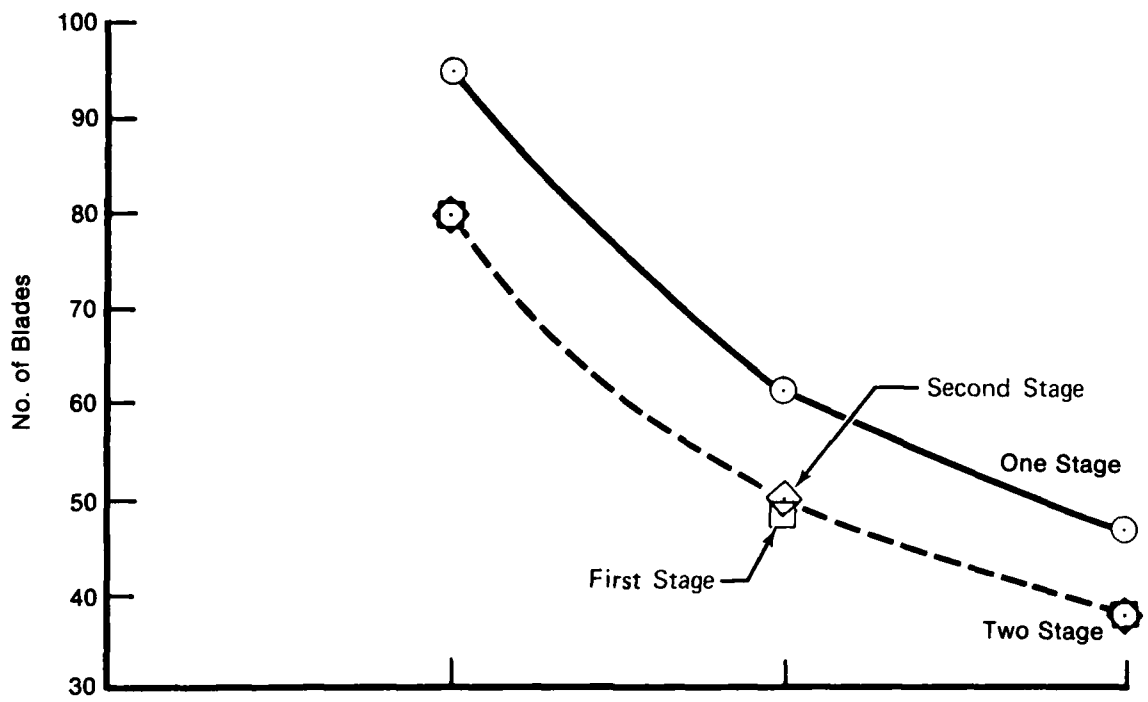
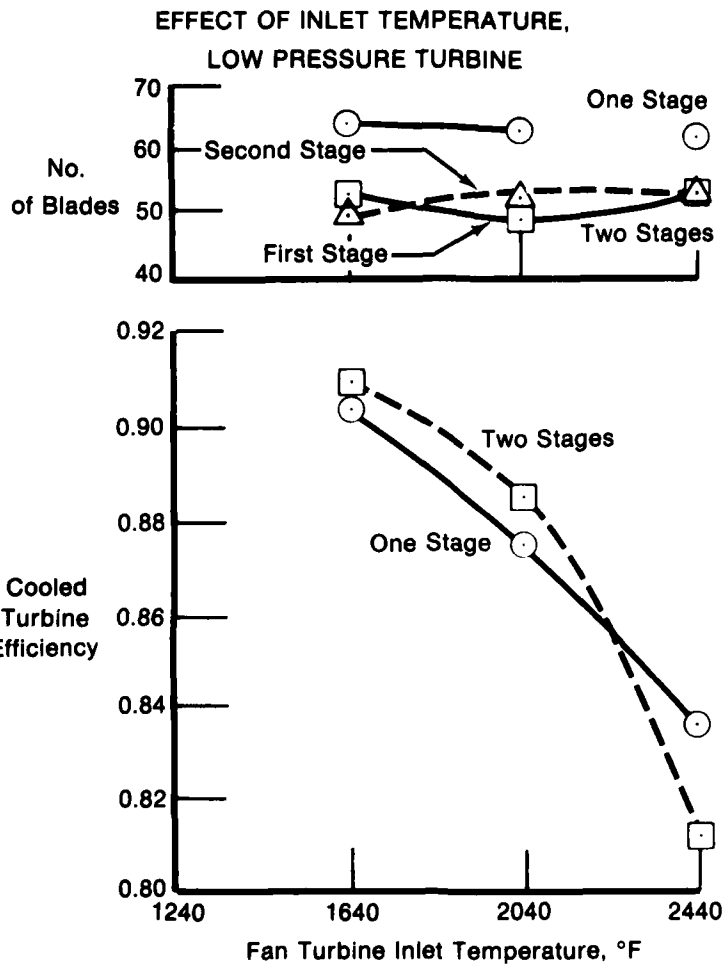
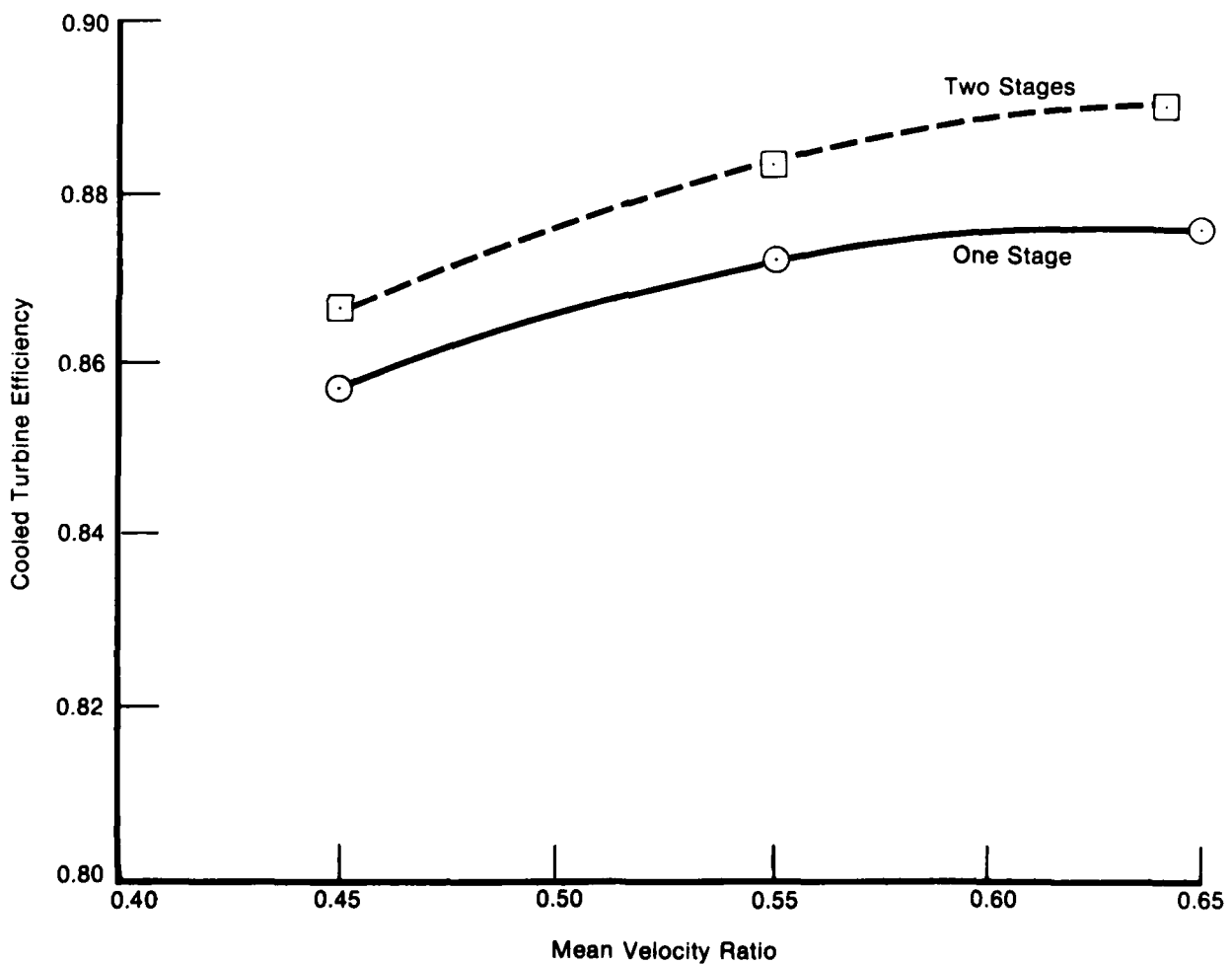
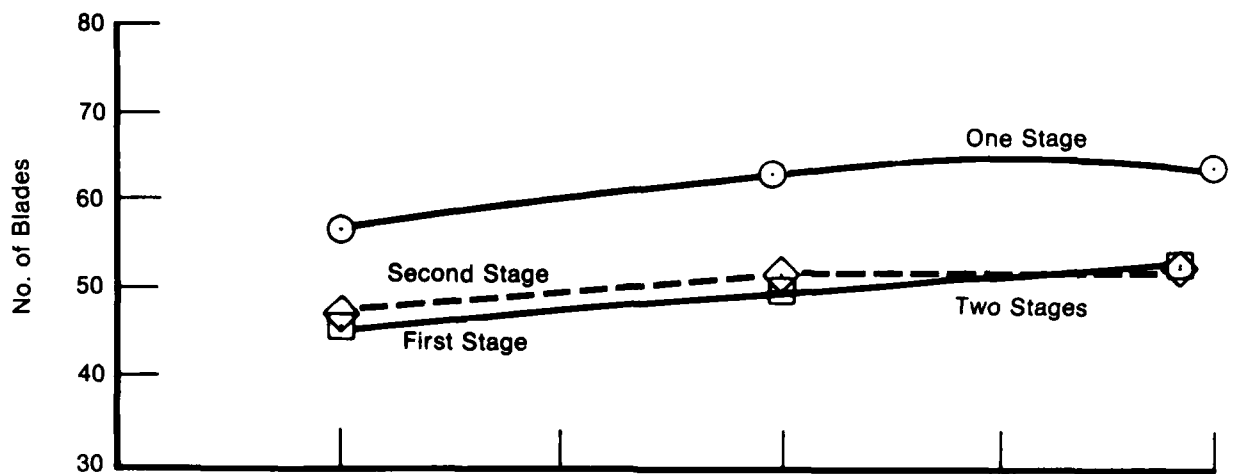


Figure 2-50. Effect of Chord, Low Pressure Turbine.



FD 184174

Figure 2-51. Effect of Inlet Temperature, Low Pressure Turbine.



FD 184173

Figure 2-52. Effect of Mean Velocity Ratio, Low Pressure Turbine.

2.3 WEIGHT PREDICTION ROUTINE

2.3.1 Engine Weight Summary

A key element of the LUCID Life Performance Weight Technique (LPWT) computer-aided design system is the Weight Prediction Routine. The routine builds up component weights for fan, compressor and turbine modules based on selected bladed-disk weights generated by the Life/Stress Deck. The multi-stage fan and compressor weight subroutines utilize weight correlations which estimate total fan rotor weight as a function of the first fan stage wheel weights. The four major component weight subroutines include hubs, shafts, seals and spacers in estimating rotor weights. Module weight is estimated by adding case and stator weights to the rotor weight.

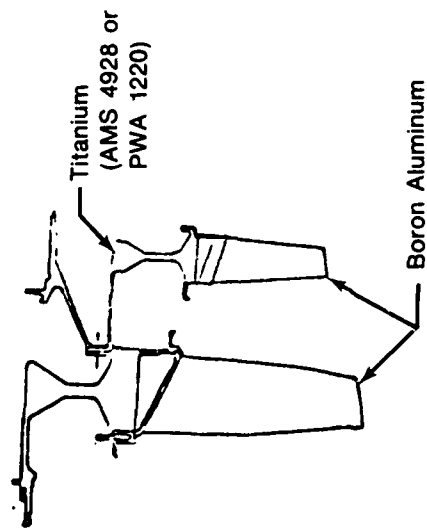
The remaining engine components (diffuser/combustor, augmentor, nozzle, gearbox, plumbing, control, etc.) are added to the major module weights in estimating the total engine weight. Thus the LPWT-generated engine weight reflects the life and utilization for the four key rotating turbomachinery elements of the gas turbine. Typically, the rotor weight comprises 25 to 30 percent of the total engine weight.

The following sections describe the Weight Prediction Routine.

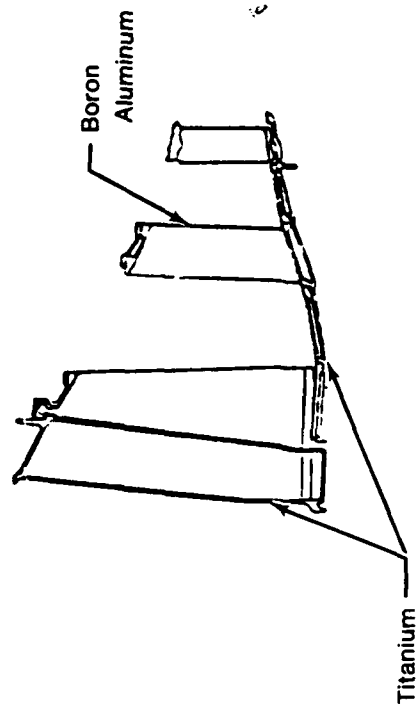
2.3.2 Fan Module Weight

The fan weight subroutine estimates fan weight for one-, two-, and three-stage boron aluminum composite fans for the size and tip speed ranges incorporated in the fan aerodynamic matrix. Figure 2-53 summarizes the mechanical arrangement and materials for a typical two-stage advanced composite fan with an inlet guide vane. Figure 2-54 illustrates the solid composite blade construction, and Figure 2-55 details the solid composite airfoil configuration used in generating the airfoil pull and weight estimates.

Centerline



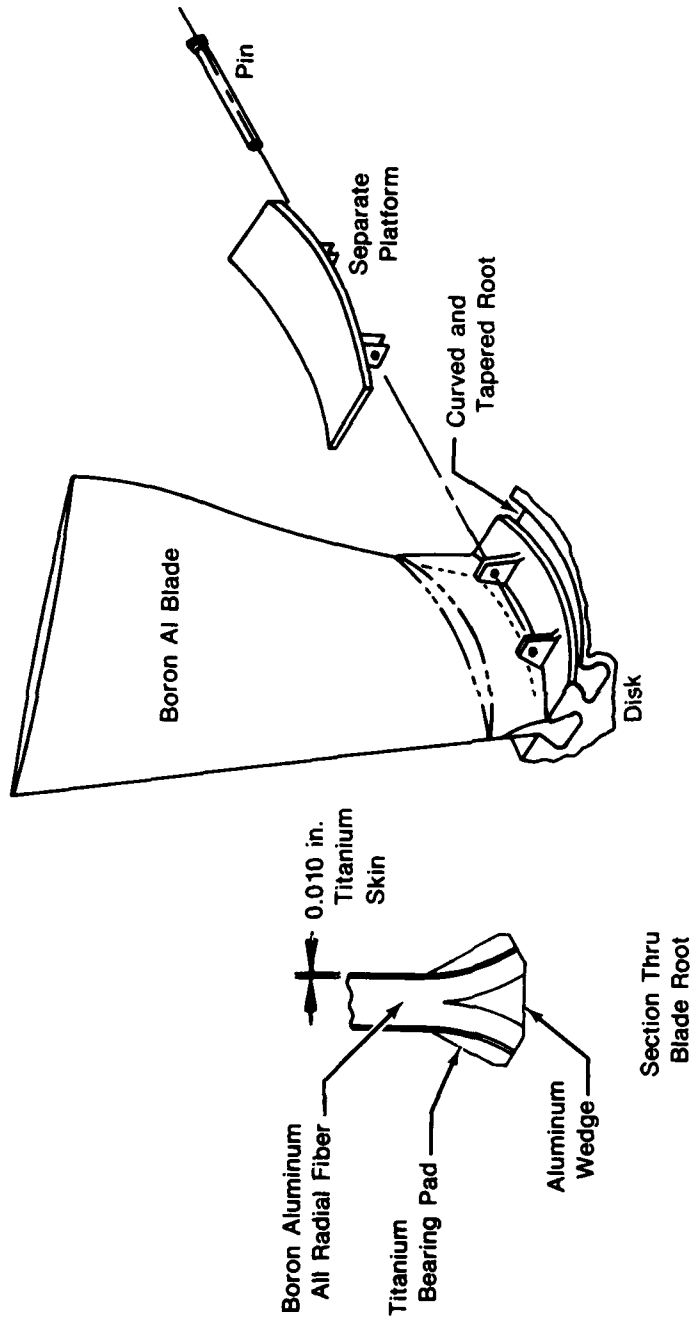
(a) Rotor Components



(b) Stator and Case Components

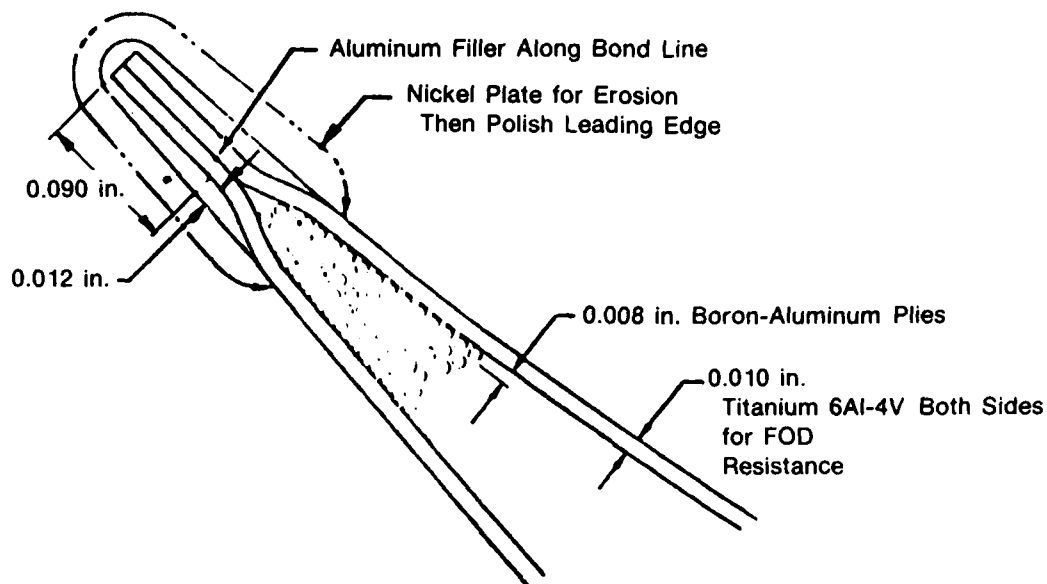
FD 223745

Figure 2-53. Fan Module Components and Materials Summary.



FD 223746

Figure 2-54. Boron Aluminum Solid Composite Fan Blade Construction.



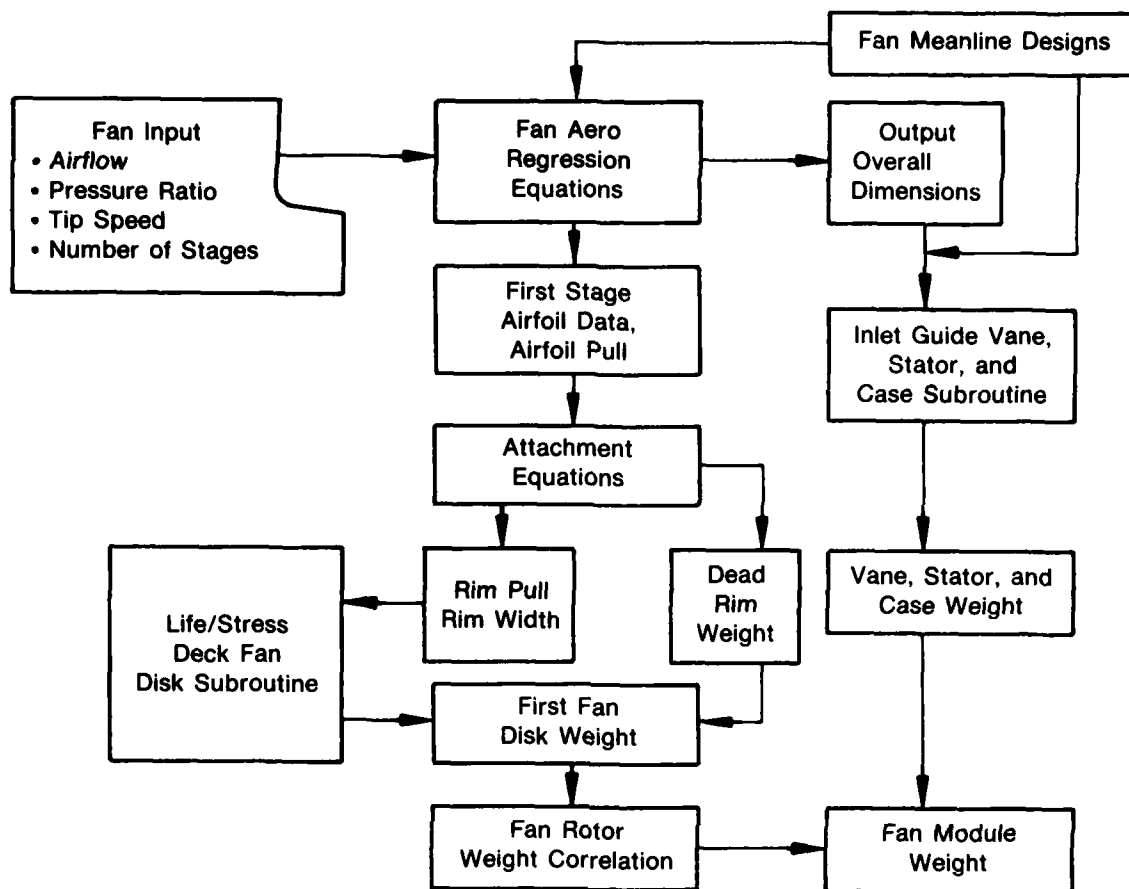
FD 22374

Figure 2-55. Boron Aluminum Solid Composite Airfoil Construction.

Figure 2-56 presents a schematic of the fan weight buildup. A fan definition (pressure ratio, size, and tip speed) drives the calculations. Fan attachment equations generate the disk requirements, and the Life/Stress Deck sizes the first fan disk. The fan rotor weight correlation generates the total fan rotor weight, given the weight of the first stage bladed-disk. Inlet guide vane, stator, and case weights are estimated; these weights and the rotor weight comprise the fan module weight.

Fan stator weights have been estimated for two-stage fans at 1600 feet/second tip speed and 2.3 average aspect ratio (Figure 2-57). Stator weight adjustment factors for tip speed, aspect ratio, and number of stages are shown in Figures 2-58 and 2-59.

Figures 2-60 through 2-63 summarize the fan weight correlation. Figure 2-60 shows the normalized rotor weight as a function of Type I cyclic life capability and fan flow size. The independence of the normalized rotor weight with respect to cyclic life is due to both the normalization and the minor increase in the two wheel weights (see Figure 2-61). The wheel weights do not increase with cyclic life because the composite blade attachment design is for fixed life, and the disk weight response with life is negligible (see Figure 2-62).



FD 223748

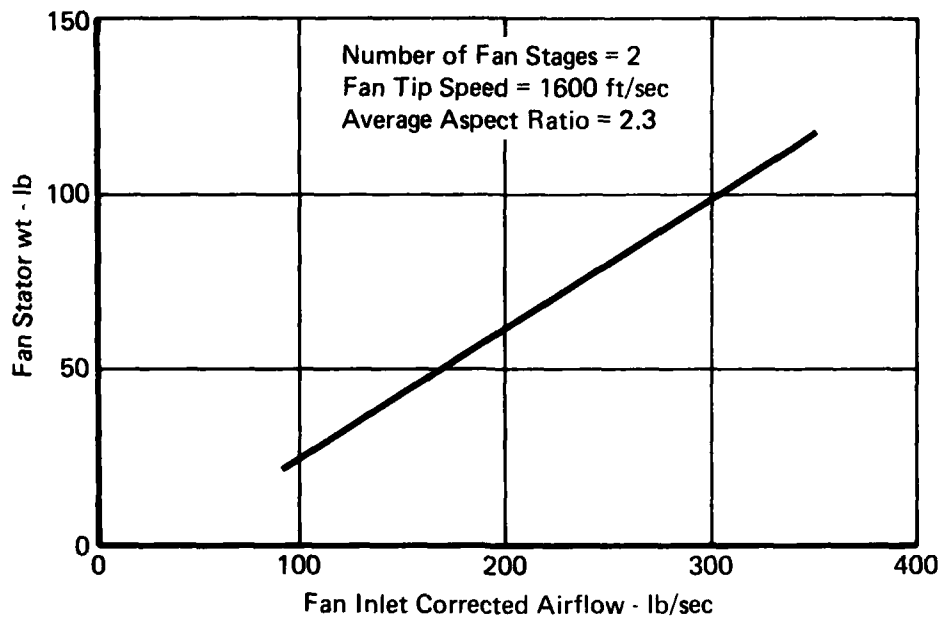
Figure 2-56. Fan Module Weight Subroutine.

The first and second-stage disks are bore fracture mechanics limited, and the weight change due to increasing life is minimal. Figure 2-63 shows the bias curves for average aspect ratio, tip speed, and number of stages.

Fan rotor weight is estimated by the equation shown below.

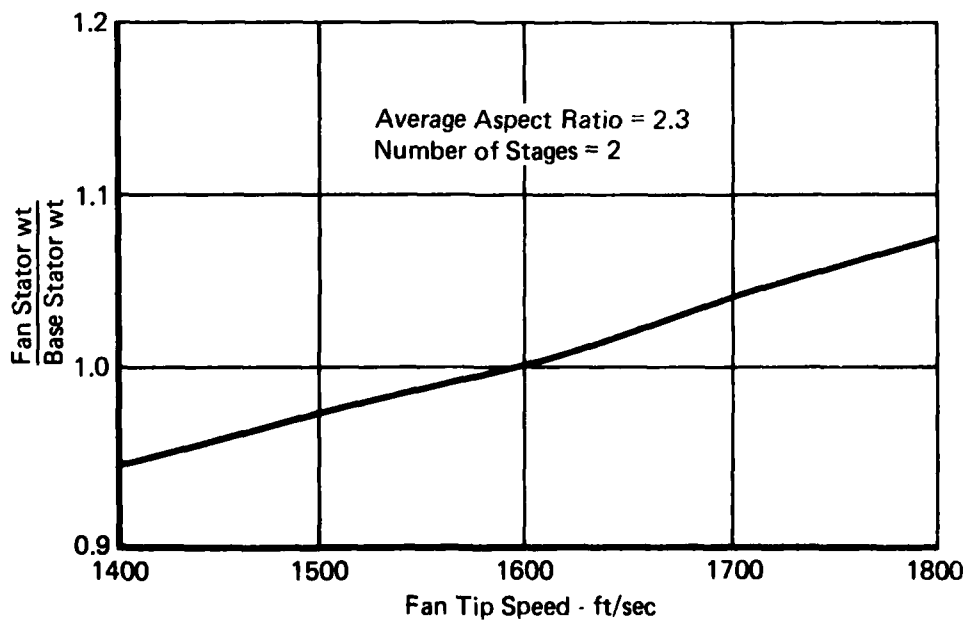
$$\text{Fan Rotor Weight} = (\text{1st Stage Wheel Weight}) (\text{Normalized Rotor Weight})(A)(S)(U)$$

- where (1) 1st stage wheel weight is estimated by LPWT
 (2) Normalized rotor weight (Figure 2-60)
 (3) A = average aspect ratio bias (Figure 2-63)
 (4) S = number of stages bias (Figure 2-63)
 (5) U = tip speed bias (Figure 2-63)



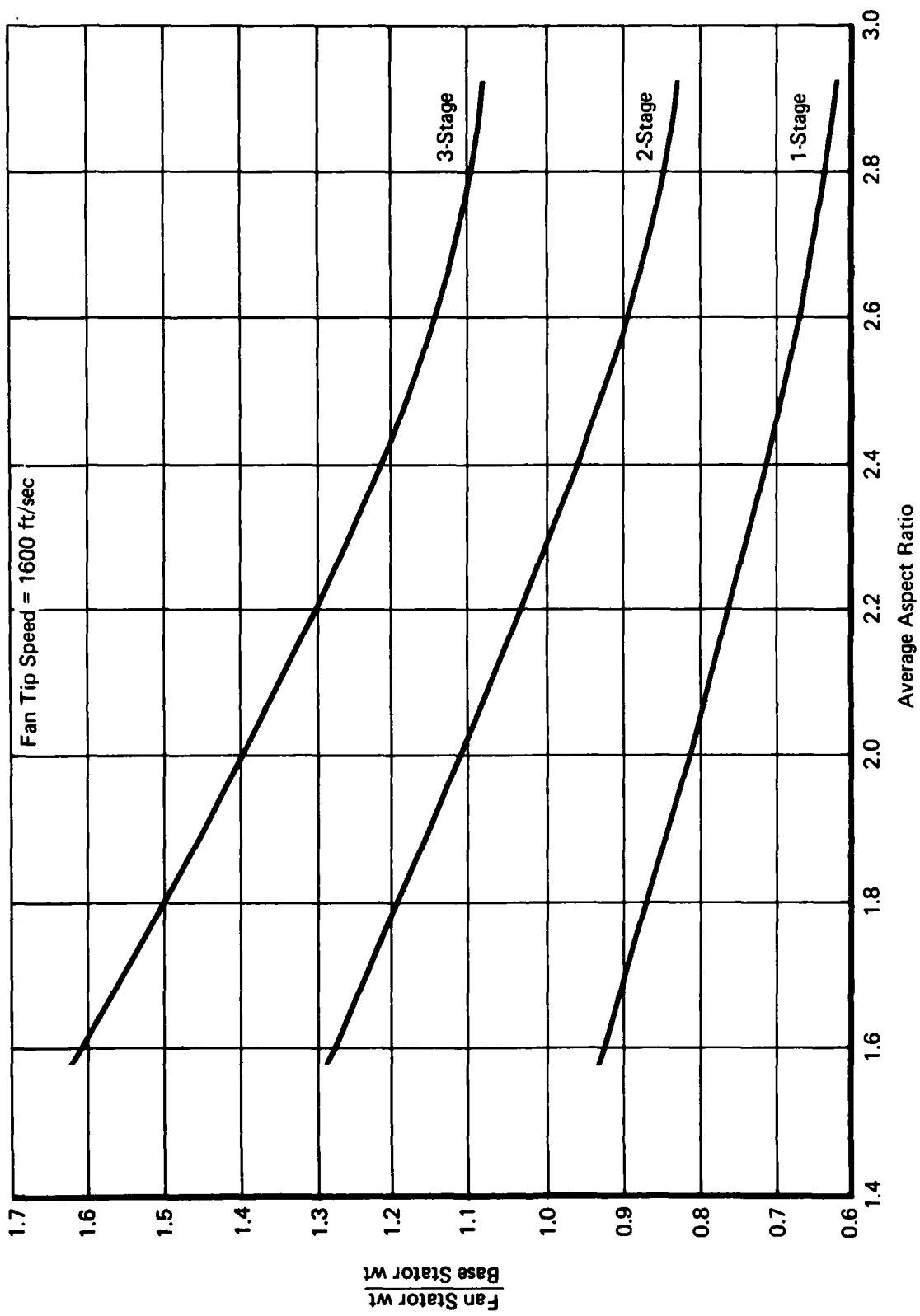
FD 184408

Figure 2-57. Fan Stator Weight as a Function of Size.



FD 184409

Figure 2-58. Relative Fan Stator Weight as a Function of Tip Speed.



FD 184410

Figure 2-59. Relative Fan Stator Weight as a Function of Number of Stages and Average Aspect Ratio.

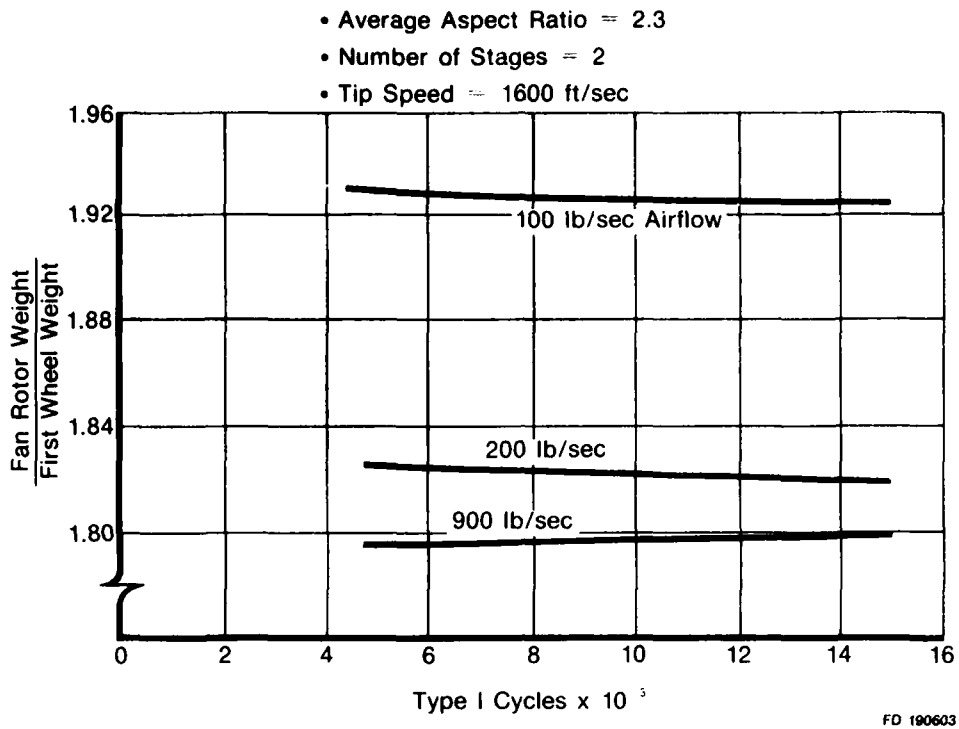


Figure 2-60. Fan Weight Correlation, Normalized Rotor Weight.

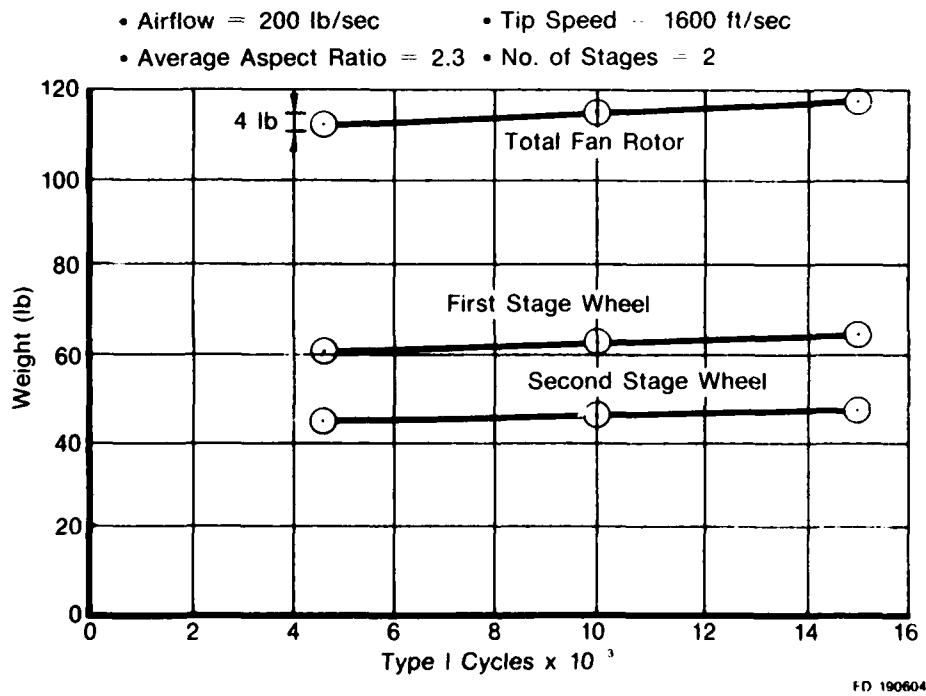
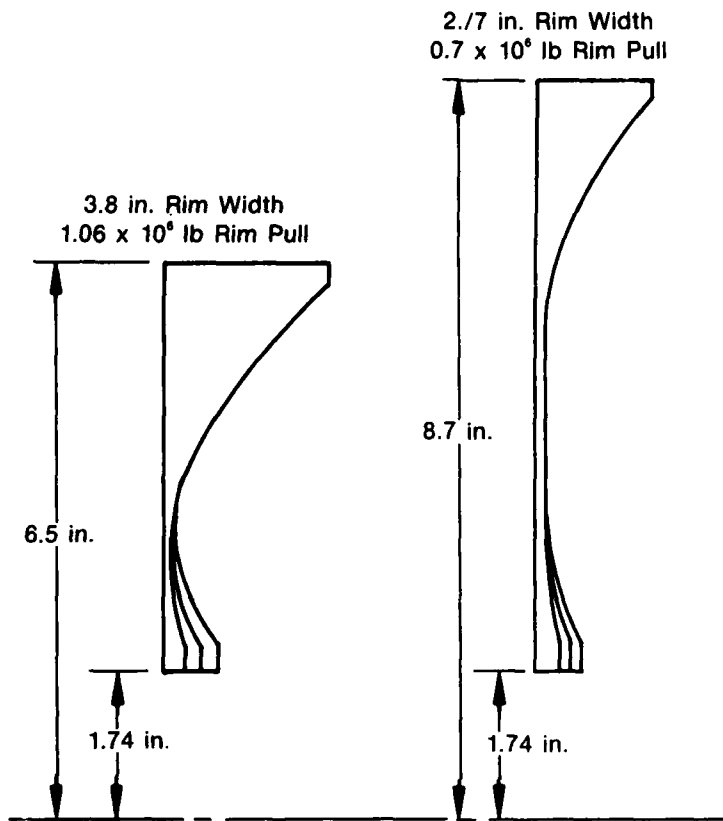


Figure 2-61. Fan Weight Correlation, First and Second Stage Wheel Weights.



	Cyclic Life Capability		
	4,500	10,000	15,000
• First Disk			
Burst Margin (%)	143	147	152.0
Disk Weight (lb)	30.1	31.1	32.4
• Second Disk			
Burst Margin (%)	132	136	139
Disk Weight (lb)	28.6	29.3	30.0

FD 190605

Figure 2-62. Fan Weight Correlation, Disk Weight and Geometry Variation With Cyclic Life Capability.

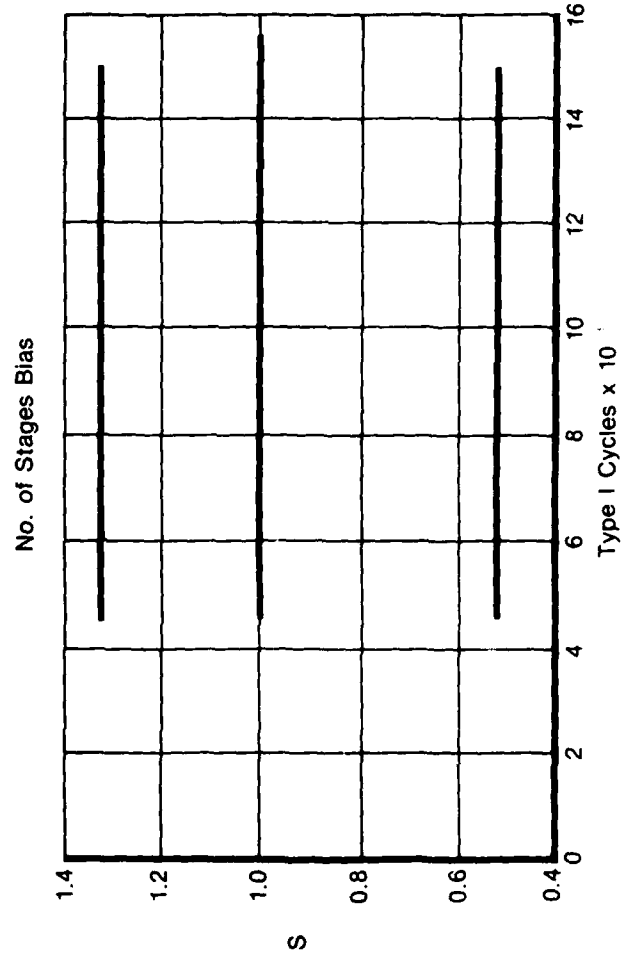
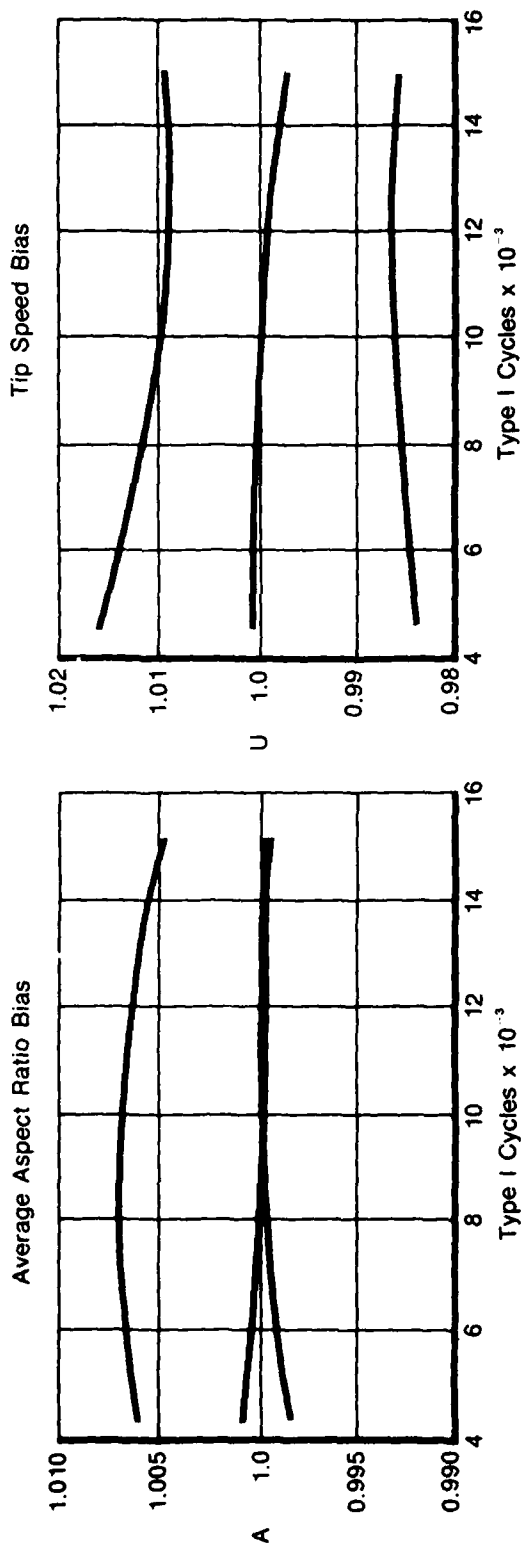


Figure 2-63. Fan Weight Correlation, Bias Curves.

2.3.3 Compressor Module Weight

The LPWT sizes blade disk attachments and disks for the first and next-to-last stages. Similar to the fan weight estimate procedure, the compressor weight subroutine requires a compressor weight correlation. The correlation estimates total compressor rotor weight given the weight of the two LPWT-sized wheels.

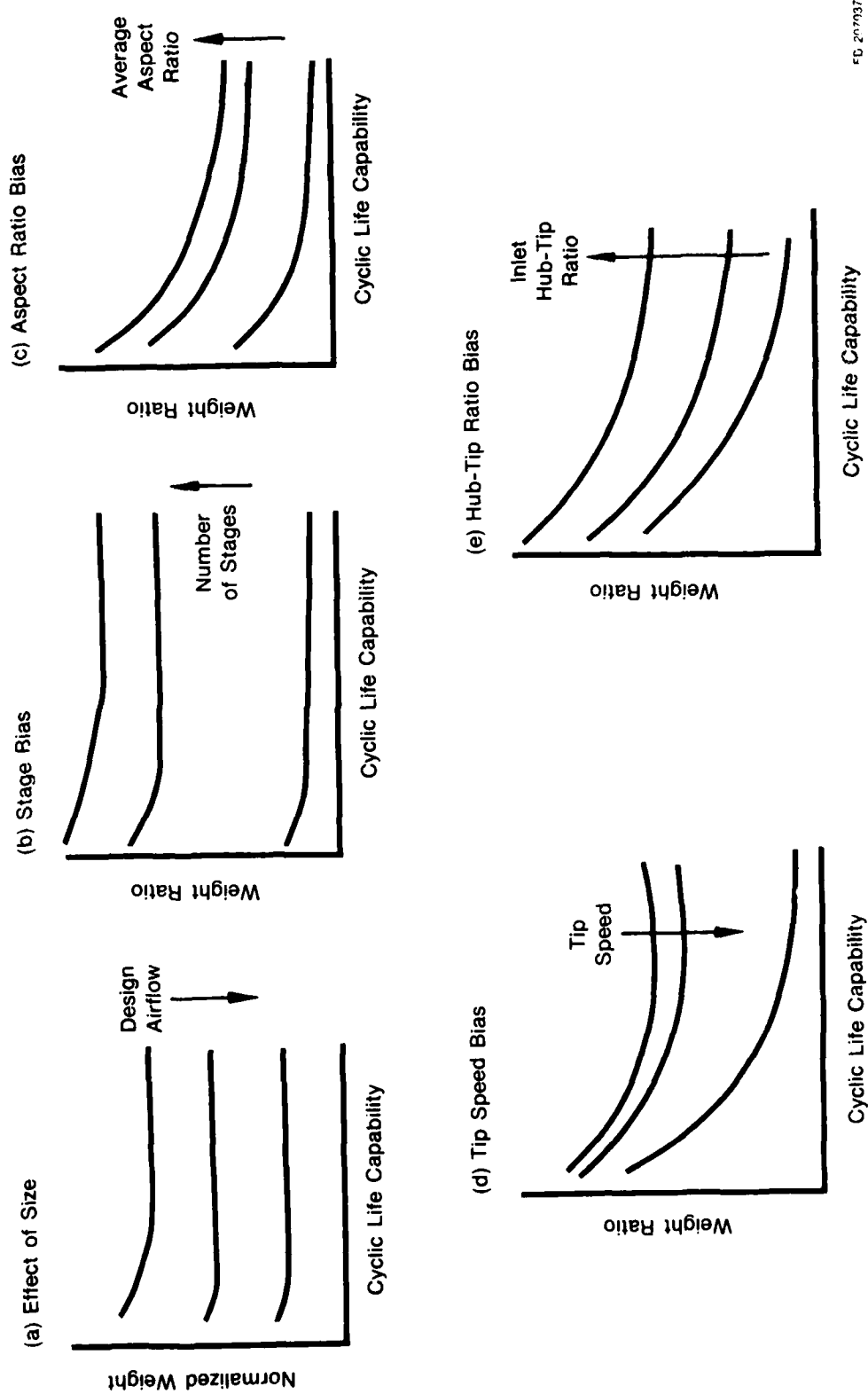
Compressor blade pulls are estimated from output of the compressor aero regression equations. Blade pull is a function of inner and outer blade diameters, mean true chord, airfoil count, and thickness/chord ratio.

Figure 2-64 presents a schematic of the compressor weight correlation basic curve of total weight divided by the sum of first stage and next to last stage wheel weights, and the four bias curves for number of stages, average aspect ratio, corrected tip speed, and inlet hub tip ratio.

The compressor weight routine is complete with the addition of subroutines for estimating vane, case, seals, shaft, and hub weights. These weight routines are functions of pressure ratio, aspect ratio, hub/tip ratio, and size. Figure 2-65 summarizes the sub-components and materials used for the compressor module weight estimates.

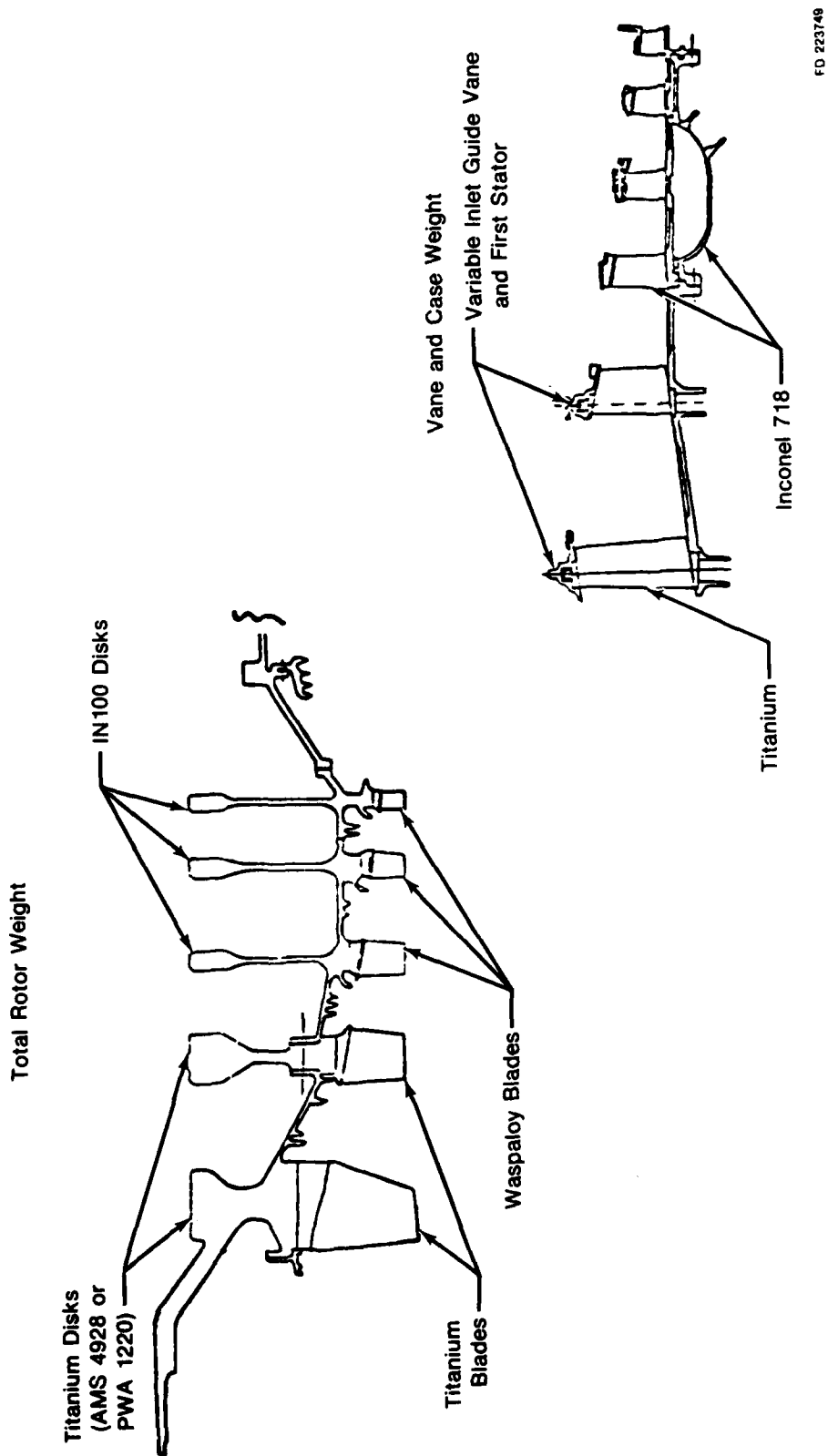
2.3.4 Diffuser/Combustor Weight

Figure 2-66 shows the diffuser/combustor geometries and materials used for estimating weight. The component is broken down into four sub-systems: prediffuser, diffuser dump, rear diffuser and combustor, and fuel nozzles and other hardware. Weights are estimated for the sub-systems; radii, diffuser inlet height, etc. are estimated by subroutines linked to outputs from the engine thermodynamic simulation.



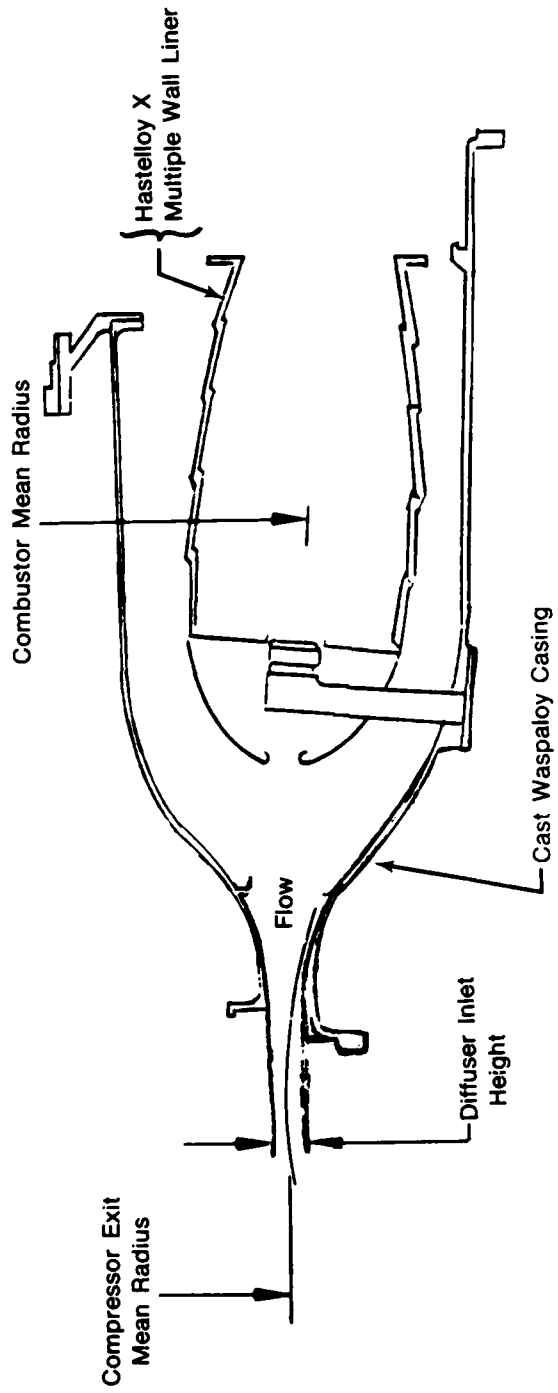
FD 207037

Figure 2-64. Schematic Representation of Compressor Weight Correlation. (Normalized Weight Is Total Rotor Weight Divided by First and Next-to-Last-Stage Wheel Weights).



FD 223749

Figure 2-65. Compressor Module Weight Summary.



FD 223750

Figure 2-66. Materials and Geometric Input for Diffuser/Combustor Weight Prediction.

2.3.5 High and Low Pressure Turbine Weight

The LPWT is currently limited to analysis of single-stage high pressure turbines. Figure 2-67 summarizes the turbine configuration and material assumptions used in generating the turbine module weight. The weight subroutine augments the bladed-disk weight generated by the LPWT with the weight of hubs, seals, and hardware based on known turbine geometries. Inner and outer shroud weight estimating subroutines are based on existing designs, as is the turbine case weight subroutine.

The low pressure turbine weight procedure is similar to the high pressure turbine procedure. Exceptions are that the LPWT has the capability for handling two-stage as well as single stage turbines, and a low shaft weight routine must be added which will interact with the fan module.

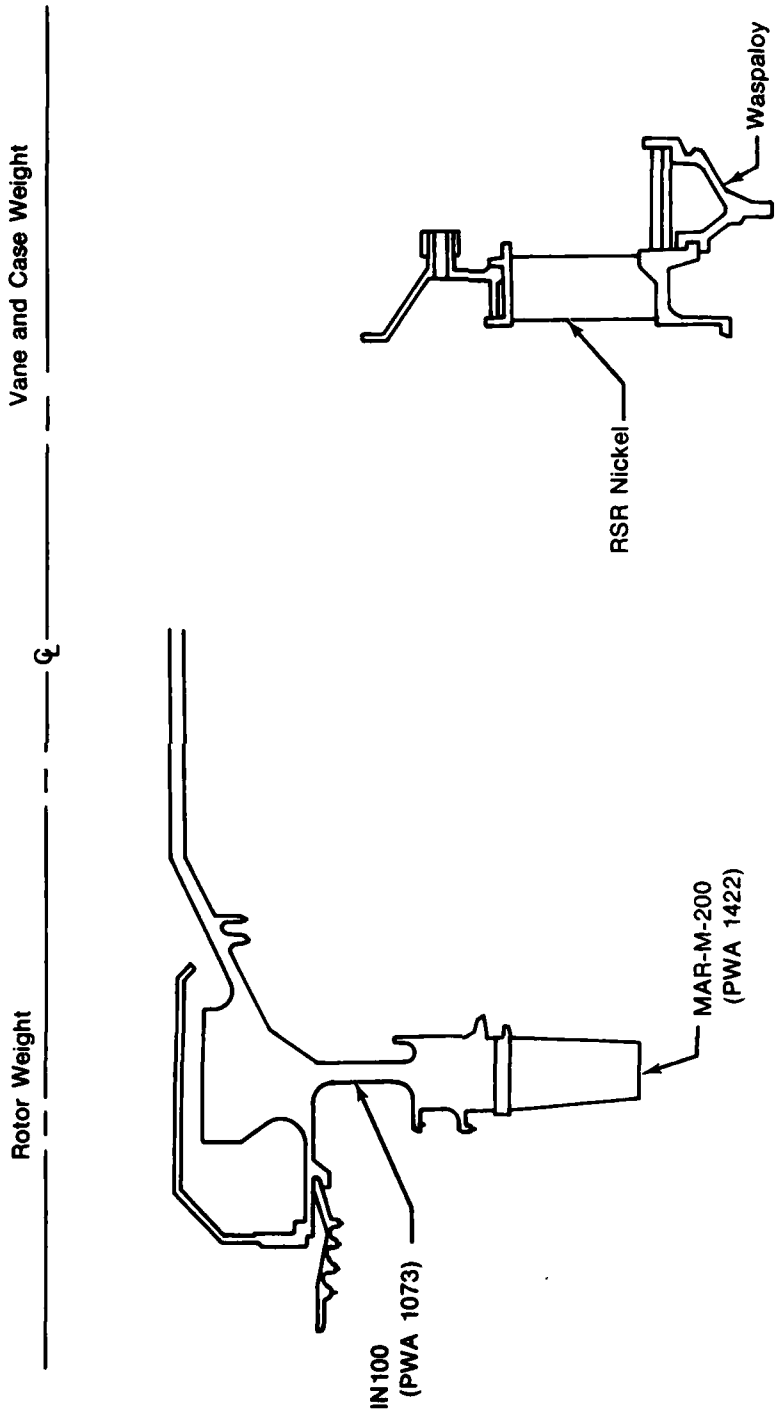
2.3.6 Turbine Exhaust Case

The turbine exhaust case weight routine addresses the components shown in Figure 2-68. Radii are available from the turbine aero regression equations. Exhaust case length is biased with turbine exit axial Mach number.

2.3.7 Augmentor and Nozzle Weights

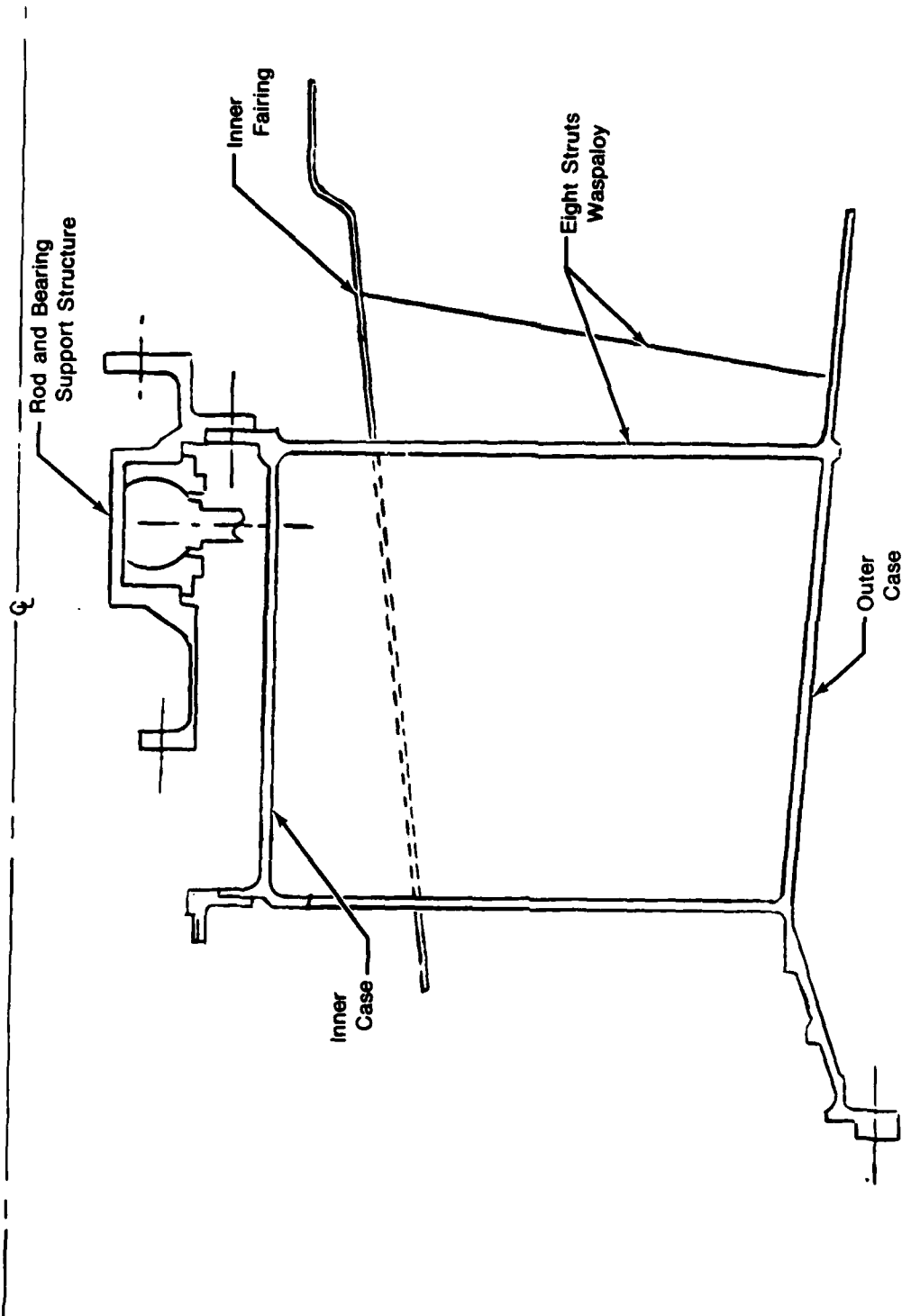
Augmentor components are illustrated in Figure 2-69. Flameholder and spraying weight are estimated as a function of augmentor diameter. The augmentor duct and liner weight subroutines develop the weights as a function of augmentor diameter and engine total airflow.

Figure 2-70 summarizes the balance beam nozzle components and materials used in constructing the nozzle weight subroutine. The general nozzle arrangement is similar to the F100-PW-100 engine. The nozzle weight subroutine develops the weights of each of the six nozzle sub-components as a function of size, nozzle pressure ratio, and nozzle area ratio.



FD 223751

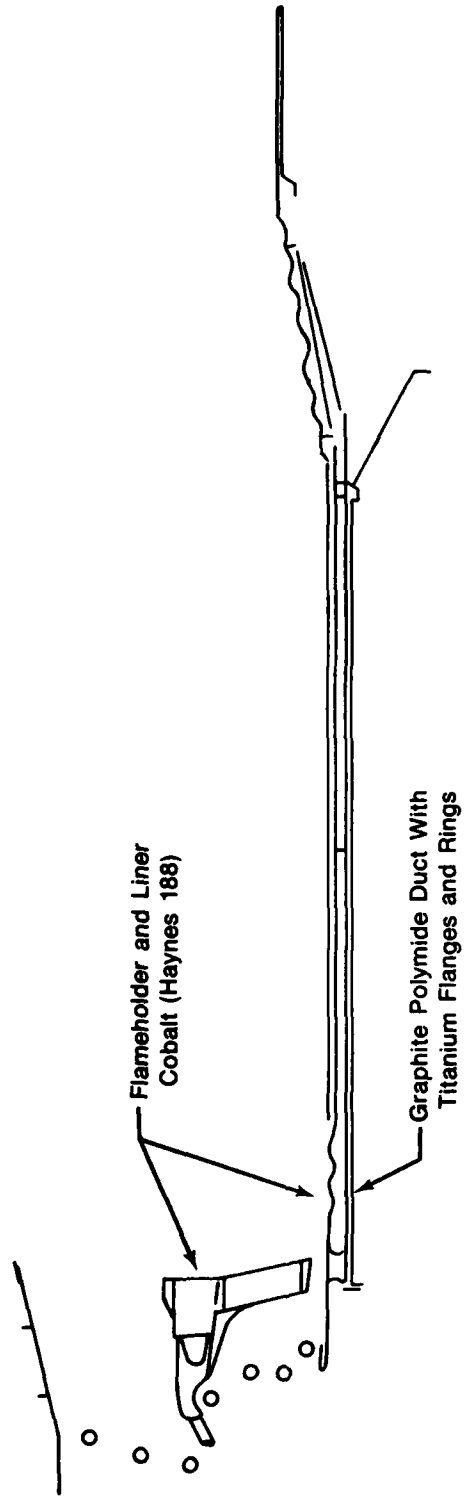
Figure 2-67. High Pressure Turbine Summary.



FD 223752

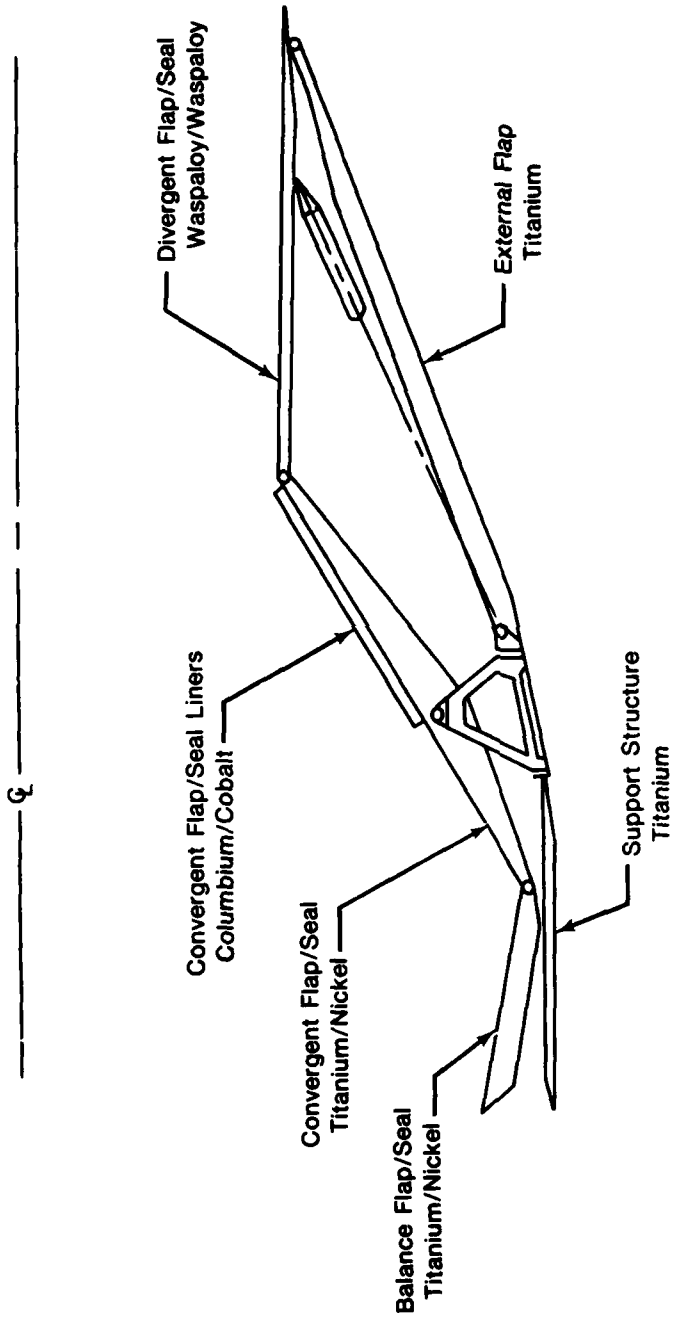
Figure 2-68. Turbine Exhaust Case Components.

6 - - - - -



FD 223753

Figure 2-69. Augmentor Components.



FD 223754

Figure 2-70. Balance Beam Nozzle Component and Material Summary.

2.4 MECHANICAL MATRICES

The mechanical, or attachment and disk matrices required by the LPWT are summarized in Figure 2-71. Four attachment and five disk matrices have been generated (note that one attachment matrix and one disk matrix suffice for the low pressure turbine, whether the turbine has one or two stages).

An example of the mechanical analyses executed by the LPWT is shown in Figure 2-72. Output from the component aerodynamic matrix consists of blade design parameters which specify the blade/disk attachment requirements. The parameters are blade root radius and axial chord, number of blades, and design speed. These parameters, plus blade and disk material properties, life, usage, and material temperatures interact with a matrix of blade/disk attachment designs in the form of regression equations. Similarly, the solution of the attachment problem generates the design parameters (rim width, rim pull, and live rim radius) required for proceeding to the disk design problem.

The following subsections describe the attachment and disk matrices generated for the fan, compressor, and turbine components.

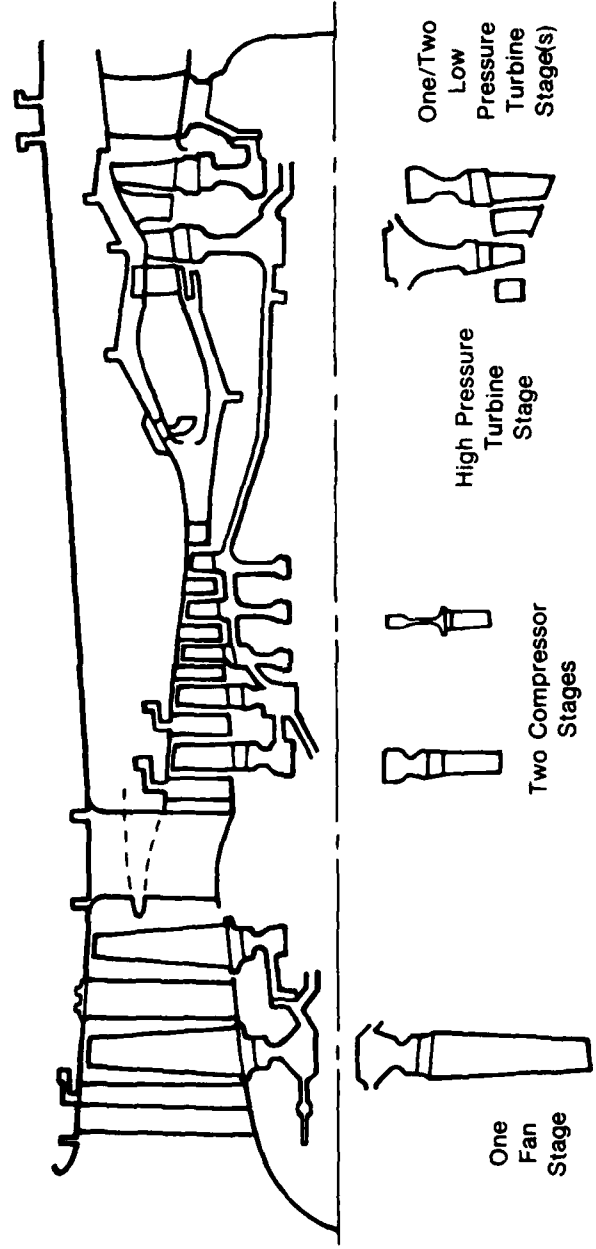
2.4.1 Compressor Blade/Disk Attachments

First and next-to-last stage compressor blade/disk attachment matrix base data generation require 45 base and 10 check designs for each matrix. Tables 2-3 and 2-4 show the independent variables and their ranges.

Fan
 • One Disk

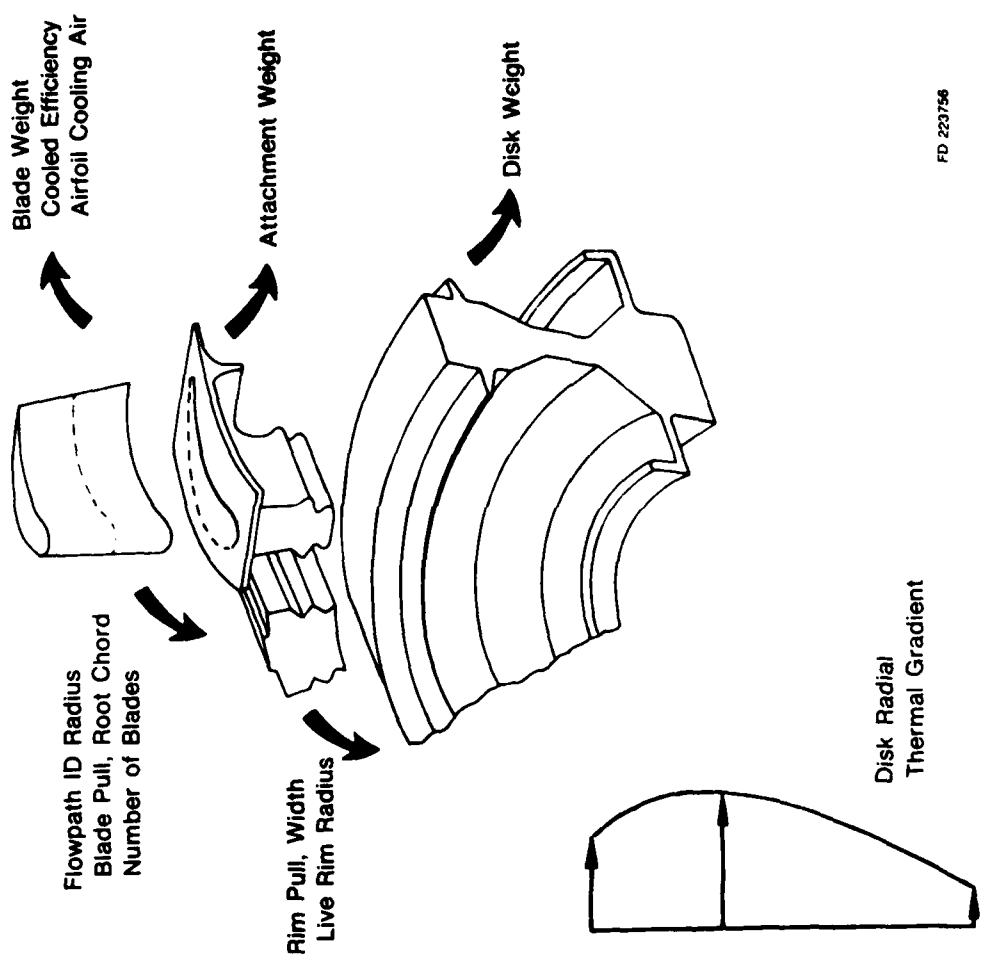
Compressor
 • Two Attachments
 • Two/Three Attachments

Turbines
 • Two Disks
 • Two/Three Disks



FO 223755

Figure 2-71. Summary of Fan, Compressor, and Turbine Attachment and Disk Matrices.



FD 223756

Figure 2-72. Blade Design Data Initiates Sequential Attachment and Disk Solutions (Turbine Example).

TABLE 2-3. FRONT COMPRESSOR ATTACHMENT
INDEPENDENT VARIABLE LEVELS

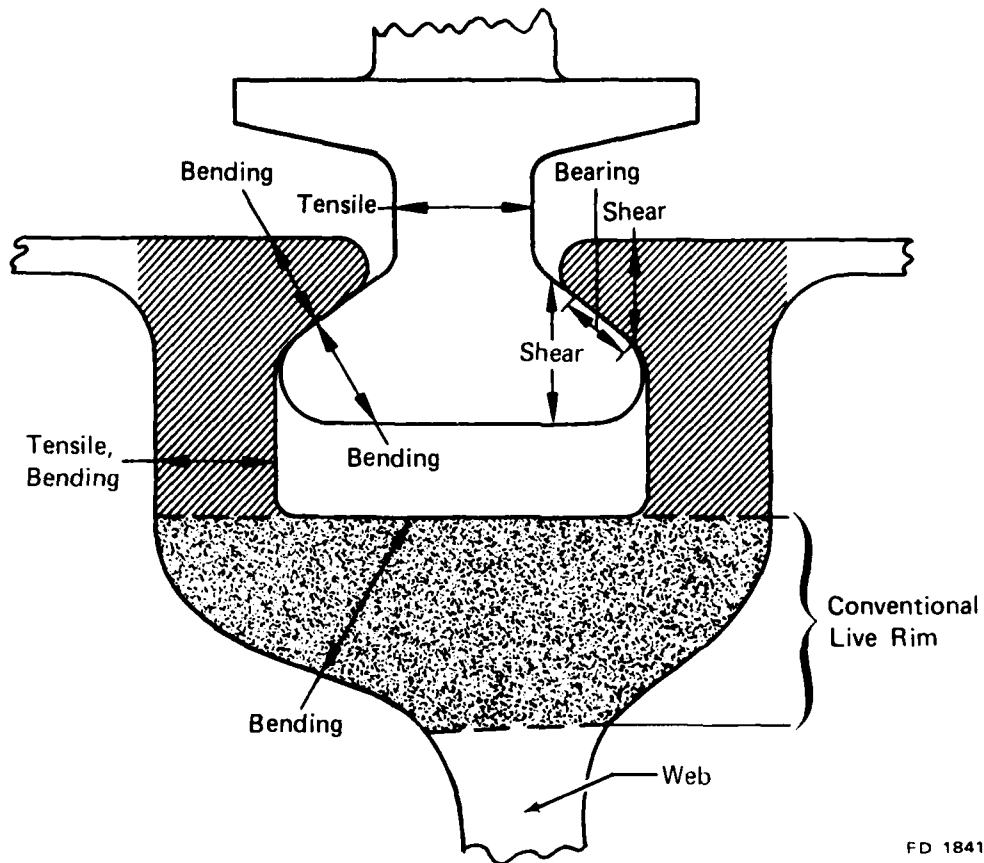
Independent Variable	Range
Rotor Speed, rpm	10,000-30,000
Blade Chord, inches	0.8-3.5
Blade Pull, pounds x 10 ⁻³	4.0-530
Number of Blades	25-80
Flowpath I.D. Radius, inches	4.4-11.8
Yield Strength, ksi	78.-100.

TABLE 2-4. REAR COMPRESSOR ATTACHMENT
INDEPENDENT VARIABLES LEVELS

Independent Variable	Range
Rotor Speed, rpm	10,000-30,000
Blade Chord, inches	0.2-3.6
Blade Pull, pounds x 10 ⁻³	2-571
Number of Blades	50-280
Flowpath I.D. Radius, inches	9.8-22
Stress Rupture Life Capability, hours	200-2,000

The circumferential slot attachment was initially selected as the LUCID baseline rear compressor configuration because projections show that these slots will be used in future engines. A circumferential attachment synthesis program was developed which partially fulfills LUCID LPWT requirements; however, the circumferential attachment synthesis program is not currently suitable for this use. The program has the capability to synthesize a minimum weight attachment by optimizing the stresses shown in Figure 2-73. The attachment program establishes the geometries of what is commonly termed the live rim (shaded portion of Figure 2-73). There is no dead rim in the usual sense, because all of the rim can carry hoop stress. The cross-hatched portions of the disk are not part of the usual live rim geometry, and the disk synthesis program does not include it as part of the live rim. The cross-hatched portions carry hoop stress but, as they are beyond the self-sustaining radius, their pull contribution varies with rotational speed and material capability. Therefore, the

circumferential slot attachment synthesis program is incompatible with the disk synthesis program, in that the attachment synthesis program cannot specify a rim pull, and both programs are constructed to determine rim geometry.



FD 184179

Figure 2-73. Compressor Blade/Disk Circumferential Attachment.

Two alternatives, further development of the circumferential attachment synthesis program, and reversion to the axial broach blade/disk attachment synthesis program were explored, and the second approach was selected. A study of axial broach versus circumferential slot attachments shows a stand-off between the weights of the two configurations (1.5 pounds each, with the axial attachment three-stage drum being marginally lighter).

Figures 2-74 and 2-75 show the effects of total blade pull, material yield strength, blade mean axial chord, and number of blades on rim pull and rim width for the front compressor blade/disk attachment. Similar plots are not shown for the rear compressor attachment due to the skewing of independent variable levels required to complete the matrix.

Compressor blade/disk attachments are typically not low cycle fatigue life limited. Therefore low cycle fatigue life capability was not included in the two compressor attachment matrices. The next-to-last stage attachment matrix life and stress driving independent variable is stress rupture life capability, while the first stage matrix uses material yield strength to drive geometry and stress levels since temperature levels are insufficient to cause stress rupture problems.

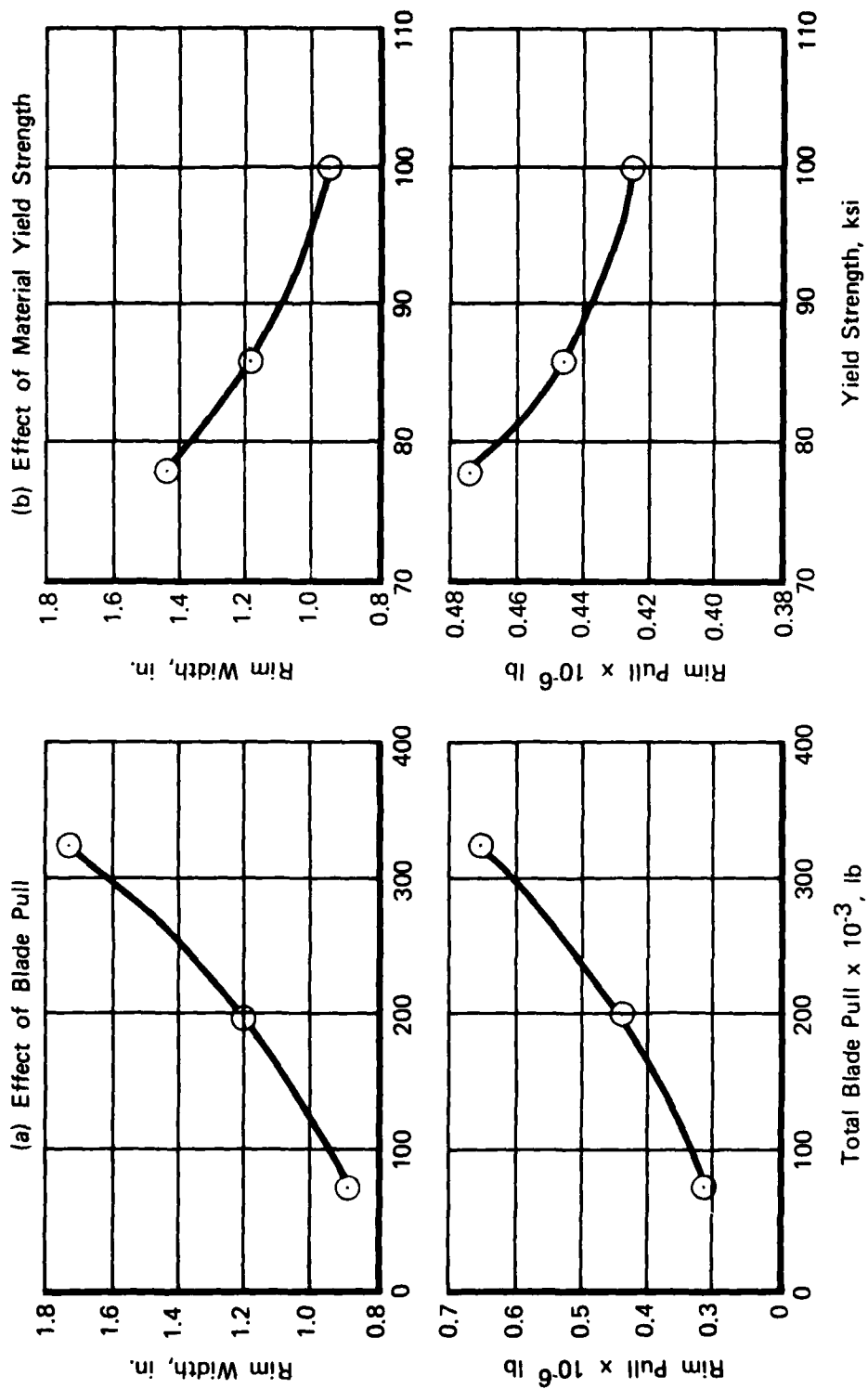
2.4.2 High Pressure Turbine Blade/Disk Attachment

In arriving at the final matrix of designs to be generated for the high pressure turbine (HPT) blade/disk attachment, several preliminary studies were conducted. These studies addressed the blade root cooling hole area and the number of teeth.

2.4.2.1 Cooling Hole Area A survey of existing blade designs was conducted, with the objective of eliminating cooling hole area from the set of independent variables, thus simplifying the overall effort.

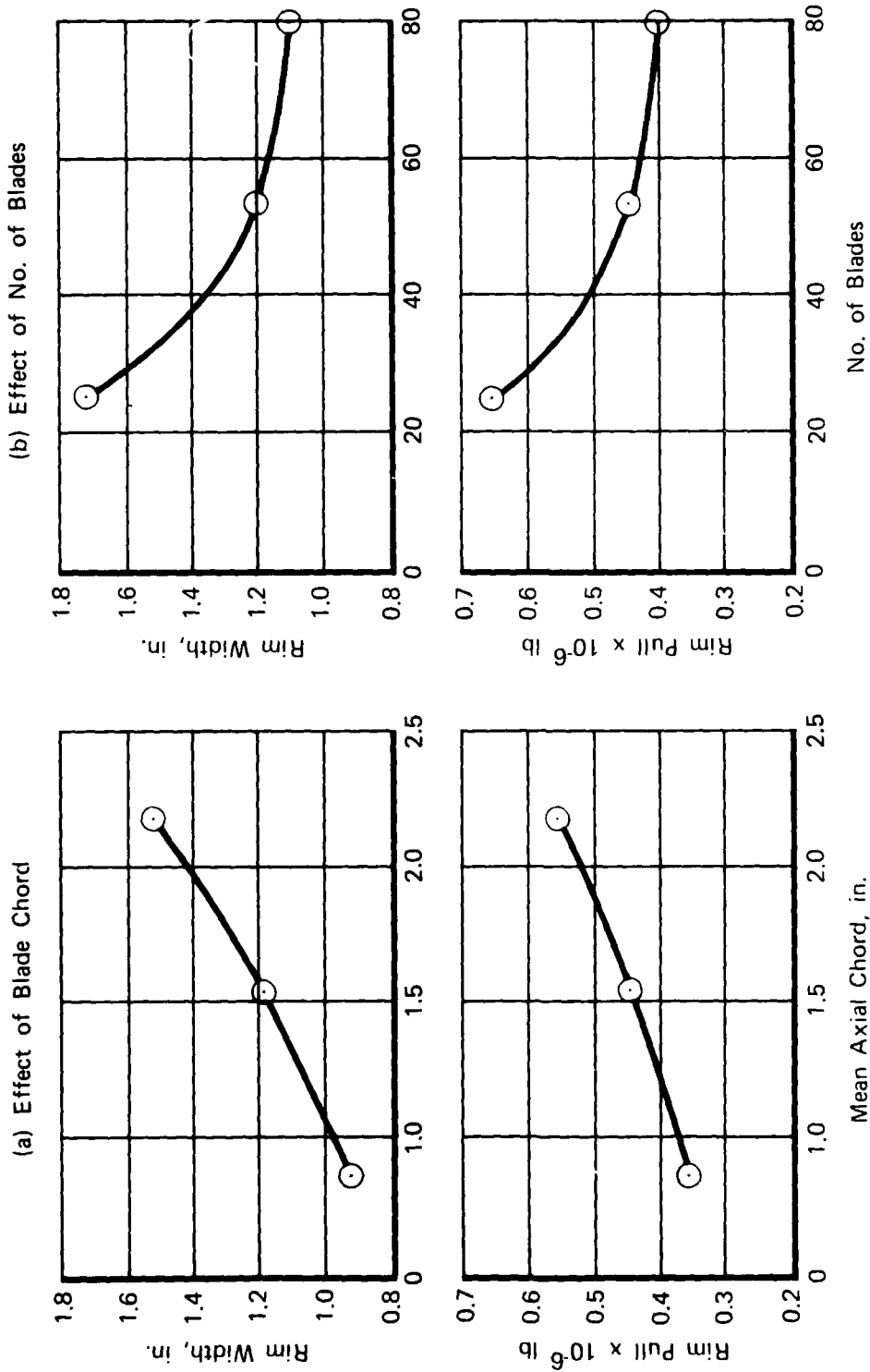
Figure 2-76 shows that for a number of existing engines and advanced designs, a tenfold increase in cooling flow only doubles the cooling flow area. Figure 2-77 shows the coolant mach numbers in the blade root for these designs (circles). The mach numbers are low because coolant flow is metered elsewhere in the engine. Also shown (as crosses) are the coolant Mach numbers which would result if the

root core area
root sweep area were made 0.06 for all designs. This would produce a maximum mach number of 0.2, which is not excessive.



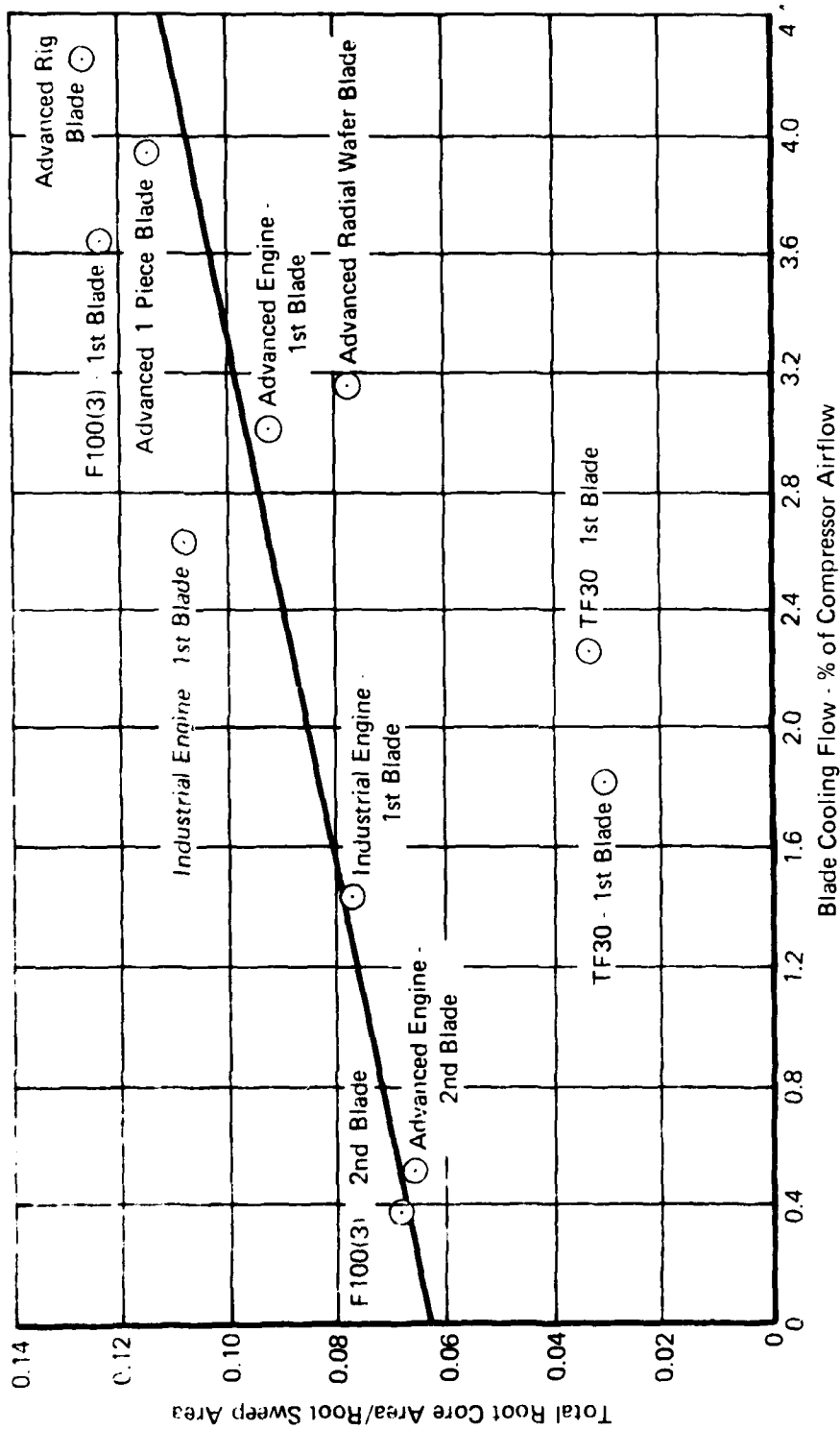
FD 193264
802804

Figure 2-74. Typical Results of Front Compressor Blade/Disk Attachment Matrix Designs.



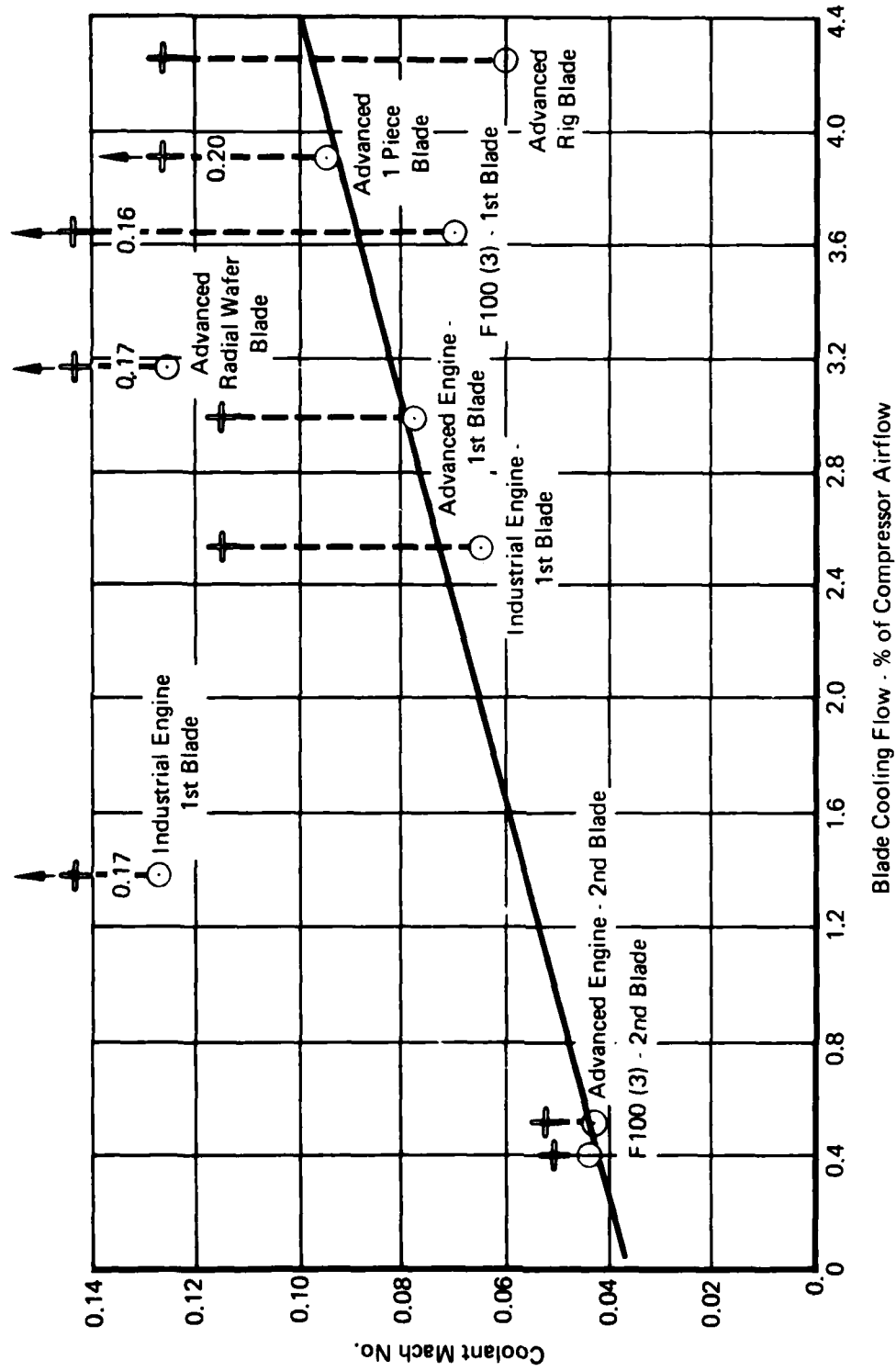
FD 193265
802804

Figure 2-75. Typical Results of Front Compressor Blade/Disk Matrix Design.



FD 184160
801701

Figure 2-76. Sensitivity of Cooling Hole Area to Cooling Flow.



FD 184161
801701

Figure 2-77. Sensitivity of Coolant Mach Number to Cooling Flow.

Since the coolant system is not sensitive to cooling hole area, it can be eliminated as a parameter without significant impact on LUCID results. This will make the LPWT more efficient and reduce computer costs.

2.4.2.2 Number of Teeth Table 2-5 shows the independent variables and their ranges of values for the HPT blade/disk attachment matrix. The rotor speed range reflects the thrust class range requirement (10,000 to 30,000 pounds augmented thrust) and ranges in aerodynamic spool parameters. This thrust range (and associated rotor speed) is large, and as a result, levels of the independent variables (except for life capability) must be skewed. Further skewing of two independent variable levels (rotor speed and total blade pull) was required to produce feasible structural designs. The seventy-nine attachment designs required for a one-half replicate of the Central Composite Design have been run for 2-tooth and 3-tooth attachments.

TABLE 2-5. HIGH PRESSURE TURBINE BLADE/DISK ATTACHMENT INDEPENDENT VARIABLE LEVELS

Independent Variable	Range
Rotor Speed, rpm	6,500 to 30,000
Blade mean axial chord, inches	1.0 to 2.8
Number of blades	2.0 to 105
Total blade pull, pounds x 10 ⁻⁶	0.4 to 4
Stress rupture life capability, hours	200 to 2,000
Low cycle fatigue life capability, cycles	1,000 to 15,000
Flowpath inside radius, inches	3.8 to 30

Three parameters, total rim load, live rim radius and rim width, were selected for comparing 2-tooth and 3-tooth attachments for the following reasons:

- o The higher the total rim pull, for a given set of blade airfoils, the heavier the disk must be to carry the load (low rim pull is goodness).

- o The larger the live rim radius, for a given gas path inner diameter, the lower the dead rim weight will be (large live rim diameter is goodness).
- o If a rim width limit is set, it will give some indication of the life capability difference in 2- and 3-tooth attachments (high life capability is goodness).

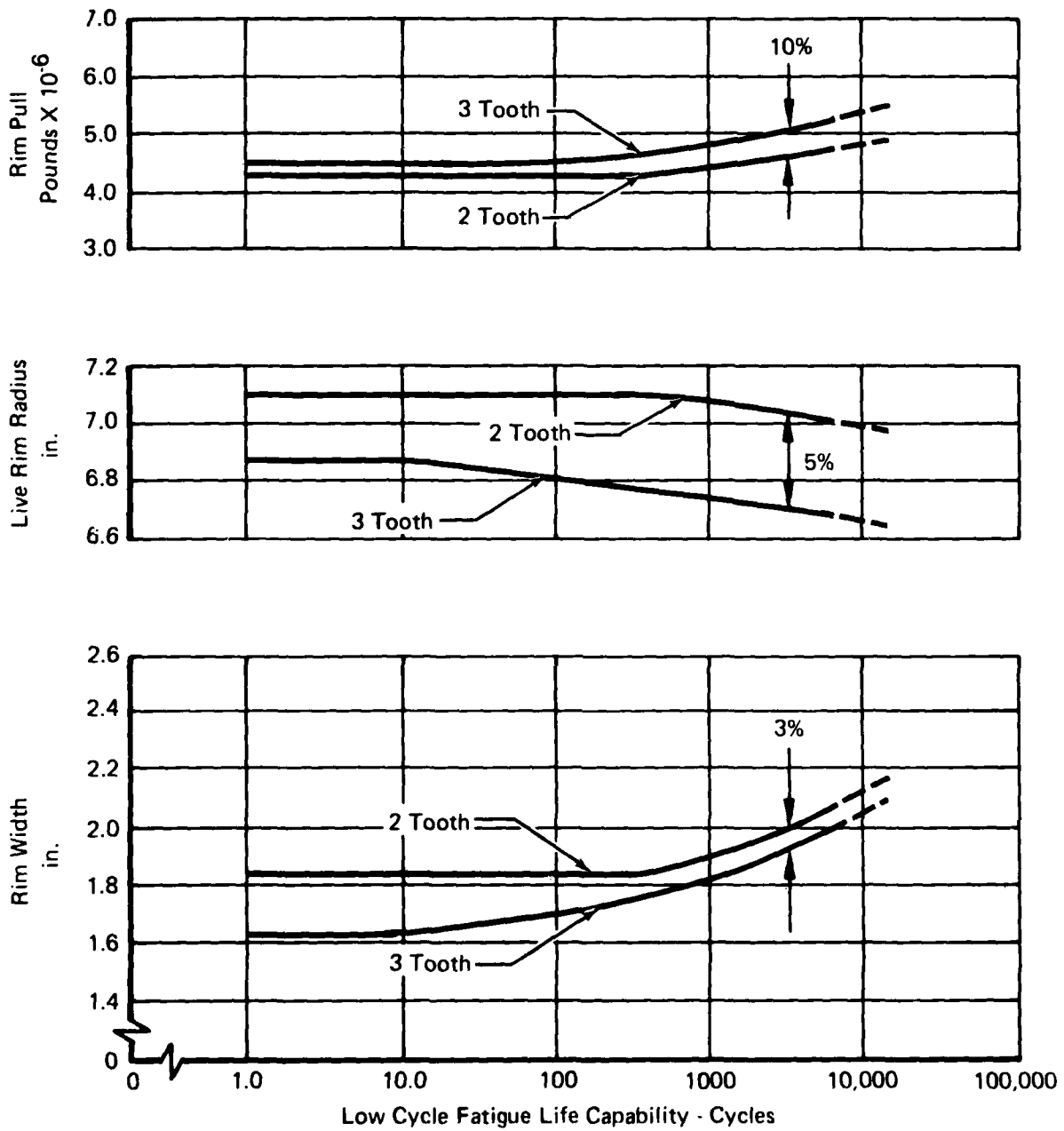
The effects on the above parameters of low cycle fatigue life requirement, stress rupture life requirement, number of blades and blade pull have been evaluated. Plots of the effects are given in Figures 2-78 through 2-81. These figures show that 2-tooth attachments produce lower rim pulls (goodness) and larger live rim radii (goodness) than 3-tooth attachments. Rim width is less (goodness) for 3-tooth attachments.

The rim width trend indicates that under extreme conditions a 3-tooth attachment might have a life advantage over a 2-tooth. However, over the life range in the matrices, the 2-tooth has the same life capability as the 3-tooth with less weight. Therefore, only 2-tooth HPT attachments were generated in the LPWT turbine attachment matrices.

2.4.2.3 Matrix Design Generation

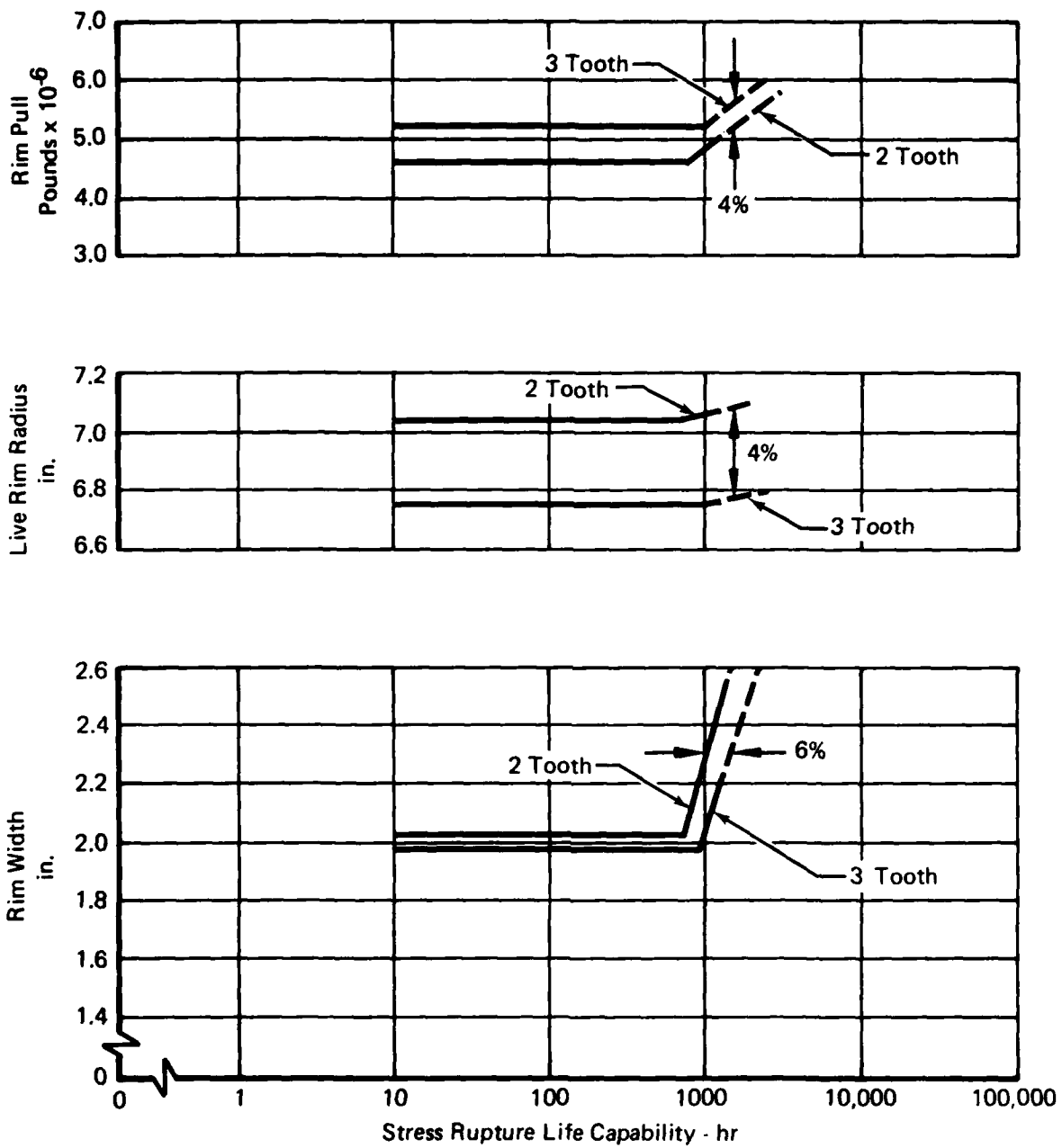
The 79 point designs for the two tooth HPT attachment matrix were generated for equal blade root and disk lug lives (or blade/disk life ratio of 1.0). To determine the effect of a reduced life ratio, 21 selected-point designs were synthesized with life ratios of 0.5 and 0.33. The effects on total rim pull, live rim radius and rim width are shown in Figure 2-82. There is no effect on live rim radius. There is a small effect (about 5 percent) on pull and rim width for most of the cases.

Life is not considered in composite fan attachments and is not a problem in compressor attachments. Should lower life ratios be desired for turbine attachments, corrections will be made to pull and rim width based on a correlation of trends illustrated in Figure 2-82.



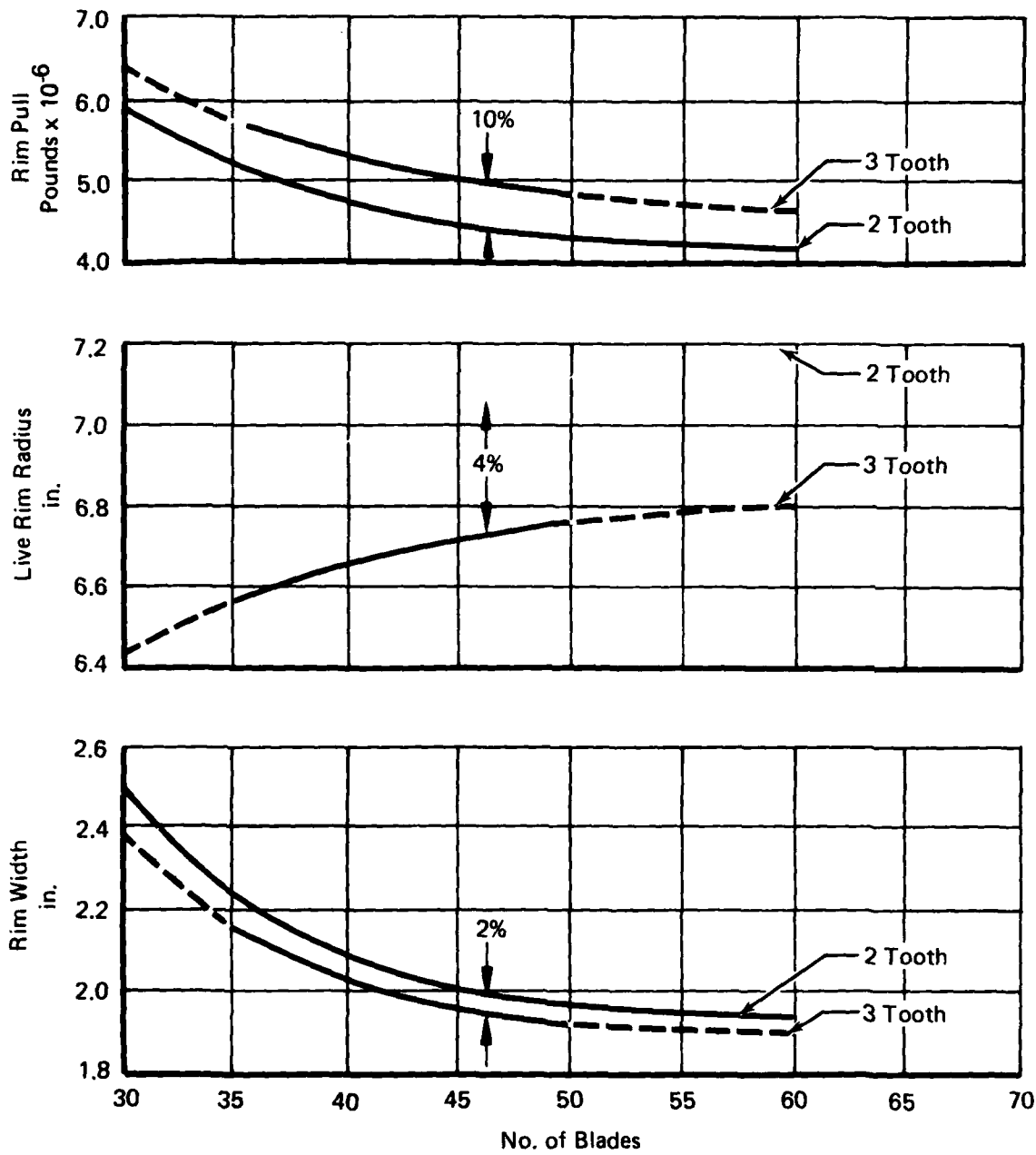
FD 18415-8
801/01

Figure 2-78. Effect of LCF Life on the Turbine Attachment.



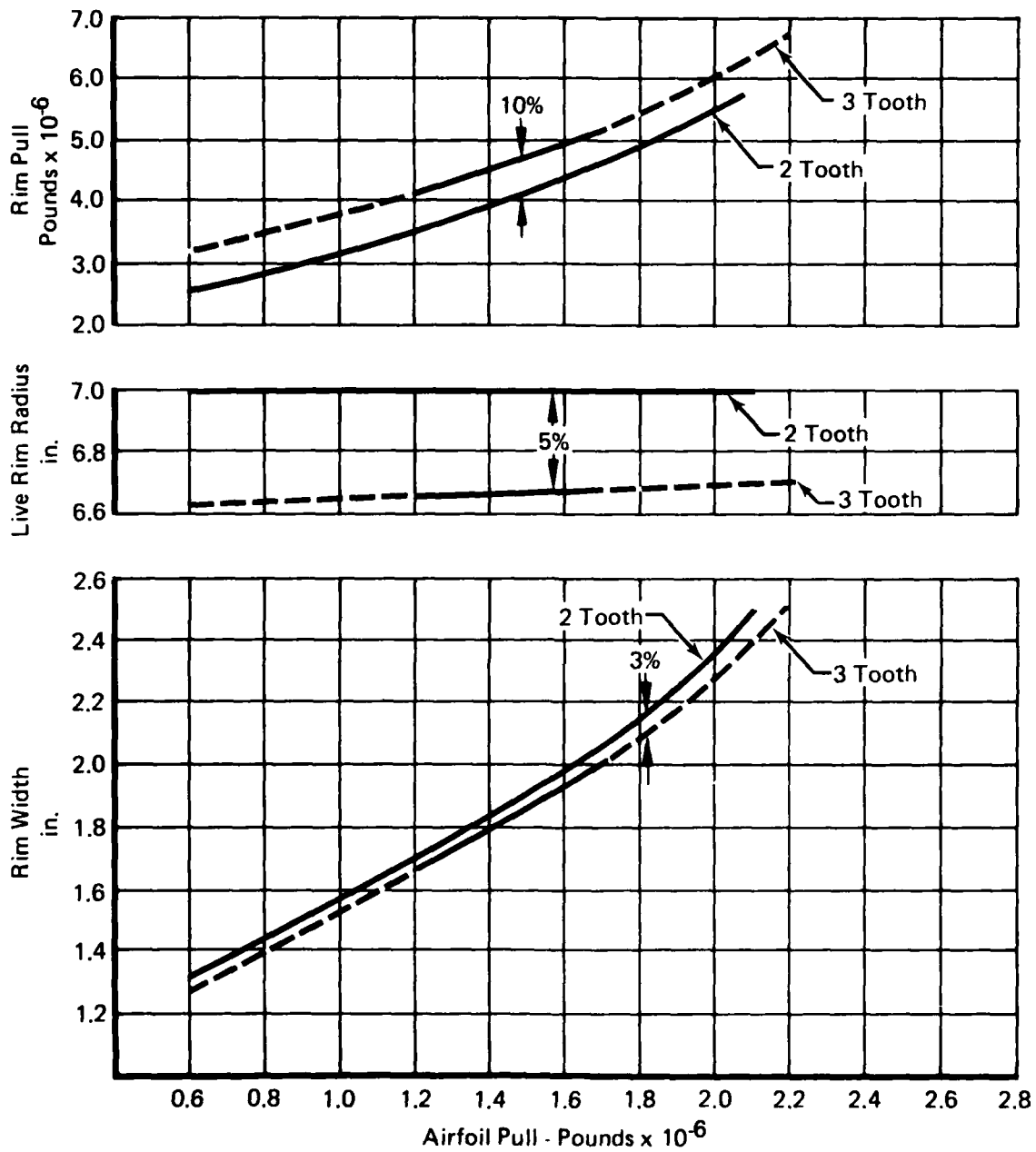
FD 184157
801701

Figure 2-79. Effect of Stress Rupture Life on Turbine Attachment.



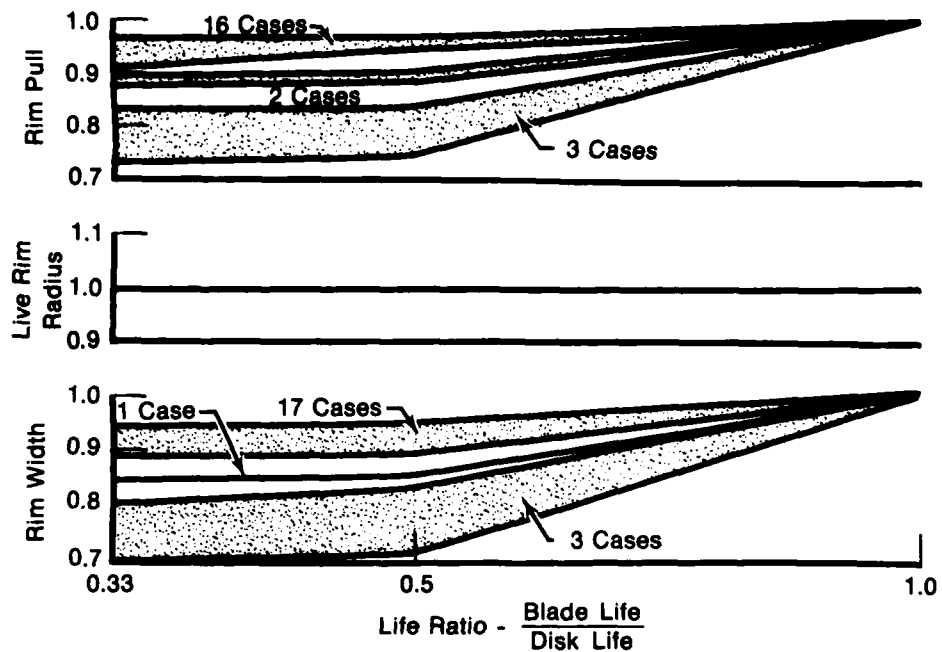
FD 184156
801701

Figure 2-80. Effect of Number of Blades on Turbine Attachment.



FD 184162
801701

Figure 2-81. Effect of Total Airfoil Pull on Turbine Attachment.



FD 184176

Figure 2-82. Life Ratio Effect on HPT Attachment.

The three most significant dependent variables in the high pressure turbine attachment matrix, with respect to disk weight, are total rim pull, live rim radius and rim width. The range of these variables over the full range of two of the blade disk attachment independent variables (gas path inner radius and rotor speed) are shown in Table 2-6. The range of attachment sizes covered is shown in Figure 2-83.

For the point designs with the highest rim pulls at each speed in the matrix, disks were sized, based on burst margin, to determine if disks capable of carrying these pulls could be designed. The seven disks with high rim pulls at 6,500 rpm are feasible, while one disk at 17,000 rpm and three disks at 30,000 rpm are not. Therefore, these four blade/disk attachment designs have been deleted from the matrix (leaving a total of 75 point designs for regression).

Seventy-nine base and 10 check case attachments were generated, consistent with the requirements of a seven variable one-half replicate central composite design.

TABLE 2-6. HIGH PRESSURE TURBINE VARIABLE LEVEL RANGES

Independent Variables		Dependent Variables		
Speed, rpm	Gas Path Inner Radius (in.)	Rim Pull x 10 ⁻⁶ (lb)	Live Rim Radius (in.)	Rim Width (in.)
4,200-6,500	30	3-29	21-28	0.8-3.6
	24	7	20.4	1.5
	18.	1.4-12.5	12-17	0.8-3.8
17,000	11.	8.9	9.1	2.5
	9.	2.4-6.5	6.2-7.8	1.2-2.8
	6.6	3.1	4.9	2.2
18,000-30,000	6.5	1.4-4.9	4.0-5.5	0.8-2.2
	5.2	2.2	3.9	1.6
	3.8	0.8-2.0	1.9-2.9	1.0-2.2

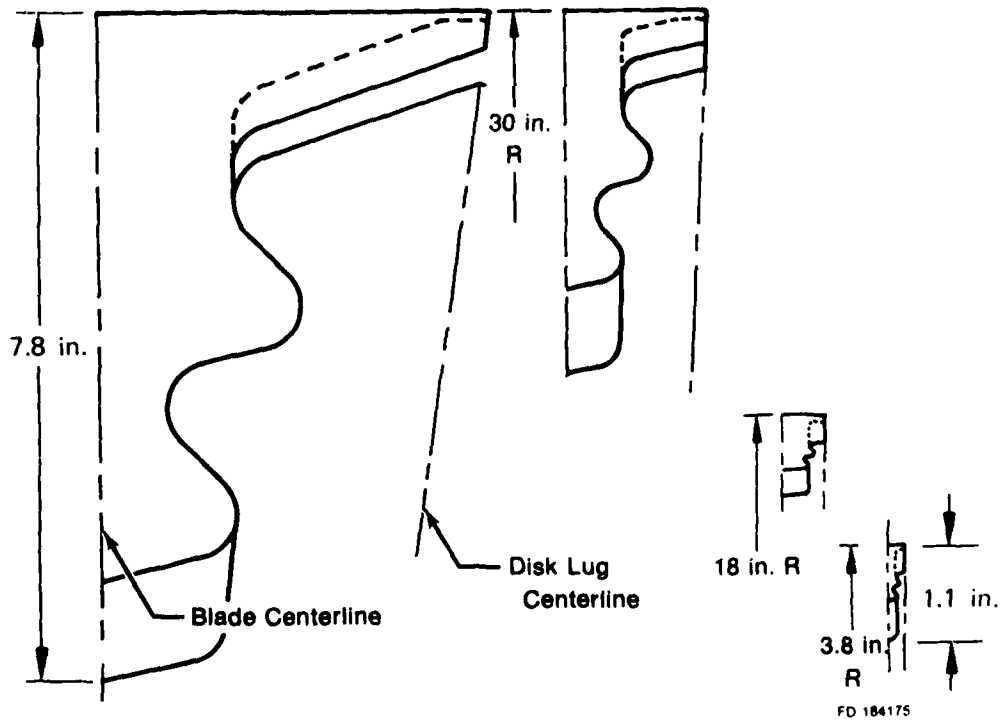


Figure 2-83. Size Range of Turbine Attachments.

Figures 2-84 and 2-85 illustrate typical results of the LPT attachment matrix. Figure 2-84 presents the response of the attachment (rim pull and rim width) to changes in blade total pull. A ten percent change in blade pull results in a 9% change in rim pull and an attendant 5% change in rim width. Figure 2-85 shows that a factor of three improvement in low cycle fatigue life capability is obtained with a twelve percent increase in rim pull, and a 19% increase in rim width. The first blade tooth local maximum elastic stress is reduced fifteen percent in achieving the three-fold low cycle fatigue life. Figure 2-85 illustrates the same type of attachment response in terms of rim pull with increased stress rupture life, since small changes in stress are required.

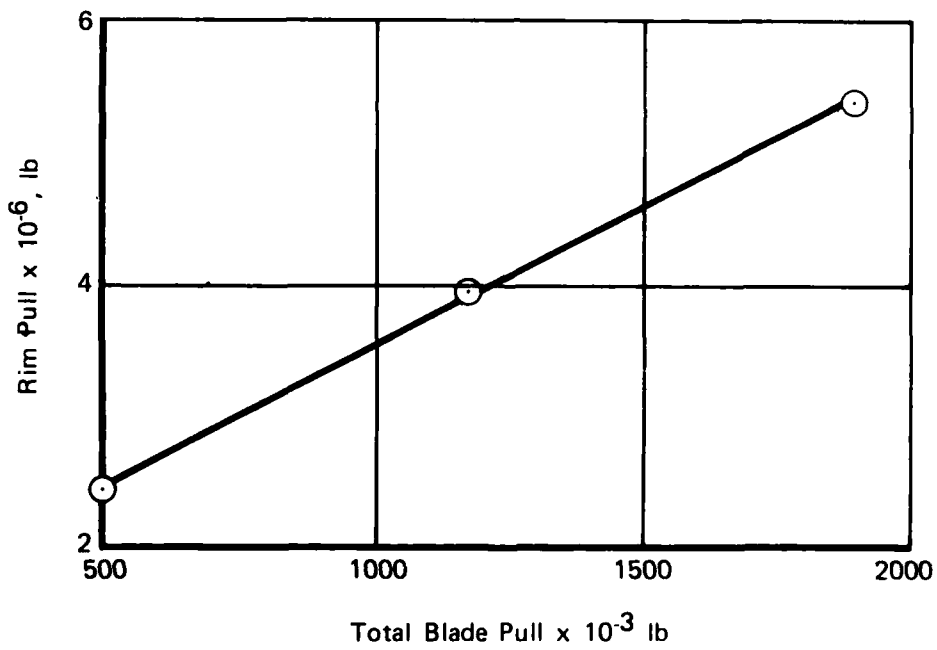
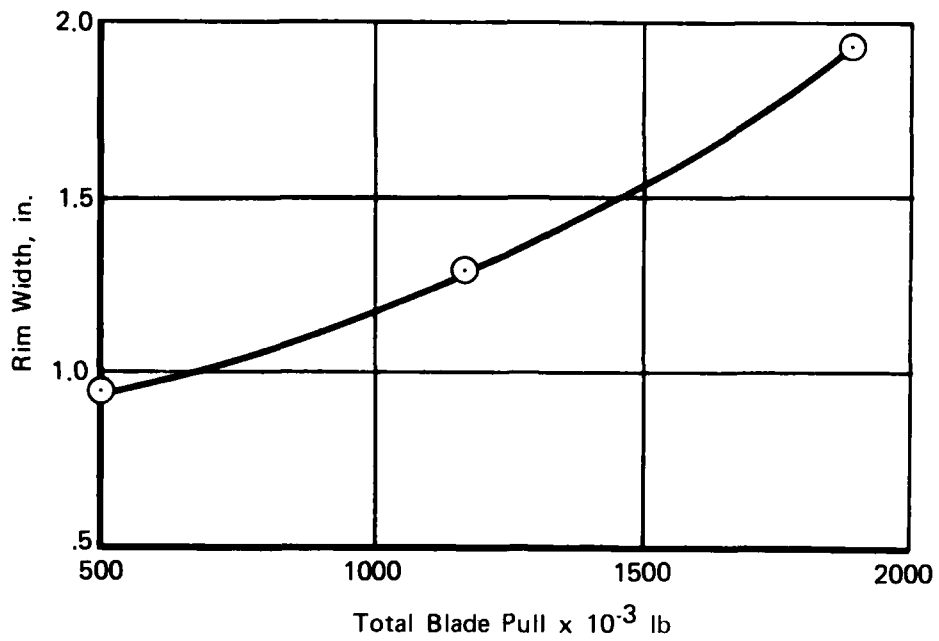
TABLE 2-7. LOW PRESSURE TURBINE ATTACHMENT

Independent Variable Levels	
Independent Variable	Range
Rotor Speed, rpm	7,000.-19,000
Blade Chord, inches	1.2-3.1
Blade Pull, pounds x 10 ⁻⁶	0.25-2.4
Number of Blades	20-115
Flowpath I.D Radius, inches	2.8-30
Stress Rupture Life Capability, hours	200-2,000
Low Cycle Fatigue Life Capability, cycles	1,000-15,000

2.4.4 Fan Disk

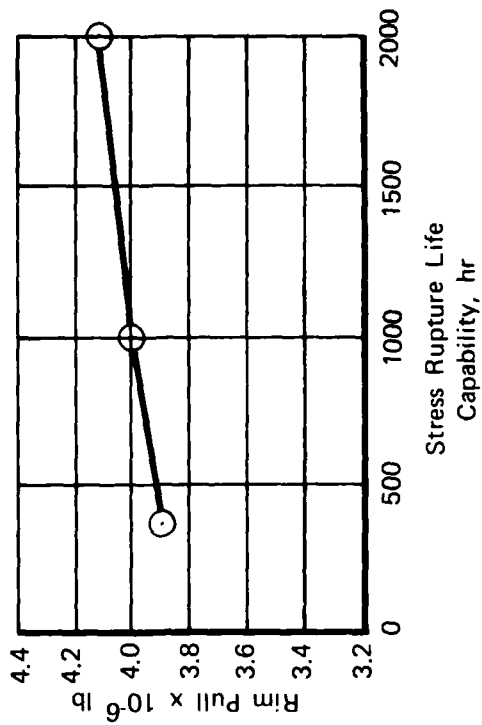
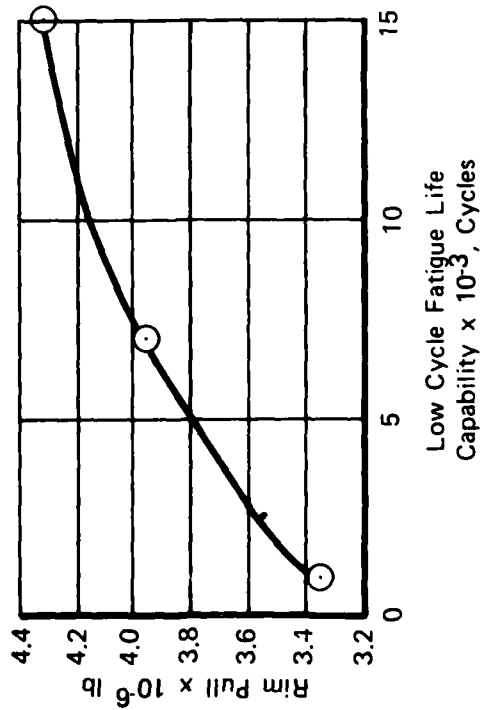
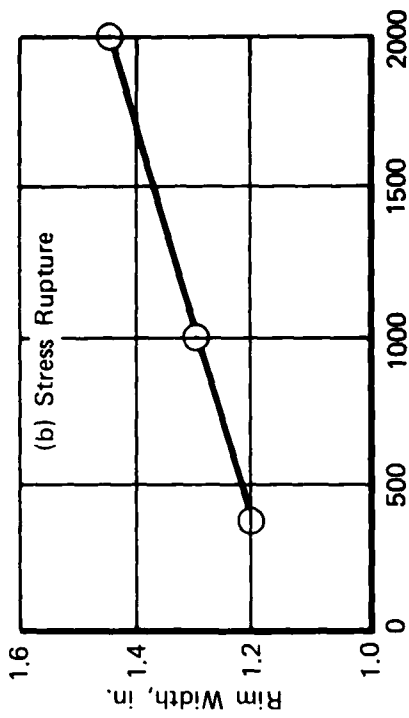
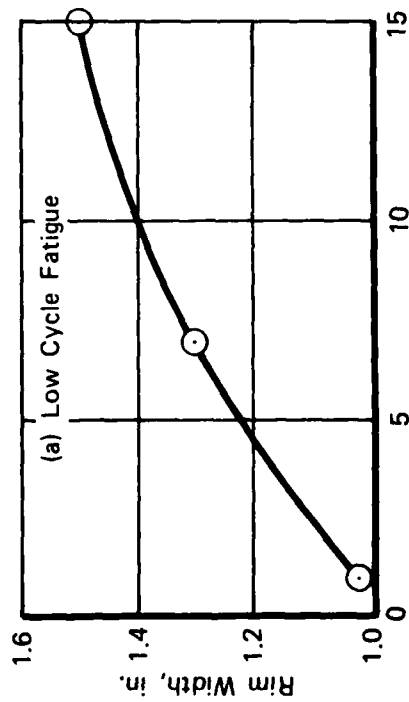
The five fan disk matrix independent variables and their ranges are shown in table 2-8.

Twenty-seven base case and five check case disks were generated consistent with the requirements of a one-half replicate central composite design.



FD 193266
802804

Figure 2-84. Low Pressure Turbine Attachment Response to Total Blade Pull Variation.



FD 193267
802804

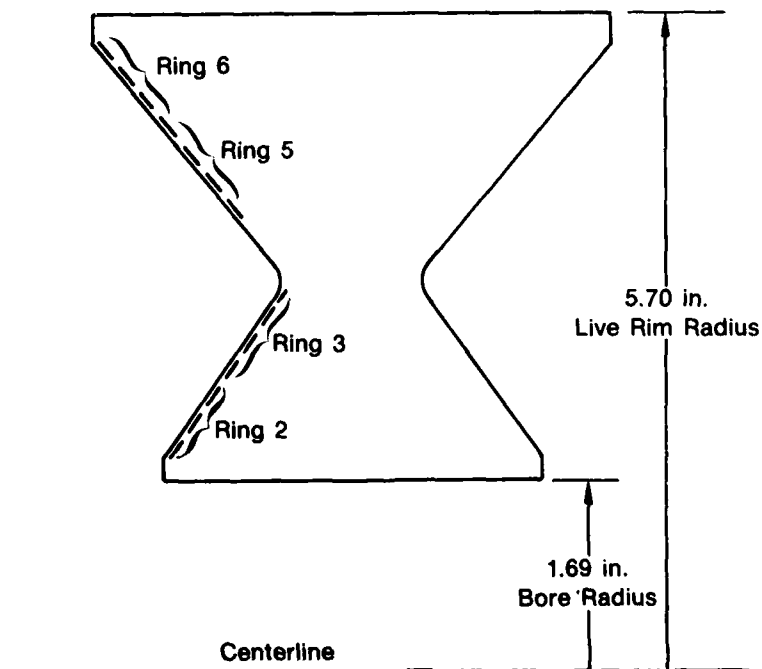
Figure 2-85. Low Pressure Turbine Attachment Response to LCF and Stress Rupture Capability.

TABLE 2-8. FAN DISK INDEPENDENT VARIABLE LEVELS

Rotor speed, rpm	7,000-17,000
Total rim pull, pounds x 10 ⁻⁶	0.47-5.7
Rim width, inches	2.-8.5
Live rim diameter, inches	1.9-19.1
Low cycle fatigue life capability, cycles	1,000-15,000

While one-fourth of the thirty-two disks generated were limited by bore effective stress, eighteen disk geometries and weights were determined by slope limits. An example of a slope-limited disk is shown in Figure 2-86. In this example, slopes in four of the seven rings are at their limits (slope-limited disks could also have only one ring at the slope limit). The balance of the disks are rim tangential stress (low cycle fatigue) and average tangential stress (burst) limited. These multiple limit functions are noted because of their potential effect on regression accuracy.

2.4.5 Compressor Disks



FD 223757

Figure 2-86. Typical Matrix Fan Disk with Four Slope-Limited Rings.

The LUCID-developed CAD technique sizes both the first stage and next-to-last stage attachments and disks.

The first stage compressor disk variables are identical to those of the fan disk. The ranges of the independent variables are shown in Table 2-9.

TABLE 2-9. FIRST STAGE COMPRESSOR
DISK MATRIX

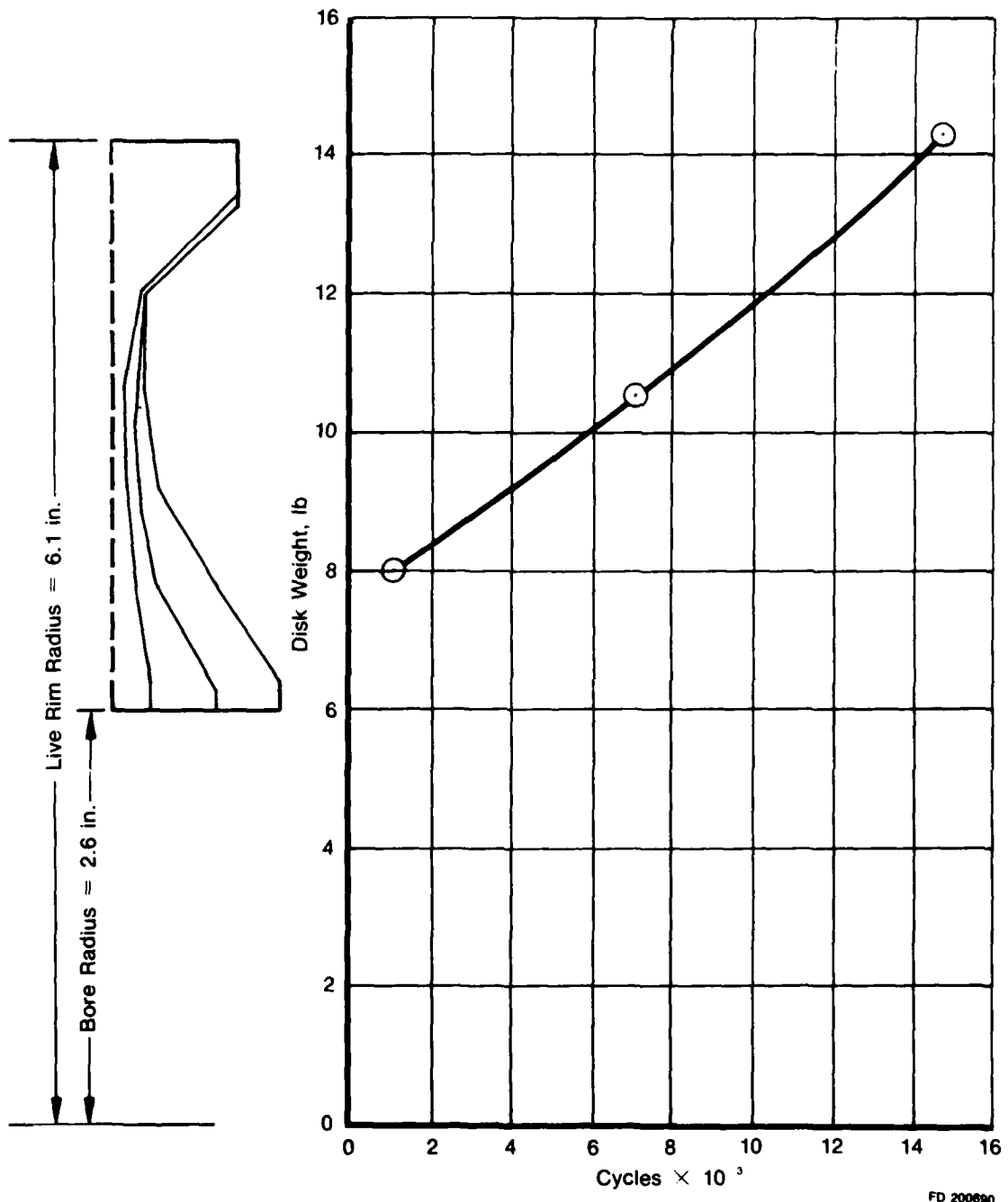
Independent Variable	Range
Rotor Speed, rpm	10,000 to 30,000
Rim Pull x 10 ⁻⁶ , lb	0.1 to 1.5
Rim Width, in.	0.3 to 3.3
Live Rim Radius, in.	3.0 to 10.7

A one-half replicate central composite design requires 27 base cases (5 check cases were also generated by the live disk synthesis program). Of the total 32 disks, 17 are bore tangential stress limited, 7 are slope limited, 6 are burst limited, one is rim tangential stress limited, and one disk is at minimum web width.

Figure 2-87 shows three disks which have the same independent variable levels except cyclic life capability, which has been varied from 1,000 to 15,500 cycles. The bore tangential stress for this change in cycles has been reduced to one-half the value at 1,000 cycles, while disk weight has been increased from 8 to 14.3 pounds.

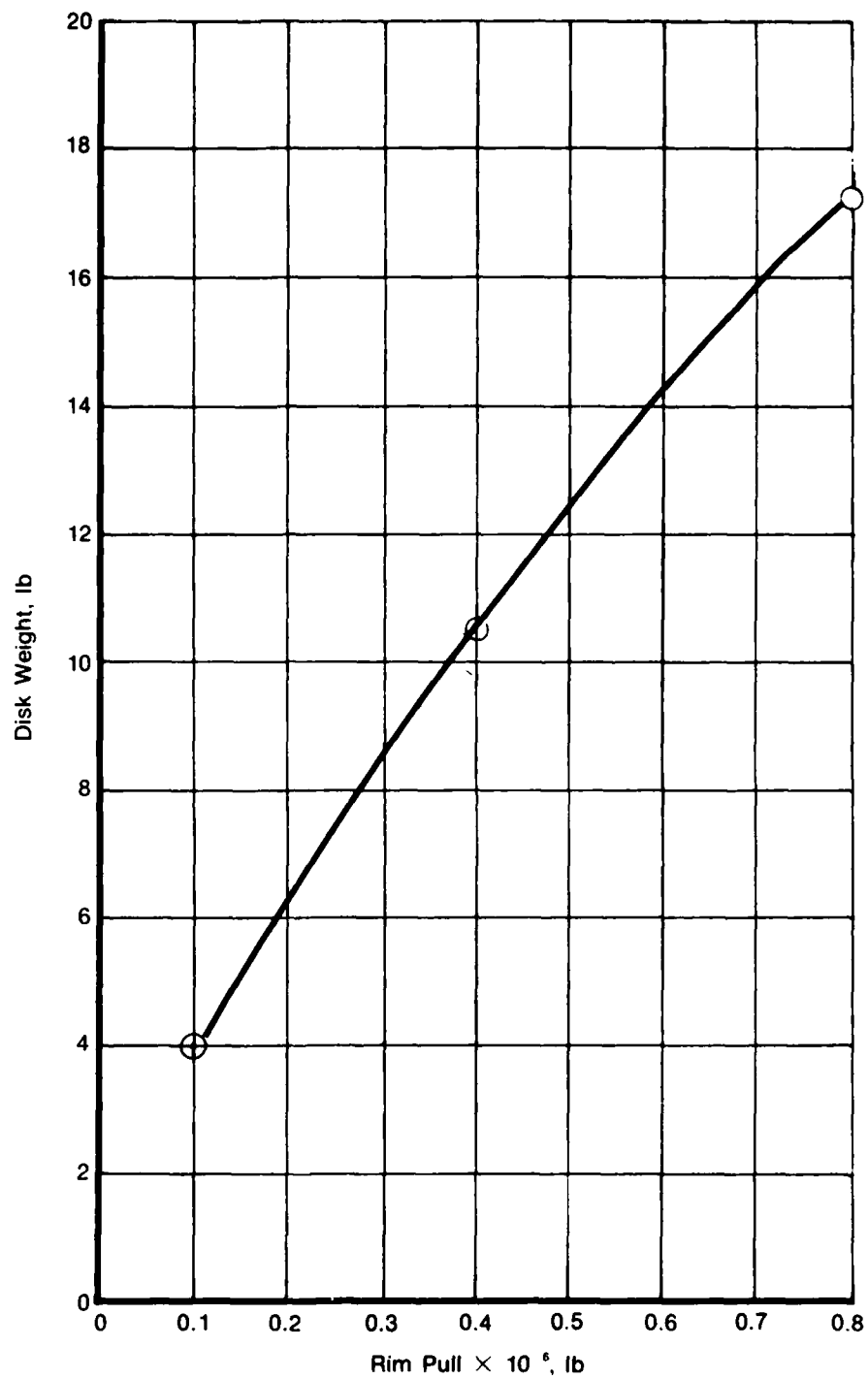
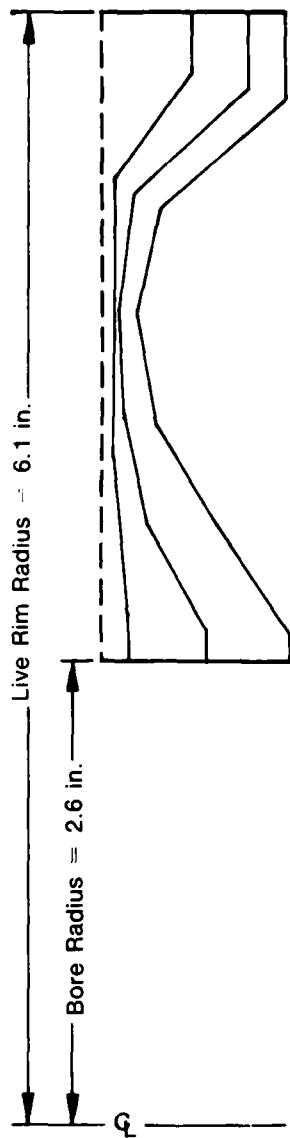
Figure 2-88 shows the combined effects of rim pull and rim width on disk geometry and weight at constant values of the remaining independent variables.

The next-to-last stage compressor disk matrix differs from the previous disks discussed in that the disk radial temperature gradient must be taken into account. While disk temperatures show some gradient from bore to rim during stabilized steady-state running, these gradients are minor relative to those incurred during engine transient operation. Accelerations of power lever angle are particularly damaging the disk bore, since the thermal contribution to total stress is added to the stresses due to the increased speed.



FD 200690
802706
gn 1 985

Figure 2-87. Effect of Cycles on Disk Weight and Geometry, First Compressor Disk.



FD 200689
802706
gn1 984

Figure 2-88. Effect of Rim Pull and Rim Width on Disk Weight and Geometry, First Compressor Disk.

Stages whose disks have significant radial thermal gradients are rear compressor and turbine stages. As a result, the approach adopted in designing the rear compressor disk matrix was to add one independent variable, temperature difference between the bore and the rim, to the other five variables. Table 2-10 shows the six independent variables and their ranges.

TABLE 2-10. NEXT-TO-LAST STAGE COMPRESSOR
DISK INDEPENDENT VARIABLES AND RANGES

Variable	Range
Rotor speed, rpm	10,000-30,000
Live rim radius, in.	4.25-10.5
Rim pull x 10 ⁻³ , lb	20-1,250
Rim width, in.	0.1-3.25
Thermal gradient, bore to rim, °F	85-675
Cyclic life capability, cycles	1,000-15,000

Consistent with the requirements of a one-half replicate central composite design, 45 base case disks were requested (10 check case disks were also requested). Repeated attempts at generating the matrix resulted in a total of 44 acceptable disks. Repeated attempts at running five disks were not successful, and six disks were eliminated because they had widths inside the rim which were at the minimum limit. Twenty-six of the disks are bore tangential stress limited, nine are average tangential stress limited, and the balance are thickness and slope limited.

2.4.6 High Pressure Turbine Disk

The high pressure turbine (HPT) disk matrix six independent variables and their levels are shown in Table 2-11.

The majority of disks generated (a total of fifty-five were attempted) were either burst limited at low cyclic life capability or bore tangential stress limited at the medium and high levels of cyclic life capability. After repeated attempts at generating the fifty-five disk matrix, only four disks were not synthesized.

TABLE 2-11. HIGH PRESSURE TURBINE DISK MATRIX
INDEPENDENT VARIABLES AND RANGES

Variable	Range
Rotor speed, rpm	10,000-30,000
Rim pull, pounds x 10 ⁻⁶	0.8-18
Rim width, in.	0.8-3.6
Live rim radius, in.	3.7-28
Radial thermal gradient, bore to rim, °F	70-470
Cycle life capability, cycles	1,000-15,000

Figures 2-89 through 2-92 illustrate the effects of cycles, disk thermal gradient, rim width, and rim pull on HPT turbine disk geometry and weight. It is noted that the middle level of speed was skewed to the three-quarters value to generate feasible disks at the high levels of cycles and rim pull.

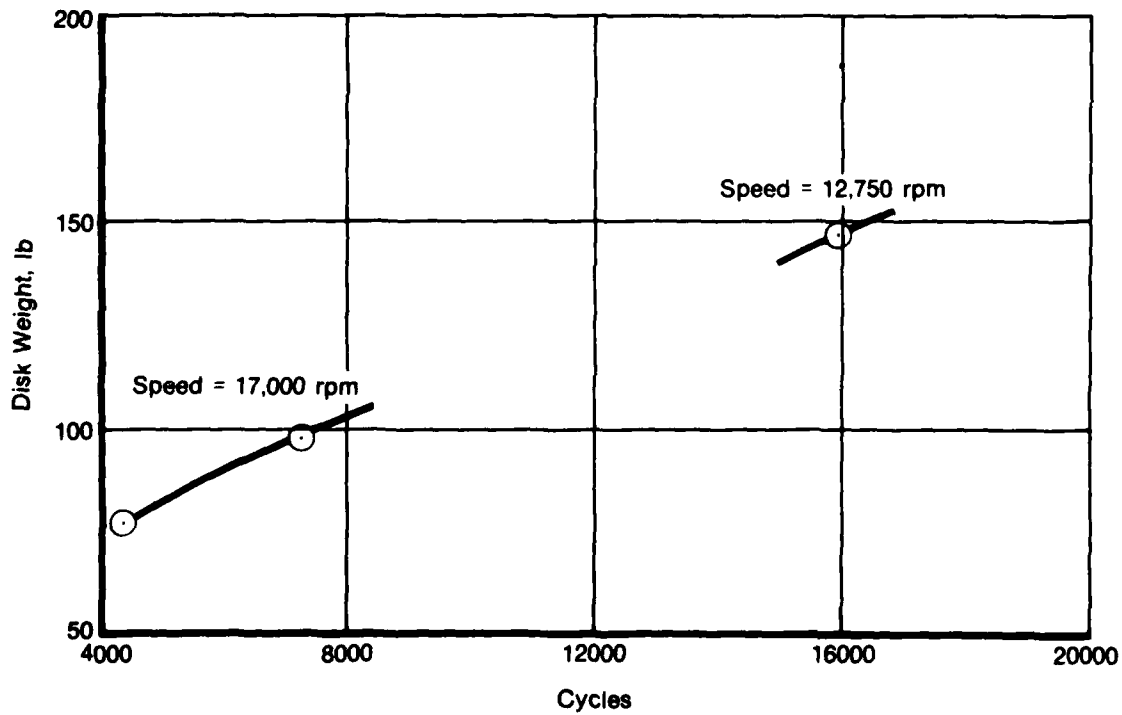
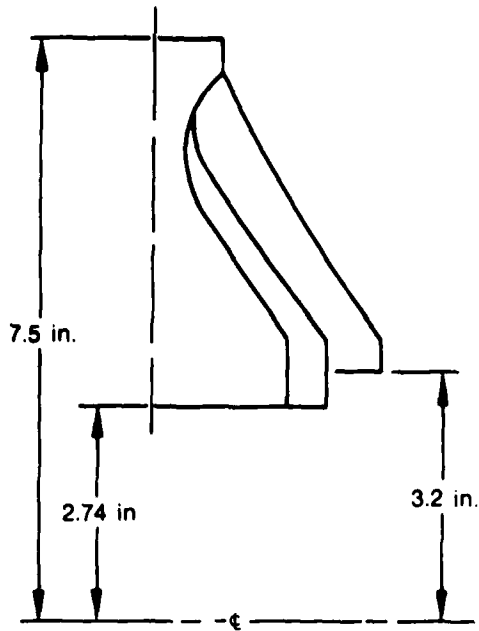
2.4.7 Low Pressure Turbine Disks

The low pressure turbine (LPT) matrix is basically quite similar to the HPT matrix. The major exception is that specification of independent variable levels included consideration of requirement for LPWT to analyze both single and two-stage LPT's. Table 2-12 lists the six independent variable levels and ranges.

The six variable LPT matrix was generated, synthesizing forty-five base and ten test case disk designs.

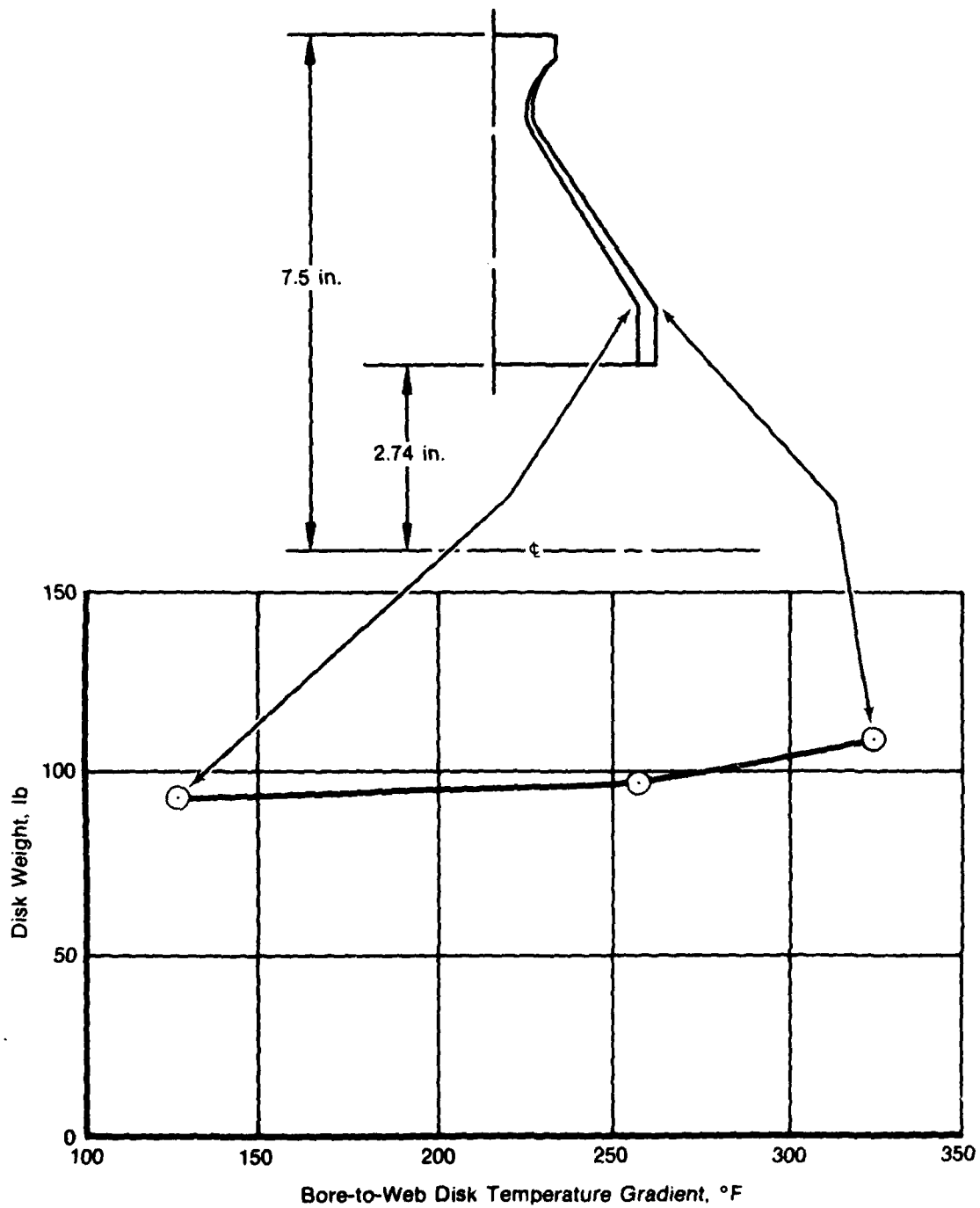
Figure 2-93 illustrates the variation in LPT disk weight and geometry as a function of bore fracture mechanics cyclic life capability. It is noted that, while the three disks shown have bore tangential stresses corresponding to the life capability shown, disks A and B are sized to burst margin.

In Figure 2-94 the effect of rim pull on disk geometry and weight is shown. Disks B and C are burst margin limited, and all disks have bore tangential stresses commensurate with a fracture mechanics life capability of approximately 11,000 cycles.



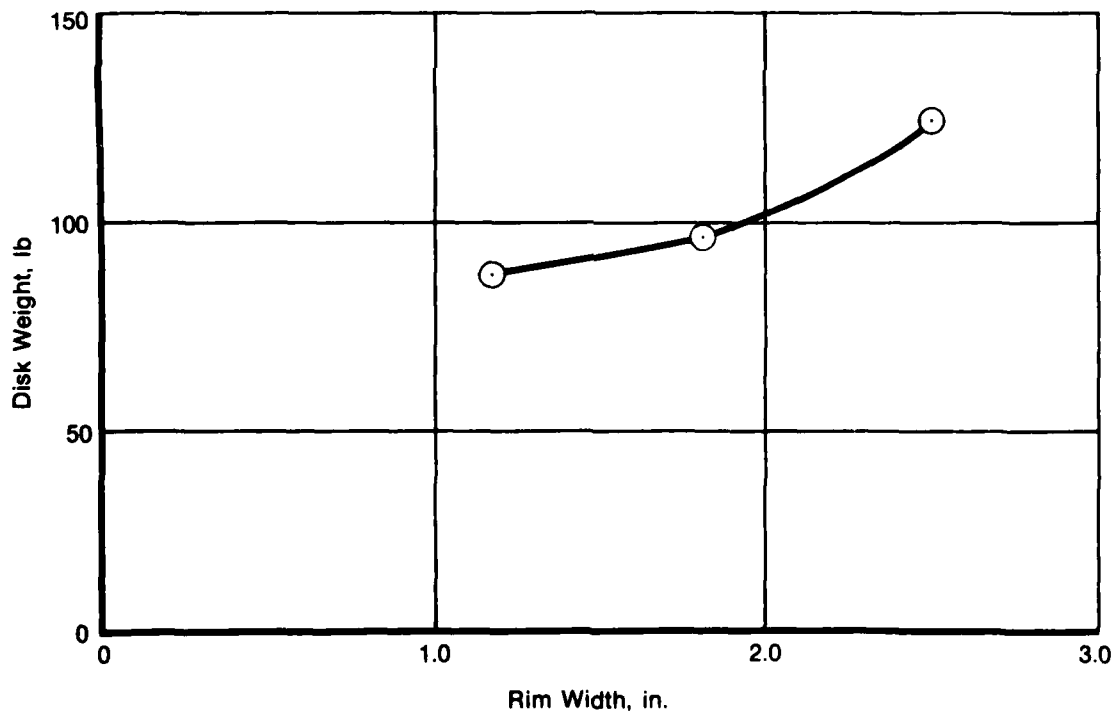
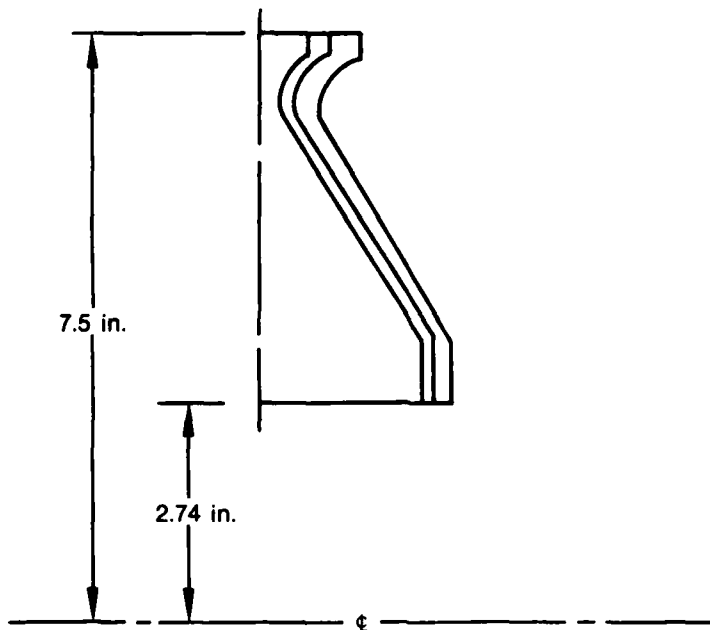
FD 200568
802807

Figure 2-89. Effect of Cycles on High Pressure Turbine Disk Weight and Geometry.



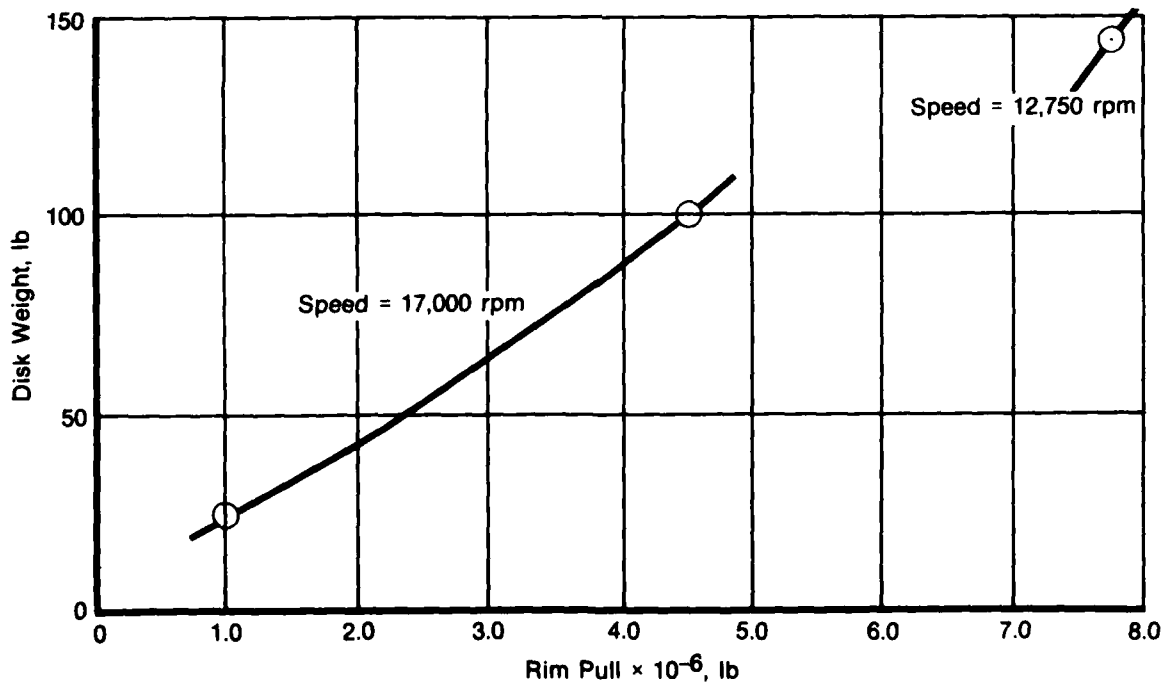
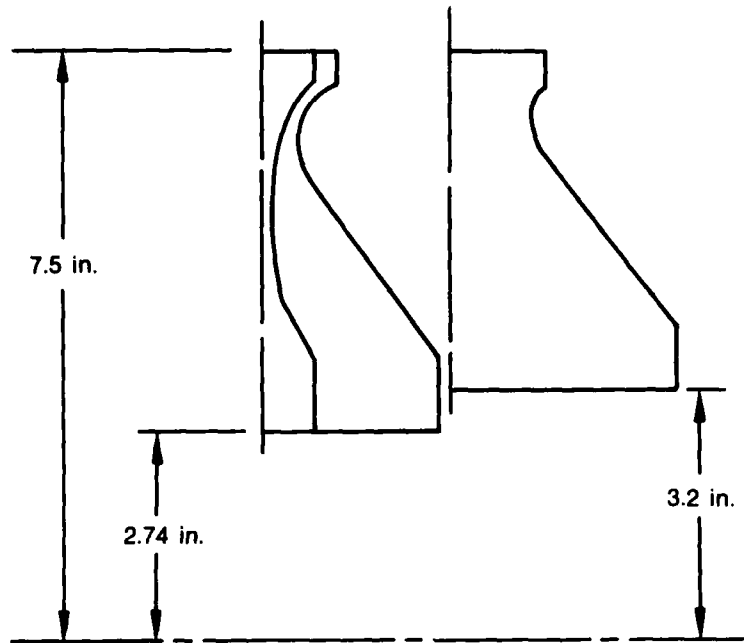
FD 200568
802907

Figure 2-90. Effect of Disk Radial Temperature Gradient on High Pressure Turbine Disk Weight and Geometry.



FD 200570
802907

Figure 2-91. Effect of Rim Width on High Pressure Turbine Disk Weight and Geometry.

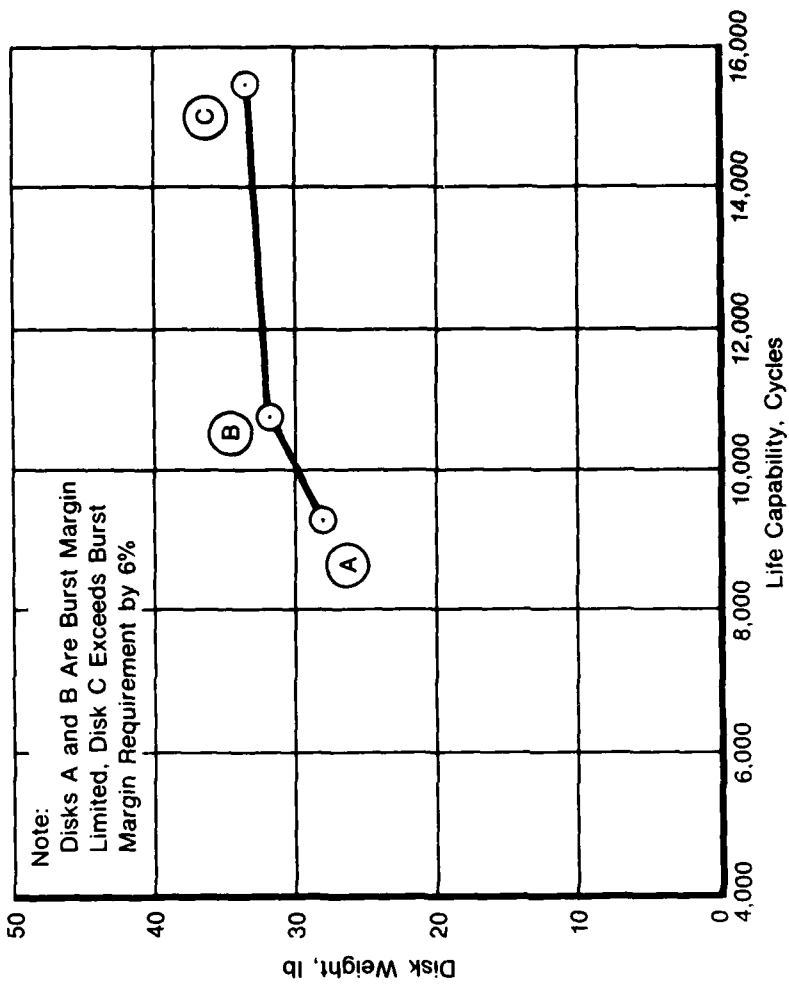


FD 200571
802907

Figure 2-92. Effect of Rim Pull on High Pressure Turbine Disk Weight and Geometry.

TABLE 2-12. LOW PRESSURE TURBINE DISK
INDEPENDENT VARIABLES AND RANGES

Variable	Range
Rotor Speed, rpm	7,000 to 19,000
Rim Pull x 10 ⁻⁶ , lb.	0.2 to 28.
Rim Width, in.	0.5 to 3.2
Live Rim Radius, in.	3.7 to 28.7
Life Capability, cycles	1,000 to 15,000
Bore-to-Rim Temperature Gradient, °F	20 to 580



FD 198748
801809
DPI 221

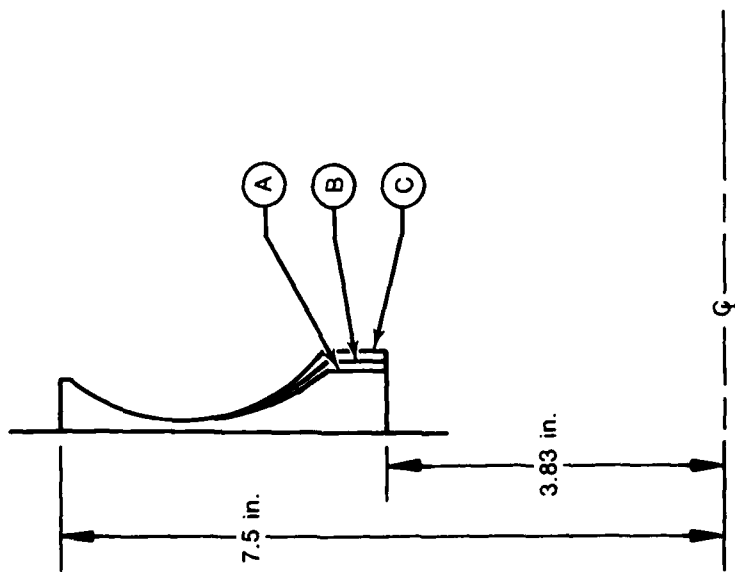
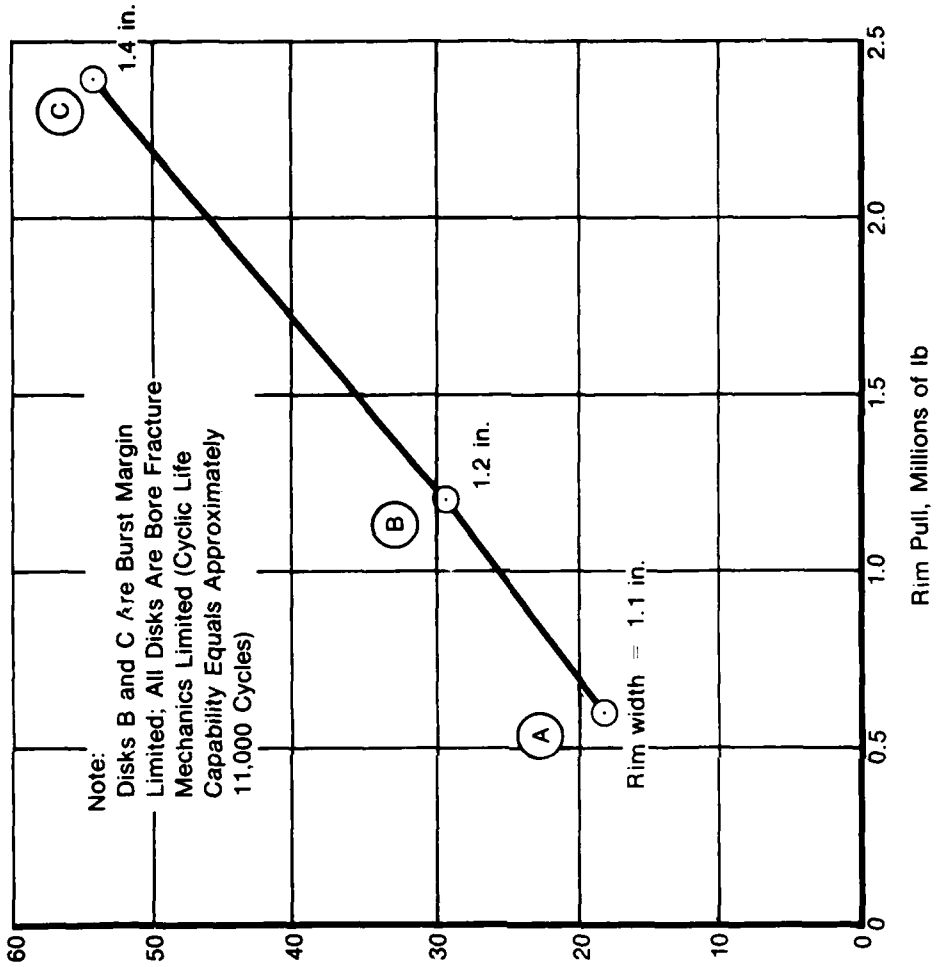


Figure 2-93. Low Pressure Turbine Disk Weight and Geometry as a Function of Cyclic Life Capability.

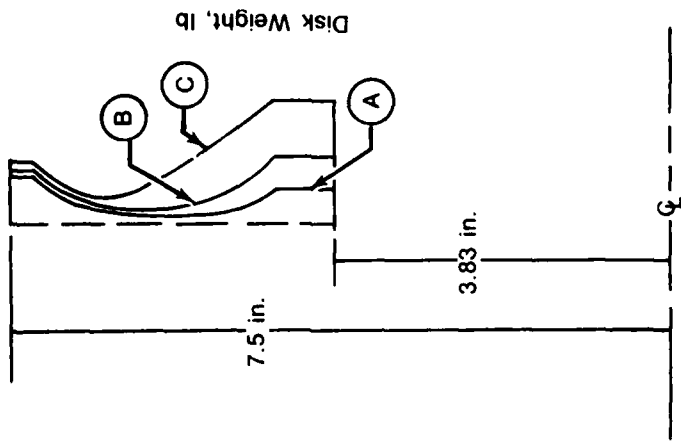


Note:
 Disks B and C Are Burst Margin Limited; All Disks Are Bore Fracture Mechanics Limited (Cyclic Life Capability Equals Approximately 11,000 Cycles)

Rim width = 1.1 in.

Rim Pull, Millions of lb

FD 198749
 901909
 9m1222



Disk Weight, lb

Figure 2-94. Effect of Rim Pull on Low Pressure Turbine Disk Geometry and Weight.

Of the fifty-five disks, twenty-one are web effective stress limited, eleven are burst margin (or average tangential stress at overspeed) limited, two are slope limited, nineteen are bore fracture mechanics limited, and two are web radial stress limited. The web effective stress limited cases are equivalent to the burst margin limited designs.)

2.5 MATRIX BASE DATA REGRESSION

An important element in the approach to formulation of the gas turbine computer-aided design system is the use of regression equations. These regression equations represent matrices of both aerodynamic components and mechanical attachment and disk designs. In the approach, regression equations were selected over use of the aerodynamic meanline design systems and mechanical synthesis computer programs for a number of reasons. Regression equations reliably provide output, while the mechanical synthesis programs may either fail to converge or provide a design solution which is not of practical interest. Use of the computer programs themselves in the LPWT would result in a program so complex as to preclude its practical use; this alternate approach would also be inconsistent with the intent in formulating the overall design system; i.e., the LPWT is meant to be a cost effective design screening tool in early conceptual design. As such, reasonably correct trends in engine performance and weight are required, rather than precision in values of weight, efficiency, stress, etc.

Pratt & Whitney Aircraft has a long history of application of regression techniques. Recent examples are the regression of a four variable compressor aerodynamic matrix in performance of contract RP1187-1 for the Electric Power Research Institute and aircraft mission performance simulations.

However, the benefit of economy in design effort via a regression approach is achieved at some risk. This risk is that one's best efforts at design, generation, and regression of a design process matrix may fail, providing insufficient accuracy. Also, design

process assumptions made in generating a matrix of designs may be obsolete as design processes evolve, requiring a new matrix of designs and regression.

The following subsections summarize regression efforts in the LUCID program. While regression accuracies of compressor and turbine aerodynamic matrices are excellent, regression attempts for attachment and disk matrices have not been as successful.

The causes of reduced mechanical matrices' regression accuracy statistics are not well understood. Consideration of the potential causes of accuracy problems yields the following list:

1. Varying design criteria in a matrix (for example burst, rim low cycle fatigue, and bore fracture limited disk designs)
2. Additional design limits (for example, minimum disk web widths specified for machining reasons)
3. Design and optimization procedures incorporated in mechanical synthesis programs
4. Incorrect assessment of matrix design due to required skewing of many independent variable levels
5. Oversimplification of the design problem (for example, five disk width independent variables could be substituted for the one stress-driver independent variable 'cycles', resulting in a ten-variable matrix).

Central composite design pattern, rather than latin square, was used to identify the designs to be generated. A second-order polynomial regression form was employed in initial regression attempts. If insufficient accuracy resulted, a SAS (Statistical Analysis Systems) regression format was attempted. In general, all aerodynamic and disk regression equations were generated with second-order polynomial models, while attachment modeling resorted to SAS terms.

2.5.1 Compressor Attachment Regression

First stage compressor blade/disk attachment regression accuracy is summarized in Table 2-13. Regression accuracy for six of the dependent variables (rim pull, rim width, live rim radius, bearing stress, blade neck nominal tensile stress, and lug neck nominal tensile stress) is judged acceptable. It is noted that check case errors are high for lug neck stress, but neck stresses are typically limiting in the blade lug and not in the disk lug. Local maximum elastic stresses in the blade and disk lug and not in the disk lug. Local maximum elastic stresses in the blade and disk lug fillets have low correlation coefficients (0.858 and 0.949 respectively), but error levels are similar to those of other dependent variables. Low cycle fatigue limited designs were not expected, but nineteen such designs resulted either at the high level of material yield strength or at low chord and blade pull levels. Of the remaining designs, 32 were limited by neck nominal tensile stress, and 4 were limited by shear stress (note that all designs are bearing stress limited).

The regression accuracy statistics are summarized for the rear compressor attachment in Table 2-14. While the multiple correlation coefficients are good for all dependent variables, average and maximum error levels are rather high, especially for the check values. There are more than one design criterion limiting the rear compressor attachment designs. Tooth bearing stress is limiting in all designs. In addition, 16 are fillet local maximum elastic stress limited, 21 are blade neck nominal tensile stress limited, 5 are shear stress limited, and 12 are limited by both blade neck tensile stress and shear stress. In addition to the above stress/life criteria, upper and lower rim width limits affected nineteen of the designs. These rim width limited designs may have a large effect on regression accuracies, but their effects are not known.

TABLE 2-13. FIRST STAGE COMPRESSOR BLADE/DISK ATTACHMENT REGRESSION RESULTS

	Base Data			Check Cases	
	Correlation Coefficient	Maximum Error (%)	Average Error (%)	Maximum Error (%)	Average Error (%)
Disk Design Terms					
Rim Pull	0.999	-4.4	1.0	-21.0	3.0
Rim Width	0.981	-17.5	3.9	-56.2	9.3
Live Rim Radius	1.000	0.8	0.1	-1.6	0.3
Stresses					
Blade Neck Nominal Tensile Stress	0.981	15.7	3.6	37.9	8.0
Lug Neck Nominal Tensile Stress	0.976	18.5	3.4	97.6	10.8
Tooth Bearing Stress	0.999	0.4	0.1	2.1	0.2
Blade Tooth Local Maximum Elastic Stress	0.858	20.0	3.2	30.0	5.8
Lug Tooth Local Maximum Elastic Stress	0.949	20.5	2.3	23.6	4.6

TABLE 2-14. REAR COMPRESSOR BLADE/DISK ATTACHMENT REGRESSION RESULTS

	Base Data			Check Cases	
	Correlation Coefficient	Maximum Error (%)	Average Error (%)	Maximum Error (%)	Average Error (%)
Disk Design Terms					
Rim Width	0.999	7.5	2.1	66.7	5.2
Live Rim Radius	0.999	0.7	0.2	5.6	0.4
Rim Pull	0.999	17.1	2.5	40.3	6.4
Stresses					
Blade Neck Nominal Tensile Stress	0.993	-12.3	2.4	106.0	8.5
Disk Neck Nominal Tensile	0.995	9.7	2.5	40.0	5.4
Blade Local Maximum Elastic	0.992	11.3	2.2	286.0	8.8
Disk Local Maximum Elastic	0.997	6.4	1.5	68.0	4.8

2.5.2 High Pressure Turbine (HPT) Attachment Regression

Regression of the 79-case HPT blade/disk attachment matrix was accomplished using both the second-order polynomial and SAS modeling techniques. The SAS model regression equations were selected because of their superior results. In addition to the above effort with a seven-variable matrix, a six-variable matrix was attempted. This simpler matrix/regression approach used optimum geometry relationships developed from results of the seven-variable matrix. This alternate approach was discarded because of inferior regression accuracy statistics.

Regression results are summarized in Table 2-15 for the dependent variables required for disk design, attachment design, and engine weight routine.

TABLE 2-15. HIGH PRESSURE TURBINE BLADE/DISK ATTACHMENT
REGRESSION RESULTS

Dependent Variable	Base Data		Check Cases	
	Average Error (%)	Maximum Error (%)	Cumulative Average Error (%)	Maximum Error (%)
Rim Pull	2.9	10.7	4.3	31.6
Rim Width	4.7	19.7	6.2	30.2
Live Rim Radius	1.3	6.0	1.8	11.3
Dead Rim Weight	3.5	17.0	4.7	20.4
Blade 1st Tooth Nominal Tensile Stress	4.4	29.5	7.1	87.8
Blade 2nd Tooth Nominal Tensile Stress	6.6	54.9	11.2	191.0
1st Tooth Bearing Stress	0.9	3.0	1.3	9.2
2nd Tooth Bearing Stress Blade	12.4	1.0	3.6	1.6
1st Blade Tooth Local Maximum	0.7	4.3	1.4	20.7
2nd Blade Tooth Local Maximum Elastic Stress	1.5	4.9	2.4	21.4

Average errors for the disk design terms (the first three in Table 2-15) range from 1.3 to 4.7% and from 1.8 to 6.2%, for the base data and check cases respectively. Dead rim weight (for the weight subroutine) average errors are 4.4 and 7.1%.

It is noted that nominal tensile stress errors for the 1st and 2nd teeth are large. These errors are principally due to only 10% of the seventy-five base data attachments being stress rupture limited. It is felt that these error levels are acceptable for the LPWT, since our perception of engine usage for 1980 tactical fighter will continue to reflect cyclic failure modes due to low levels of Intermediate-and-above power hours.

Tooth bearing stress is always limiting in minimum rim pull attachments, hence the excellent regression accuracy results achieved.

First and second tooth local maximum elastic stress regression accuracies also reflect the preponderance of attachment designs which are low cycle fatigue limited.

2.5.3 Low Pressure Turbine (LPT) Attachment Regression

A summary of LPT blade/disk attachment regression accuracy statistics is shown in Table 2-16.

TABLE 2-16. REGRESSION RESULTS FOR LOW PRESSURE TURBINE
BLADE/DISK ATTACHMENT MATRIX

	Base Data			Check Cases	
	Correlation Coefficient	Average Error (%)	Maximum Error (%)	Cumulative Average (%)	Maximum Error, (%)
Disk Design Terms					
Rim Pull	0.999	3.2	16.8	4-2	32.6
Rim Width	0.974	4.4	18.2	6.0	45.1
Live Rim Radius	0.999	1.2	-9.0	1.3	2.8
First Tooth Terms					
Blade Neck Tensile Stress	0.974	3.9	17.3	5.7	-42.0
Lug Neck Tensile Stress	0.964	5.1	16.2	6.6	46.5
Blade Maximum Fillet Stress	0.996	1.0	-3.0	1.3	-9.4
Lug Maximum Fillet Stress	0.993	3.1	10.8	4.0	37.2
Bearing Stress	0.999	0.1	0.6	0.8	0.2
Second Tooth Terms					
Blade Neck Tensile Stress	0.943	7.0	31.2	9.9	99.3
Lug Neck Tensile Stress	0.974	3.1	-11.6	4.7	-42.1
Blade Maximum Fillet Stress	0.969	3.1	11.0	4.1	24.5
Lug Maximum Fillet Stress	0.989	2.4	9.2	3.3	46.5
Bearing Stress	0.999	0.5	-1.8	0.7	-9.4

Two of the three disk design terms' (rim pull and live rim radius) dependent variable regression accuracies are good, with 0.999 correlation coefficients and average error levels from 1.2 to 4.4%.

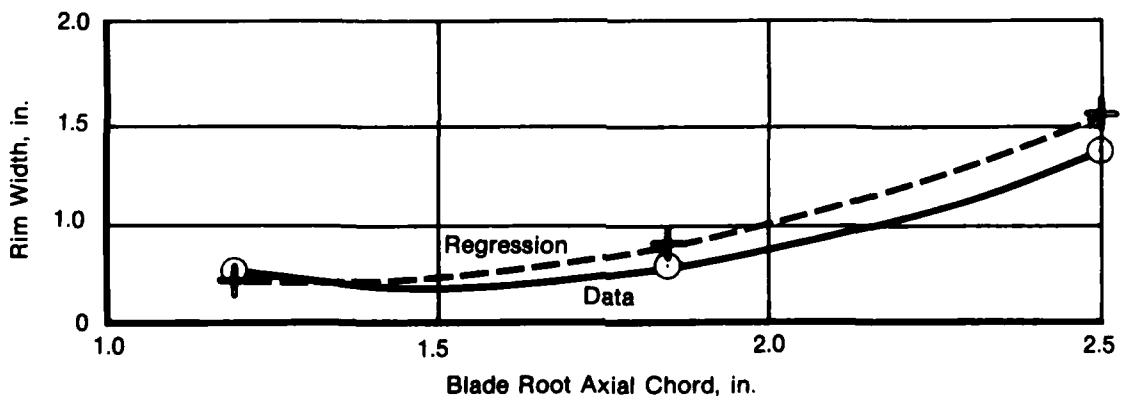
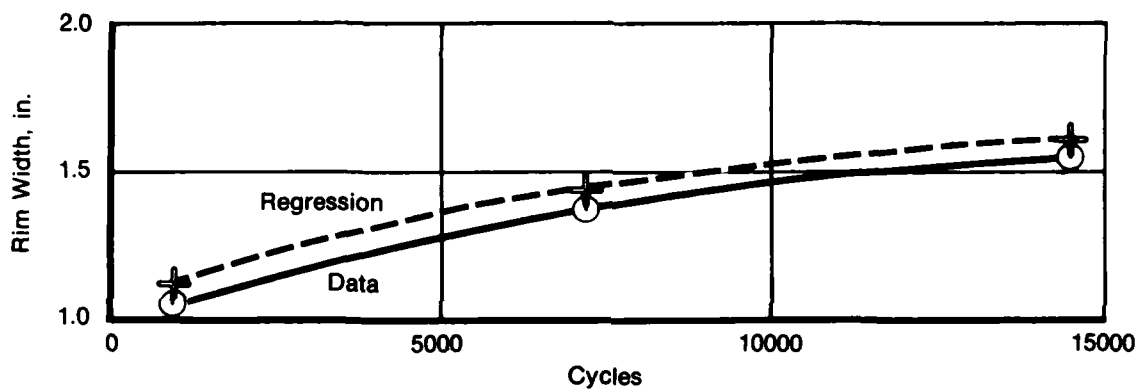
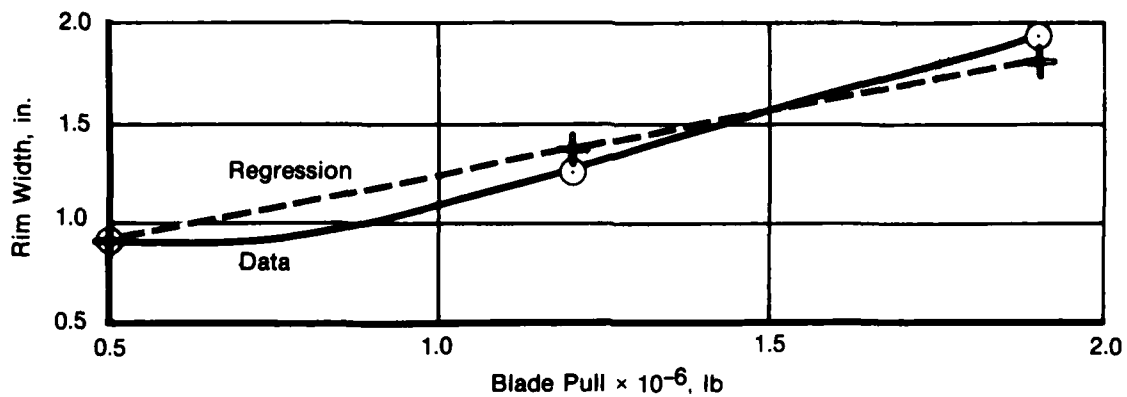
Regression accuracy of the remaining disk design term, rim width, is not as good as the above with a correlation coefficient of 0.974 and a cumulative average error of all data of 6.0%. Figure 2-95 shows rim width trends with three of the independent variables, blade pull, cycles, and blade root axial chord. Trend agreement of the data and regression is good.

First and second tooth regression results are also shown in Table 2-16. Results are similar to the high pressure turbine blade/disk attachment, in that tooth fillet local maximum elastic stress and bearing stress regression accuracies are good, while blade and disk lug nominal neck tensile stress regression accuracies are poor. In the LPT blade/disk attachment data 13 of the 79 base data cases and two of the ten check cases are stress-rupture limited, and the remaining attachments are low cycle fatigue limited. With these dual life-limiting modes, total data regression accuracy of blade and disk nominal neck tensile stresses is poor. Figure 2-96 compares the distribution of LPT attachment second tooth nominal neck tensile stress regression errors of all regressed data with the errors of the 13 attachments which are stress-rupture limited. Four of the stress-rupture limited cases have errors which are above 10%, but are not as high as the maximum errors of the total data.

2.5.4 Aerodynamic Matrices' Regression

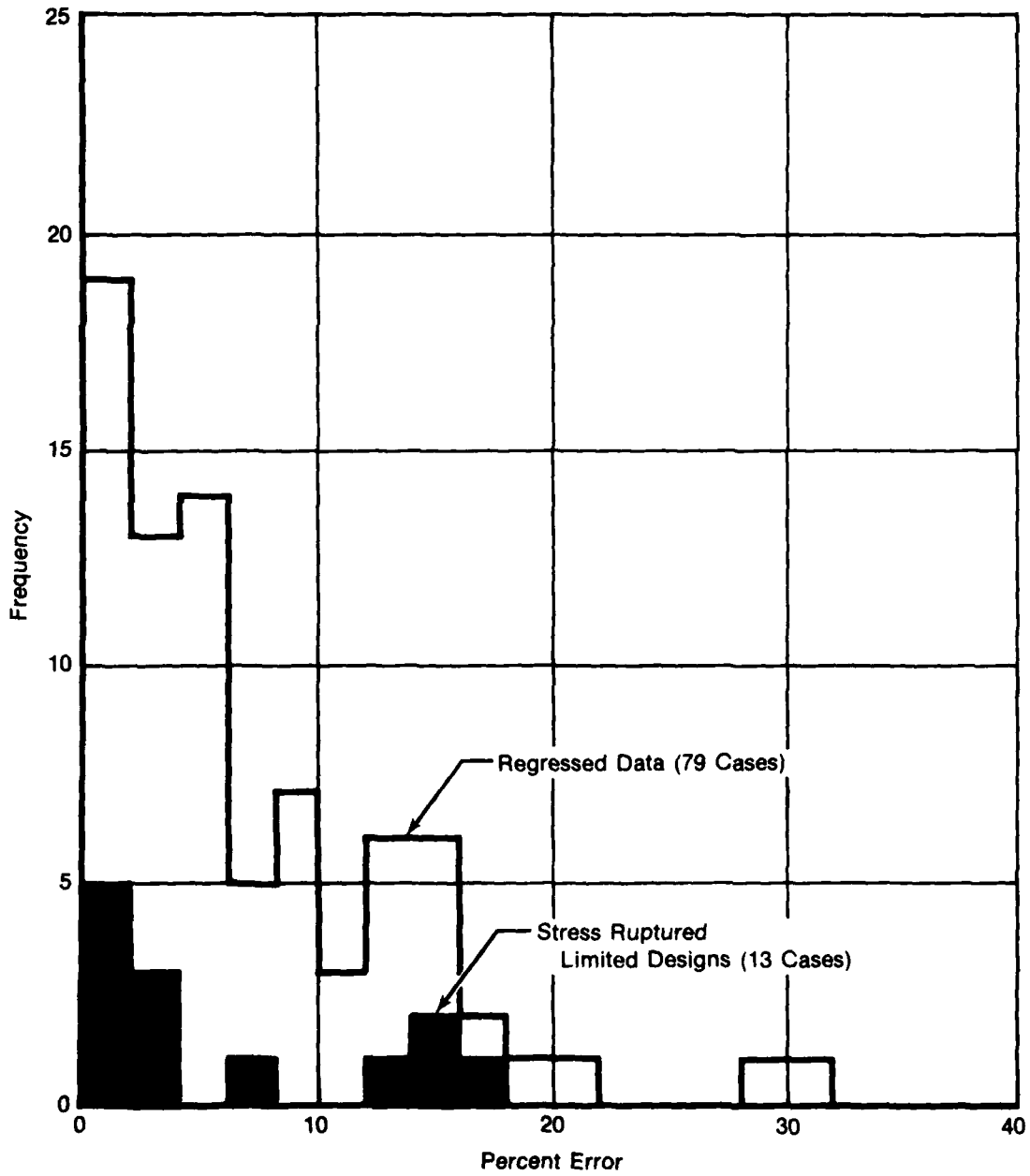
The following subsections (a) thru (c) summarize regression accuracy statistics for the three aerodynamic matrices.

2.5.4.1 Compressor Aerodynamic Matrix Regression Regression analysis results for the compressor aerodynamic matrix are excellent, and are shown in Table 2-17. Overall dependent variable terms (pressure ratio, efficiency, etc.) base data and check cases' maximum errors are 3% or less, and average errors are 1% or less. First stage and next-to-last stage blade count and geometry dependent variables' regression accuracy levels are also 3% or less.



FD 200672
802907

Figure 2-95. LPT Blade/Disk Attachment Rim Width Trend Comparison of Data and Regression Equations.



FD 200573
802907

Figure 2-96. LPT Blade/Disk Attachment Blade Second Neck Nominal Tensile Stress Regression Error Comparison.

TABLE 2-17. COMPRESSOR AERODYNAMIC MATRIX REGRESSION ANALYSIS RESULTS

Dependent Variable	Base Data			Check Cases	
	Standard Error of Estimate (%)	Maximum Error (%)	Average Error (%)	Maximum Error (%)	Average Error (%)
(1) Overall Terms					
Pressure Ratio	1.8	2.8	1.0	2.8	1.2
Efficiency	0.8	0.9	0.5	1.2	0.6
Length	1.0	1.8	0.5	0.7	0.6
Exit Outer Radius	0.1	0.2	0.1	0.1	0.1
(2) First Stage Terms					
Blade Root Axial Chord	0.2	0.4	0.1	1.0	0.2
Number of Blades	0.8	1.1	0.4	1.6	0.6
Blade Inlet Radius (i.d.)	0.6	1.4	0.2	0.6	0.3
Blade Exit Radius (i.d.)	1.9	4.0	0.7	2.6	1.0
(3) Next-to-Last Stage					
Flowpath Radius, Inside	0.4	0.7	0.2	0.5	0.2
Blade Root Axial Chord	2.2	4.0	1.1	1.8	1.3
Number of Blades	3.0	4.0	1.5	1.5	1.6

2.5.4.2 High-Pressure Turbine (HPT) Aerodynamic Matrix Regression

Table 2-18 summarizes HPT aerodynamic matrix regression accuracy statistics.

TABLE 2-18 REGRESSION RESULTS FOR HIGH PRESSURE TURBINE AERODYNAMIC MATRIX

	Base Data			Check Cases	
	Correlation Coefficient	Maximum Error (%)	Average Error (%)	Maximum Error (%)	Cumulative Average Error, % (%)
Cooled Efficiency	0.987	1.3	0.3	0.7	0.4
Blade Pull	0.985	26.7	4.2	15.2	5.4
Number of Blades	0.996	7.5	2.1	16.8	3.1
Flowpath Inside Radius	0.998	7.7	1.9	5.9	2.3
Rotor Speed	0.999	1.6	0.4	0.4	0.4
Annulus Area	0.999	3.3	0.8	1.2	0.8

All multiple correlation coefficients exceed 0.99, with the exception of cooled efficiency and blade pull. Average and maximum error statistics in general are excellent, and check case average errors are consistent with base data levels.

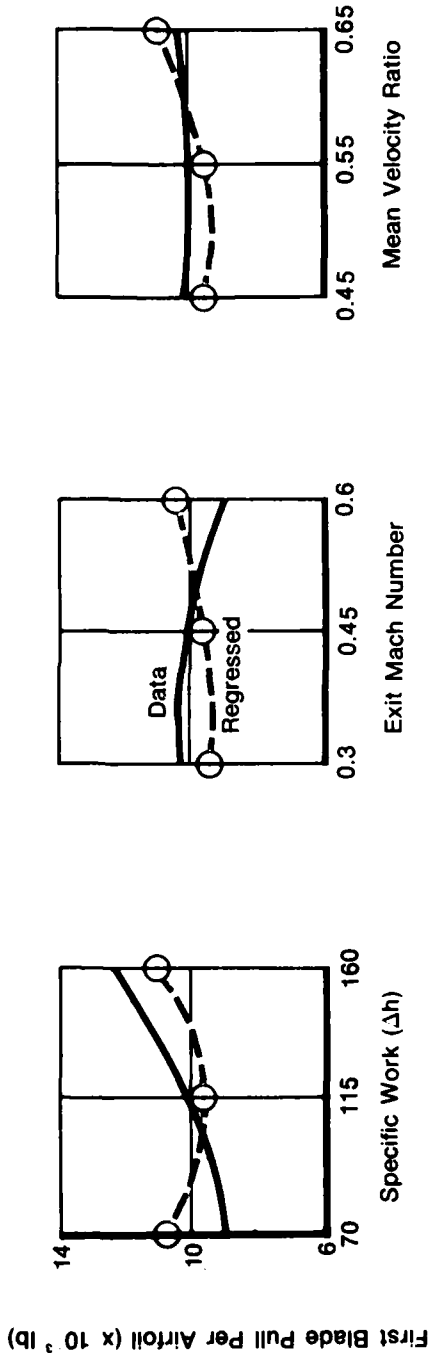
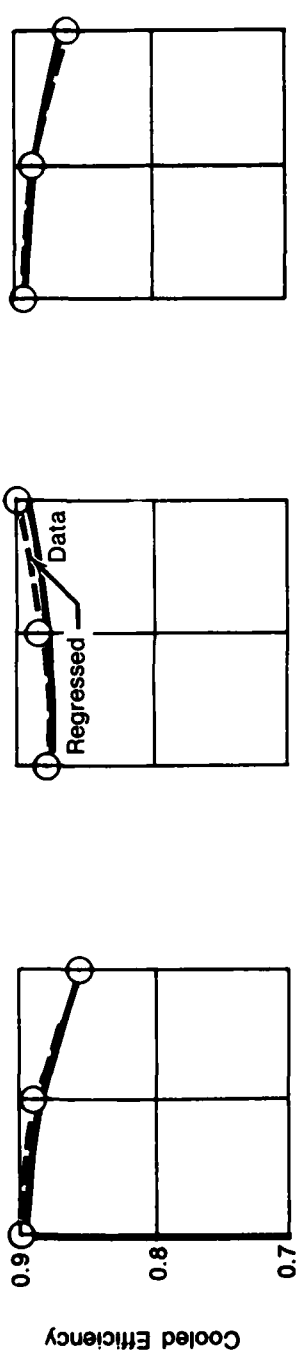
2.5.4.3 Low Pressure Turbine Aerodynamic Matrix Regression

Tables 2-19 and 2-20 summarize regression accuracy statistics for the single and two-stage low pressure turbine (LPT) aerodynamic matrices. Single stage LPT regression results (Table 2-19) are generally good, as evidenced by the correlation coefficient levels (0.99) and average percent errors of 0.4 to 3.1. LPT blade pull per airfoil maximum and average percent errors of 13.0 and 3.1, respectively are lower than the high pressure turbine errors (26.7 and 4.2 percent). Check case errors are low, and at the same levels as the base data.

TABLE 2-19. REGRESSION RESULTS FOR SINGLE-STAGE LOW PRESSURE TURBINE AERODYNAMIC MATRIX

	Base Data			Check Cases	
	Correlation Coefficient	Maximum Error (%)	Average Error (%)	Maximum Error (%)	Cumulative Average Error, % (%)
Cooled Efficiency	0.989	1.3	0.4	1.4	0.4
Blade Pull Per Airfol	0.994	13.0	3.1	7.0	3.1
Number of Blades	0.998	-6.6	1.6	-6.8	1.7
Rotor Speed	0.999	1.8	0.5	-1.2	0.5
Exit Annulus Area	0.999	5.6	0.8	-2.7	0.9

Table 2-20 presents the final low pressure turbine (LPT) regression results for the two-stage aerodynamic matrix. LPT regression results are excellent for rotor speed, blade counts, and exit annulus area, with correlation coefficients of 0.993 or more, and cumulative average error levels (including check cases) of 0.6 to 2.5%. Regression results for the remaining independent variables (cooled efficiency and blade pulls per air foil) are not as good as other terms. Figure 2-97 shows cooled efficiency and first stage pull



FD 190607
802608

Figure 2-97. Cooled Efficiency and Blade Pull Trends.

per airfoil trends as a function of three of the independent variables. Cooled efficiency trends are good, while pull per airfoil trends are adequate.

TABLE 2-20. TWO-STAGE LOW PRESSURE TURBINE AERODYNAMIC MATRIX REGRESSION RESULTS

	Base Data			Check Case	
	Correlation Coefficient	Maximum Error (%)	Average Error (%)	Maximum Error (%)	Average Error (%)
Overall Data					
Cooled Efficiency	0.978	-3.8	0.8	-2.0	0.8
Rotor Speed	0.999	1.7	0.4	6.3	0.6
First Stage					
Blade Pull Per Airfoil	0.967	23.2	6.4	10.2	6.3
Number of Blades	0.993	8.5	2.5	-4.7	2.5
Second Stage					
Blade Pull Per Airfoil	0.997	-7.4	1.8	12.3	2.0
Number of Blades	0.999	4.3	0.9	-6.2	1.0
Exit Annulus Area	0.999	-3.2	0.7	-2.2	0.7

2.5.5 Fan Disk Matrix Regression

Regression accuracy statistics for the first stage fan disk matrix are shown in Table 2-21.

With the four multiple correlation coefficients above 0.99 and average percent errors for 1.0 to 3.2, the regression accuracies are judged to be adequate.

TABLE 2-21. FAN DISK MATRIX REGRESSION RESULTS

	Base Data			Check Cases	
	Correlation Coefficient	Average Error (%)	Maximum Error (%)	Cumulative Average Error (%)	Maximum Error (%)
Disk Weight	0.999	3.2	12.2	4.4	10.1
Average Tangential Stress	0.994	1.0	4.8	1.9	13.7
Bore Tangential Stress	0.996	1.1	4.9	2.1	14.6
Rim Tangential Stress	0.993	1.0	5.7	1.7	7.8

2.5.6 Compressor Disk Matrices Regression

2.5.6.1 First Stage Compressor Disk Regression Table 2-22 summarizes first stage compressor disk matrix accuracy statistics. The second-order polynomial form for modeling the matrix was selected. SAS model check case errors were higher. These regression results are only fair for the weight and the three tangential stress variables. Though the web radial and effective stress regression equations have also been incorporated in the LPWT, these stress checks will not be implemented.

Table 2-23 summarizes regression accuracy statistics for the next-to-last stage compressor disk matrix. Weight, average tangential stress, and bore tangential stress accuracies are judged adequate for the LPWT program requirements. Web radial stress, web effective stress, and rim tangential (or LCF) checks will not be implemented in the LPWT.

TABLE 2-22. FRONT COMPRESSOR DISK REGRESSION ACCURACY SUMMARY
(SECOND ORDER POLYNOMIAL)

	Base Data			Check Cases	
	Correlation Coefficient (R^2)	Maximum Error (%)	Average Error (%)	Maximum Error (%)	Cumulative Average Error (%)
(a) Weight	0.9943	21.1	5.5	35.8	7.1
(b) Stresses					
Average Tangential	0.9839	15.2	3.4	39.9	5.2
Radial, Outer Ring 4	0.9792	60.8	10.9	44.4	12.9
Rim Tangential	0.9890	9.4	3.2	40.9	5.6
Bore Tangential	0.9669	19.7	5.2	57.3	7.1
Effective, Inside Ring 5	0.9852	17.2	3.2	57.9	6.5

TABLE 2-23. REAR COMPRESSOR DISK REGRESSION ACCURACY SUMMARY
(SECOND ORDER POLYNOMIAL)

	Base Data			Check Cases	
	Correlation Coefficient (R^2)	Maximum Error (%)	Average Error (%)	Maximum Error (%)	Cumulative Average Error (%)
(a) Weight/Thickness					
Weight	0.9966	24.4	4.8	69.2	11.5
Outer Ring 1 Thickness	0.9976	12.2	3.6	56.4	7.7
Outer Ring 2 Thickness	0.9934	19.0	7.2	82.3	16.6
Outer Ring 3 Thickness	0.9825	46.7	11.4	93.6	20.5
Outer Ring 4 Thickness	0.9981	23.1	4.7	84.4	11.4
Outer Ring 5 Thickness	0.9962	24.9	5.0	99.8	14.7
(b) Stresses with Radial ΔT					
Radial, Outer Ring 4	0.9601	50.7	12.8	245.	28.3
Rim Tangential	0.9642	128.1	20.0	385.	39.1
Bore Tangential	0.9992	4.6	1.3	21.0	2.3
Effective, Inner Ring 5	0.9483	45.1	10.7	237.	19.6
Average Tangential	0.9974	9.4	1.8	37.1	4.1
(c) Stresses without Radial ΔT					
Bore Tangential	0.9982	9.0	1.8	24.3	3.1

The rear compressor disk (as well as the turbine disks) is in an environment which results in significant disk radial thermal gradients. As a result, the disk thicknesses for rings one through five (ring one is the bore) must be regressed. Cumulative average errors of 10 to 20 percent, and check case maximum errors up to 100 percent, were obtained for thickness regression accuracies. These thicknesses are required for input to the Disk Radial Thermal Gradient Program incorporated in the LPWT. Thickness accuracy requirements are not critical to successful operation of the LPWT.

2.5.7 High-Pressure Turbine (HPT) Low-Pressure Turbine (LPT) Disk Matrix Regression

Tables 2-24 and 2-25 summarize the regression accuracy statistics for the HPT and LPT disk matrices, respectively. HPT regression modeling of thicknesses, weight, and web radial/effective stresses was accomplished for both second-order polynomial and SAS models. Second-order polynomial regression accuracies are superior to the SAS results.

LPT disk regression results show better weight, stress, and thickness accuracies in comparison with HPT statistics.

Web (disk rings 3, 4 or 5 are shown in Tables 2-24 and 2-25) radial and effective stress regression results are generally poor as expected, since web radial and effective stresses did not influence HPT disk sizing, and web radial stress does not influence LPT disk sizing. The exception is that web effective stress does not influence 40% of the LPT disks in the matrix, and both base data and check case errors are improved for the ring 4 effective stress dependent variable.

Analysis of HPT and LPT disk regression results indicate that:

- (1) disk stresses that limit the disk designs fit well with second order polynomial (2 to 4 percent cumulative average error)
- (2) weight regression accuracies (cumulative average error) are 5.4% and 11.7% for LPT and HPT matrices respectively, suggesting that additional effort on HPT disk regression has potential of improving accuracy

- (3) disk thicknesses do not model well using either second order polynomials or current Statistical Analysis Systems (SAS) candidate terms
- (4) in general the LPT disk regression errors are lower (approximately one-half) than those of the HPT
- (5) for both HPT and LPT disks' matrices, regression accuracies for the disk web radial and effective stresses are insufficient to warrant the incorporation of these design checks in the LPWT.

TABLE 2-24. HIGH PRESSURE TURBINE DISK REGRESSION ACCURACY SUMMARY
(SECOND ORDER POLYNOMIAL)

	Base Data			Check Cases	
	Correlation Coefficient	Maximum Error	Average Error	Maximum Error	Cumulative Average Error
	(R ²)	(%)	(%)	(%)	(%)
(a) Weight/Thickness					
Weight	0.9926	35.2	8.4	85.4	11.7
Outer Ring 1 Thickness	0.9837	25.3	7.9	77.3	11.6
Outer Ring 2 Thickness	0.9778	41.7	11.1	81.7	13.2
Outer Ring 3 Thickness	0.9683	42.0	13.4	86.7	17.0
Outer Ring 4 Thickness	0.9412	75.0	19.8	176.0	25.3
Outer Ring 5 Thickness	0.9207	64.0	17.0	165.2	22.2
(b) Stresses with Radial ΔT					
Average Tangential	0.9633	16.0	3.8	34.2	4.6
Rim Tangential	0.9852	53.6	6.3	91.2	7.7
Bore Tangential	0.9746	10.7	2.7	87.4	5.2
Web Ring 4 Outer Radial	0.8356	74.8	18.3	344.	24.5
Web Ring 3 Inner Effective	0.9562	13.0	4.5	52.7	5.9
Web Ring 5 Inner Effective	0.8476	45.1	10.5	69.0	11.9
Web Ring 3 Outer Effective	0.8914	22.0	6.0	61.2	7.8
Web Ring 4 Outer Effective	0.8342	27.3	9.3	67.1	10.7
(c) Stresses without Radial ΔT					
Rim Tangential	0.9568	11.1	3.3	40.7	4.2
Bore Tangential	0.9718	15.7	3.1	79.7	5.3
Web Ring 4 Outer Radial	0.8791	156.	19.8	415.	27.3
Web Ring 3 Inner Effective	0.9661	12.9	3.4	52.2	4.7
Web Ring 5 Inner Effective	0.8424	24.4	7.8	58.4	10.2
Web Ring 3 Outer Effective	0.9007	22.1	6.1	57.8	7.8
Web Ring 4 Outer Effective	0.8480	23.7	8.8	63.2	10.0

TABLE 2-25. LOW PRESSURE TURBINE DISK REGRESSION ACCURACY SUMMARY
(SECOND ORDER POLYNOMIAL)

	Base Data			Check Cases	
	Correlation Coefficient	Maximum Error	Average Error	Maximum Error	Cumulative Average Error
	(R ²)	(%)	(%)	(%)	(%)
(a) Weight/Thickness					
Weight	0.9958	15.0	4.0	30.3	5.4
Outer Ring 1 Thickness	0.9972	8.0	2.4	77.2	5.3
Outer Ring 2 Thickness	0.9930	24.2	6.3	59.0	9.7
Outer Ring 3 Thickness	0.9869	31.1	8.2	42.6	11.0
Outer Ring 4 Thickness	0.9882	38.3	7.8	52.1	10.6
Outer Ring 5 Thickness	0.9834	42.2	9.1	56.4	12.2
(b) Stresses with Radial ΔT					
Average Tangential	0.9834	4.4	1.1	18.6	2.1
Rim Tangential	0.9931	22.2	3.0	67.0	6.6
Bore Tangential	0.9870	4.5	0.9	20.2	2.1
Web Ring 4 Outer Radial	0.9794	26.5	8.3	120.	12.8
Web Ring 5 Outer Radial	0.9492	85.8	12.0	88.2	16.6
Web ring Outer Effective	0.9547	12.3	3.3	50.5	6.0
(c) Stresses without Radial ΔT					
Rim Tangential	0.9811	4.5	1.3	15.3	2.2
Bore Tangential	0.9880	4.0	0.9	18.0	2.0
Web Ring 4 Outer Radial	0.9800	25.7	8.5	122.	12.9
Web Ring 5 Outer Radial	0.9810	399.	35.0	431.	40.3
Web Ring 4 Outer Effective	0.8683	10.5	2.8	38.7	4.7

2.6 LIFE, PERFORMANCE, WEIGHT TECHNIQUE (LPWT) CAD SYSTEM

The following describes the technical approach used to integrate the techniques and design procedures described in Sections 2.1 through 2.5.

Engineering formulation, programming, and checkout of the CAD system was an ambitious undertaking. This effort utilized the balance of program resources in the last twelve months of the program (thru 1 May 1981). A team of skilled computing analysts and engineering personnel were assigned to the LUCID program in the Spring of 1980, with the objective of assembling and checking out the LPWT. The size of the total LPWT is three million bytes. Though the program is

large, a typical case requires approximately three minutes of computer run time. At a computer cost of roughly one dollar per second, an LPWT run costs two hundred dollars. Of course, this does not include the engineering labor required to set up and define the input to the program. Stipulation of life, cycle, component configuration variables and composite usage are not labor intensive input items. The definition of material properties can require an extensive effort if one is defining advanced material properties; however, the associated cost would be prorated over many LPWT executions.

A summary of the major elements/subroutines in the LPWT is shown in Table 2-26.

TABLE 2-26. LIFE, PERFORMANCE, WEIGHT TECHNIQUE (LPWT)
SIZE OF MAJOR ELEMENTS/SUBROUTINES

Program (or Subroutine)	Size, Lines of Code
Compressor and Turbine Disk Radial Thermal Gradient Program	1,400
Material Data Library	2,300
Engine Performance Program (and Pre-Processor)	10,000
Aerodynamic, Attachment, and Disk Regression Equations	12,600
Turbine Airfoil Life Proration Program	1,500
Driver and Life/Stress Decks	6,600

The LPWT schematic (see Figure 2-99) illustrates some of the major subroutines and program logic. Table 2-27 lists these subroutines, dividing them into two categories: the Driver Deck, which is initiated by specification of engine size and cycle, and generates blade design parameters, and the Life/Stress Deck, which is initiated by the above blade parameters from the Driver Deck, and generates attachment and disk geometries, stresses, and weights consistent with the required life and utilization.

TABLE 2-27 LPWT DRIVER AND LIFE/STRESS DECK
MAJOR SUBROUTINES

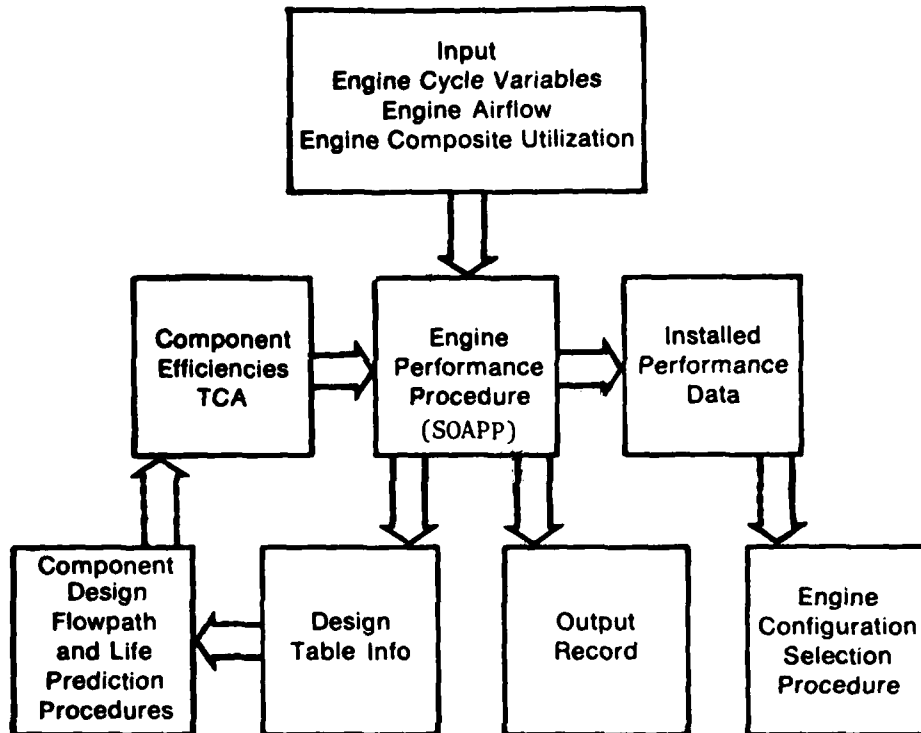
(a) Driver Deck
(1) Engine performance simulation
(2) Size scaling subroutine
(3) Component aerodynamic regression equations
(4) Turbine airfoil life prorotation program
(b) Life/Stress Deck
(1) Material data library
(2) Attachment and disk subroutines
(3) Attachment and disk regression equations
(4) Disk radial thermal gradient program

2.6.1 Engine Performance Simulation and Associated Driver Deck
Routines

This LPWT subroutine calculates engine performance for flight conditions specified in the composite engine utilization, and required for trading aircraft takeoff gross weight in the system design mission. Because component performance and turbine airfoil cooling air levels affect gas path and metal temperatures, which in turn affect component stress levels, the component flowpath, Life/ Stress Deck, and engine performance simulation are interactive.

A turbofan engine State-of-the-Art Performance Program (SOAPP) constitutes the major portion of the LPWT's engine performance simulation. SOAPP provides the engine performance parameters which serve as a basis for the component designs, engine weight, and size estimates.

Figure 2-98 is a schematic of the SOAPP performance simulation and related Driver Deck routines. Additions to the program for use as a routine in the LUCID LPWT include definition of the input routines which control the engine performance simulation program execution, provision of the interfaces to the component flowpath, life prediction, and configuration selector routines, and definition of special output formats to provide user visibility.



FD 10077

Figure 2-98. Schematic of SOAPP, LPWT Engine Performance Simulation, and Associated Driver Deck Routines.

The input routine controls execution of the engine performance program by defining flight conditions, power settings, and sequence of points to be simulated. The input routine is programmed to include automatic execution of engine design points, as well as execution of off-design match points necessary for component life calculation and mission performance estimates.

Interface with the component design routine occurs for both input and output because the component design is an iterative procedure. The engine performance program will execute a first pass through the component design match points with first estimate values of component efficiency and turbine cooling air. The output from the performance program provides the necessary design information (pressures, temperatures, etc.) for executing the component design routine. This routine then provides revised estimates of component efficiencies and cooling air requirements. These estimates, in turn, provide the input for subsequent iterations through the performance program. After each

iteration, a check is made to determine whether component performance level has closed sufficiently to preclude another pass through the performance program.

After completing the component design loop, mission points are executed and the resulting performance data is transferred to a storage matrix. This occurs for all subsequent passes through the program for engines with other flowpath designs. The performance matrix is then transferred to the engine configuration selection routine.

The output format has been constructed to provide the desired visibility, Current output procedures used in the SOAPP programs provide adequate output information for the engine performance routine.

SOAPP Description All of the steady-state performance estimates are carried out using a sophisticated powerplant performance analysis computer system, State-of-the-Art Performance Program (SOAPP). This system utilizes modular representations for each type of powerplant component, permitting virtually complete freedom in selecting the desired configuration. It is easy to use, versatile and fast, and it incorporates the most up-to-date calculation techniques available. The full system is currently in use in both batch and interactive modes of operation.

The unique feature of SOAPP is a pre-processor, which establishes the proper sequential logic required for the component calculation modules, and also performs the detailed communication bookkeeping work specific to any given powerplant configuration. Figure 2-99 is a pictorial representation of how SOAPP operates. The desired configuration is specified using a simple modeling language, along with specific module and component characteristic (map) identification codes. The pre-processor then selects the corresponding module and map routines from the library and writes the FORTRAN code for a main control program which calls the modules in the proper sequence to provide complete mass and energy balances for the desired configuration. It also provides all the necessary input-output flexibility, and provides iteration balances as required, in and out

bleed or extraction streams, external schedules and controls and communication of data between modules and input-output routines.

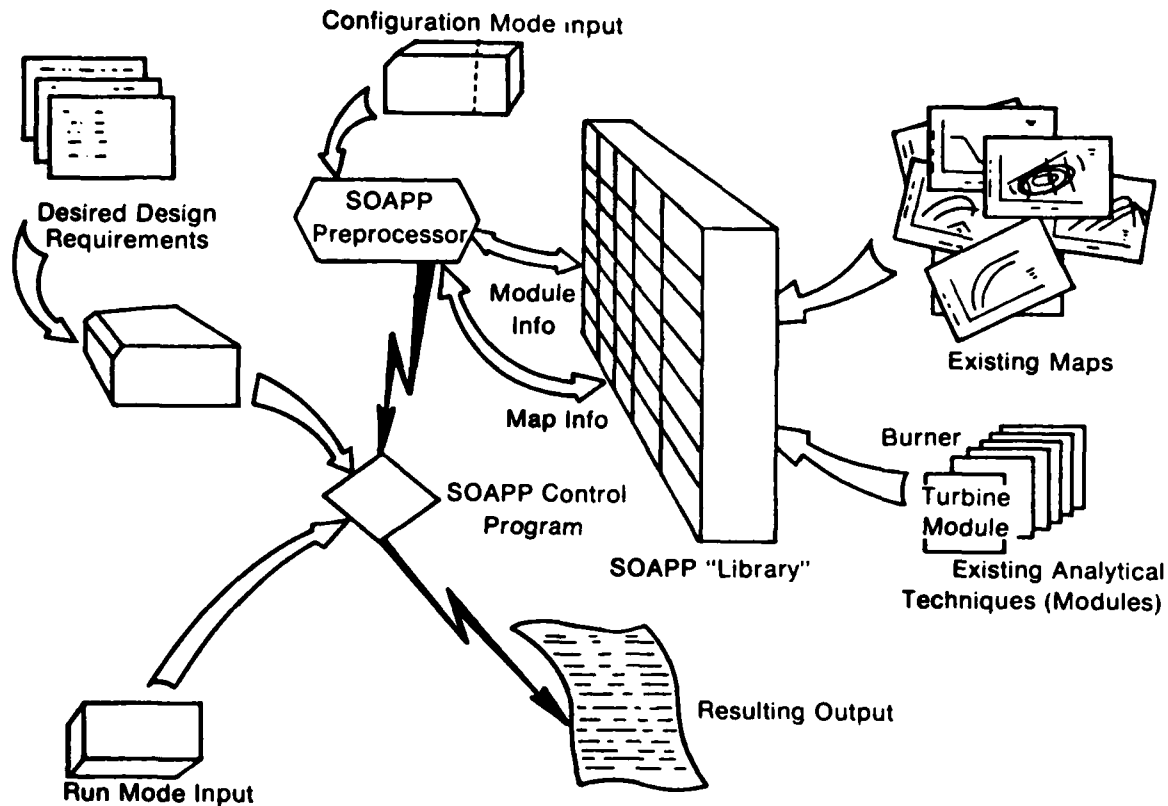


Figure 2-99. Pictorial Representation of SOAPP System.

The configuration flexibility described above was the primary goal of SOAPP. Other advantages include user convenience features such as automatic cycling of run data, data input/output manipulation and logic flexibility, automatic balancing of constraints imposed on parameters at intermediate locations in the powerplant cycle.

The development of SOAPP was done at corporate expense. The basic system structure, communication techniques and mathematical routines were developed by Pratt & Whitney Aircraft in 1970, as were the first component calculation modules and component map routines. Other maps and modules for aircraft gas turbines have been added continually by P&WA. During the early 1970's, P&WA assisted the United Technologies Research Center and the Power Systems Division

with the extension of the SOAPP library to include modules necessary for advanced industrial powerplants, such as boilers, heat exchangers, fuel cells, coal and oil gasifiers, and fuel gas clean-up systems. SOAPP has been used on a large number of corporate and Government-funded projects involving aircraft gas turbines, industrial gas turbines, combined-cycle power systems, turbocharged electrical fuel cells, integrated coal gasification/combined-cycle power systems, fossil- and nuclear-fueled closed-cycle systems using fluids such as helium and argon, and nuclear aircraft powerplants.

The turbine airfoil life proration program is a second major element of the Driver Deck. This prediction system is described in Section 2.1.4.

Integration of the preliminary design system was accomplished; however, various problems were encountered and solved in the integration process. The primary problem was one of high computer costs, and was solved by minimizing the number of passes through the turbine airfoil design system and the SOAPP routine. Other programming problems were related to multi-stage low pressure turbine configurations and program tolerances.

Section 2.2 summarizes the fan, compressor, and turbine aerodynamic designs generated in support of the flowpath computer routine. Section 2.5 summarizes the regression of the component flowpath parameters. Integration of the flowpath data in the Driver Deck was relatively straightforward, and primarily required the programming of a scaling routine. The scaling routine merely scales the component size of the particular engine being executed to the flow sizes of the matrices. The output of the component aerodynamic matrices are then scaled back to the actual component sizes. These parameters are radii, rotor speeds, lengths, and airfoil chords. Photo-scaling of components does not alter airfoil stage counts, aspect ratios, or tip speeds.

2.6.2 LIFE/STRESS DECK

Major elements of the Life/Stress Deck are shown in Figure 100 (located at the rear of the book). Preceding sections cover the

technical approaches, data generated, and other efforts which provide the programs/subroutines for integration in the LPWT's Life/Stress Deck. Section 2.6.2 summarizes the work accomplished integrating these support elements in the Life/Stress Deck.

2.6.2.1 Material Data Library A computerized material data library was available with ultimate strength, yield strength, creep, and stress rupture material properties for integration in the Life/Stress Deck. However, notched and smooth low cycle fatigue property curves for the three blade materials and the four disk materials were in curve form only (Section 2.1.5 summarizes the Material Data Library related LUCID effort). Fracture mechanics material properties were also in curve form. The LCF and fracture curves (fifty-seven LCF and twelve fracture mechanics property curves) were curve fit and incorporated in the material data module of the Life/Stress Deck.

2.6.2.2 Disk Radial Thermal Gradient Program The compressor and turbine disk radial Thermal Gradient Program was integrated in the Life/Stress Deck with relatively few problems. The rear compressor and turbine disk regression equations utilize one independent variable, the temperature difference from bore to rim, to define the radial thermal gradient of the disk, which is defined as the design gradient. It is noted that the design bore to web temperature gradient is a function of the bore to rim gradient.

In the process of solving a typical disk problem, the LPWT is estimating disk stresses at the multiple flight conditions specified in the composite utilization, and not just the sea level static flight conditions. To accommodate this calculation procedure, each disk matrix includes stress dependent variables with zero thermal gradient, as well as stresses for the total disk environment of dynamic and thermal contributions. Thus stresses at the off-design flight conditions are obtained by modifying the thermal contribution to stress by the gradient ratio and adding this revised stress change to the dynamic stress. The dynamic stress at the off-design flight condition reflects the level of speed at off-design.

2.6.2.3 Attachment Modules The Life/Stress Deck attachment modules perform the calculations which check the empirical stress criteria and the low cycle fatigue life. These modules mainly interface with their respective regression equation subroutines and the Material Data Library. The turbine blade/disk attachment modules are slightly different from the compressor attachment modules, in that two stress/life limits are simultaneously estimated. The compressor attachment modules drive only one criterion to a limit. Turbine attachments are typically low cycle fatigue and tooth bearing stress limited, while neck tensile and/or tooth bearing stresses may be limiting in compressor attachment designs.

Our approach to formulating and programming the attachment modules was to generate the more complex turbine attachment module first, then the compressor modules were obtained by modifying the turbine modules.

Attachment modules include the logic for making all stress checks defined by current design criteria. Of course, life/stress checks are not currently being made for those stresses which did not limit the matrix base data, and therefore did not correlate well.

2.6.2.4 Disk Modules The Life/Stress Deck disk modules mainly interface with the Material Data Library, the output from their respective attachment modules, and the disk regression equation subroutines. The disk modules perform the calculations which check the various stress and life criteria. All five disk modules (fan, front compressor, rear compressor, high pressure turbine, and low pressure turbine) use one independent variable, cyclic life capability, in generating a live-disk geometry and weight with one criterion at the limit, and the remaining criteria with stress below limits and estimated lives which exceed the required life.

2.6.2.4 Engine Weight Prediction Routine The LPWT engine weight routine (see Section 2.3) is the last major LPWT element whose integration into the CAD technique is described in this section. Section 2.3 discusses the technical approach and subroutines generated

for incorporation in the LPWT. These subroutines generate fan, compressor, high pressure turbine, and low pressure turbine module weights. Incorporation of these weight prediction subroutines was straightforward.

The weights of the remaining engine components are estimated by weight routines which are common to other conceptual design tools/techniques in use at Pratt & Whitney Aircraft.

These components are primarily the combustor, augmentor, nozzle, control and accessories. Weight estimating routines for the above components are straightforward, and in general are keyed directly to output from the engine performance simulation.

2.6.3 Life, Performance, Weight Technique Validation

LPWT validation effort was focused on those elements of the CAD system which utilize regression modelling in estimating aerodynamic/mechanical parameters. In the Driver Deck, the regression-based elements are the fan, compressor, high pressure turbine, and low pressure turbine aerodynamic matrices. The Life/Stress Deck regression-based subroutines are the four blade/disk attachment systems (front compressor, rear compressor, high pressure turbine, and low pressure turbine); the five disk matrices are the four attachment areas (see above) and the first fan disk components.

Regression accuracy problems in the component Flowpath Computer Routine were not expected, nor were they encountered in the validation effort outlined in the following section, because of the excellent regression accuracy statistics reported in Section 2.5.

However, regression accuracy statistics for the blade/disk attachment matrices and disk matrices are generally not as good as the aerodynamic matrices. Sections (b) and (c) outline the results of the validation effort in these areas.

(a) Flowpath Computer Routine Validation

Checkout of the component aerodynamic equations was accomplished by duplicating the fan, compressor, and both turbines of an existing turbofan conceptual design with the LUCID-developed LPWT.

The gas turbine cycle is 22.8:1 overall pressure ratio, 2800° maximum combustor exit temperature, 0.8:1 bypass ratio, and 1.06 throttle ratio. Design fan inlet airflow is 192 lb/sec. Table 2-28 summarizes the two-stage fan comparison. The variable levels of the two designs compare very well, given the five percent difference in inlet specific flow.

TABLE 2-28. COMPARISON OF LPWT-GENERATED FAN AERODYNAMIC VARIABLES WITH EXISTING CONCEPTUAL DESIGN

Variables	Conceptual Design	LPWT
a. Independent		
Average Pressure Ratio	3.27:1	3.27:1
Number of Stages	2	2
Inlet Hub/Tip Ratio	0.4	0.4
Inlet Specific Flow, lb/sec/ft ²	40	42
Tip Speed, ft/sec	1800	1800
Flowpath Shape	CMD	CMD
b. Dependent		
Average Aspect Ratio	2.20	2.18
Efficiency	0.819	0.825
Rotational Speed, RPM	12,740	13,070
Blade Tip Diameter, in.	32.4	31.6
First Stage Number of Blades	34	32

Table 2-29 summarizes the compressor aerodynamic comparison. This comparison differs from that shown in the September Progress Report in that the LPWT-generated inlet hub/tip ratio has been increased to 0.696. With the resulting 2 percent larger inlet tip diameter, the LPWT compressor has equal pressure ratio, rotational speed, and average aspect ratio, thus compensating for its CMD flowpath shape. Table 2-29 also shows that blade counts are in fair agreement.

Table 2-30 shows the high pressure turbine aerodynamic comparison. The LPWT-generated high turbine levels of efficiency and number of blades are not in good agreement with those of the baseline design. The baseline load coefficient is ten percent higher than that of the LUCID turbine matrix, explaining half of the blade count difference.

TABLE 2-29. COMPARISON OF LPWT-GENERATED COMPRESSOR AERODYNAMIC VARIABLES WITH AN EXISTING CONCEPTUAL DESIGN

Variables	Conceptual Design	LPWT
a. Independent		
Pressure Ratio	7	7
Inlet corrected flow, lb/sec	40	40
Number of stages	5	5
Inlet hub/tip ratio	0.67	0.696
Inlet specific flow, lb/sec-ft ²	36.5	37.5
Average aspect ratio	1.10	1.10
Flowpath Shape	CMD/COD	CMD
Rotational speed, RPM	18,650	18,650
b. Dependent		
Inlet tip radius, in	9.54	9.74
Efficiency	0.869	0.865
Corrected tip speed, ft/sec	1280.	1306.
Number of blades, first stage	36	40
Number of blades, next-to-last stage	80	70

TABLE 2-30. COMPARISON OF LPWT-GENERATED HIGH PRESSURE TURBINE AERODYNAMIC VARIABLES WITH AN EXISTING CONCEPTUAL DESIGN

Variables	Conceptual Design	LPWT
a. Independent		
Inlet flow parameter	16.5	16.5
Specific work, BTU/lb	161	161
Product of exit annulus area and speed squared, RPM ² x in. ²	500	500
Axial exit Mach number	0.45	0.43
Blade mean axial chord, in.	1.11	1.11
Mean velocity ratio	0.57	0.57
b. Dependent		
Flowpath inside radius, in.	8.8	8.8
Rotational speed, RPM	18,650	18,650
Cooled efficiency	0.885*	0.866*
Number of blades	46	59

*LPWT and baseline design efficiencies are quoted for different systems

Approximately 4% difference in exit Mach number is required to obtain equal annulus areas. The turbine efficiencies are not comparable because they are quoted for different calculation systems.

Table 2-31 compares low pressure turbine aerodynamic variables for the two design methods. As in the high-pressure turbine comparison, a direct comparison of the cooled efficiencies cannot be made because the calculation methods are different. At identical speed and AN^2 , the exit axial Mach numbers are only approximately 4% different. The blade count disagrees by 4 blades; 6% is not representative of the matrix regression accuracy statistics reported on page 135.

TABLE 2-31. COMPARISON OF LPWT-GENERATED LOW PRESSURE TURBINE AERODYNAMIC VARIABLES WITH AN EXISTING CONCEPTUAL DESIGN

Variables	Conceptual Design	LPWT
a. Independent		
Inlet flow parameter	45.3	45.3
Specific work, BTU/lb	109.5	109.5
Product of exit annulus area and speed squared, $RPM^2 \times in^2$	500	500
Axial exit Mach number	0.52	0.54
Blade mean axial chord, in.	1.35	1.35
Mean velocity ratio	0.511	0.511
b. Dependent		
Flowpath inside radius, in.	8.8	8.8
Rotational speed, RPM	12,740	12,740
Cooled efficiency	0.900*	0.874*
Number of blades	58	62

*LPWT and baseline design efficiencies are quoted for different systems.

(b) Blade/Disk Attachment Validation

The LPWT-generated from compressor attachment is 34 percent higher in rim pull than the corresponding blade/disk attachment

generated by the synthesis program. The LPWT-generated attachment is at the low level limit of the stress-driver independent variable (blade yield strength of 78 Ksi), and stress limits of both tooth bearing and blade neck tensile are estimated. It is noted that tooth shear is not checked in the current version of LPWT.

The blade/disk attachment synthesis program lighter attachment has three design limits: blade tooth bearing stress, blade tooth shear stress, and blade nominal neck tensile stress. These stress levels are within 4.5 percent of those of the LPWT generated attachment.

The rim width generated by the LPWT is also significantly higher than that of the synthesis program. The rim pull and rim width discrepancies are slightly greater than the maximum errors of the check cases.

An attempt at validation of the low pressure turbine blade/disk attachment indicates regression accuracy problems also. The LPWT-derived attachment's rim pull and rim width are 23% and 41% greater than the blade/disk attachment synthesis program levels. The two components share blade first tooth bearing and local fillet maximum elastic stress (low cycle fatigue) limits. A stress comparison shows good agreement in these stress levels, and in general fair agreement in other stress levels. These pull and width errors are slightly below the check case maximum errors of 33% and 45% respectively, but higher than the average errors of the check case data.

(c) Disk Validation

Validation of the five disks which the LOPWT addresses (first stage fan, first stage compressor, next-to-last stage compressor, high pressure turbine, and low pressure turbine) was attempted. As in the cases of some of the attachments, various factors prohibited a valid comparison of the LPWT-generated front compressor disk, rear compressor disk, and high pressure turbine disk.

(1) Fan Disk

Table 2-32 summarizes fan disk validation results, with the LPWT-derived disk's weight ten percent less than the synthesized disk. Not only did the LPWT identify the disk's life-limiting mode (bore fracture mechanics), but it also generated rim tangential and average tangential stresses which are in very good agreement with those generated by the Live-Disk Synthesis Program.

TABLE 2-32. FAN DISK VALIDATION

Variables	LPWT	Synthesis
Stress Variables		
Bore tangential, ksi	74.7 (limit)	72.8 (limit)
Rim tangential, ksi	38.1	35.4
Average tangential, ksi	52.8	48.4
Other Variables		
Disk weight, lb	27.8	30.9
Ring 3 thickness, in.	0.96	1.67
Bore thickness, in.	5.17	4

(2) Fan Turbine Disk

As in the case of the fan disk, the low turbine disk's life-limiting mode is bore fracture mechanics, as predicted by both the LPWT and the Live-Disk Synthesis Program (see Table 2-33).

Although rim tangential stress (low cycle fatigue) and average tangential stress (burst) are relatively far from limiting the disk design, these stresses are in reasonable agreement. The estimated weights are in excellent agreement (1.2% difference), and the bore and web widths are in good agreement.

TABLE 2-33. FAN TURBINE DISK VALIDATION

Variables	LPWT	Synthesis
Stress Variables		
Bore tangential, ksi	118 (limit)	118.0 (limit)
Rim tangential, ksi	31.3	24.4
Average tangential, ksi	85.2	79.8
Other Variables		
Disk weight, lb	59.7	60.4
Ring 3 thickness, in.	2.90	3.05
Bore thickness, in.	0.80	0.84

SECTION 3
RESULTS AND CONCLUSIONS

The thirty-two months of LUCID engineering effort have altered and benefitted the conceptual design process at Pratt and Whitney Aircraft. The generation of effective life prediction computer programs (see Sections 2.1.1 through 2.1.4) now allow more detailed analysis of mechanical components in our conceptual design efforts at minimal cost. In addition, these same life prediction programs are being applied in some areas of preliminary design. For example, the simplified Disk Radial Thermal Gradient Program is being used in the initial stages of turbine disk preliminary design, in preference over the more detailed thermal analyses. Also, the disk synthesis program, in identifying disk design/life problems within two days of receipt of the related vane/blade flowpath data, has resulted in component aerodynamic changes being made to designs while this flexibility is available. Our experience has sometimes been that these types of mechanical problems are found after schedules and lead times prohibit alteration of the component design. These computer programs are excellent examples of the economies which are realized by the use of computer software in solution of multi-variable optimization programs. These computer programs are in constant use at Pratt & Whitney Aircraft Government Products Division.

The computer-aided design (CAD) engine component/life screening technique has been executed many times during checkout and validation. Software development has progressed to the point that many subroutines are performing correctly. The various subroutines in the Driver Deck (see Section 2.6.1 of this report) are executing with very good results, as shown in Section 2.6.3 of this report. The Driver Deck is mainly comprised of the SOAPP engine performance program, the turbine airfoil life proration program, the fan/compressor/turbines aerodynamic matrices, subroutines for estimating blade airfoil pulls for the stages to be analyzed, and an executive routine which links these subroutines. We project that all

(or part) of the LUCID-developed Driver Deck will find application in our future conceptual design efforts.

While adaptation of the Driver Deck elements to our conceptual efforts is recommended, a more cautious approach is appropriate in evaluation of the cost versus benefit picture for the Driver Deck. The issues here are (1) man-in-the-loop generation of blade/disk attachments and disks via synthesis programs may be more effective than the overall computer-based LUCID approach, (2) the benefits of further pursuit of the overall analysis technique would be thwarted by evolution/innovation in mechanical execution, continually obsolescing the Life/Stress Deck.

The first issue, one of effectiveness, may be answered through contrasting the effectiveness of the two design techniques in performance of the typical engine conceptual design problem. The difficult part of this evaluation would be estimating the costs of further development and validation of the various elements of the Life/Stress Deck. This evaluation is recommended.

The second issue, concerning the correctness of the design execution details embodied in the assumptions inherent in the mechanical matrices, overrides the effectiveness issue. It is recommended that an assessment addressing these issues of flexibility and relevance be reviewed. If the consensus of designers' views are that the single computer-aided design technique is not feasible, then this totally computer-based approach would be discarded outright.

Regression accuracy statistics of the attachment and disk matrices and the conceptual engine component validation effort (refer to Sections 2.5 and 2.7) indicate that there are unresolved technical problems associated with modelling the weight/stress relationships of these components. Attachment rim pulls generated by the LPWT can exceed those of the synthesis program by as much as thirty-five percent. While the LPWT generates a low turbine disk weight within one percent of the synthesis program weight, fan disk validation

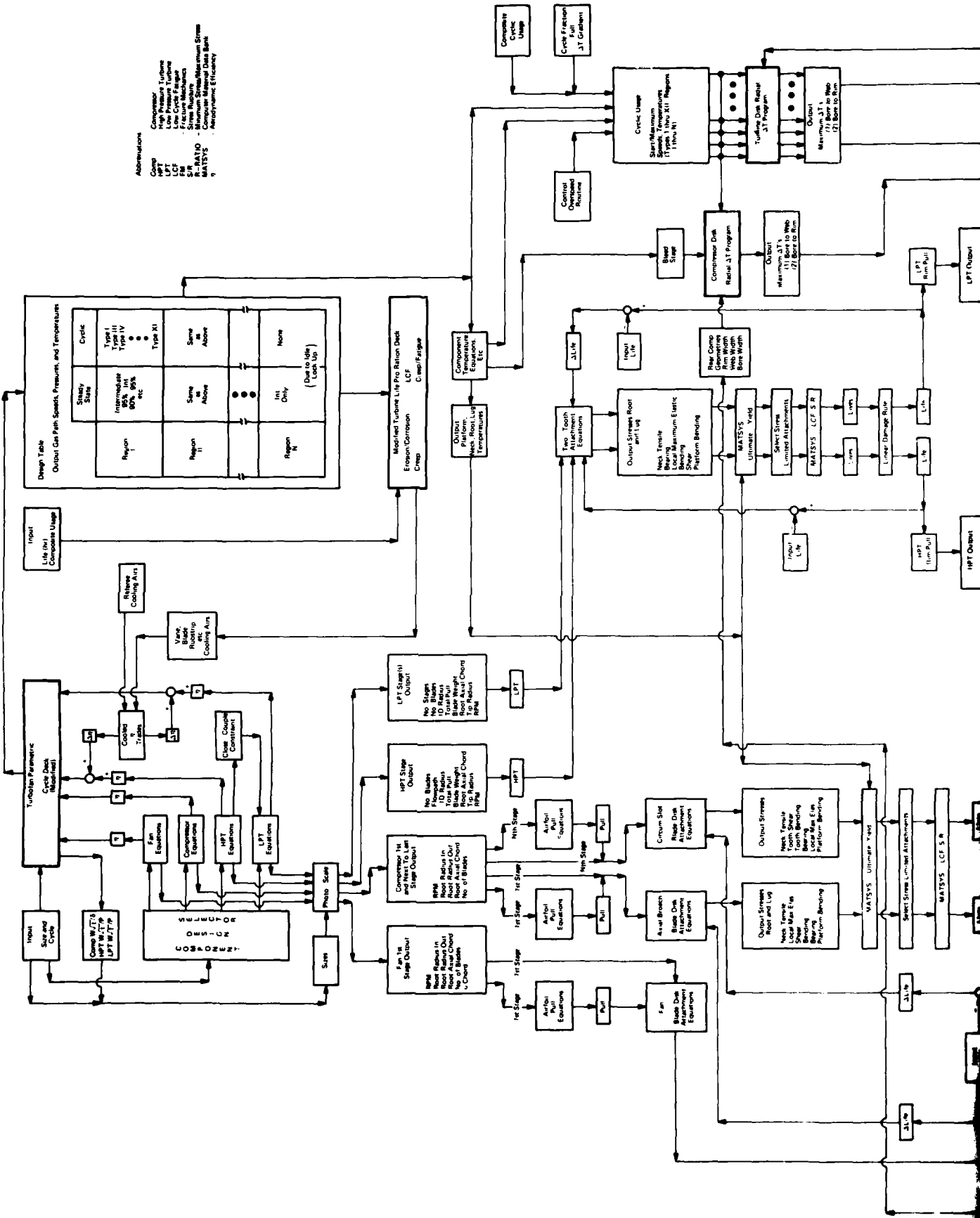
indicates a ten percent discrepancy. Though proof is not available, the addition of one independent variable to the attachment matrices and a rigorous approach to assessment of the validity of the design pattern while generating heavily skewed disk matrices may solve the Life/Stress Deck technical problems. It is noted that there are other relatively minor areas (material low cycle fatigue and fracture mechanics property curve fits, for example) which will require further effort.

Though these CAD system technical problems persist, other LUCID efforts have been extremely successful. The turbine airfoil, attachment, and disk life prediction techniques have met with acceptance and are being improved and used continually in our conceptual design efforts. The LUCID-developed Driver Deck has evolved to the point that it performs as planned.

With these accomplishments, a re-evaluation of LUCID Program objectives is recommended. This recommendation is made based upon the current program's emphasis on more detailed life/utilization analyses in early conceptual design. This emphasis resulted from a perception that parametric performance decks are deficient in these areas. Two factors should be pointed out in discussion of this topic: (1) cycle selection efforts in conceptual design do not stop with completion of initial system (engine and aircraft) optimization effort at the airframe company, (2) cycle selection efforts continue, both in the form of engine point designs covering ranges of important cycle variables (bypass ratio and combustor exit temperature, for example) and revised parametric performance decks are generated if these point designs indicate the requirement. In general, the Advanced Technology Engine Studies (ATES) program results indicate that engine point design estimates of weight and performance are in good agreement with military aircraft gas turbine parametric deck output, and that parametric deck relations are appropriate for the types of analyses intended.

At this time, Pratt & Whitney Aircraft is investigating potential areas of conceptual and preliminary design which are in need of enhanced analysis techniques. The objective is definition of on-going developments of effective design systems, so that the excellent progress of the current LUCID program can be continued.

FLOWCHART - LUCID LIFE PREDICTION PROCEDURE



Abbreviations

COMP - Compressor
 HPT - High Pressure Turbine
 LCF - Low Pressure Turbine
 FEM - Finite Element Method
 FRM - Fracture Mechanics
 MRE - Mean Residual Elastic
 MRE - Maximum Strain
 MATSYS - Computer Material Data Bank
 AEF - Aerodynamic Efficiency

Design Table

Output: Gas Path Speeds, Pressures, and Temperatures

Region	Steady State	CYCLE		
		Type I	Type II	Type III
Region I	Intermediate 95% Int 80% Ext etc.	•	•	•
Region II	Same Above	•	•	•
Region N	1st Only	•	•	•

None (Due to life) (Lock Up)

Modified Turbine Life Pro Ratio Deck

Output: Creep, Erosion/Corrosion, C-Map/Fatigue

Cyclic Usage

Output: Span/Maximum Span/Minimum Span/Maximum Temperature (1 Type, 10 to 11 Regions, 10 to 11 N)

Turbine Disk Rate

Output: Maximum JT's Web (2) Bone to Rim (2) Bone to Rim

Output

Maximum JT's Web (2) Bone to Rim

Compressor Disk

Output: Maximum JT's Web (2) Bone to Rim

Input Life

Output

Maximum JT's Web (2) Bone to Rim

Input Life

Output

Maximum JT's Web (2) Bone to Rim

Input Life

Output

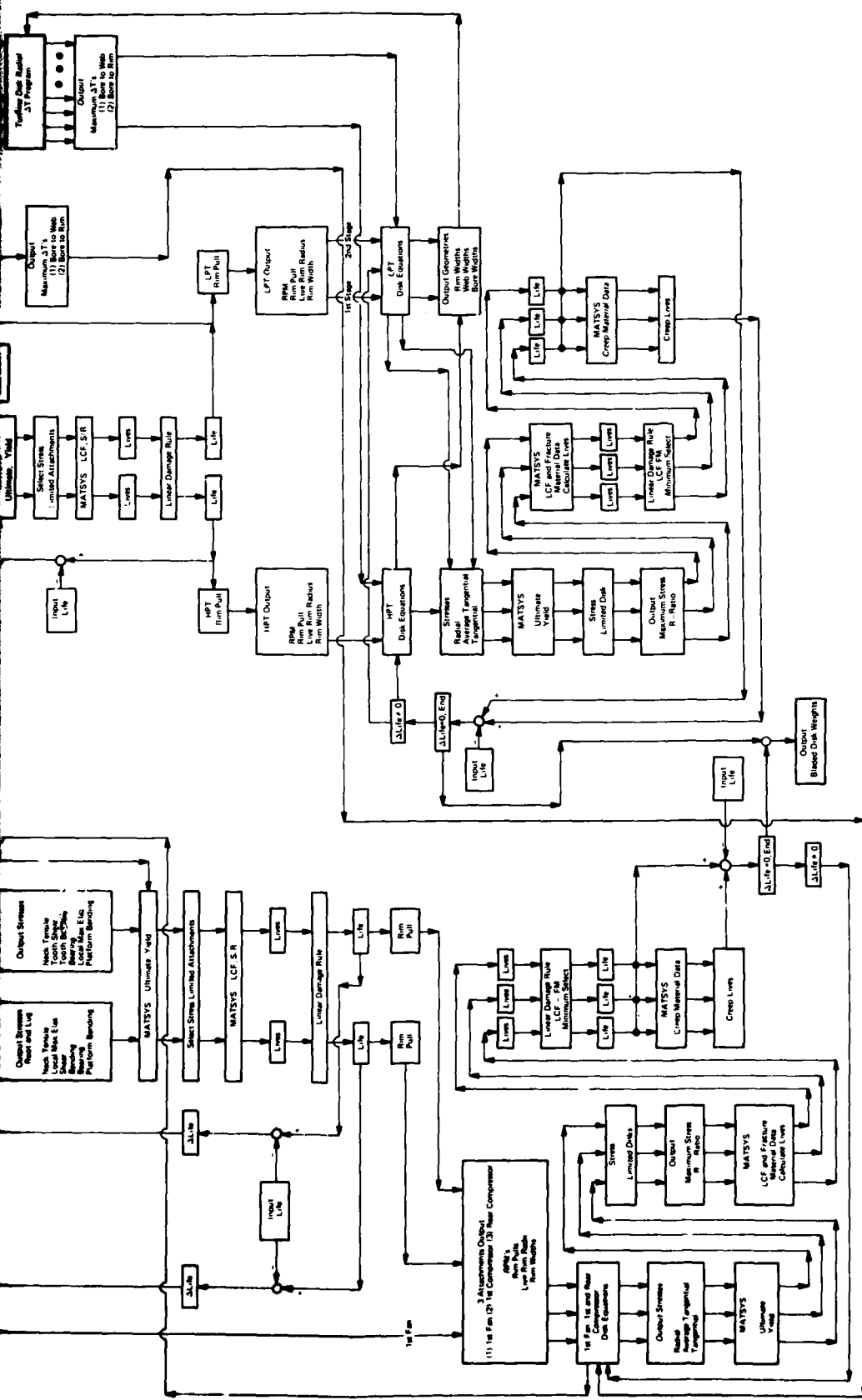
Maximum JT's Web (2) Bone to Rim

Input Life

Output

Maximum JT's Web (2) Bone to Rim

LPT Output



2-100. Flowchart of LUCID Life Prediction Procedure.